# On-line ship performance monitoring system for biofouling and its control

Alessandro Carchen


A thesis presented for the degree of

*Doctor of Philosophy*

School of Engineering
Marine, Offshore and Subsea Technology Group
Newcastle University
UK

August 2019

## Abstract

Marine biofouling has a significant impact on the overall hydrodynamic performance of a vessel. The literature shows that powering penalties for heavy fouled ships may reach up to 80% in the worst-case scenario, clearly resulting in higher operational costs and overall greater $CO_2$ emissions.

In the 1920's, ship performance monitoring emerged as one of the most suitable means of estimating these effects using full-scale on-board measurements coupled with various analysis techniques. The primary difficulty of such method stands in differentiating the effect of biofouling from the effects of such disturbances as waves, wind, change of operating conditions and so forth. A deterministic approach to this problem employs physical laws to estimate the contribution of the most relevant disturbances and hence to 'deduct' them from the measured in-service resistance.

However, very few deterministic Ship Performance Monitoring Systems (SPMSs) have been successfully implemented to estimate all the effects of hull and propeller performance monitoring with both a scrutinised uncertainty and state of the art standards. The present research investigates this knowledge gap.

The main aim of this research is to develop a working on-line SPMS based on the first published deterministic performance analysis method dedicated to the measurement of the effects of hull and propeller fouling on ship performance.

In achieving these aims, Newcastle University's R/V *The Princess Royal* was employed as a development and testing platform of the prototype SPMS, proving to be one of the few applications on small-size vessels. Four Key Performance Indicators (KPIs) were developed to estimate the impact of biofouling on hull and propeller. A novel method to derive $\Delta C_f$ is also proposed.

The accuracy of the estimations provided by the SPMS developed on-board *The Princess Royal* was assessed conducting a comprehensive Uncertainty Analysis, which includes all data treatment stages, from acquisition to performance analysis.

*To Maria, Agnese and Benedetto*

# Acknowledgements

This PhD has been an important milestone in my life and career. It has been a humbling experience, which has challenged my mind as well as my heart. I feel grateful to God not only for the expertise and knowledge gained in these years, but especially for the unexpected events.

Firstly, I would like to express my deepest gratitude to those people that more than others inspired me at the beginning of this journey and throughout it. Their enthusiasm for science is infectious and I dare say it is passed to co-workers by osmosis. A huge *thank you* goes therefore to Prof. Mehmet Atlar, for having inspired the pursuit of this degree from that very first interview to these days. Working with him is both an honour and a pleasure, not only for the knowledge, passion and energy he puts in all his work, but also for his humility and for the affection he has towards his team members. I would also like to extend my sincere thanks to Prof. Noriyuki Sasaki for having inspired me with his deep scientific wisdom and for teaching me to always dig deeper into the numbers.

My highest appreciation goes then to my supervisory team — Prof. Mehmet Atlar, Dr. Kayvan Pazouki and Dr. Alan J. Murphy. Their wise and kind guidance and patient support has always been a terrific help even in the difficult circumstances we found ourselves in.

My gratitude is due to Prof. Noriyuki Sasaki and Stone Marine Propulsion for having established the Sasaki-SMP fund by which this PhD was funded.

This research project has seen the involvement of a few third parties in the design, manufacture and maintenance of experimental equipment. I would therefore like to thank International Paint, for the support given throughout the development of the on-board system and for the supply of testing material. A big thank goes to Design Unit of Newcastle University, manufacturers of the instrumented shafts, for the customer support provided throughout the years in the person and kindness of Mr. Andy Hamer. Finally, I'm grateful to Stone Marine Propulsion and Dr. Stephan Helma for the support given through the design and manufacture of the NPT propeller model.

Several people have contributed to the success of this study. I would like to express my gratitude in particular to:

- Dr. Serkan Turkmen and Dr. Serena Lim, for their unconditional help and the friendship they have blessed me with. Even through the roughest trips on the North Sea.

- The *The Princess Royal*'s crew, Mr. Neil Armstrong and Mr. Barry Pearson, particularly for their patience during the development of the on-board system and the several long trials.

- The technicians of the Hydrodynamic labs, Mr. Bob Hindhaugh, Mr. Phil Letouze, Mr. Kieron Fallows, Mr. Ian Howard-Row and Mr. Liam Rogerson.

- The IT staff, always of great support when needed.

- The administrative staff, particularly Mr. James Armston for his outstanding efficiency and kindness.

- Miss Mincui Liang, for being of tremendous help in the submission process.

Throughout these years, I have been blessed with being surrounded by several people. Their presence taught me once again that what we are given is greater than what we imagine. I therefore embrace the opportunity to send my deepest gratitude especially to:

- My colleagues of the *Emerson Cavitation Tunnel* Team and Office 2.66. Working with them has been one of the most amazing experiences ever for their passion and for the uncommon true friendship that allowed not only work but life to be shared.

- To Brian Newman, my 'third grandfather'. For his inspirational fresh enthusiasm towards nearly everything and his loving affection.

- To Neil Armstrong, for his friendship, blossomed in very unexpected and painful circumstances.

- To my loving friends at St. Andrews Parish and those of Communion and Liberation, for always redirecting my heart to the essential.

- To my new line managers, Dr. Tomaso Gaggero, Dr. Diego Villa and Dr. Giovanni Besio for their endless patience and understanding during the completion of this thesis.

I am deeply grateful for the loving presence of my parents and my sister, whose unconditional love is the foundation of my being.

Finally, my most profound gratitude goes to God for my wife Maria and for my children Agnese and Benedetto, precious gifts born during the course of this PhD. In the joys and the difficulties, each and every day they have helped me putting all my life into perspective with their docile presence and their intensity.

# Contents

# Nomenclature

### Greek Symbols

| | | |
|---|---|---|
| $\beta$ | Drift angle | deg |
| $\delta$ | Rudder angle | deg |
| $\eta_b$ | Propeller behind efficiency | - |
| $\eta_d$ | Propulsive efficiency | - |
| $\eta_g$ | Gearing efficiency | - |
| $\eta_h$ | Hull efficiency | - |
| $\eta_o$ | Propeller open water efficiency | - |
| $\eta_r$ | Propeller relative rotative efficiency | - |
| $\eta_s$ | Stern gland efficiency | - |
| $\gamma$ | Wave filter strictness parameter | - |
| $\mu$ | Wave direction. 0 deg for Northbound wave train | rad |
| $\mu_R$ | Relative wave direction. 180 deg for head waves | rad |
| $\mu_{AR}$ | Relative wind bearing. 0 deg for head wind | rad |
| $\mu_A$ | Wind bearing. 0 deg for a northerly wind | rad |
| $\nu$ | Kinematic viscosity of sea water | $m^2/s$ |
| $\omega$ | Wave frequency | rad/s |
| $\omega_e$ | Wave encountering frequency | rad/s |
| $\phi$ | Fouling coefficient | - |
| $\psi$ | Ship heading | deg |
| $\psi_g$ | Ship course over ground | deg |

| | | |
|---|---|---|
| $\rho$ | Water density | kg/m$^3$ |
| $\rho_A$ | Density of air | kg/m$^3$ |
| $\sigma_{AW}$ | Nondimensional added wave resistance transfer function in regular waves | - |
| $\theta_L$ | Trim angle | deg |
| $\vartheta$ | Ship-specific time constant | s |
| $\zeta$ | Wave amplitude | m |

**Latin Symbols**

| | | |
|---|---|---|
| $\overline{R}_{AA0}$ | Air resistance due to ship motion | N |
| $\overline{R}_{AA}$ | Mean direct wind resistance | N |
| $\overline{R}_{AW}$ | Mean added wave resistance in irregular waves | N |
| $A_L$ | Projected lateral plane area | m$^2$ |
| $AHR$ | Average Hull Roughness | $\mu$m |
| $B$ | Ship breadth | m |
| $C_f$ | Skin friction drag coefficient | - |
| $C_T$ | Total ship resistance coefficient in service conditions | - |
| $C_v$ | Viscous resistance coefficient | - |
| $C_w$ | Wave-making resistance coefficient | - |
| $C_X$ | Wind resistance coefficient in surge direction | - |
| $D$ | Propeller diameter | m |
| $EAR$ | Expanded Blade Area Ratio | - |
| $F_N$ | Rudder normal force | N |
| $Fn$ | Froude number | - |
| $g$ | Gravitational acceleration | m/s$^2$ |
| $h$ | Water depth | m |
| $H_{S_\zeta}$ | Directional wave height threshold | m |
| $IQR$ | Inter-Quartile Range | - |

| | | |
|---|---|---|
| $J$ | Advance coefficient | - |
| $k$ | Form factor | - |
| $K_Q$ | Torque coefficient | - |
| $K_T$ | Thrust coefficient | - |
| $L_{oa}$ | Length overall of the ship | m |
| $L_{pp}$ | Length of the ship between perperndiculars | m |
| $m_x$ | Nondimensional added mass in surge direction | - |
| $N$ | Data bin size | datapoints |
| $n$ | Propeller rate of revolutions | rev/s |
| $n_e$ | Engine rate of revolutions | rev/s |
| $P/D$ | Pitch-to-Diameter ratio | - |
| $p_a$ | Absolute air pressure | Pa |
| $P_B$ | Brake power | W |
| $P_D$ | Delivered power | W |
| $P_E$ | Effective power | W |
| $P_T$ | Thrust power | W |
| $p_v$ | Vapour pressure | Pa |
| $Q$ | Propeller behind hull torque | Nm |
| $Q_\phi$ | Added torque due to propeller fouling | Nm |
| $Q_B$ | Engine brake torque | Nm |
| $Q_o$ | Propeller open water torque | Nm |
| $Q_S$ | Shaft torque | Nm |
| $R_\phi$ | Added resistance due to biofouling | N |
| $R_\rho$ | Added resistance due to changes in water properties | N |
| $R_T$ | Total ship resistance in service conditions | N |
| $R_v$ | Viscous resistance | N |

| | | |
|---|---|---|
| $R_w$ | Wave-making resistance | N |
| $R_\delta$ | Steering resistance | N |
| $R_{add}$ | Added resistance due to disturbances | N |
| $R_{AW}$ | Added wave resistance in regular waves | N |
| $RH$ | Relative air humidity | % |
| $Rn$ | Reynolds number | - |
| $S$ | Ship wetted surface area | $m^2$ |
| $S_\zeta$ | Directional spectral density ordinate | $m^2$ s/$rad^2$ |
| $S_A$ | Salinity of the water | PSU |
| $T$ | Propeller thrust | N |
| $t$ | Thrust deduction factor | - |
| $T_a$ | Temperature of air | K |
| $T_M$ | Midship draugth | m |
| $t_R$ | Steering resistance deduction factor | - |
| $T_w$ | Temperature of the water | K |
| $U_A$ | True horizontal wind velocity | m/s |
| $u_s$ | Forward component of the ship speed through the water | m/s |
| $U_{AR}$ | Relative wind velocity | m/s |
| $V_a$ | Speed of advance | m/s |
| $V_g$ | Ship speed over ground | m/s |
| $V_s$ | Ship speed through the water | m/s |
| $v_s$ | Athwart component of the ship speed through the water | m/s |
| $w$ | Effective wake fraction | - |
| $w_\phi$ | Wake fraction gain due to biofouling | - |
| $w_{app}$ | Apparent wake fraction | - |
| $w_Q$ | Torque-identity wake fraction | - |

| | | |
|---|---|---|
| $w_T$ | Thrust-identity wake fraction | - |
| $Z$ | Reference wind height above water | m |
| $z$ | Anemometer height above water | m |

**Other Symbols**

| | | |
|---|---|---|
| $\mathbb{t}$ | Time | s |
| $\nabla$ | Ship volumetric displacement | $m^3$ |

**Suffixes**

| | |
|---|---|
| 0 | Ideal service sailing conditions |
| ref | Clean hull reference sailing conditions |

**Accents**

| | |
|---|---|
| $\hat{a}$ | Approximate value |
| $\overline{a}$ | Mean |
| $\tilde{a}$ | Median |
| $a'$ | Nondimensional value |
| $a^*$ | Design value |

**Acronyms**

| | |
|---|---|
| AIAA | American Institute of Aeronautics and Astronautics |
| BSRA | British Ship Research Association (now BMT) |
| CFD | Computational Fluid Dynamics |
| DD | Dry-Docking |
| DGPS | Differential Positioning System |
| DOF | Degrees Of Freedom |
| EDD | Extended Dry-Docking |
| EFD | Experimental Fluid Dynamics |
| ESD | Extreme Studentized Deviate test |
| FR | Foul-Release |

GPD Generalised Power Diagram

GPS Global Positioning System

GUM Guide to the Expression of Uncertainty in Measurements

IDI Inter-Docking Interval

IEC International Electrotechnical Commission

ISO International Organization for Standardization

ITTC International Towing Tank Conference

IWS In-Water Surveys

LPF Low-Pass Filter

MCM Monte Carlo Methods

MIT Massachusetts Institute of Technology

NMEA National Marine Electronics Association

NOAA National Oceanic and Atmospheric Administration

R/V Research Vessel

RANS Reynolds Averaged Navier-Stokes

SPC Self-Polishing Copolymer

SPMS Ship Performance Monitoring System

SPMS Ship Performance Monitoring System

SSI Steady-state Identification

TBT Tributyl Tin

VLCC Very Large Crude Carrier

WAAS Wide-Area Augmentation System

WHOI Woods Hole Oceanographic Institue

# List of Figures

# List of Tables

# CHAPTER 1

# Introduction

## 1.1 Introduction

This chapter provides the reader with a general overview of the subject of ship performance monitoring and sets the aims and objectives for this research. In doing so, Section 1.2 introduces the problem of biofouling growth on ships and speculates on the contemporary drivers of ship performance monitoring. Section 1.3 outlines the cardinal assumptions and some important concepts as the necessary basis of the aims and objectives presented in Section 1.4. Section 1.5 then briefly discusses the possible applications of the Ship Performance Monitoring System (SPMS) and the scope of this research. Finally, Section 1.6 describes the layout of this thesis by briefly introducing the main contents of each chapter.

The notation introduced in this chapter was conceived to be consistent with both ITTC and ISO 19030 standards as much as feasible.

## 1.2 Overview

Biofouling growth on ship hulls was always recognised as critical for the ship's navigation, not only because of its detrimental effects on powering, but also due to its fast advancement and the problem of its prevention and removal. The observation of vessel performance in-service is therefore a long standing practice, which is believed to be even older than written records. It is known that the loss of speed and manoeuvrability of ships caused by biological growth was more than a nuisance to the ancient sailors, as some of the older written reports credited shell-fish and sea-weed for stopping ships dead in the water (e.g. Lemnius, 1571).

Although sailors have always been aware of the detrimental effects of biofouling, its monitoring and prevention was initially entrusted to the mariner's wisdom alone. Only in the late 18th century the first service trials and ship performance monitoring dedicated to biofouling research were carried out on the *HMS Alarm* from 1758 to 1761. It may be speculated that historically the Royal Navy's investigation initiated the systematic moni-

toring of biofouling effect on ship performance. The scientific commitment to the subject continued irregularly over the 19th Century, until the relatively new screw propulsion and the novel model testing practices sparked a renewed interest in the ship-scale hydrodynamic phenomena (WHOI, 1952). In this context, a renowned study was conducted by Telfer (1926), which is credited to have paved the way to the modern SPMSs. For the first time, Telfer showed how on-board collected measurements of speed and power can be used to calculate the effect of biofouling on the ship performance.

Today, well known studies have shown that fouling penalties are in the worst cases reaching 80% of the shaft power when the hull is covered with heavy calcareous fouling (see e.g. Schultz, 2007). Such circumstance can be avoided if the fouling penalties are kept under control not only by a suitable fouling-control strategy, but also by the regular monitoring of the ship performance deterioration over time.

### *1.2.1 Contemporary drivers of ship performance monitoring*

Nowadays, the focus of the industry is not as much on avoiding worst-case fouling settlements, but rather on the fine optimization of the vessel management — from the timing for hull and propeller cleaning and the selection of fouling control strategies to the assessment of energy saving devices and route planning.

The significant fall of the freight prices by the end of the first decade of the 2000's had yet again stimulated the adoption of fleet management strategies aimed at improving the shipping efficiency. Practices to reduce fuel consumption such as slow steaming and smart steaming were direct answers to a rapidly changing market where the minimization of bunkering costs was paramount. In recent years, however, it is the environmental legislation to have the most significant impact on the design and operation of ships. The growing concern for the Green House Gases (GHG) fostered the action of the International Maritime Organization (IMO) and its regulatory organs to further reduce the emissions of seagoing vessels. Already in 2009, the IMO had recommended the use of the Ship Energy Efficiency Management Plan (SEEMP) for the improvement and management of the ship's energy efficiency over time (IMO, 2009). As a monitoring tool, the Energy Efficiency Operational Indicator (EEOI) was at first proposed as a cost-effective measure of the in-service fuel efficiency. The EEOI was later complemented by the Energy Efficiency Design Index (EEDI), which has been the most influential technical measure in ship design since its introduction. The EEDI and SEEMP, made mandatory by IMO's Resolution MEPC.203(62) in 2011, urge the continuous advancement and implementation of measures to increase the fuel efficiency of ships — respectively at design stage and during the ship's lifetime. This procedure became even more stringent when the monitoring of ship emissions was later made mandatory by both the IMO and the European Commission, respectively with Resolution MEPC.278(70) and the Monitoring, Reporting

and Verification scheme (MRV) (EC, 2015, 2016). The enforcement of these measures was a consequence of the extensive studies that the IMO has been conducting on the GHG emissions from ships. The goals for the reduction of GHG were finally drafted in 2016 and an 'Initial Strategy' was enacted in April 2018 with the adoption of Resolution MEPC.304(72). Among the objectives of this strategy is the reduction of GHG and $CO_2$ emissions respectively by 50% and 70% by 2050 (IMO, 2018). The impact of these global regulations on shipping is expected to be huge, from both a design and operational point of view (see e.g. Clarksons Platou, 2018).

In this context, the control of biofouling is an important asset in the fight for the reduction of air pollution from ships and is taken into account in the IMO guidelines regarding the SEEMP (IMO, 2016). On the other hand, the market of fouling-control strategies offers a plethora of different solutions, each with a specific performance in clean and fouled condition (see e.g. Yebra *et al.*, 2004; Yeginbayeva, 2017).

In this framework, ship performance monitoring stands as one of the strategies that can be effectively used in achieving the objectives set by the IMO (Stopford, 2019). In order to be kept under a certain threshold during the service life of the ship, performance decays have to be monitored and analysed to plan the investments and the most suitable maintenance strategies. The sensibility of research institutions and industry to the subject was recently reflected by the development of the ISO 19030 (2016), the first standard dedicated to the analysis of hull and propeller performance. Therefore, SPMSs remain the primary aid in the assessment of a fuel management strategy, the effectiveness of a new energy saving retrofit and the performance of different coating systems on the short and long terms.

## 1.3 Main assumptions and initial considerations

According to the ISO 19030,

> "the hull and propeller performance refers to the relationship between the condition of a ship's underwater hull and propeller and the power required to move the ship through water at a given speed" ISO, 2016

In this framework, the least ship resistance and an efficient propulsion system are the objectives of the performance improvement.

As a vessel enters into the water, the physical condition of its hull begins to deteriorate, particularly because of biological growth on the hull and propeller surfaces. The effect of this degradation of the hull surface roughness is not directly measurable and difficult to evaluate in the vast majority of the cases. One reason is that the whole environment the vessel sails into and its operational profile contribute to alter its power absorption, thus

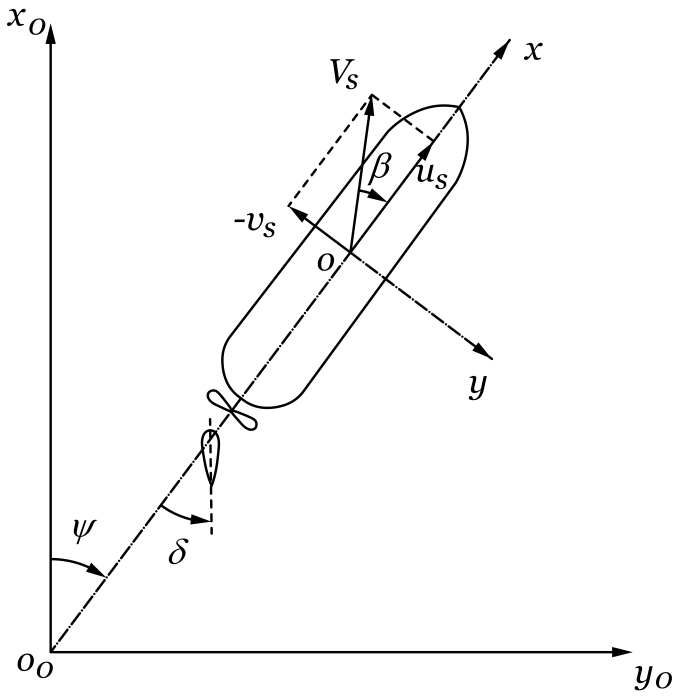


**Figure 1.1** – *Reference Coordinate System.*

causing the performance data to be contaminated by many factors. Hence, isolating the sole effect of biofouling from performance data collected on-board is an arduous task.

In this section, the main assumptions used to obtain a good estimation of the effect of biofouling by means of the SPMS propose in this thesis are laid out.

The reference coordinate system used in this research is shown in Figure 1.1. The axis $x_0$ and $y_0$ lay on the still water surface, $o$ coincides with the midship, $u_s$ and $v_s$ are the axial and normal components of the total ship speed through water $V_s$ on the ship axis system and $\beta$, $\psi$, $\delta$ the drift, heading and rudder angles respectively.

From the basic relations of ship resistance and propulsion, the steady-state ship powering equations are defined as follows (e.g. Carlton, 2012):

$$P_S = \frac{TV_s}{\eta_o \eta_r \eta_s}(1-w) \tag{1.1a}$$

$$T = \frac{R_{T0}}{1-t} \tag{1.1b}$$

These are the equations to be addressed to solve the ship performance problem. It should be recalled that the variables $T$ and $\eta_o$ cannot, most of the times, be directly measured and are indirectly evaluated measuring the propeller torque $Q$, the propeller speed $n$ and knowing the propeller open-water curves. Chapter 2 will show in detail how biofouling primarily affects the viscous resistance of the ship, the viscous component of the wake and the propeller torque. The effects on other components and variables are sufficiently small to be neglected. It will also be shown that the complex environmental conditions and operational profile of a ship introduce alterations in its powering requirements. Under

equal environmental and operational circumstances, every increase in power requirement to move the ship at a same speed through water stands to indicate an efficiency loss in the hull, the propeller or both. As soon as the environmental and operational conditions vary, the initial $V_s$–$P_S$ relationship becomes altered by the presence of additional forces. This fact has two major implications:

1. In order to understand the effect of biofouling, the $V_s$–$P_S$ relationship has to be analysed under the same ideal conditions.

2. Auxiliary measurements are necessary to identify the state of the real conditions met by the vessel.

The ideal conditions are most conveniently chosen to be similar to those suitable for conducting sea trials — see ITTC (2014*c*). Firstly, we define *ideal* sailing conditions having the following characteristics:

- Calm deep water
- No wind
- No current
- Defined air and water properties
- Defined displacement and trim
- Steady-state sailing

Predetermined values of displacement, trim and air and water properties are arbitrary. However, they can be conveniently chosen as the design values. This is coherent with the relevant work conducted in the past on this topic and with most current standards (e.g. ITTC, 2014*c*; ISO, 2015*a*).

We also define a *reference* (or baseline) performance as that obtained by a ship sailing in *ideal* conditions with a defined hull and propeller fouling state. In most cases, this is taken as clean hull and propeller.

Four assumptions can at this point be introduced.

**Assumption 1.** The total in-service resistance of a vessel can be defined as the superposition of the resistance in ideal conditions, $R_{T0}$, and the added resistance caused by the disturbances, $R_{add}$. When biofouling starts to grow on the hull, $R_{T0}$ will include the effect of the increased surface roughness. The total in-service resistance can therefore be thought of as the sum of the reference resistance (i.e. ideal conditions with clean hull), $R_{T\text{ref}}$; the resistance induced by biofouling growth, $R_\phi$; and the added resistance, $R_{add}$:

$$R_T = R_{T\text{ref}} + R_\phi + R_{add} \tag{1.2}$$

The growth of biofouling was shown to affect both the frictional resistance and the viscous pressure drag (Oliveira *et al.*, 2018), whilst having minimal effects on potential-related forces. The total resistance as it is described in eq. (1.2) may be therefore rewritten in its in-service form as:

$$R_T = (1 + \phi)R_v + R_w + R_{add} \tag{1.3}$$

where $\phi$ is the effect of biofouling growth on the viscous forces.

It should be noted that in principle, $\phi$ would indicate a change in the hull surface roughness and $R_\phi$ the relative induced resistance. However, since fouling is the major contributor to the change of hull roughness and is the object of the present study, $\phi$ shall be herein termed fouling coefficient.

**Assumption 2.** The effects of the external disturbances on the effective wake fraction are negligible in the range of sailing conditions useful for performance analysis. Therefore, the effective wake fraction for in service hull conditions, $w$, can be redefined as:

$$w = w_{\text{ref}} + w_\phi \tag{1.4}$$

where $w_{\text{ref}}$ is the effective wake fraction for the reference performance (i.e. ideal sailing conditions and clean hull) and $w_\phi$ is the wake fraction gain due to the biofouling growth on the ship's hull.

**Assumption 3.** As biofouling also increments the propeller torque, the in-service measurement of propeller torque can be expressed as:

$$Q = Q_{\text{ref}} + Q_\phi \tag{1.5}$$

where $Q_{\text{ref}}$ is the propeller torque in reference fouling conditions and $Q_\phi$ is the added propeller torque caused by fouling growth on the propeller blades.

**Assumption 4.** The type of analysis here sought is a relative assessment of parameters measured under different hull and propeller roughness. In this perspective, the absolute accuracy of the measurements assumes a secondary importance compared to their relative consistency over time (ISO, 2016).

The study of $\phi$, $w_\phi$ and $Q_\phi$ by means of full-scale ship performance monitoring and analysis is the subject of this work. Some important aspects need however to be addressed prior to setting the aims and objectives.

***Dealing with*** $R_{add}$***.***—From a data analysis perspective, $R_{add}$ is fundamentally a noise in the reference $V_s$–$R_{T0}$ relationship that hinders the derivation of $\phi$. As it will be mentioned in Chapter 2, nowadays there are several types of SPMS analysis principles, of which the most important are the *deterministic* and the *data-driven*. Deterministic ship performance monitoring and analysis systems substantially employ two methods to minimise the impact of $R_{add}$, namely data filtering and data correction. Data correction procedures attempt to eliminate $R_{add}$ by correcting the measured data to ideal conditions from the available information of the encountered environmental and operational conditions. This process is also called *normalization*. Filtering techniques instead attempt to minimise $R_{add}$ by discarding all measurements conducted with environmental and operational conditions outside pre-defined ranges (i.e. too 'far' from the ideal conditions). This includes conditions that cannot or should not be corrected for. Data filtering is carried out prior to the normalization stage during the data preparation.

Whereas it is possible in principle to use only one of the two methods, it is customary to use a blend of filters and corrections, in the same fashion of sea trials analysis (ITTC, 2014*a*). Regardless, the weaknesses of both methods ought to be known. Excessive data filtering drastically diminishes the quantity of useful data, weakening the statistics derived in performance analysis. Excessive correction, on the other hand, may lead to an increase in the data noise if corrections are carelessly applied or if they are simply not accurate.

Therefore, the wise selection of filtering thresholds and the application of resistance corrections is ultimately beneficial only if they both contribute to handling the noise without jeopardising any subsequent analysis.

***Raw data collection and handling.***—The above consideration must be ultimately instrumental in the choice of the measurement system characteristics and of the raw data handling method. A state-of-art measurement system needs to be installed on-board not only to measure the fundamental variables presented by eq. (1.1), but also to retrieve information useful to reversely calculate $R_{add}$. The system will thus measure fundamental or *primary* variables as $V_s$, $n$ and $Q_S$, but also additional *secondary* variables of the like of wind speed and direction, wave height, ship draught, etc. The secondary measurements should be then chosen based on the capabilities of the employed normalization methodology.

On the other hand, the raw measurements often present outliers and some filtering needs to be carried out prior to the data analysis itself, for example in the detection of steady-state periods. As a consequence, suitable raw data handling techniques need to be devised to prepare the data for the normalization and performance analysis. The ensemble of these techniques is here termed data *preparation*. Whilst this is a fundamental step in ship performance analysis, not always is carried out properly nor it has been deeply investigated in the past literature.

***Uncertainty of the performance analysis.***—Every SPMS retains the characteristics of a common experimental setup, whereby a measurement and a mathematical model are employed to yield a result. As such, the quality of the whole process needs to be verified in a scientific manner by assessing the 'goodness' of all the information used and, ultimately, of the result. Failure in doing so, renders any result the less meaningful the greater is targeted resolution of the experiment. In other words, the smallest is the change in performance to be quantified, the strongest the need and responsibility to assess how certain our estimation is. Yet, it appears that despite the large number of SPMSs currently in commerce, seldom is such estimation clearly stated and only very few studies have been conducted to modern scientific standards to evaluate the uncertainty and data quality of SPMSs.

## 1.4 Aims and objectives

Based on the above stated complimentary aspects of ship performance monitoring, the aims of the present study are described as follows:

**Aim 1.** To devise a deterministic performance analysis method dedicated to the measurement of the effect of biofouling growth on hull and propeller and to the selection of a suitable fouling control coating system in retrospective.

**Aim 2.** To develop a physical, working, on-line SPMS with the capability of carrying out automatic continuous monitoring of the vessel hydrodynamic performance and of the relevant secondary parameters.

**Aim 3.** To assess the uncertainty related to the performance estimation, eventually allowing modification of the system to target higher levels of accuracy.

In achieving these aims, the following objectives are set:

**Objective A.** To review the past and existing ship performance monitoring solutions in order to justify the present study.

**Objective B.** To employ a transparent physics-based deterministic approach, which is built for ship performance monitoring but can be easily extended to multi-purpose applications.

**Objective C.** To carry out a detailed investigation on all the data treatment stages (i.e. collection, preparation, normalization and performance analysis) in order to clarify and generalise some aspects of performance monitoring that are often assumed implicitly or are devised for ship-specific applications.

**Objective D.** To develop suitable Key Performance Indicators for the estimation of the biofouling effect.

**Objective E.** To employ Newcastle University's R/V *Princess Royal* as a development and testing platform of the proposed SPMS and performance analysis method. Using a proprietary vessel which operates closer to the campus allows a greater flexibility and easier control over its operation.

**Objective F.** To conduct any experimental and/or numerical campaign necessary to reversely calculate $R_{add}$ from the measured secondary parameters with a pragmatic perspective on the employed resources. The experimental facilities of Newcastle University used for this research part include the cavitation tunnel, the towing tank and a wind tunnel.

**Objective G.** To conduct dedicated full-scale sea trials to test the SPMS and the proposed analysis.

**Objective H.** To carry out a detailed uncertainty analysis of the ship performance estimation with the methods proposed by the relevant international standards.

In accordance with the above, the SPMS proposed in this research will have the general structure shown in Fig. 1.2.

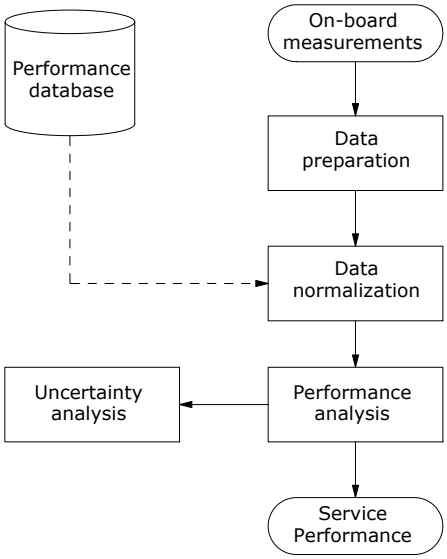


**Figure 1.2** – *Simple schematic of the proposed SPMS.*

## 1.5 Scope of the work

Despite the renewed attention and the well established use of SPMSs, the research in this field is far from being exhausted. The current and past literature calls for further study on the drag penalties of slime films in particular (Townsin, 2003). Several drivers exist for new research in this field, which may be identified as follows:

1. The complexity of the ship's operating conditions and the lack of hitherto ultimate, analytical solutions to several of the problems they imply.

2. The development of commercially owned SPMS that often lack transparency or independence from the service beneficiaries.

3. The rapid advancements of computer and sensors technologies, which permit superior data management in quantity, quality and analysis.

The SPMS developed with this research has been fitted to a small fast craft, proving to be one of the few applications of a SPMS on small-size vessels. However, it was devised to be easily commercialized and applied to vessels of any size.

This work not only addresses the need to assess the effect of biofouling build-up on hull and propeller or the effectiveness of a fouling control coating application. It also provides a system capable of general energy saving assessment, voyage planning, condition monitoring and retrofit evaluation. For instance, the first installation of New Profile Technology (NPT) propellers (Stone Marine Propulsion) on a fast vessel has benefited from *The Princess Royal*'s monitoring equipment as advanced full-scale assessment of their superior performance. The SPMS has also provided critical support for studies on marine anti-fouling and FR coatings. In this respect, collaborating with external marine coating companies has been complimentary to the project. Two dry-dockings have been used to replace the existing coating with newer and more performing ones, tested in the subsequent IDI period. One of these coatings was tested in the framework of the EU project SeaFRONT (Carchen, 2017).

## 1.6 Thesis layout

The above reviewed research is presented in this thesis according to the following structure.

Following this introductory Chapter 1 of the thesis, Chapter 2 provides an overlook at background naval architecture theory and describes the phenomena that affect ship performance in general terms. The effect of fouling is described in detail to facilitate the identification of suitable means to evaluate it in the course of research.

In fulfilment of **Objective A**, Chapter 3 provides a detailed literature review of the relevant studies concerning ship performance monitoring. The Author attempts here

to outline the knowledge gaps at the time of writing and justifying the novelty of this research.

According to **Aim 1** and **Objective B** and **C**, Chapter 4 provides the reader with a comprehensive and detailed description of the methodology from a theoretical point of view. The chapter begins with a presentation of the capabilities of the deterministic SPMS to deduct the different effects of external factors from ship performance. These are regarded as the basic principles for designing the system. Next, the SPMS is described following the flow of data within the system. At first, the data collection is tackled, with a description of the sensors that may be used to acquire useful performance data. Then, a method is proposed to prepare the raw data for further analysis, including Steady State Identification, outlier handling, conditional filtering and measurement validation. The deterministic procedure to deduct the effects of disturbances, based on the renowned Taniguchi–Tamura method, is then described. Finally, a novel long-term performance analysis is presented with a detailed description of four KPIs conceived to provide clear estimations of the effect of biofouling on ship hydrodynamic performance (**Objective D**).

In achieving **Objective E**, Chapter 5 describes in detail how the methodology laid out earlier in Chapter 4 is applied to the case study vessel — Newcastle University's R/V *The Princess Royal*. The same layout of Chapter 4 is used, whereby the data flow through the SPMS is followed and presented in relation to their real-case application. According to **Objective F**, the experimental and numerical campaigns that were used to calculate the added resistance components on the R/V are presented. The results of the full-scale implementation of the SPMS are shown and embody the validation of the proposed ship performance analysis methodology (**Objective G**).

In Chapter 6, the uncertainty of the ship performance analysis proposed in this research is evaluated and discussed by means of a comprehensive and first-seen Uncertainty Analysis on the real measurements carried out on-board *The Princess Royal* (**Objective H**). Monte Carlo methods are employed together with the law of propagation of the uncertainty to estimate the impact of elemental uncertainties (e.g. sensor precision, measurement variability etc.) on the primary variables (i.e. speed an power) and on the KPIs.

Finally, general conclusions and recommendations for future work are provided in the final conclusive Chapter 7.

## 1.7 Summary

This chapter has provided initially an overview to the subject of ship performance monitoring in relation to biofouling. The aims, objectives and scope of the current research were thereafter laid out. Four main assumptions were introduced concerning the applicability of the superposition principle to the expression of ship resistance, wake fraction

and propeller torque and the relevance of conducting a relative assessment. The founding aspects of the SPMS structure were then discussed. These covered the concepts of data *collection*, *preparation* and *normalization* and the need for a scientific uncertainty assessment of the performance analysis results. At last, the layout of the thesis was presented.

# CHAPTER 2

# Ship Performance and Biofouling

## 2.1 Introduction

In this Chapter, a general background of the definitions and of the topics treated in this work is given to contextualise the problem of interest and outline the research direction. The background information will aid to support the Author's motivation as well as the aims and objectives of this research which were described in 1. Most of the concepts here presented will be known to those familiar with the discipline of Naval Architecture, but have nonetheless been included for the sake of completeness.

Therefore, Section 2.2 presents the basic principles of ship propulsive and hydrodynamic performance considering the basic relations and the influence of the interaction between the ship and several circumstances encountered during its in-service life. Section 2.3 introduces to the reader the biofouling problem with some of its main characteristics and most used methods for its prevention. Finally, Section 2.4 discusses the effects of biofouling on ship performance and examines the available methods for their estimation giving a brief review of the relevant state-of-art.

## 2.2 Principles of Ship Performance

### *2.2.1 Basic relations*

When a ship sails in steady motion in calm deep waters and calm weather, resistance forces are exerted on it by the water and by the air through which the upper hull and superstructure moves across. The calm water resistance is traditionally considered formed of several components that can be subdivided as shown in Fig. 2.1 by Carlton (2012). Though each of these components interacts to some degree with the others, external factors may have a stronger influence on some of them only. It is the case for example of hull surface roughness, which mainly affects the viscous resistance. To reflect this, in the present study the most suitable representation of ship calm water resistance would therefore be that firstly introduced by Hughes (1954). This approach separates the viscous-related forces,

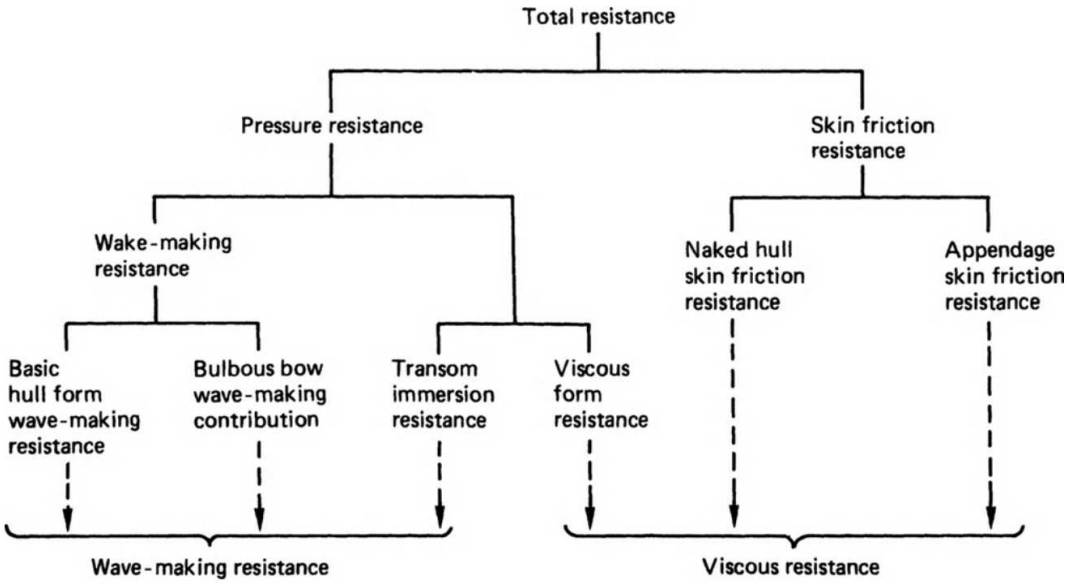


**Figure 2.1** – *Components of ship resistance [Source: Carlton (2012)].*

tangential to the hull surface, from the potential forces, normal to the hull surface:

$$R_{T0} = R_v + R_w \tag{2.1}$$

Where $R_{T0}$ is the resistance of the ship in calm water, $R_v$ the viscous resistance and $R_w$ the wave making resistance. Note that in this representation, the air resistance is incorporated into the pressure-related forces, $R_w$. In nondimensional terms:

$$C_{T0} = C_v + C_w \tag{2.2}$$

The generic nondimensional resistance coefficient is found by dividing the dimensional resistance by the dynamic head $0.5\rho V_s^2$ and the wetted surface area $S$, where $\rho$ is the water density and $V_s$ the ship speed through the water.

At the hull surface, the no-slip condition implies a velocity of the water flow equal to the hull velocity. Moving away from the hull, the flow velocity will approach the free stream velocity in a transitional region called boundary layer (Fig. 2.2). The changes in flow velocities within the boundary layer are responsible for the generation of a shear stress on the boundary wall that is proportional to the velocity gradient and the viscosity of the fluid (Larsson and Raven, 2010). The viscous resistance defined in eq. (2.1) and (2.2) encompasses both the tangential skin friction drag, main responsible for the thickness of the boundary layer along the hull's length, and the eddy making resistance, which is responsible for the three dimensional effects of the viscous resistance (wake) — what is termed viscous pressure drag. The viscous resistance coefficient can be thus described as:

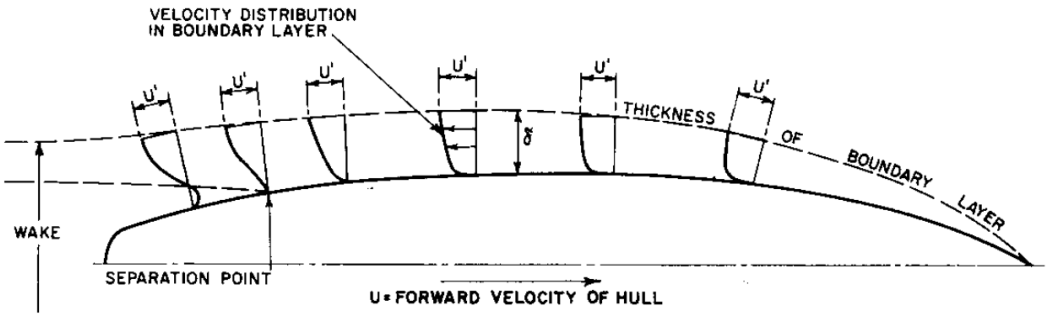


**Figure 2.2** – *Flow around the turbulent friction belt of a ship's hull [Source: Lewis (1988)].*

$$C_v = (1 + k)C_f \tag{2.3}$$

Where $k$ is the form factor, which relates the viscous pressure drag to the ship's form, and $C_f$ is the skin friction drag coefficient. Figure 2.3 shows the components of the ship calm water resistance, namely $C_f$, $k\,C_f$ and $C_w$, as fractions of the total. Values are plotted against the Froude number $Fn = L_{oa}/\sqrt{V_s\, g}$, where $L_{oa}$ is the overall ship length, $V_s$ is the speed through the water and $g$ is the gravitational acceleration. Note the larger impact of the frictional drag on the slower tanker and, conversely, the strong effect of wave making resistance on the fast catamaran, particularly at the transient $Fn$.

In principle, a speed–resistance relation would be sufficient to describe the performance of a vessel under steady motion and calm weather. However, since the ship's resistance is not directly measurable, the propulsive power stands as its closest proxy. For a ship moved by a conventional underwater screw propeller, the total calm water resistance $R_{T0}$ is related to the propulsive system by the known relations shown in Fig. 2.4. The following are here defined:

$w$: Effective wake fraction, which defines the loss of velocity inflow at the propeller plane with respect to the ship speed (eq. (2.6) below). It largely depends on viscous phenomena, but also on potential and ship wave effects.

$t$: Thrust deduction factor, which defines the effect of the propeller suction on the resistance increase or, traditionally, the effect of the presence of the hull on the loss of propeller thrust. It mostly depends on potential properties (Harvald, 1983).

$T$: Propeller thrust in relation with the total resistance according to:

$$R_{T0} = (1 - t)T \tag{2.4}$$

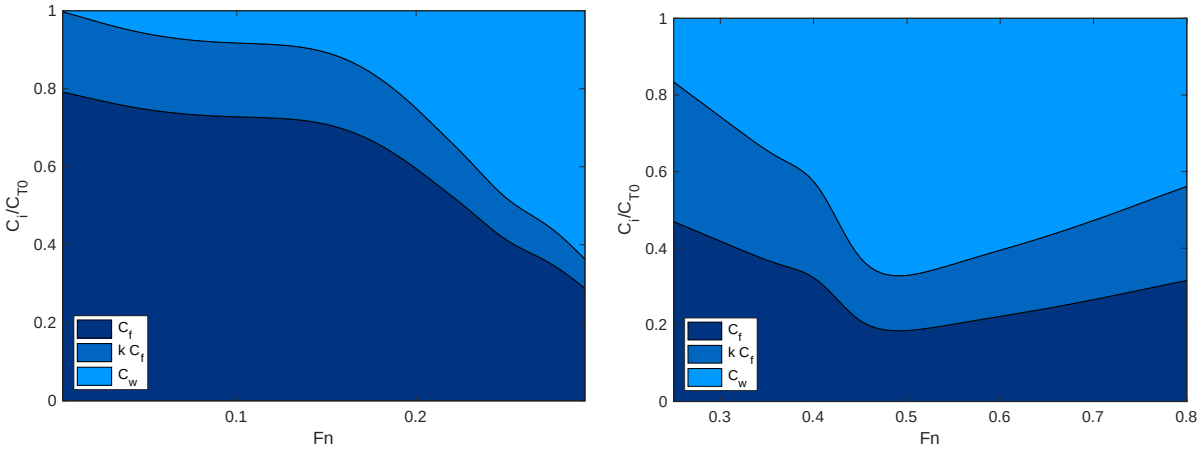


**Figure 2.3** – *Friction, viscous pressure and wave making components of the calm water resistance presented against Fn as fraction of the total resistance for:* (a) *a 12,000 DWT tanker;* (b) *a fast catamaran.*

$V_s$: Ship speed through the water, which can be also described by its forward and athwart components as:

$$V_s = \sqrt{u_s^2 + v_s^2} \tag{2.5}$$

$V_a$: Speed of advance or speed of the propeller inflow defined by:

$$V_a = (1 - w)V_s \tag{2.6}$$

$P_E$: Effective power or power needed to overcome the calm water resistance at speed $V_s$, defined as:

$$P_E = R_{T0}V_s \tag{2.7}$$

$P_B$: Brake power developed by the engine and measured at the engine's flywheel, defined as:

$$P_B = 2\pi n_e Q_B \tag{2.8}$$

Where $n_e$ is the engine's revolutions per second and $Q_B$ the engine brake torque.

$P_S$: Shaft power, measured on the shaft and after all machinery.

$$P_S = 2\pi n Q_S \tag{2.9}$$

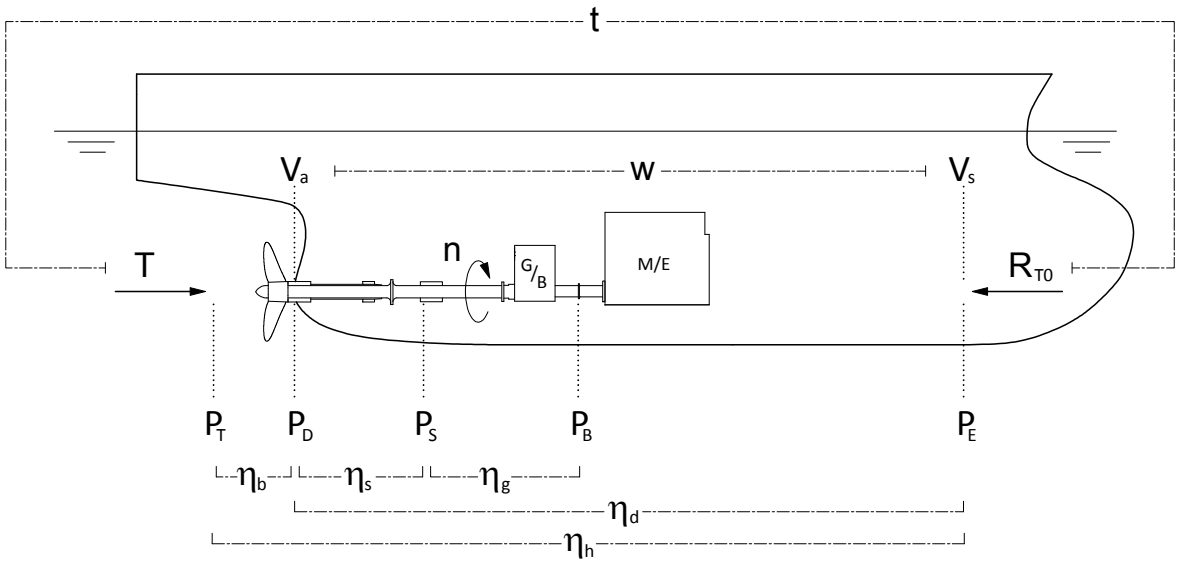


**Figure 2.4** – *Generic ship powering definitions, after Atlar (2013).*

where $n$ is the shaft (i.e. propeller) revolutions per second and $Q_S$ is the shaft torque measured in proximity of the stern gland.

$P_D$: Delivered power to the propeller taken outside the hull ideally between the stern gland and the propeller disc, defined as:

$$P_D = 2\pi n Q \tag{2.10}$$

Where $Q$ the torque absorbed by the propeller behind the hull.

$P_T$: Thrust power developed by the propeller thrust in a flow with speed of advance $V_a$, defined as:

$$P_T = TV_a \tag{2.11}$$

$\eta_b$: Propeller efficiency behind the hull, defined as $\eta_b = \eta_o \eta_r$, where:

$\eta_o$ is the propeller open water efficiency defined as:

$$\eta_o = \frac{TV_a}{2\pi n Q_o} \tag{2.12}$$

$\eta_r$ is the relative rotative efficiency defined as:

$$\eta_r = \frac{Q_o}{Q} \tag{2.13}$$

where $Q_o$ is the torque absorbed by the propeller operating in open water condition.

$\eta_g$: Gearing efficiency (if fitted).

$\eta_s$: Stern gland efficiency, defined as:

$$\eta_s = \frac{Q}{Q_S} \tag{2.14}$$

$\eta_d$: Propulsive efficiency, or Quasi Propulsive Coefficient (QPC).

$\eta_h$: Hull efficiency, defined as:

$$\frac{1-t}{1-w} \tag{2.15}$$

In accordance with Fig. 2.4, the following relations hold:

$$P_T = P_S \eta_o \eta_r \eta_s \tag{2.16a}$$

$$P_E = P_T \eta_h \tag{2.16b}$$

$$P_E = P_S \eta_o \eta_r \eta_s \eta_h \tag{2.16c}$$

In virtue of eq. (2.16) above, the calm water performance can thus be described by the steady-state equations:

$$P_S = \frac{TV_s}{\eta_o \eta_r \eta_s}(1-w) \tag{2.17a}$$

$$T = \frac{R_{T0}}{1-t} \tag{2.17b}$$

The propeller open water characteristics are in the present work expressed in the common non-dimensional form as follows. Let $D$ be the propeller diameter, we define:

$$\text{Thrust coefficient} \quad K_T = \frac{T}{\rho n^2 D^4} \tag{2.18a}$$

$$\text{Torque coefficient} \quad K_Q = \frac{Q_o}{\rho n^2 D^5} \tag{2.18b}$$

$$\text{Advance coefficient} \quad J = \frac{V_a}{nD} \tag{2.18c}$$

The steady-state ship performance in calm weather described thus far is however seldom encountered in real navigation. The environment a vessel sails in and the conditions in which the vessel is operated all contribute to alter the relation described by eq. (2.17). These disturbances usually affect both the vessel resistance and the interaction between propulsor and hull causing what are known as *involuntary performance losses*. The following sections describe the characteristics of the factors that affect the performance of ships. Their effect of ship performance will be considered in more detail in Chapter 4.

### 2.2.2 Disturbances due to the environment

**Air mechanics**

***Wind.***—When a wind blows, an extra force is exerted on the upper hull and superstructure of the ship. This force depends upon the characteristics of the wind and of the part of the ship exposed to its action, and its effect on a ship is generally twofold:

1. Speed loss, or direct wind resistance;

2. Indirect resistance due to drift, yaw and steer motions induced to keep the course.

The wind action is however of an evident fluctuating nature. Wind speed and direction easily exhibit variations temporally and geographically. At the same location, the wind might vary with frequencies of days or even display turbulences in the scale of seconds (see Fig. 2.5). The frequencies of interest to ship performance monitoring are to be found in the high ranges.

Wind turbulence is a phenomenon happening at high frequencies, usually in the order of minutes, or even less (see the right-most peak in Fig. 2.5). Because of its complex nature, turbulence is normally expressed in statistical terms as the the standard deviation $\sigma_u$ of the wind speed $U_A$, assumed normally distributed around the mean value $\overline{U}_A$. It is observed that at relatively low heights above the ground, $0.13\overline{U}_A < \sigma_u < 0.25\overline{U}_A$, meaning that the speed fluctuations are of significantly smaller entity compared with the free stream velocity (Burton *et al.*, 2011). It is therefore useful for the purposes of our research to simply express the wind velocity components as an average over a reasonable amount of time (Hasselaar, 2011; ITTC, 2014*a*).

Two effects are the main drivers of turbulence — the aforementioned thermal effects and the friction forces with the Earth's ground. It quite naturally follows that turbulence is predominant in that lower thin band of the atmosphere called the Ekman layer, whose thickness varies with latitude reaching a maximum of a few hundred meters (Stewart, 2008).

For practical purposes, the wind velocity profile within this layer is often approximated by a power law of the kind:

$$\overline{U}_A \propto z^{\alpha} \tag{2.19}$$

where $z$ is the vertical height above the ground. In open seas, the standard developed by the IEC (2005) recommends $\alpha$ ranging from 0.14 for normal to 0.11 for extreme wind conditions. The ITTC (2014*a*) instead recommends a fixed value of 1/7.

***Air properties.***—Changes in air density have a direct relationship with the force caused by the air or by the wind's action. In contrast to wind speed and direction, local density variations are slower as they are often a consequence of direct solar radiation and the passage of weather systems.

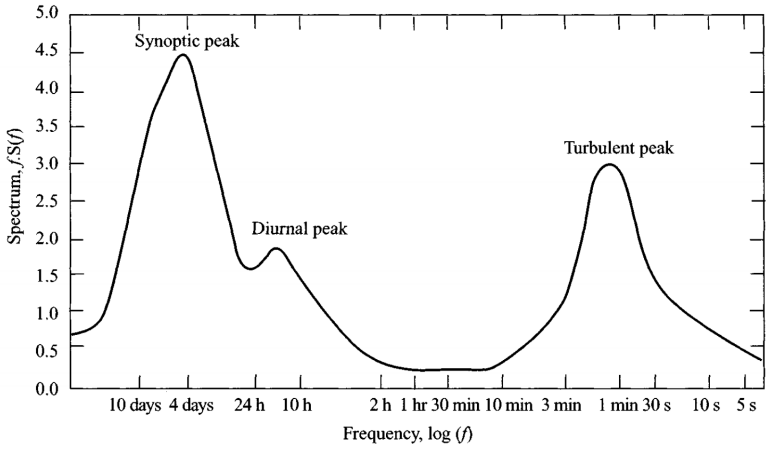


**Figure 2.5** – *Wind speed spectrum as recorded at the Brookhaven National Laboratory. The abscissa is a log-scale of frequency, whilst the spectral ordinate is proportional to the wind energy contained at that frequency [Source: Burton* et al. *(2011), after Van der Hoven (1957)].*

Geographical variations in air density are however larger than temporal variations over the same location. Hasselaar (2011) reckoned that variations of 25% in air density are not uncommon between the north Atlantic dry, cold areas and Tropical locations boasting a hot, humid weather. In these areas, the air properties remain fairly constant over the whole year. Conversely, the mid-latitudes are subjected to more seasonal and daily variability depending on the moving weather systems.

### Water mechanics

***Waves.***—When a ships sails in a seaway, the action of waves induces on it hydrodynamic forces of several orders. First-order forces are generally larger and are assumed linear with the wave height. Second-order forces depend on non-linear hydrodynamic phenomena and are assumed proportional to the square of the wave height. First-order forces induce the ship's oscillatory motions, whilst the second-order forces are responsible for the added wave resistance as well as the slowly varying ship motions. Broadly speaking, the action of waves has two main effects on ship performance, namely:

1. Increase of the ship resistance, chiefly related to potential (i.e. non-viscous) effects.

2. Alteration of the propeller inflow and of the hull-propeller interaction (both wake and thrust deduction fraction) as a consequence.

Most of the sea states commonly found at sea comprise a combination of wind and swell waves. Swell waves have generally a more regular aspect than wind waves and they are unrelated to the local wind speed and direction. Confused seas therefore arise when the

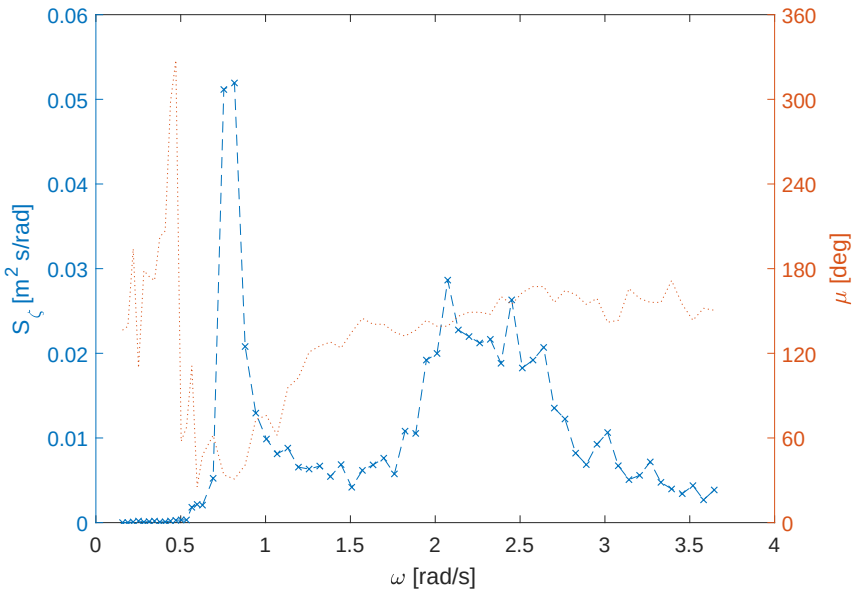


**Figure 2.6** – *An irregular wave spectrum measured off the North East coast of England by the Channel Coast Observatory. The two energy peaks of swell at the lower frequencies and wind waves at the higher frequencies can be observed, respectively bearing 40*deg *and 150*deg *[Data source: CCO (2017)].*

two merging wave systems have comparable height but different directions. The type of waves thus generated are called short crested and, depending on several circumstances, will show the tendency to spread to some degree around a mean direction.

The sea state can be represented by the superposition of an infinite number of regular sine wave components according to the principles of spectral analysis. However, the open sea environment rarely creates the unidirectional so-called long crested waves. Therefore the relative 'strength' of wave components bearing different directions is best expressed by the directional wave energy spectrum, whose spectral ordinate is proportional to the total (i.e. kinetic and potential) energy per square meter contained at every wave frequency band for any direction interval, viz.:

$$S_\zeta(\omega, \mu) = \frac{\zeta^2}{2\delta\omega\delta\mu} \tag{2.20}$$

where $S_\zeta$ is the spectral ordinate, $\zeta$ the wave amplitude, $\omega$ the wave frequency and $\mu$ the wave direction. Often, double peaked spectra are observed of the kind plotted in Fig. 2.6. Here, a directional wave spectrum is plotted from data recorded by the Channel Coast Observatory off the North East coast of England. The left-hand side y-axis shows the spectral ordinate whereas the right-hand side one shows the mean wave direction $\mu$. The swell and wind waves can be seen clearly bearing different mean directions at different frequencies.

Should the directional wave spectrum be known, the wave height can be reversely

calculated from eq. (2.20) as:

$$\zeta = \sqrt{2S_\zeta(\omega, \mu)\delta\omega\delta\mu} \tag{2.21}$$

For practical purposes, several one-directional idealised wave energy spectra have been developed over the years to represent actual wave spectra of open seas and coastal locations using only an exiguous number of parameters. They can be thereafter combined with ideal directional spreading functions to generate a more realistic directional wave energy spectrum. The three idealised spectra mostly employed in seakeeping analysis are the Pierson–Moskowitz, Bretschneider and JONSWAP spectra.

Directional spreading functions mostly use $\cos^m$ operators, with $m = 2$ being the most used (Lloyd, 1989). Obviously, as these functions provide a single peak wave energy spectrum with respect to both frequency and direction, the superposition of multiple idealised spectra is often a due choice.

Nevertheless, since they are designed to fit a wide range of real sea conditions, all idealised wave spectra mostly exhibit large inaccuracies in their predictions. Direct measurements or hind-casting stands therefore as the best means of obtaining the actual wave energy spectrum for performance monitoring purposes (Hasselaar, 2011).

***Currents.***—Besides the movements caused by waves, ocean waters are subjected to a large variety of currents, whose speeds vary from fraction of knots to even 5-7 knots at some particular locations and time of the year (Kent, 1959). Currents act as existing incident water flows on ships and have different effects on them depending on their relative directions. In case the ship sails with or against the current, the effect on the ship will mostly be limited to a difference between her speed through the water and over the ground. In other cases, a current may more severely distort the flow field around the hull and propeller inducing changes in the vessel attitude (e.g. drift and yaw motions), loss of propeller efficiency and additional resistance.

The two principal causes of ocean currents are tides and thermal phenomena similar to those driving atmospheric winds. The interaction of these currents with the surrounding environment (e.g. winds and bathymetry) adds complexity to this phenomenon. As a consequence, ocean currents are often depth dependent. Figure 2.7 shows the variation of the current in knots at the entrance of Miami Harbor over a depth of 12m and 20 hours of time. As already stressed by Hasselaar (2011) and the recent work conducted by MARIN (van den Boom and Hasselaar, 2014), this phenomenon affects particularly large ships whose draughts span a depth significant for these velocity variations. Estimating the correct speed through the water experienced by the ship's hull, on average, becomes thus a challenge.

***Restricted waters.***—Limited water depths or channel widths affect quite severely both the resistance and the propulsive characteristics of a ship by altering the potential

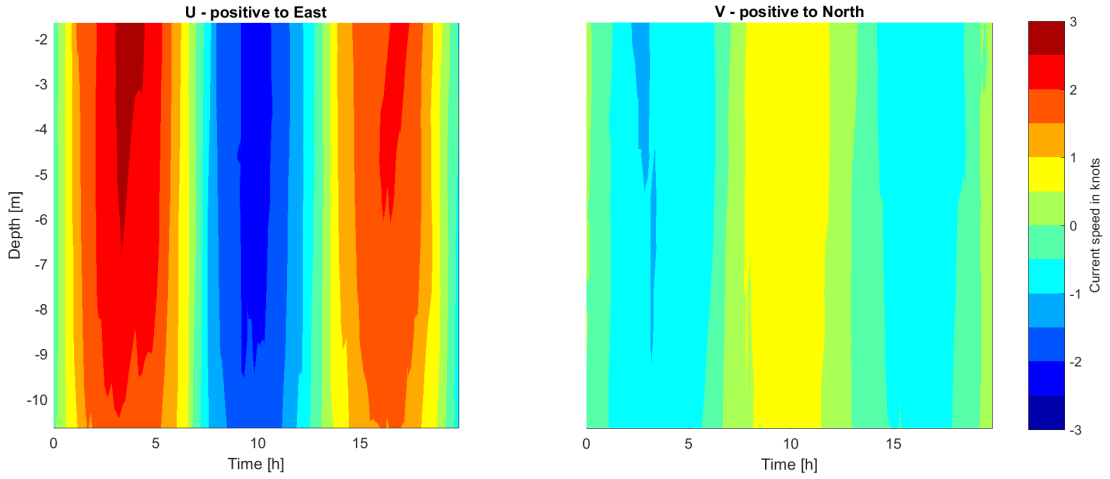


**Figure 2.7** – *Current at the entrance of Miami Harbor, in knots, recorded by NOAA buoy MIH0901 over a period of 20h during the 2008 current survey [Data source: NOAA (2009)].*

flow field around the hull and even the viscous-related forces. Because of the scope of the present work, we shall however focus on shallow waters only.

The first evident effect of a reduced amount of water under the hull is the increase of the wave height and the change in the wave pattern (Larsson and Raven, 2010). The second is a Venturi-like effect originating by the relative vicinity of the ship's keel with the sea bottom, which acts effectively as a reduction of the inflow cross-sectional area. This results in an increased water speed and the consequent pressure drop under the hull, which is balanced by an increase in the ship's draught ('sinkage'). According to the classic work of Lackenby (1963), the combination of these two effects can lead, for example, to speed losses in excess of 10% when the ratio between midship sectional area to water depth is higher than 0.05 at a speed of 15 kn.

Shallow waters significantly alter also the propeller wake and the thrust deduction factor due to the different pressure field around the hull.

***Water properties.***—Two water properties chiefly contribute to affect the ship's performance, namely the water density and the water viscosity.

Changes in water density are related to the same thermal phenomena earlier described for currents. The pressure gradients that drive thermal ocean currents are actually caused by the different water densities resulting from the uneven heating of the water surface (Stewart, 2008). However, since the maximum density variations encountered ocean-wide are less than 7% (Fofonoff and Millard Jr., 1983), they can be easily demonstrated to have very small incidence on ship performance (e.g. Hasselaar, 2011).

In contrast, viscosity normally exhibits larger variations between tropical and polar

waters. Changes in viscosity have thus a more significant impact on the bare hull viscous drag and on the propeller efficiency.

**Biofouling**

The definition of biofouling and its effects on performance will be discussed in detail in Section 2.3.

### *2.2.3 Disturbances due to the ship*

**Structural**

***Roughness.***—In the broader context, roughness defines the difference between the theoretical and the true surface of the underwater hull. An often used measure of small-scale roughness is the Average Hull Roughness ($AHR$), which is a weighted average of the mean local roughness measurements at different hull locations, in $\mu$m. Prochaska (1977) distinguished two roughness components, namely:

A. Permanent roughness

B. Removable roughness

Item (A) refers chiefly to macro-scale structural imperfections like weld beads and plate waviness, but also to smaller-scale roughening of the hull and propeller caused by the natural decay of the surfaces with ageing. This latter group includes corrosion, build-up of old paint and poor paint application standards — the last two items up to a certain extent. Whereas these processes can somehow be reduced by e.g. frequent grit-blasting, it is impossible to stop them or repair completely the damaged surface, resulting in a slow, progressive worsening of the performance throughout the life of the ship (Fig. 2.8).

Item (B) refers to those changes in hull and propeller local surface topography that can be considered temporary and can be completely removed by a suitable treatment. These include the roughening by effect of fouling accumulation (see Section 2.3), paint porosity, paint deterioration, damage (e.g. grounding, ice, anchor etc.) and poor paint application (e.g. cold flow phenomena, detachments, poor pre-cleaning etc.).

It is worth mentioning that (A) has often some effects on (B), in that a hull surface that is in itself rough accelerates several of the processes that lead to accumulation of removable roughness. For instance, several biofouling species are 'thigmotoxic', i.e. they prefer rough surfaces for settlement.

Whereas the performance effects of roughness are within the scope of the present research, the focus is on the quantification of the effects of the removable roughness and particularly of fouling. Nonetheless, the effects of the permanent roughness can be observed on the longer term.

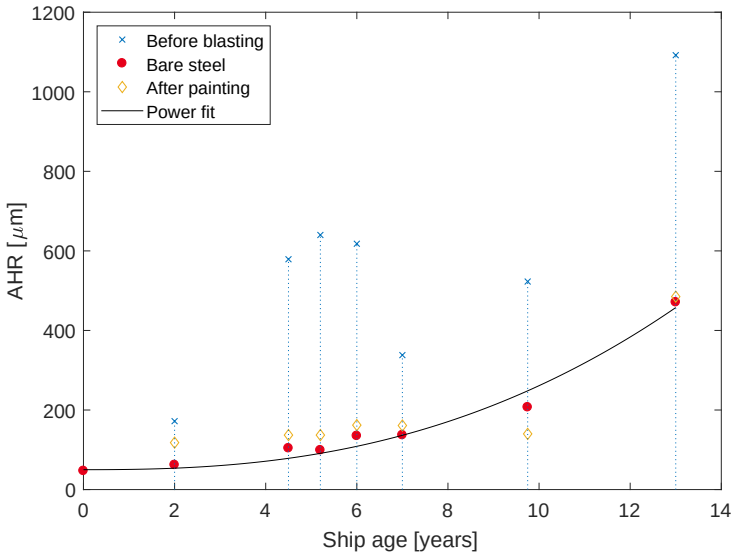


**Figure 2.8** – *AHR of old coating, bare steel and new coating application plotted against the ship's age in years since launch as obtained from dry-docking measurements and excluding shot blasting, after BSRA (1981).*

***Damage.***—Hull and particularly propeller damage may severely alter the overall performance of a ship. Even minimal bending of the propeller blades can result in a severe alteration of the propeller open water performance. For instance, the relatively small damage shown in Fig. 2.9 — with a maximum blade deformation of 5mm — caused an estimated change in propeller efficiency of 16% (Sasaki and Carchen, 2015). Whereas the proposed methodology is capable of detecting the effects of the sudden change in performance due to hull and/or propeller damage, it is assumed that no such damage occurs and therefore its effects will be herein ignored.

### Mechanical

***Engine.***—As the input energy on ships is essentially marine fuel, it is quite clear that the engine efficiency has an impact on the overall ship performance. Hasselaar (2011) reports a few studies on the topic and summarises the causes of changes in engine performance in air temperature, humidity, cooling water temperature, fuel quality, engine loading point and ageing of the engine components. He concludes that in order to assess with a certain degree of accuracy the efficiency of the engine, most of the above parameters must be measured and their relative influence be accounted for. It naturally follows that the uncertainties related to evaluating the ship performance from such measures as the fuel consumption — i.e. from $P_B$, Fig. 2.4 — are significantly high, as also reported by the recent ISO (2016) guidelines.

***Shafting.***—Albeit to a much smaller extent, the shafting arrangement can contribute to changes over time in propulsive performance. The factors playing a role in this are:

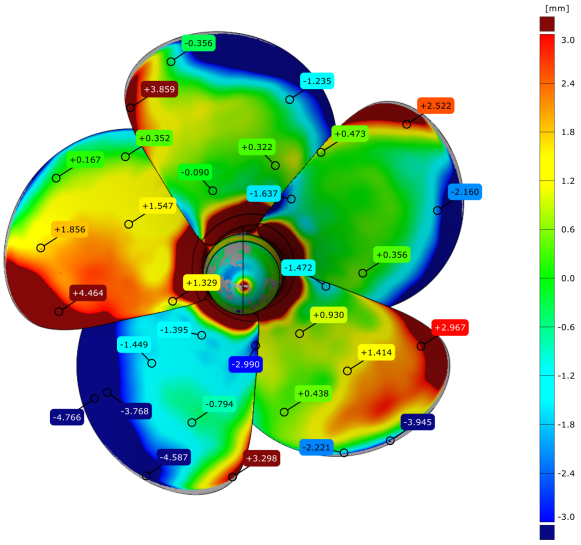


**Figure 2.9** – *Propeller deformation on a fast catamaran obtained by 3D laser scanning. Measures are reported in mm (positive numbers mark a displacement toward the reader). Note the twisting of the blades and the erosion at the blade tips (grey areas).*

shafting alignment; journal and thrust bearing lubrication; stern gland lubrication; and, if fitted, the overall gearing efficiency.

In past studies, the Author has acknowledged the significant importance of low shafting efficiency arising from prolonged lay-up periods (Carchen, 2015*b*). These in turn cause build-up of residual shaft stresses which must be dissipated prior to conducting any performance measurements (ITTC, 2014*c*).

In general, if enough lubrication is provided to the shafts and no alignment issues arise, shafting losses are normally very low — up to 6%, of which 5% is attributable to gearing. Moreover, they have a 'constant torque' character, meaning that their effect will decrease with increasing shaft speed and usually they stabilise to an almost constant value at cruising propeller speed.

The inconvenience of engine and shafting efficiencies appearing in the performance powering balance of eq. (2.17) is overcome by taking power measurements just forward of the stern tube and abaft the engine and gearing systems; in other words, by measuring $P_S$ instead of $P_B$ (Fig. 2.4). In this way, the only stern gland efficiency $\eta_s$ will need to be accounted for.

### Operational

***Displacement.***—An increase in displacement has mainly two effects, namely the increase of the wetted surface area and the change of the shape of the immersed hull, which on most ships results in a fuller shape. These two effects lead to an increase in the frictional drag and in the pressure-related forces respectively. Modern ships with bulbous

bows and partially submerged transom sterns are in this greatly disadvantaged by the dramatic changes of underwater hull shape between different draughts.

This is shown for example in the work of Krapp and Schmode (2017) as they simulate the speed-power curve of an LNG vessel at different draughts, finding power changes in excess of 5% over the normal operating range of displacements.

Changes in draught will also affect the wake fraction as a result, for instance, of the bluffer hull form at a higher draught.

Very shallow draughts may also lead to propeller emergence, with obvious direct impact on the propulsive efficiency. These conditions must be therefore avoided when monitoring the ship performance (Hasselaar, 2011).

***Trim.***—Trim affects the ship performance in a way at all similar to the above, though with larger effects for smaller changes. This in part due to the changing underwater shape, particularly in relation to the misalignment of the body with the flow streamlines, and the position of the centre of buoyancy.

All ships are naturally subjected to dynamic changes of attitude in navigation — the so-called sinkage and dynamic trim — to counterbalance the changing pressure field on the hull. Despite the impact that these have on the resistance on the ship, they are safely assumed constant for equal loading condition and speed (Larsson and Raven, 2010) and their effects are therefore implicit in the analysis explained in the following chapters.

***Manoeuvring.***—Any voluntary action taken to alter the ship's course or speed can be described as a manoeuvre. Any such action occurs with the appearance of one or more acceleration components that unbalance the steady-state powering of eq. (2.17). This is quite obvious for instance in the case of a straight line acceleration or deceleration, where eq. (2.17b) would become:

$$(1-t)T - R_{T0} = \rho\nabla(1+m_x)\frac{\mathrm{d}u_s}{\mathrm{d}\mathbb{t}} \tag{2.22}$$

where $\mathbb{t}$ is the time, $\nabla$ is the ship's volumetric displacement and $m_x$ is the nondimensional added mass in surge direction.

When the ship is changing its course, the rudder is given an angle, which produces a lift and a drag force. To counteract the rudder forces, the ship changes its sailing attitude by drifting and yawing. As a result of the strong hydrodynamic forces exerted on the hull and rudder, displacement ships tend to heel outboard with respect to the turning centre (i.e. starboard heel to port turn, Fig. 2.10), whilst planing crafts heel inboard. Rudder action and changes in attitude all produce additional resistance components. In addition, it quite naturally follows from the above that the wake will be altered to a certain degree. Figure 2.11 shows the records taken during a zig-zag manoeuvre of a fast vessel at constant RPM and rudder angle. Note the speed loss and the simultaneous torque increase during

**Figure 2.10** – *The aircraft carrier* USS Harry S. Truman *while performing a full-ahead turning cirle. Note the severe heel angle and the clear wake deviation [Source: Young (2012)].*

the manoeuvre. The increasing difference between Course Over Ground (COG) and ship heading are signals of the drifting motion to which the vessel is subjected.

The added resistance and changes in wake, that is, the effects of the above disturbances on ship powering will be discussed in detail in Chapter 4. However, it is clear that monitoring the ship performance during transient periods of the like of accelerations and strong manoeuvres must be avoided (see Hasselaar, 2011; ISO, 2016).

***Heel.***—During a manoeuvre or strong side winds, or owing to exceptional circumstances such an incorrect loading plan or damage, the ship may heel at an angle. When this happens, the shape of the underwater hull becomes asymmetrical and fuller in the same side of the heeling. As a consequence, the wave making resistance increases and the propeller wake is altered. Sometimes, viscous forces are also affected (Lewis, 1988). Excluding strong manoeuvring transients and the exceptional circumstances, it will be seen in Chapter 4 that the heel angles occurring in normal sailing are generally smaller and bearing weaker effects than other induced forces.

***Drift.***—A ship sailing in still water with a drift angle can be seen as a wing or fin in a flow at an angle of attack. The resulting added resistance in this circumstance is caused by the induced drag related to the inception of lift forces. Because of the blunt shape of most vessels, flow separation on the afterbody occurs quite rapidly at low drift angles (usually around 5 deg), dramatically increasing the induced resistance.

Regardless, drift resistance is normally well below 5% of $R_{T0}$ for drift angles smaller than 5 deg. Depending on the duration of the drifting motion and on the yaw rate of the vessel, the effect of drift can be however very large on the propeller wake (Inoue *et al.*, 1981).

Drift may be caused by manoeuvring, side winds, side currents and, to a lesser extent,

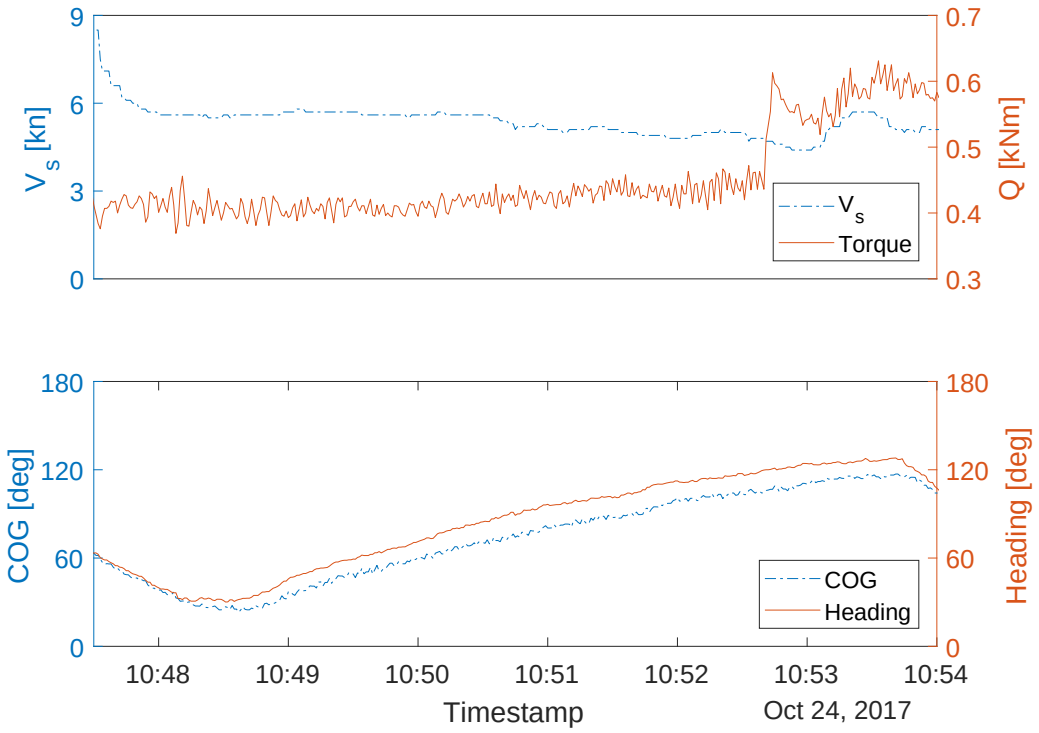


**Figure 2.11** – *Records during a zig-zag manoeuvre of a fast vessel at constant RPM.*

waves. When the drifting motion is caused by wind, wave and current forces, it is called leeway drift.

***Yaw.***—The change and the rate of change of heading are referred to as yaw and yaw rate respectively. The longitudinal component of the centripetal acceleration resulting from the ship's yawing is therefore the source of the induced resistance, which usually accounts for up to 1–2% of $R_{T0}$ in normal sailing conditions.

Apart from manoeuvring, yawing motions arise when encountering the side action of wind, waves and currents. To counteract the side forces thus generated, the helmsman is forced to the use of rudder to steer the ship to course. However, the natural variations of the external disturbances necessarily results in an oscillatory yaw motion. Incidentally, this phenomenon occurs to vessels with very poor course-keeping abilities even when sailing in calm weather.

As before, in most circumstances suitable for performance monitoring, yaw motions are very small and their effect on ship performance limited (Hasselaar, 2011).

## 2.3 Biofouling

### *2.3.1 Characterisation of biofouling*

The term 'biofouling' generally refers to the accumulation of animal and vegetal organisms on the ship's parts in contact with the water. The settlement process may be considered to progress in three stages, namely:

I. Slime formation or primary fouling;

II. Algal settlement or secondary fouling;

III. Animal fouling, including secondary and tertiary fouling.

Although more than 4000 fouling species have been identified, (Anderson and Hunter, 2000), the principal classes of constituent species and brief descriptions are reported in Table 2.1, loosely reproduced from Bengough and Shepheard (1943) and WHOI (1952). Animal fouling classes are grouped according to common features (e.g. hard shell) and presented in ascending order of structural complexity.

These three fouling stages may or may not be in temporal sequence, albeit stage (I) usually preludes the other two in that it appears to condition the surface and in some way favour the attachment of other species. In fact, slime is a thin layer or film of bacteria, diatoms (unicelluar plants) and microalgae that immediately starts growing on a surface immersed in water (Yeginbayeva, 2017). Its thickness ranges from a few microns to even 1mm in the case of 'heavy slime', and albeit rootless it is known to resist very high shear stresses (Townsin, 2003). It has been observed that the species forming slime and diatoms in particular adhere to a surface by producing a mucilaginous matrix of extracellular polymeric substances. This gel-like compound, despite not properly attracting other species, helps retaining spores, diatoms and small larvae of other species; may serve as food for larger fouling animals; dulls the brightness of the surfaces; and helps increasing the alkalinity in the proximity of the surface (Yebra *et al.*, 2004).

Should the environmental conditions be favourable, the algal spores and the animal larvae entrapped by the mucilaginous slime may then develop into algae and animal fouling. It is observed that on seagoing ships the most prominent algal species are the *Ectocarpus* and the *Enteromorpha*, respectively the most common brown and green weeds found on ships (Bengough and Shepheard, 1943; WHOI, 1952). Other species, particularly *Ulva* and *Cladophora*, may appear on relatively stationary vessels or in those areas of the ship's hull that are not subjected to strong shear stresses from water (e.g. dry transom of a fast ship).

Animal fouling incepts contemporaneously to algal settlement, but it is reckoned to cover much larger areas. In addition to this, the integument of animals with hard shells

TABLE 2.1
*Stages of biofouling progress on ships.*

| *Stage* | *Constituents* | *Description* |
|---|---|---|
| Slime formation | Bacterial slime | In a grey, green or brown mucilaginous slime |
| | Diatoms | |
| | Spores | |
| | Larvae | |
| | Silt | |
| | Ulothrix | Filamentous micro algae |
| Algal settlement | Ectocarpus | Brown algae |
| | Enteromorpha | Green filamentous algae |
| | Cladophora | Green reticulated algae |
| | Ulva | Green 'sea lettuce' |
| | Polysiphonia | Red reticulated algae |
| Animal fouling | Ciliates | Single-celled eukaryotes |
| | Porifera | Sponges |
| | Hydrozoans | Hydroids e.g. polyps |
| | Polychaetes | Sea worms e.g. tube-worms |
| | Cirripedes | Barnacles |
| | Bivalves | Mussels, oysters etc. |
| | Bryozoans | Moss-animals |
| | Tunicates | Sea-squirts |
| | Ascidians | |

contributes to make fouling species of the like of barnacles the most critical in the incrementation of a hull's surface roughness. Animal fouling has the advantage over algae to grow even in parts of the hulls not benefiting from direct sunlight, as the hull bottom or a sea chest. *Cirripedes* (e.g. barnacles) are among the first animal species of significant size to adhere to the hull surface, followed by *Polychaetes* (e.g. tube-worms), *Hydrozoans* (hydroids) and *Bryozoans* (e.g. moss animals). If let to cover a conspicuous area, these species will easily form a more favourable surface for other and more complex species to attach, for instance mussels and sea-squirts.

Figure 2.12 shows an example of fouling development on a small fast catamaran. A slime layer is the first to form after only a few months of sailing (a). To demonstrate its softness, it can be seen purposely 'scratched' with fingertips. An advanced settlement of algal species can be seen in (b): the more common *Enteromorpha* and *Cladophora* are complemented by some attachment of *Ulva* and even *Laminaria* (the large brown 'oarweed'), which is rather rare on slower ships. In (c), a common fouling state is shown that includes an underlying (mostly covered) slime film, some *Ulva*, acorn barnacles, a colony of tube-worms and diffused *Membranipora* (a genus of Bryozoans known as 'sea-mat') covering them. Finally, an advanced animal fouling state is pictured from a bow thruster tunnel in (d). Because of the limited amount of light and of the reduced water speed, several animal species can be seen to populate the enclosed space. Among them are acorn barnacles, tube-worms, sea-squirts, hydroids, moss animals and sea-mat.

### *2.3.2 Factors of influence in the biofouling growth*

The growth of fouling species on ships depends upon several factors, which are not easily taken into account should one wish to predict in how much time and what fouling species would settle on a hull. Bengough and Shepheard (1943) distinguish the following categories:

1. Port factors
    (a) Time in port
    (b) Water contamination
    (c) Salinity
    (d) Season and climate of mooring period and location
    (e) Light intensity
    (f) Geology of the port
2. Ship factors
    (a) Hull shape

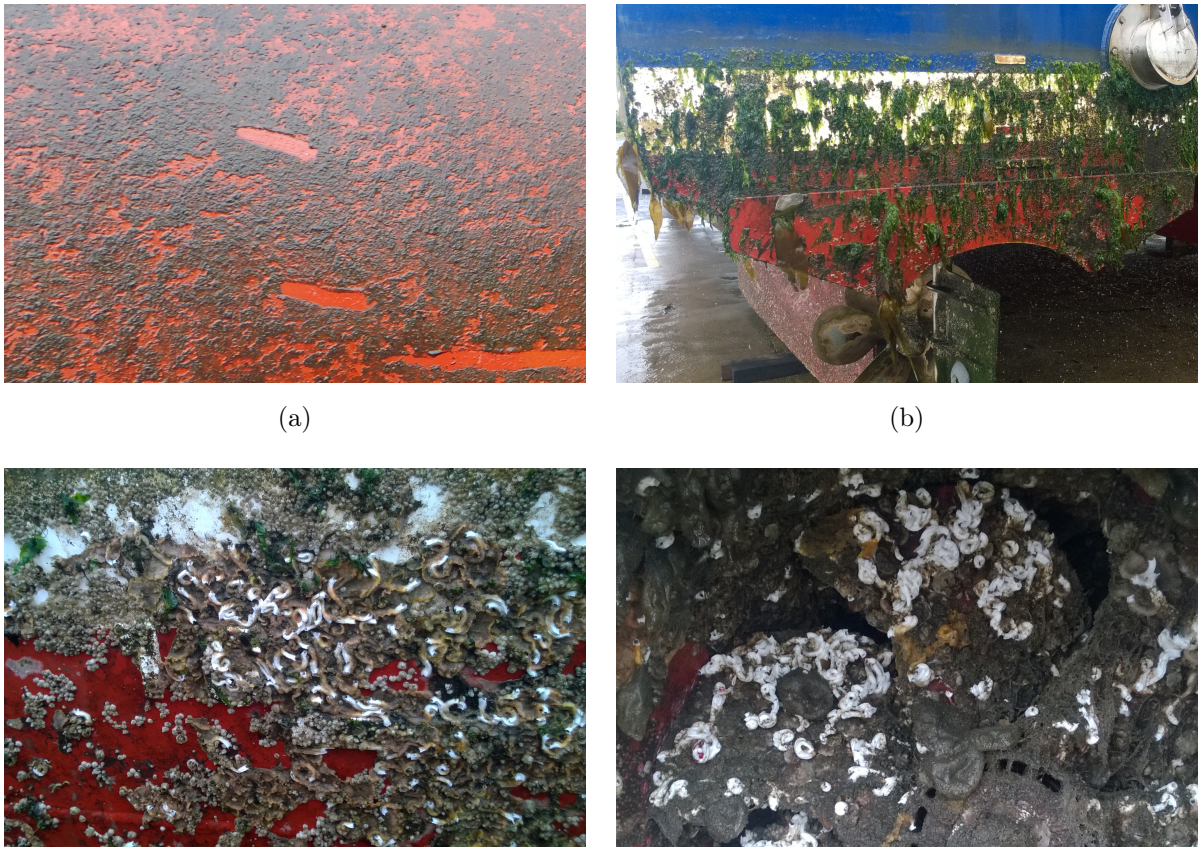

(a) (b)

(c) (d)

**Figure 2.12** – *Fouling stages on a small fast catamaran observed during different dry-dockings:* (a) *significant slime layer after a few months' sailing;* (b) *diffused algal fouling on the dry transom of the vessel;* (c) *slime, algal and animal fouling after one year of sailing;* (d) *advanced animal fouling in the bow thruster tunnel.*

(b) Design speed

(c) Propeller speed

3. Coating factors

(a) Anti-fouling principle

(b) Chemical formulation

The port factors are acknowledged to be the most influential, starting from the time spent in port to the quality of the water. However, it is observed that the natural environment also plays an important role: rocky shores tend to favour the settlement of most of fouling animals, which would therefore be found in large quantities by ships mooring nearby. Quite the opposite effect is observed when the coastline is sandy (Bengough and Shepheard, 1943).

The shape and operational profile of a ship are also important. The frictional forces are differently perceived in different locations of the ship, as investigated for example by Vargas and Shan (2017), Fig. 2.13. This leads to different species settling on different hull areas. Several studies reviewed by Yeginbayeva (2017) indeed produced evidence that in high shear stresses the fouling species are less diversified than those developed under lower shear stresses.

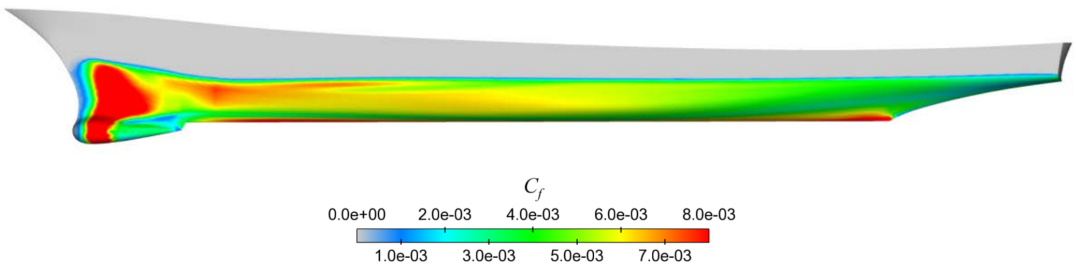


**Figure 2.13** – *Change in skin friction coefficient over the ship length for a state of medium calcareous fouling [Source: Vargas and Shan (2017)].*

Finally, the hull (and eventually the propeller's) coating plays a fundamental role. The adhesion of fouling depends upon its fouling control principle and its chemical composition. This will be discussed further in the following.

### *2.3.3 Prevention and treatment of biofouling*

#### Marine coatings

The prevention of fouling growth on ships has always been critical since the beginning of trades. After the advent of iron hulls, the application of protective coatings on hulls and

also on propellers has been the preferred line of action (Atlar *et al.*, 2003), with two main goals:

A. Preventing fouling, and

B. Reducing the surface roughness.

Item (B) is related to the smoothing capabilities of the coating, which is generally achieved either at application or during in-service life. In the '70s, the introduction of biocidal self-polishing copolymer (SPC) coatings based on tributyl tin (TBT) as biocide was the first revolution in fouling control technology from the advent of iron-built ships. Nowadays, after the 2001 ban of the TBT from the coating market, several solutions are available in replacement to TBT-based coatings, of which a good review is given by Yebra *et al.* (2004). Most of these coatings are able to deter or slow down the settlement of secondary fouling for relatively long periods, but still accumulate slime, which has become the focus of several recent studies. The main marine coatings available to date may be grouped under two headings, namely biocidal and non-biocidal coatings (Anderson, 2013).

***Biocidal coatings.***—Broadly speaking, they have acidic binders that release biocide particles in the water by dissolution and at a certain leaching rate — even when stationary. The released biocide concentrates in the proximity of the hull (or propeller) surface, inhibiting the adhesion of juvenile fouling or simply making the surface less appealing for settlement. The most used biocide to replace TBT is Copper, whilst a good variety of binders exists that allows a further classification.

The cheapest biocidal coatings are based on rosin binders with insoluble components that build up in an outer 'leached layer'. On one hand, this considerably hinders the biocide release, on the other it doesn't particularly smooth the surface and keeps most of its initial weight. Rosin-based coatings last generally up to 2 years.

Higher performance coatings are based on acrylic self-polishing copolymers (SPC) that solve into sea water by reacting with it, resulting in a constant leaching rate and thinning of the coating. These coatings have excellent in-service smoothing properties and gradually loose weight throughout their long life (up to 5 years).

***Non-biocidal coatings.***—They are based on various biocide-free principles. Among the most successful (and expensive) are Foul-Release (FR) coatings. They are based on the principle of low surface energy, which minimises the adhesion of fouling by creating extremely smooth 'non-stick' surfaces. This is achieved by the use of binders such as silicone or fluoropolymers. The resulting paints exhibit the lowest thickness, overall weight and own frictional coefficient on the market, whilst boasting excellent foul release properties at speed. Whereas they can last very long (even over 5 years), repair of damaged areas is a costly operation that requires significant skills.

A less performing alternative to FR coatings are hard coatings that rely on periodic scrubbing of the outer fouled layer. Their smoothness and fouling control properties however is heavily dependent on the scrubbing frequency and quality. They normally last up to 2 years of service.

Table 2.2 summarises the principal fouling control coatings on the market with their main properties.

TABLE 2.2

*Main fouling control coatings available to commercial shipping and their properties.*

| *Type* | *Principle* | *Anti-foulant* | *Cost* | *Smoothness* | *Duration* |
|---|---|---|---|---|---|
| Biocidal | Rosin-based | Copper, Silyl, Zinc, etc. | $ | ⋆ | • |
| | SPC | Copper, Silyl, Zinc, etc. | $$ | ⋆⋆ | ••• |
| Non-Biocidal | FR | Low surface energy | $$$ | ⋆⋆⋆ | ••• |
| | Scrubbable | Regular scrubbing | $$$ | ⋆⋆ | •• |

### Hull and propeller cleaning

Whilst hull and propeller coatings can prevent to a certain extent the adhesion of fouling, a periodical cleaning of the surfaces is necessary. Hull and propeller cleaning would normally be carried out during the due dry-docking class surveys, but may be carried out in advance should the ship operator estimate a higher profitability in an early cleaning.

It is worth recalling that the advancements in marine coating technology have allowed to extend the Inter Docking Interval (IDI) to longer periods. An example of a normal surveying regime is:


where the Dry-Docking (DD) is carried out every 5 years since the completion of the ship and the intermediate survey is replaced by an approved In-Water Survey (IWS). Dry-docking is a time consuming and costly maintenance operation and can often be carried out only at convenient locations, farther from the ship's route. IWS are quicker and require a lesser downtime. Underwater hull cleaning and propeller polishing can at this time be carried out, most commonly by means of diver-operated machines, as the one pictured in Fig. 2.14.

Modern high-end marine coatings significantly delay the onset of algal and animal fouling, allowing particular ship types to apply for an Extended Dry-Docking (EDD) plan

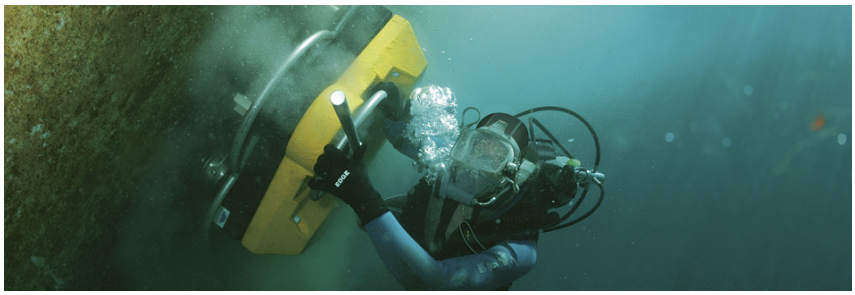

**Figure 2.14** – *Manned underwater machine for hull cleaning [Source: Hydrex (2018)].*

that expands the IDI from 5 to 7.5 years. Such plans are nowadays offered by most Class Societies and require two IWS to be carried out in a period of 7.5 years — for instance:


These programs are very beneficial to ship owners and operators because they are less disruptive of the ship's schedule and leave much more flexibility on time and location of the IWS. However, EDD programs are not allowed on all ships irrespectively. Currently, only container, general and dry cargo ships are permitted to apply. Moreover, the approval of the flag state is needed prior to the single ship's application to be filed and there are restrictions for the age of the vessel.

One of the most important factors in the evaluation of the ship fitness for the EDD is the state and quality of its hull coating. The coating must be certified to last for 7.5 years or over and must fit the ship's operational profile (e.g. design speed, area of operation, time in ports etc.). Ultimately, the right time for IWS and dry-docking can be controlled within the survey time window, if accurate information is available on the impact of biofouling on the ship's performance.

The ship operator is therefore responsible for two major decisions in this framework:

- Choice of fouling control strategy;
- Choice of dry-docking time within the given time window.

Long standing research in this topic has shown that Ship Performance Monitoring Systems are suitable tools to both carry out a retrospective assessment of the selected coating and planning the dry-docking schedule. These are indeed some of the major tasks of ship performance monitoring.

## 2.4 Effect of biofouling on ship performance

The detrimental effects of biofouling on the ship's hull and propeller are well known to affect primarily the viscous-related forces acting on them. The related penalties were

defined by Townsin (2003) as

> "ship speed loss at constant power, or, power increase at constant speed, or, consequentially, an economic penalty due to increased fuel consumption and scheduling penalties and other delays."

Several studies have been devoted to the estimation of these penalties over the years, a comprehensive reviews of which can be found e.g. in WHOI (1952); Townsin (2003).

### Effect of hull fouling

Biofouling impacts the ship performance largely because of the increased hull surface roughness, resulting in a thickening of the turbulent boundary layer and an increase of the ship wake (Fig. 2.2). This has the effect of increasing the viscous drag $R_v$ and changing the propeller inflow field. It can be speculated from Fig. 2.3 how large the impact of biofouling can be particularly on slower vessels, where $R_v$ accounts for up to 90% of the total resistance.

Much research has been hitherto undertaken in the attempt to quantify such effects. The classic work of Kempf (1937) was one of the first trying to correlate measures of size and spread of fouling (in his case, the size of the barnacles and the percentage of coverage) to the increase in ship frictional drag. Kempf's work followed an impressive set of systematic towing tests carried out on-board the Japanese ex-destroyer *Yudachi* after various periods spent at anchor (Izubuchi, 1934). The resistance measurements clearly showed the effect of fouling, estimated on a days-out-of-dock basis (Fig. 2.15). Years later, the renowned experiments on the *Lucy Ashton* recorded an increase in frictional resistance of about 5% for slime (Conn *et al.*, 1953) and almost 50% for weed and sparse shell fouling (Livingston Smith, 1955).

A notable research conducted by Townsin and Svensen (1980) resulted in the establishment of a correlation between $AHR$ and ship powering that was soon adopted by the ITTC. The works of Loeb *et al.* (1984) and Lewthwaite *et al.* (1985) confirmed these findings with experimental and full-scale techniques. Haslbeck and Bohlander (1992) conducted laboratory experiments and sea trials showing that heavy slime increased of about 18% the shaft power needed to push the 4,000 tons single screw USS *Brewton* at the speed of 25kn.

More recently, the seminal work of Schultz (2004, 2007) has set the standards for modern predictions of the effect of hull surface roughness on ship resistance. Flat plates were initially coated with different coatings and fouling states and their frictional resistance measured from towing tank tests. The frictional coefficients were thus extrapolated to full scale using the Granville similarity law showing, for example, that heavy slime and heavy calcareous fouling increased the shaft powering requirements of a frigate sailing at 30kn by 12% and 51% respectively (see Table 2.3).

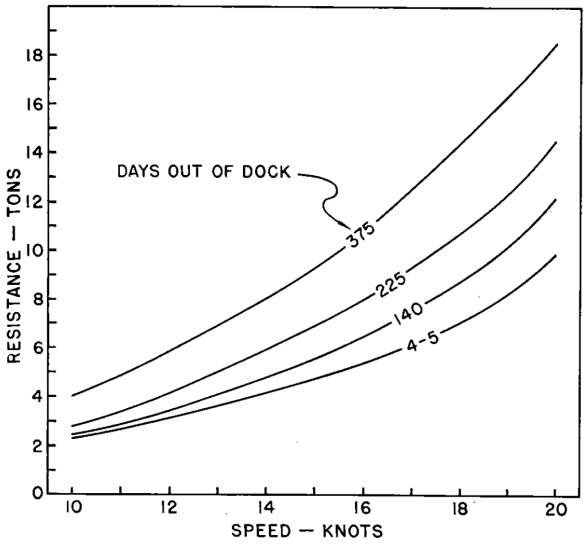


**Figure 2.15** – *Resistance tests on the* Yudachi *after various lay-up periods [Source: WHOI (1952), after Izubuchi (1934)].*

TABLE 2.3

*Predicted increase in total resistance for a frigate with various hull roughness conditions at two speeds, after Schultz (2007).*

| *Description of condition* | $\%\Delta R_T$@15*kn* | $\%\Delta R_T$@30*kn* |
|---|---|---|
| Light slime | 9% | 6% |
| Heavy slime | 18% | 12% |
| Weed fouling | 32% | 21% |
| Medium calcareous fouling | 50% | 32% |
| Heavy calcareous fouling | 78% | 51% |

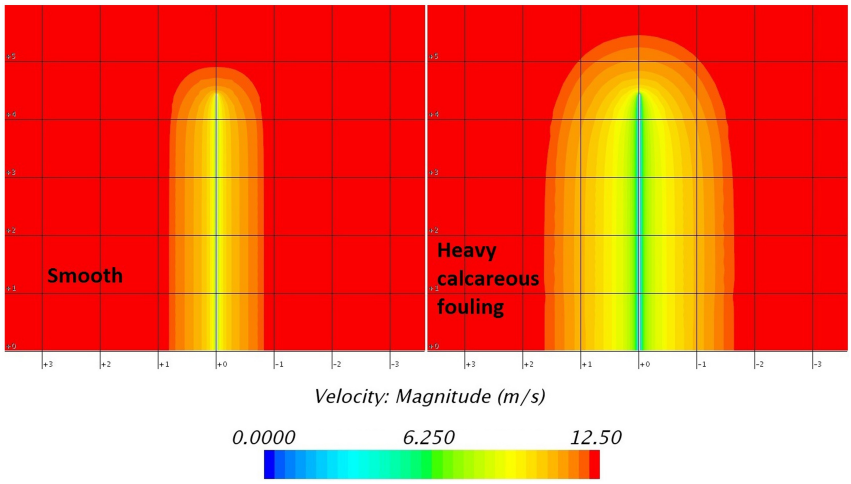


**Figure 2.16** – *Increase in boundary layer on a flat plate caused by heavy calcareous fouling obtained by CFD simulations [Source: Demirel* et al. *(2017*a*)].*

Extensive research is following Schultz's. Work by Demirel *et al.* (2017*a*,*b*) included the systematic use of 3D printing and pioneered the use of CFD to predict the effect of biofouling roughness on a ship's resistance, staying in the ballpark of Schultz's predictions (Fig. 2.16). Oliveira *et al.* (2018) extended these studies by studying the effect of the hull surface roughness on the form factor.

Yeginbayeva (2017) conducted perhaps the most comprehensive systematic experimental campaign on the roughness, boundary layer and drag characterization of commercial marine coatings. 'In-service' fouled surface conditions were achieved by growing natural slime both in laboratory and full-scale conditions on purpose-designed test panels. Interestingly, the results confirmed that different species of slime populated surfaces subjected to different wall shear forces.

### Effect of propeller fouling

Marine propulsors and in particular screw propellers are not immune from fouling. Despite most of them are built from copper alloys, the cathodic protection to which they are subjected hinders the dissolution in water of the toxins and their fouling control properties as a consequence. Nevertheless, the high Reynolds numbers ($Rn$) at which they normally operate act as a natural in-service 'polishing' together with blade cavitation (if present). If the vessel is not laid up for significant time, the combination of high $Rn$ and cavitation in general is sufficient to 'wash off' most macro-fouling species.

The effect of fouling on propeller performance is twofold: it increases the frictional drag of the blades and reduces their lift, altering the characteristics of the propeller described by $K_T$ and $K_Q$. This results in a decrease of propeller efficiency, as shown by eq. (2.12), and adds to the change in the propeller loading point caused by the increased wake fraction $w$, as seen in eq. (2.6) and (2.18c).

The already cited research conducted by Bengough and Shepheard (1943), reported the unusual case of the HMS *Fowey*, which after the launch had been berthed for a period of about five weeks. When the sloop failed to reach the design speed of about a knot during trials, the cause was found to be very heavy calcareous fouling covering all of the propellers. The relevance of propeller fouling and service oriented design and maintenance was later to be advocated by the studies of e.g. Broersma and Tasseron (1967) and Prochaska (1977).

Later during the '80, the work conducted at Newcastle University by the 'Ship Performance Group' gathered by Prof. Townsin provided invaluable information on the impact of propeller fouling on performance. Above all, the researches of Svensen and Medhurst (1984) and Mosaad (1986) concluded that, despite its smaller impact relatively to hull fouling, propeller fouling can induce a few percentages of power loss (or speed loss) in a case of common fouling condition. For example, sparse barnacle and weed on the propeller blades of a 9000 DWT cargo ship would result in about 3% power penalty (Mosaad, 1986). Moreover, it was shown how the drag characteristics of the propeller blades are affected more than its lift (Fig. 2.17). As a result, the torque coefficient $K_Q$ increases in greater percentage than the thrust decreases.

This was later supported by Seo *et al.* (2016), who integrated the methodology developed by Schultz (2007) in a lifting surface code predicting a 9.5% propeller efficiency loss in case of heavy slime. Lutkenhouse *et al.* (2016) corroborated these findings by applying full-scale measured roughness parameters to the PSF-10 lifting surface code developed by Greeley and Kerwin (1982). The annual fuel penalty due to propeller fouling was estimated as 2.5% of propulsion fuel use.

It can be concluded that although the effect of propeller fouling is not as significant as that of the hull, it is however well more important in terms of energy loss per unit area (Anderson *et al.*, 2003).

For the above reasons, coating marine propellers is sometimes carried out to stop fouling whilst simultaneously preventing corrosion and chalk build-up from the cathodic protections (Atlar *et al.*, 2003). However, propeller cavitation most notoriously erodes soft coatings particularly in the tip regions, leading to paint damage and additional roughness. As propeller coating is still an attractive solution for a good part of the shipping, research on the topic is therefore far from completion.

### *2.4.1 Estimation of biofouling effect on ship performance*

Hull and propeller fouling is one of the most important aspects of a ship's performance during her service life. The preceding sections hopefully provided an insight over the extent and quality of the effect of biofouling not only on the resistance but on the whole powering of ships.

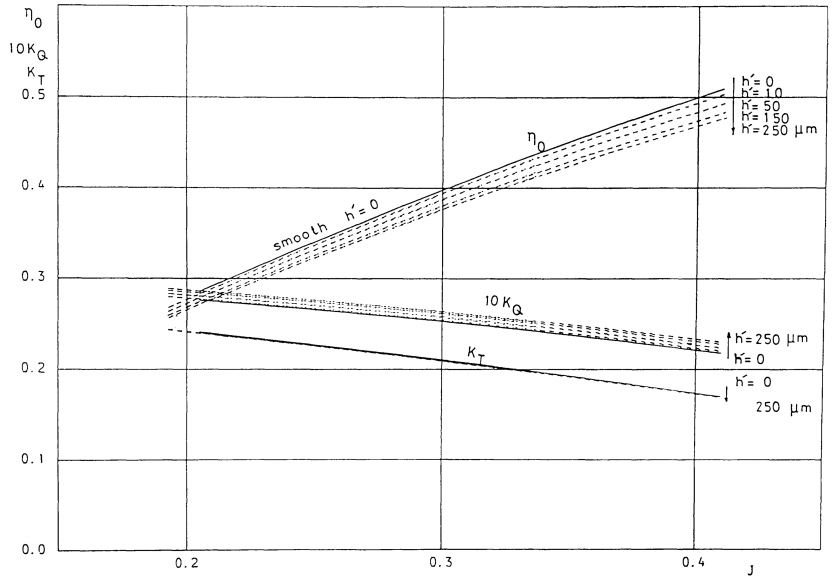


**Figure 2.17** – *Effect of propeller roughness on $K_T$ and $K_Q$ [Source: Mosaad (1986)].*

We must therefore acknowledge that if on one side the growth of biofouling cannot be avoided completely, the quantification of its effects upon the ship performance is of the utmost interest to the ship owner or operator. This topic, however, opens up to several challenges.

Recent and current research shows that prediction of fouling powering penalties from the knowledge of the elemental surface roughness — the so-called 'bottom-up' approach — is becoming increasingly accurate. However, two great challenges are found in the application of these methods to accurate full-scale predictions:

1. A complete definition of the typical 'roughness' of a ship is very complex to give. In part, this is due to the impractical mapping of the fouling species populating hull and propeller — particularly their size and extent over the wetted surfaces. It has already been mentioned how different lighting and shear stresses generate a significant differentiation of fouling species even on the same ship, between sides and bottom. Making an overall estimate of the average spread of slime, algal and animal fouling over the whole hull and propeller from underwater inspections would be possible, but questionably practical.

   Obtaining a roughness parameter from size and spread of fouling is the next hurdle. Townsin (2003) rightfully points to the critical aspect of defining the average roughness of slime and weed, where the former is prone to change in structure and shape under shear stress (Yeginbayeva, 2017) and the filaments of the latter often protrude into the turbulent boundary layer.

2. Even if the above estimation was possible, relating that to the full-scale power increase is not in the least an easy task. Roughening of the surface leads to multiple

effects, the dynamics of which are very complex and not yet fully understood. This therefore prevents the formulation of rigorous analytical solutions. Roughness functions are attempts to overcome this hurdle by empirically relating the wall shear stress to the surface roughness. As remarked by Schultz and Swain (2000), however, the scatter in the roughness functions of certain types of surfaces (particularly when covered with algae) still calls for further research.

It may be concluded that if the effect of biofouling (and roughness in general) needs to be accurately and efficiently assessed in a practical application, we must resort to on-board ship performance monitoring systems — i.e. a 'top-down' approach.

***Ship Performance Monitoring Systems.*** —Broadly speaking, a Ship Performance Monitoring System (SPMS) allows, with various degrees of accuracy and complexity, the analysis of the time-dependent speed–power curve as it changes against a *reference* curve. This is most conveniently chosen to be that for a clean hull and calm weather.

As shown in Section 2.2, the powering of ships is however affected by several factors, which must be in some way accounted for when carrying out the performance analysis. In fact, if the disturbances caused by the environment and the ship itself can be 'isolated', the remaining difference between the reference speed–power curve and that taken at some later point in time can be related to fouling only.

To achieve this, the on-board measured speed-power curve can be corrected to calm water conditions by applying knowledge of the physical phenomena, or they can be analysed by using pure statistical inference, or even manipulated using a combination of both methods. SPMSs applying physical knowledge are termed *deterministic*, whilst those purely based on statistical power are said to be *data-driven*.

On-board data collection methods can be manual or automatic. The need to understand the effects of operational and environmental factors on navigation and the want of improved route planning made the regular observation and recording of vessel speed and position a standard on most ships by the onset of the *Age of Sail* (Sannino, 2007). Simple techniques were employed to analyse the recordings of the Captain's logs, enriched by bunkering data with the appearance of the first steamboats at the end of the 19$^{\text{th}}$ Century. With modern manual data collection, deck officers and engineers record navigational, engine and cargo loading data on logbooks which are then aggregated in daily noon reports. Almost all ships were (and still are) fitted with a manual logging system, which easily made this data collection method the most used for performance monitoring throughout history. However, its two major drawbacks are the low sampling frequency and the heavy involvement of human action in the data collection process, both of which increase the measurement uncertainties and errors (Hasselaar, 2011; Aldous *et al.*, 2015). Therefore, despite noon reports are still used for performance monitoring, they are not to be preferred.

On the other hand, automatic data logging systems are already a standard on several ships. The IMO requirements on Voyage Data Recorders and the pressures arising from the needs for state-of-art performance monitoring solutions are among the drivers of such change. Indeed, automatic measurement systems provide data having the highest precision and sampling frequency and allow to carry out on-line (i.e. immediate on-board) analysis. Automatic systems have obvious advantages when it comes to measurement quality. However, they also imply that a suitable method must be in place to handle the big data they generate. This aspect and the capability of integrating the SPMS with equipment-based internet connections — a network system commonly called the 'Internet of Things' — is currently a very debated topic. However, whilst a significant part of the shipping industry has at present invested in the structure and facilities required by such networks, the majority of shipping companies do not make an efficient use of the acquired data as yet (Halfhide, 2018). Any newly proposed SPMS should therefore be conceived with a view towards network integration and 'big data' handling.

The practical implications of automatic on-line SPMSs render on-board monitoring a great challenge that demands the dedication from all the involved parties — the naval architect, the ship owner, the ship builder and the crew members. Nevertheless, despite its challenges on-board ship performance monitoring still marks the way ahead for real-time assessment of the effect of biofouling on ship performance and stands as the ultimate assessment of numerical predictions.

## 2.5 Summary

In this chapter the scientific background for the present study has been given. Section 2.2 introduced the general definition of ship performance and attempted a description of the several factors that may affect it. These were distinguished between the disturbances caused by the environment and those caused by the ship operation, structure or machinery. The ship service performance was therefore introduced as a complex problem involving several interrelated phenomena.

Section 2.3 gave an insight on biofouling and attempted to define its characteristic traits in terms of principal constituent species, sequential settlement, and conditions favourable to its growth. An overview of the methods currently available to deal with the accumulation of biofouling on ships was then given with descriptions of the most common types of marine coatings and an insight on their role in the dry-docking planning. It may be summarised that the growth of biofouling is a natural phenomenon that depends on a great variety of factors and is for this reason very difficult to predict. At the same time, its prevention and treatment provide several challenges and detain a considerable share of the operating costs of a ship.

In Section 2.4, an overview of the effects of biofouling on the powering of ships in

service is complemented by a brief review of the relevant studies. These were subdivided in reason of their focus on either hull or propeller fouling. In making such review, the Author tried to point out the importance of the biofouling penalties on ship powering, concluding that on-line ship performance monitoring is still the most convenient and efficient means of assessing them.

# CHAPTER 3

# Review of literature on Ship Performance Monitoring

## 3.1 Introduction

Whereas naval architects focussed on different aspects of ship performance throughout history (e.g. estimation of sea margin, model scale correlation, etc.), hull and propeller fouling has always received a certain degree of attention. As stated in Chapter 1, the effect of fouling on ship performance and the effectiveness of marine fouling control strategies will be assessed in this study by means of full-scale monitoring of service performance. It is therefore appropriate to concentrate this review on the achievements made in the field of ship performance monitoring (**Objective A**).

In doing so, a general overview of ship performance monitoring is given in Section 3.2, with particular emphasis on the evolution of monitoring methodologies throughout history. Section 3.3 reviews the state of art in ship performance monitoring, categorising SPMSs in reason of the method used to analyse the service performance of ships, namely deterministic, statistical, data-driven and hybrid. Section 3.5 summarises the achievements and implications of the recent and first ISO standard dedicated to the measurement of hull and propeller performance. Section 3.6 then reviews the few studies conducted to evaluate the uncertainty of performance estimations using modern SPMSs. The motivations of the current study in light of the literature available to-date are then consolidated in Section 3.7 to justify the aims and objectives of the thesis. A discussion is also included in the same section regarding the different performance monitoring solutions.

## 3.2 Overview

Rational ship performance analysis methods first appeared at the beginning of the 20th Century with the early work conducted by Edmund Telfer on the analysis of ship performance in trials and service conditions (e.g. Telfer, 1926; Bonebakker, 1951; Clements,

1957). Most of the service performance monitoring studies that followed were based on relatively simple trend analysis of on-board measured data. Shore offices received the data in the form of logs manually recorded at every watch or noon. Rarely were the ships fitted with automated measurement systems, and only out of a pure research interest. In addition, the added resistance caused by weather and operational changes were seldom calculated, mostly due to the lack of reliable theories. Only in the 50s more advanced statistical tools were applied to performance data in an effort to benefit even from small samples of mediocre quality. Several studies successfully showed the power of statistical analysis on the voyage data recorded on log books.

The introduction of spectral analysis and potential theory in seakeeping in the late 50s promoted advances in the prediction of added wave resistance in irregular sea states. This encouraged the early implementations of deterministic added weather resistance corrections in service performance analysis. Early normalization methods, however, often estimated the combined effect of wind and waves, assumed to have the same direction, and hence did little to reduce the scatter of full-scale measurements. One reason is that the assumption of same wind and waves direction seldom holds, especially in cases of severe swell (see Chapter 2). The other major cause was reckoned to be the lack of reliable and stable speed through water measurements. It would take yet another decade to see significant improvements in the weather corrections and in the accuracy of service performance estimations.

Meanwhile, other innovations were developing alongside. The advent of microprocessors in the late 60s brought huge changes in the entire society and with it in the discipline of ship performance monitoring. The availability of relatively inexpensive computers allowed faster calculation times and fostered the development of advanced self-learning 'adaptive' algorithms (e.g. Jazwinski, 1969; Sage, 1972). In the late 1980s, ship performance analysts eventually borrowed the algorithms giving origin to data-driven analysis methods. These developments have been the seeds of the alternatives to traditional methods from the 1990s.

Both traditional and statistic-based approaches coexist to date with several degrees of in-betweens. However, the considerable pressure of environmental regulations and the economic benefits implied by performance monitoring has in recent times put the debate on the quality of SPMSs under the spotlight.

In a first attempt to standardise SPMSs, several class societies, research institutions, paint companies and shipbuilders made a joint effort to release the first international standard on hull and propeller performance monitoring, the ISO 19030 (ISO, 2016). Nonetheless, the available literature proves that the effectiveness of different performance monitoring methods is still open for discussion and no firm conclusion has been drawn regarding the achievable minimum uncertainty of each.

The following sections will thus give a review of the existing SPMSs and other relative

studies.

## 3.3 Performance modelling methods

The early literature displays a wide spectrum of SPMSs and their underlying principles. Nonetheless, two major streams appear to have taken separate routes that are relevant to contemporary applications — the *deterministic* approach and the *statistical* approach. The latter was to be enhanced by the advent of computational power, paving the way to *data-driven* and *hybrid* approaches.

### *3.3.1 Deterministic approach*

The representation of a physical phenomenon is termed deterministic when physical governing laws and causal relationships between them are, with the due assumptions, employed to create a model of the phenomenon itself. When modelling the ship's performance, experimental or numerical techniques are employed to model parts of $R_{add}$ in real scale. As stated in Chapter 1, the primary variables (e.g. $V_s$ and $P_S$) are obtained from on-board measurements and are then normalised to standard conditions using $R_{add}$ reversely calculated from secondary measurements and the $R_{add}$ models. The complete performance model is thus built considering the physical relationships between measured variables and models.

Consider the simple example of an SPMS, the aim of which is to determine the in-service performance of a ship in no wind. A simplified schematic representation of a typical deterministic approach to the problem is shown in Fig. 3.1. In this example, the SPMS uses cavitation tunnel tests to build a propulsion model based on the actual propeller's open water characteristics. It then employs wind tunnel tests to calculate the direct wind resistance on the ship's superstructure and to create a wind resistance model. Both propulsion and wind resistance models are needed to normalise the on-board measurements to standard conditions — which in this case corresponds to 'no wind'.

Depending on the project, employing Experimental Fluid Dynamics (EFD) in the development of a deterministic SPMS might involve the use of towing tank data, cavitation tunnel experiments and wind tunnel measurements. EFD techniques are, however, often complemented by Computational Fluid Dynamics (CFD). Both methods are ship-specific and very accurate, but they require substantial resources to undertake extensive testing or simulation campaigns. Therefore, their use is usually confined to the assessment of only the propeller open water characteristics and relevant conditions of additional resistance components. For example, CFD may be used to estimate the added wave resistance in head seas only and for a specific draught. When the case allows it, semi-empirical methods can be used, for instance to calculate wind resistance coefficients. Care has to be taken,

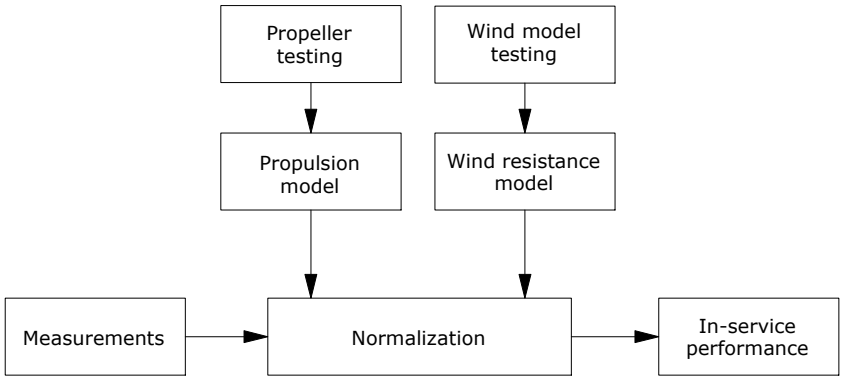


**Figure 3.1** – *Schematic of a typical deterministic approach..*

however, in checking the limits of applicability of such methods.

Sometimes in the literature is found a misleading definition of 'deterministic approach'. There seems to be a tendency to sometimes consider parametric powering prediction methods as the deterministic performance models described so far. Well known prediction methods of this kind have been published e.g. by Guldhammer and Harvald (1974); Holtrop and Mennen (1982); Hollenbach (1998), but albeit they are fast, inexpensive and relatively simple techniques, their natural inaccuracy makes them unsuited for deterministic performance modelling.

The deterministic approach has its roots in the work carried out by Edmund Telfer (1926) at the time he was affiliated with Monitor Shipping Ltd. In discussing the possible solutions for the determination of ship full-scale performance, his classic paper proposes the use of the propeller as the link between ship speed, propeller rate of revolution and power. For each ship, load trials are carried out to calibrate the propulsion model over the normal slip range and stock propeller model test data are used to expand the model for a wider range of propeller slip ratios. A ship-specific Generalized Power Diagram (GPD) is generated that would hold in any seagoing condition provided that the propeller remains unchanged. The study also addresses the monitoring of service performance introducing four weather classes to subdivide ('bin') the data. This allows only clean weather data to be used in the derivation of the GPD and fouling assessment, whilst leaving the other measurements for eventual weather assessments.

The concept of weather classes is sometimes referred to as 'data bucketing' and it is ultimately a particular kind of condition-based data filtering still widely used in contemporary performance monitoring (see e.g. Dinham-Peren and Dand, 2010; Cusano *et al.*, 2016). The literature of almost a century shows that Telfer's method has been the basis of most SPMSs of the 20th Century, to the extent that his method was to be fully reprised by Bustard (1978) and, more recently, by Kevin Logan (2011). In Logan's revision, the weather classes are abandoned and only calm weather data are retained for analysis. The shortcomings of Telfer's method (and its revisions) are firstly due to the drastic reduction

in analysable data following weather classification. Secondly, to the assumption of linear relationships amongst several variables, which are often violated on vessels sailing beyond transition speeds due to the inception of nonlinear planing forces.

In the last quarter of the 20th Century, Prof. Townsin's 'Ship Performance Group' was very active in performance monitoring as well. Townsin *et al.* (1975) describe a method to monitor the speed of ships in service using on-board data and a GPD similar to that described by Telfer. The paper interestingly proposes several recommended measurements and the pitfalls in speed through water and power readings. The need of reliable speed logs is underscored by the authors and supported by the significant data scatter presented in the measurements. Data bucketing is again used to separate the weather effect from reference performance data and study the involuntary speed losses caused by different directions and intensity of winds and waves. Corrections are applied to speed data to normalise it for an arbitrary displacement and power.

To the Author's knowledge, the first example of modern-day on-line SPMS targeting hull and propeller performance was presented by Journée *et al.* (1987) in the form of a mathematical model run on a common PC. The paper describes in detail the SPMS as being comprised of a calculation 'module' for the propeller performance and for each disturbing factor (i.e. wind and waves) for a fixed ship draught. Added wave resistance is split into the contributions of wind waves and swell. Two simple roughness allowances are let free to adjustments for hull and propeller fouling. The authors suggested to obtain the wind coefficients from Isherwood (1973) and to calculate the added wave resistance using a combination of the methods developed by Gerritsma and Beukelman (1972) and Boese (1970). Other added resistance factors are ignored. The SPMS described in this study is also one of the first making use of an automatic measurement system. Very valuably, the authors stress the ultimate importance of both reproducibility and repeatability of the measurements, despite no further analysis is carried out in support of the given figures. The paper also does not mention any raw data handling procedure.

Though less complete, similar works are those by Andersen *et al.* (2005) and by Hunsucker (2016), where the former uses noon reports whilst the latter automatic continuous monitoring. In both studies, approximated empirical formulations are used for wind and waves corrections, but a propeller model is not included. Therefore, the changes in total propulsive efficiency are taken into account by quite loose approximations. Andersen *et al.* (2005) mention the uncertainty in performance estimation, noting that the significant data scatter allegedly arises from errors in weather observation, weather correction methods and speed through water measurements. Hunsucker's research in addition draws upon aspects of big-data handling and the choice of a correct indicator of hull performance against fouling. Both studies, however, do not discuss either uncertainty or big data handling.

Recently, one of the most complete studies on ship performance monitoring was con-

ducted by Thijs Hasselaar (2011) at Newcastle University. Much has to be credited to him for his extensive review of on-board sensor technology, existing deterministic methods and for having explored state of art possibilities of deterministic performance monitoring. Following a substantial investigation, he developed a working SPMS on Newcastle University's former Research Vessel (R/V) *Bernicia*. He later installed it on a large VLCC. The systems targeted small changes in hull hydrodynamic performance and therefore aimed for high quality standards of signal acquisition, processing and analysis. The SPMS described in his thesis involves continuous automatic measurements from several on-board sensors, including speed log, torque-meter, shaft meter and environmental sensors. The raw data is checked for steady state periods and outliers are removed using established statistical techniques. Smoothing and suitable averaging is then applied before data normalisation and performance analysis. In the case of the *Bernicia*, Hasselaar conducted towing tank experiments to derive the added wave resistance transfer function, but used wind coefficients from the literature. He used empirical formulations for the VLCC to derive both added wave resistance and direct wind coefficients. Hasselaar neglected other added resistance factors because of their small impact on performance. The core of the analysis methodology is the propeller performance in open water. The effects of disturbances are treated in view of changes of the propeller loading point for unchanged ship speed and wake fraction according to the well-known method developed by Taniguchi and Tamura (1966). Unfortunately, the unavailability of propeller geometry of either ship introduced large approximations that were exacerbated by the poor speed logs. Due to time restrictions, alternative solutions couldn't be sought, and nor was a detailed investigation of the uncertainty of performance estimation. Despite its limitations, however, the study remains a milestone in the investigation of deterministic performance monitoring in contemporary shipping.

Hansen (2011) conducted a similar work, albeit with the different aim of aiding a shipping company in the transition from noon reporting to automatic computerised monitoring. Although the normalization method and performance analysis parameters are relatively coarse, a valuable review of state of the art measurement systems and raw data handling is given.

Foteinos *et al.* (2017) used one-year worth of noon reports and engine data collected on four bulk carriers to estimate the impact of biofouling on ship performance. Due to the purported unreliability of the torque meters installed on-board, $P_S$ was calculated by inputting real measurements into a power prediction software based on a comprehensive engine model. Corrections for wind and waves were estimated based on the Fujiwara and Nimura (2005) and the STAwave-2 methods (van den Boom *et al.*, 2015) and from deck observations or hind-casting. Other corrections were not included in the analysis. The open water characteristics of the propeller were not available and it is unclear how the propeller thrust was thus derived to relate the normalization to the ship performance.

Two indicators of fouling were thus chosen; the first related to the propulsive power and the second to the ship resistance. Whereas the overall trends of these indicators could be related to fouling, their scatter prompted the authors to consider that the employed normalization procedure needed further improvements.

Lately, Orihara and Tsujimoto (2017) published an interesting work on performance monitoring describing the successful application of one of the most complete deterministic SPMS found in literature. The aim of the study pertains the validation of earlier design powering predictions of a large bulk carrier. The paper gives a good description of the sensors used, the filtering techniques and the data normalization procedure, but does not provide information about the uncertainty of the performance predictions. The adopted methodology is very similar to that set forth by Hasselaar (2011). The main differences stem from the employed filtering procedure and parameters and from the application of corrections for rudder, drift and yaw resistances in addition to the usual wind and waves'. Furthermore, added wave resistance is treated as a superposition of wind waves and swell systems. Unfortunately, the origin of the corrections effectively used is not explained, nor is the extent to which such corrections have been applied.

Several other studies can be found in recent literature that will not be summarised in this work. Deterministic SPMSs have indeed a long standing and thriving history and owing to their versatility they are still being implemented in a wide spectrum of applications. Nonetheless, the literature demonstrates that not many of these systems have been successful in measuring small changes in performance. Fewer still are those addressing the whole of the data processing — from data collection to performance analysis. At the same time, the applied normalization procedures are very different, ranging from complete absence to extremely detailed, and often they are unjustified. Whilst deterministic SPMSs have proven to be effective and versatile, the literature thus calls for further research.

### *3.3.2 Statistical approach*

The statistical approach appeared early in the 50s and developed alongside the already established deterministic methods. Its main principle stands in the derivation of all the relevant relationships between variables — and hence of the ship service performance — solely by means of advanced statistical techniques applied to raw measurements. In some occurrences, the raw data is normalised with statistical corrections, though data bucketing is the most common practice. The previous example of an SPMS with aim to determine the in-service performance of a ship in no wind is represented in Fig. 3.2 for a typical statistical SPMS. Here, the data is firstly categorised for weather intensity. Hence, advanced statistical algorithms are used to analyse data recorded in no wind to build a calm water performance model for the ship. This model is then used as a baseline to analyse the data in the remaining weather classes to obtain additional statistical models

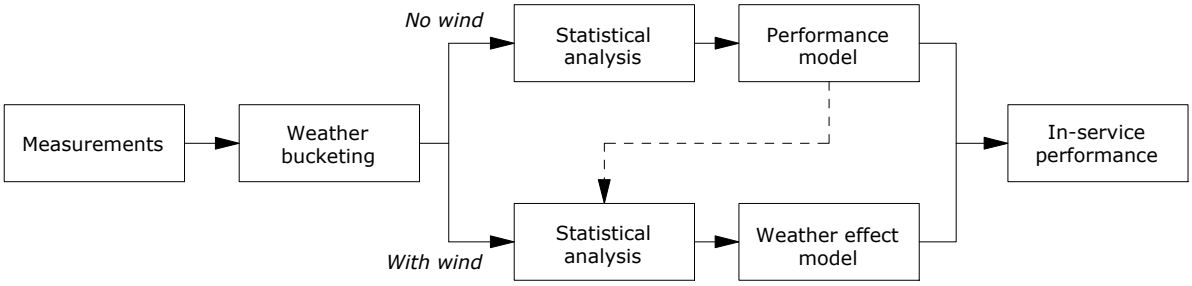


**Figure 3.2** – *Schematic of a typical statistical approach..*

of the effect of wind on performance. It is very relevant to note that these methods require heavy involvement of the data analyst, that actively operates as supervisor of the statistical analysis with expertise and judgement. A more advanced version of this concept is fostered by data driven methods that will be later discussed.

Jan Bonebakker pioneered the statistical approach with two milestone studies (Bonebakker, 1951, 1953) that were to inspire several others until nowadays. The innovation he introduced regarded the application of Telfer's method without resorting to any model test. All the information of concern was to be obtained from on-board measurements, making extensive use of multiple correlation algorithms. Bonebakker achieved very reasonable results in his ship performance studies, despite finding quite a reluctance on part of fellow naval architects to accept the novelties of his research. Nevertheless, his approach survived until our days as one of the simplest methods to analyse performance data.

Papers by Aertssen (1953, 1961) and by the British Ship Research Association (Clements, 1957) followed Bonebakker's work shortly after, supporting the findings and the introduction of multiple-regression analysis in ship service performance monitoring.

Of slightly different concept is the work by Scott (1971), who adopted a combination of statistical and deterministic approach to normalise the measured speed through water using statistically derived weather, displacement and fouling corrections.

More recently, Bialystocki and Konovessis (2016) apply a very similar approach to noon measurements of fuel consumption and ship speed, quantifying the effect of different weather conditions. Despite the aim of the paper is rather to provide ship owners with a simple service power estimation algorithm, the study shows how the statistical approach is still a valuable asset in performance monitoring.

The accuracy of the statistical models, however, is found not satisfactory for accurate hull and propeller performance monitoring since it is jeopardised by two chief factors. Firstly, by the several nonlinearities encountered in hydrodynamic interactions, often overlooked by the simplifications of the models. Secondly by the reliance of the statistical algorithms on the variability of the data, starting from ship speed and propeller rate of

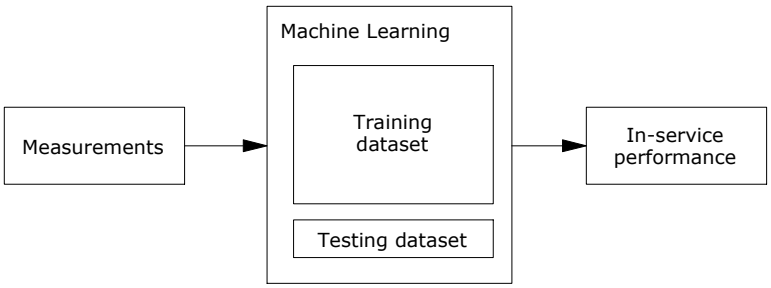


**Figure 3.3** – *Schematic of a typical data-driven model..*

revolutions. It should also not be understated that in nowadays' era of big data analysis the use of these scientist-driven methods can be quite a daunting task due to the enormous quantity of data to analyse.

### *3.3.3 Data-driven approach*

Data driven and statistical methods share a common origin in that they do not require any knowledge of the physical phenomena they aim to model. Even more so since all the data manipulation and statistical analysis is entirely carried out by computers using powerful self-learning (adaptive) algorithms. For this reason, they are often referred to as *Machine Learning* or *Black Box* methods in analogy with the theory of electronic circuits. Incidentally, for this reason deterministic methods are sometimes called *White Boxes*. Pure statistical inference is used on measured data for the derivation of the transfer functions relating one or more measurands (e.g. wind speed and direction) with one or more observed variables (e.g. ship's speed and power).

Similarly to the previous sections, the same example of SPMS is represented in Fig. 3.3 as if it were built with a data-driven method. The implementation of a data-driven model is based therefore on the history of measurements, a large portion of which (usually more than half of the total sample) is initially used to *train* the model. In practice, the statistical algorithm finds a best fit for the data (in the form of correlation matrix and coefficients) exploiting different techniques and criteria for the minimisation of the fit residuals. The remainder of the measurements history are then used for validation and testing, that is, the assessment of the model found with the training dataset. Machine Learning methods can be very accurate even in the prediction of non-linear problems and their implementation is relatively inexpensive. However, they are at most *as* accurate as the measured data from which the models are developed.

The successful application of data-driven methods to ship performance monitoring has a relatively recent history. Pioneering of adaptive algorithms and system identification theory indeed belonged to the application of Kalman filters to the guidance of aerospace

vessels (see e.g. Jazwinski, 1969; Sage, 1972; Lainiotis, 1976).

An unsupervised Machine Learning implementation (i.e. where the adaptive algorithm is let alone to find the structure in the input without external intervention) is found in the works conducted by Pedersen and Larsen (2009*a*,*b*). Artificial Neural Networks are employed for the forecast of the propulsion power of a large tanker and demonstrate that a good agreement can be reached between the model and the used dataset. This includes high-speed automatic measurements (1 Hz), noon report data and hindcast weather observations divided in four groups, each corresponding to a different draft. The studies also show the superiority of Artificial Neural Networks against simpler adaptive algorithms, namely optimised linear and non-linear methods.

A very similar attempt was coincidently carried out in the same period by Petersen *et al.* (2012*b*), who again used Artificial Neural Network in the prediction of fuel consumption, with similar results. The work on Artificial Neural Networks is expanded by another paper (Petersen *et al.*, 2012*a*) and, in a very similar and almost contemporary study, by Pedersen and Larsen (2013), both of which introduce the use of Gaussian Process Regressions and compare them to the accuracy and computational characteristics of Artificial Neural Networks. Pedersen and Larsen (2013) specifically demonstrate how Gaussian Process Regression can be used for a more computationally efficient prediction of powering performance without jeopardising the predictive accuracy.

With the slightly different aim of designing a weather routing tool, Maki *et al.* (2011) successfully employs a Real-Coded Genetic Algorithm to the definition of the optimal route in consideration of several objectives of efficiency and safety in vessel operation.

Although their application to ship performance monitoring has been hitherto limited, data-driven model have proven to be an accurate and viable alternative to more traditional methods. However, whereas the cited studies give detailed descriptions of the precision of the models with respect to the training and testing datasets, it would be beneficial to also obtain information regarding the uncertainty of the models on larger and more varied data samples.

### *3.3.4 Hybrid approach*

The implementation of data-driven methods supervised by some degree of physical knowledge originates hybrid models. Underlying these methods there is generally a simple physical model (e.g. Holtrop's powering prediction) which is adjusted and refined by the analysis of historical on-board measurements with any of the Machine Learning techniques earlier presented. This technique is called supervised Machine Learning and, in analogy to the Black and White Box terminology, it is also referred to as *Grey Box* modelling. The same example used in the above sections is reproduced in Fig. 3.4 for a hybrid method. Hybrid methods are therefore intended to benefit from a certain degree of knowledge of

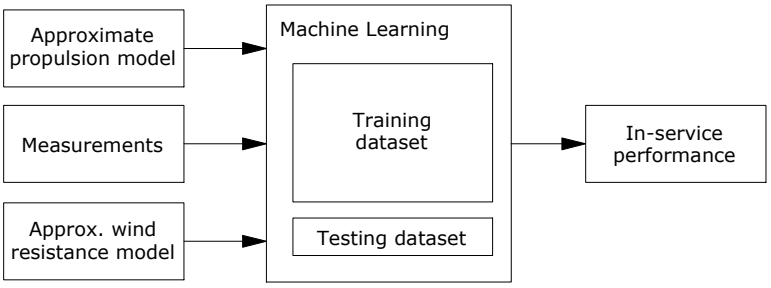


**Figure 3.4** – *Schematic of a typical hybrid model..*

the physical phenomena and from the qualities exhibited by Machine Learning techniques in finding the structure behind complex correlations. For this reason, they are widely used in commercial applications due to their good accuracy and relatively quick implementation. Hybrid methods indeed require less historical data than pure data-driven methods as they already retain a certain 'knowledge' of the relations they attempt to model.

Contrarily to what could be expected, hybrid methods were introduced in ship performance monitoring before 'pure' data-driven methods and effectively are based on the same concept on which Telfer's method was based. An impressive work was conducted by Reid (1985) for the US Navy and consisted in embedding approximate models for ship resistance and propulsion systems in one of the first SPMSs based on microprocessor technology. To achieve this, sea trials and model tests were carried out for the sea barge clipper SS *Almeria Lykes* on which the SPMS was tested. Several parameters of the approximate models could be thence adjusted using adaptive algorithms from on-board measurements. Reid stresses the importance of an accurate measurement of speed through water data, obtained in his case by combining the log measurements with other estimates form propeller and speed over ground. Interestingly, he also discusses the importance of the data variability for adaptive algorithms to achieve accurate results.

Important advancements in hybrid models came also from the studies conducted at MIT by Abkowitz (see e.g. Abkowitz and Liu, 1988; Abkowitz, 1989) and in Berlin by Schmiechen (1991), who used similar algorithms to calculate propulsive and manoeuvring coefficients from full-scale trials.

More recently, Munk (2006) and Munk and Kane (2011) describe a commercial hull performance monitoring system based on a hybrid method and devoted to the detection of fouling effect. The papers foster the proposal of a compromise between automatic measurements and noon reports in the form of weekly observations conducted over a time of at least two hours of steady navigation in ideal conditions. The parameters of the approximated physical model need at least 10–12 observations to be defined and are said to stabilise after about 30–40 sets of observations, corresponding to the best part of a

year. Added resistance at design speed is used as a performance indicator and claimed to be as accurate as 1% with a deviation of about 3% from the mean value.

Leifsson *et al.* (2008) presented a hybrid approach to the operational optimization of a medium sized container vessel that combines Holtrop and Chan (1984) powering prediction, Isherwood (1973) wind resistance estimations and van Lammeren *et al.* (1969) propeller diagrams with feed-forward Artificial Neural Networks. The authors discussed the similar accuracy achieved by adopting a serial and a parallel approach in the combination of White and Black Box models. They eventually remarked Reid's findings on the importance of obtaining complete and accurate environmental measurements and of widening the variance of the parameters.

In a recent paper, Haranen *et al.* (2016) discussed different commercial performance modelling approaches at NAPA Ltd. The company uses a deterministic model, a Black Box solution based on Multivariate Adaptive Regression Splines, and a Generalised Additive Model implemented on simple powering predictions. The authors draw upon the challenges related to the data-driven approach, namely data variety, measurement independence and minimum data quantity. The importance of data quality, on which data-driven models mostly rely, was further stressed.

In an exhaustive comparative study of Machine Learning methods, Coraddu *et al.* (2017) demonstrated the performances of several approaches, namely the Regularised Least Squares, the Lasso Regression and the Random Forest methods as Black Boxes or Gray Boxes combined with Guldhammer's parametric powering estimation method. Measurements from the automatic on-board monitoring system of a Handymax tanker were used, with exclusion of wave data. The authors discussed the shortcomings of data-driven techniques at the same time praising the superiority of the Random Forest method over parametric powering prediction and other Black Box models. Speed through the water and propeller pitch were indicated as the most important variables in the prediction.

Similar conclusions were drawn also by Solonen (2016) and Jonsson and Fridriksson (2016), whilst a comprehensive description and comparison between White, Gray and Black Box approaches can be also found in Górski (2016).

The hybrid approach is the natural evolution of statistical methods in the wake of the modern technological advancements. Their capability of assessing the vessel performance with little outsourced information and good accuracy makes them the best competitor of deterministic performance, though not as versatile.

## 3.4 Commercial SPMSs

Spurred by the renewed interest in ship performance monitoring, several commercial SPMSs are currently available on the market. Broadly speaking, each SPMS is based on either of the above presented approaches and targets a certain level of accuracy de-

pending on its purpose and structure. Some of the most popular SPMSs are briefly introduced in this section based on the available published information.

***Napa.***—With a long standing ship performance expertise, Napa offers a wide range of ship performance monitoring solutions. A deterministic approach forms the basis of a ready-to-use SPMS, which is employed from early design stage onwards for a large array of purposes (e.g. feedback to the design, optimization of operations and performance monitoring). On-board measured data is then used to improve the deterministic predictions and change performance monitoring approach by using data-driven and hybrid techniques — respectively a Multivariate Adaptive Regression Splines model and a Generalized Additive Model. A more detailed description of Napa solutions is provided in Haranen *et al.* (2016).

***Eniram.***—This SPMS is based on a generic deterministic model comprehensive of several corrections. The comparison between the reference and the in-service performance is carried out 'as-is', i.e. correcting the reference curve to the actual in-service conditions. On-board data is then acquired by means of pre-existing measurement systems which may be eventually integrated by proprietary equipment. As soon as a sufficient amount of on-board data becomes available, the performance model is heavily improved by means of Bayesian regressions and other Machine Learning methods, producing one of the most popular commercial SPMS based on the hybrid approach. A description of Eniram's SPMS is found in Solonen (2016).

***Marorka.***—A proprietary deterministic approach forms the basis of a SPMS which is generally aimed at short-term performance analysis. The SPMS can be coupled to existing on-board instrumentation. Marorka appears to employ relatively coarse filters to exclude unwanted environmental and operational conditions from the performance analysis. Finally, statistical tools are used to provide estimations of the accuracy of the performance assessment. Two case study applications of this SPMS are presented in Jonsson and Fridriksson (2016).

***Japan Marine United Corporation.***—The already cited work by Orihara and Tsujimoto (2017) provides a description of one of the most comprehensive commercial SPMSs based on the deterministic approach. The system is based on the Taniguchi–Tamura method and applies several correction models (i.e. wind, waves, drift, yaw and steering resistance) to normalise the in-service performance. Strict filtering criteria are applied. The paper presents the SPMS in the assessment of an energy saving retrofit.

***NYK-MTI.***—A deterministic model similar to that of Japan Marine United Corporation is interpolated over a multi-dimensional space (speed, draft and trim) using B-splines. This approach then provides both the reference performance curve and corrects for disturbances the in-service measurements. More details are included in Kakuta

*et al.* (2016).

***Propulsion Dynamics.***—Munk (2006) and Munk and Kane (2011) describe this SPMS as based on a simple deterministic model which is refined over time by means of statistical tools. This SPMS is conceived much in the same fashion of Eniram's, which allows to classify it as a hybrid method.

***Enamor.***—In a similar way, Enamor's approach suggests the combined use of experimental and numerical tests (where available), which are to be integrated by empirical formulas to describe off-design conditions. The deterministic model thus obtained is then extrapolated to improve the interpolation of the vessel performance across multiple speeds, draughts and trim angles. The approximation of this multi-dimensional ship performance problem is achieved through NURBS hypersurfaces, which are defined by means of a Genetic Algorithm. More details about Enamor's SPMS are presented by Górski (2016).

***Kyma.***—In Hagestuen *et al.* (2016), a description is given of a SPMS based fundamentally on a statistical approach focused on the management of the big data produced by ship performance monitoring.

Albeit not exhaustive, the above brief descriptions show how the majority of commercial SPMSs are based on the hybrid approach. This may be explained by considering that, compared to a deterministic SPMS, hybrid SPMSs usually result in a relatively cheaper implementation (no CFD/EFD involved) and do not need a large amount of ship information (e.g. linesplan, propeller geometry, etc.).

## 3.5 The ISO 19030

In the previous sections, the Author attempted to provide the reader with an insight over the spectrum of performance monitoring solutions available to-date. The ISO 19030 (ISO, 2016) was conceived with in mind the standardisation of the general principles common to most of them for large commercial vessels. The introduction to the standard states that its aim is to

> "prescribe practical methods for measuring changes in ship specific hull and propeller performance and to define a set of relevant performance indicators for hull and propeller maintenance, repair and retrofit activities."

Even more so since in recent years several SPMSs have been privatised and their principles are kept confidential. Whereas the standard is neither mandatory nor regulatory, in its three parts the ISO 19030 defines:

I. general principles of hull performance monitoring and suitable indicators of dry-docking, in-service, maintenance, repair and retrofit performances of both hull and

propeller;

II. a 'default' method for performance monitoring with the relevant performance indicators and

III. alternatives to the default method.

An interesting feature of the document is the subdivision of measured parameters in 'primary' and 'secondary' in relation to the impact they have on ship performance. Hence, speed through the water and power belong to the primary whilst environmental and operational parameters to the secondary parameters list.

The data flow through a standard SPMS is therefore identified in the three phases of:

1. Data acquisition;

2. Data storage;

3. Data preparation.

The default method is fundamentally a deterministic system based on automatic and direct measurements of all variables (e.g. the shaft power must be measured with a torque-meter). Powering characteristics of the vessel should be made available by use of sea trials data, approved model tests or CFD simulations. The data is binned in batches of 10 min, and each batch filtered for outliers with Chauvenet's criterion (Chauvenet, 1863). The normalization is carried out following the ITTC (2014*a*) recommendations, with the exclusion of wave correction which is deemed too inaccurate for performance monitoring applications. The performance indicators are defined after dry-docking during reference periods of 3–12 months and are characterised by calm weather in standard deep-water conditions and steady state sailing (i.e. ideal conditions). The indicators are subsequently assessed during evaluation periods to detect fouling and other performance degradations. The standard suggests the use of speed loss as the performance indicator.

Alternative methods are also described that are generally considered to yield a lesser accuracy since they adopt proxies for the measurements of parameters (e.g. delivered power from fuel consumption). In addition, the standard draws from relevant literature estimates of the expected uncertainty of the SPMSs developed according to the guidelines of the standard.

Being in its early years of development, the ISO 19030 appears to lack certain aspects as yet. Firstly, measurements and corrections of the environmental effect on ship performance are loosely treated, if not omitted at all in the case of waves. No mention is then made of the difficulties in obtaining reliable speed through water measurements nor to variable cross-checking methods to assess the strength of ocean or tidal currents. Thirdly, the standard is aimed at a particular class of vessels, namely large commercial

ships fitted with fixed pitch propellers. Extending the standard to other categories would be certainly beneficial. In addition, the uncertainty values given in the analysis are derived from simulations of a likely SPMS, not from a real SPMS. Finally, the data filtering techniques can be improved by the introduction of more advanced statistical tools as the ones later proposed in this research.

If the standard cannot provide thus far complete guidelines on ship performance monitoring, it is however to be greatly credited with having set the basis for a promising definition of the features of the state-of-art SPMSs.

## 3.6 Uncertainty Analysis studies

A still under-explored area in the ship performance monitoring discipline is that of Uncertainty Analysis. It has already been mentioned that most contemporary SPMSs belong to private companies and consultancies, which more often than not are reluctant to share detailed information of their founding principles and uncertainties.

At the same time, a regulated approach to the estimation of uncertainty was introduced only after the 80's (see e.g. Coleman and Steele, 1989). These efforts resulted in the development of the Guide to the Expression of Uncertainty in Measurements, often referred to as GUM. This is the method currently adopted by the American Institute of Aeronautics and Astronautics (AIAA) and the ITTC (ITTC, 2014*b*). It assesses the uncertainty as it propagates through the mathematical relations of the variables.

Further advancements came with the standardisation of Monte Carlo Methods (MCM), which are instead based on an iterative random sampling from probability distributions assigned to the input variables. A detailed explanation of Uncertainty Analysis methods will be given in Chapter 6.

To the Author's knowledge, the first Uncertainty Analysis study associated with ship performance was conducted by Insel (2008). He applied the MCM to evaluate the uncertainty in sea trials measurement and analysis carried out according to ITTC specifications on 12 sister ships. All the measurements recommended by the ITTC guidelines were taken, with the primary variables being recorded automatically. Corrections to standard calm water conditions were carried out using Blendermann (1996) for wind; Havelock (1940) and Kreitner (1939) for waves; and the ITTC recommendations for shallow waters, displacement change and water properties. Much in the same fashion of the traditional approach given by Coleman and Steele (1989), Insel calculated separately:

a) Uncertainty of measurements and normalization

b) Uncertainty induced by weather and other random factors

Item (1) was calculated from MCM using representative data, whilst (2) from the direct observation of the spread of the $V_s$–$P_S$ curves of all 12 sister vessels. Results showed

that the combined uncertainty of these two factors amounted to a limit 7–9% in power and that MCM can be successfully applied in the complex field of full-scale propulsion estimation.

The greatest advancements in Uncertainty Analysis for ship performance monitoring has however to be credited to the work conducted over the years by Aldous (2016). In Aldous *et al.* (2013, 2015), the authors used a simulated ship performance model that embedded effects of the hull and propeller degradation and a virtual SPMS that included the effects of sensor errors (i.e. precision, bias and drift), model errors and sampling effects (averaging and sample size). In must be noted that the virtual measurements were not normalised, but only filtered. Uncertainty caused by normalisation was therefore not included in the analysis, nor it was that arising from human error. The papers explore the uncertainty difference related to the use of noon reports opposed to continuous measurement systems, reckoning that the uncertainty in power estimation is in the former case somewhat 90% higher than in the latter. A detailed sensitivity analysis shows that the larger impact on uncertainty depends from the goodness of the speed through water sensor, closely followed by draft and power measurements.

Very relevant is also the conclusion that an ultimate role is played by the performance model, that is, the model fit to evaluate the baseline of a performance indicator. This aspect is often underestimated in current SPMSs. As already stressed by Munk (2006), quality performance data can be obtained from the state-of-art measurement systems and from e.g. detailed normalisation procedures. However, if the baseline model is carelessly selected, the whole performance analysis will produce wrong results. For instance, Haranen *et al.* (2016) fitted a 2-nd order polynomial to the evolution over time of a hull degradation performance indicator, whereas an asymptotic behaviour is more realistic.

As expected, Aldous *et al.* (2015) also agreed with Insel's findings that, on the short term, precision errors contributes more prominently to uncertainty than bias and drift. Precision errors do however decrease over longer monitoring periods, whereas those caused by bias and drift obviously display the opposite trend. A point is also made that the use of normalisation procedures would significantly help reducing the total uncertainty, should the uncertainties of the corrections be kept to a minimum by their careful selection and application.

The researches on full-scale uncertainty analysis of vessel performance conducted by Lucy Aldous and Insel are two milestones that will be regarded as reference in this field for a long while. Nevertheless, some flaws can be identified in view of the assessment of the biofouling effect. Firstly, none of the studies carries out the uncertainty analysis on a working SPMS — Insel (2008) disposes of a simple measurement system whilst Aldous (2016) of a mathematical model and some real data. Further, the second study doesn't include a normalization method, whose uncertainty is therefore not assessed. In addition, both authors do not calculate the uncertainty of specific performance indicators,

limiting their analysis to $V_s$ and $P_S$. All of these aspects are fundamental for a SPMS that targets the effects of biofouling on the vessel performance and therefore more dedicated uncertainty analysis studies are needed.

## 3.7 Research rationale

The Author has hitherto attempted to provide the framework in which this study is set. In this section, he consolidates the reasons for the selection of the deterministic approach and for conducting this research based on this approach.

### *3.7.1 The adopted approach*

It has been shown that the relevant approaches to modern ship service performance monitoring are either deterministic, data-driven or hybrid. Despite being able to achieve comparable accuracy, all three of these methods have benefits and drawbacks and all require relevant expertise to apply.

Machine Learning methods are easy to be implemented on-board and can reach good levels of accuracy without any need for physical or external knowledge. However, tuning the statistical parameters to avoid model overfitting is not in the least a simple task (Coraddu *et al.*, 2017) and requires its in-depth knowledge. On the other hand, these methods normally need several months of on-board recorded data, as reported e.g. by Haranen *et al.* (2016) and Górski (2016).

Hybrid methods are superior, because the base physical knowledge already entails an approximate representation of physics and thus the freedom of the employed Machine Learning technique is more restrained. Nevertheless, the accuracy of both methods excels only within the boundaries of their training data set (Coraddu *et al.*, 2017). Moreover, they heavily rely on the on-board data quality, consistency and variety, the latter of which is often the most challenging to obtain since ships normally sail at a fixed RPM, power or speed. The major consequence is that Black and Gray Box models are prone to suffer from multicollinearity and variable confounding (Leifsson *et al.*, 2008; Haranen *et al.*, 2016; Górski, 2016). This happens when a parameter is wrongly identified as causally related to another, generating a spurious correlation between the two.

In contrast, accurate deterministic methods may require, in various degrees, technical information that is at times not easily accessible and may require a reasonable investment of resources. However, SPMSs based on a detailed deterministic approach can be used immediately after their on-board implementation and are more suitable than the other two methods for the analysis of on-board measurements collected over shorter periods (Haranen *et al.*, 2016).

By definition, deterministic methods are also transparent, thus the model and all

the data used can be inspected, validated and extracted at any time. Therefore, it is possible to utilise the deterministic SMPS itself to validate corrections, to provide feedback to earlier design stages, verify performance predictions and obtain additional physical information to aid further design or operational investigations. Since the accuracy of the deterministic methods naturally does not change over time, their use is also suited to long term studies, such as fouling assessment on ship hulls. The scope of their possible applications is thus wider, e.g. ranging from long term monitoring, short-term retrofit analysis (e.g. Carchen *et al.*, 2015), to the validation of performance prediction techniques (e.g. Atlar *et al.*, 2018).

Another factor taken into account in this research was the limited sailing time of Newcastle University's R/V (an estimated 15% of the total time over a year). This would certainly hamper the accuracy of a Machine Learning-based SPMS over the short length of a 3-year project.

Within the above framework, despite the economical advantages often fostered by the Machine Learning methods, a deterministic method is preferred as the basis of the Ship Performance Monitoring System developed in this study.

### *3.7.2 Motivation and novelty of the study*

From the literature hitherto presented, it appears that only few state-of-art studies involve the use of a working deterministic SPMS purposely implemented for hull and propeller performance monitoring. The majority of the attempts in the literature either targets a more general assessment of vessel performance (thus aiming at looser uncertainty levels), or analyses data recorded with pre-existing on-board measurement systems. In this framework, the following knowledge gaps are evident:

- The application of a normalisation procedure for environmental and/or operational factors, which affect the hydrodynamic performance of a vessel, often appears to be somewhat of a subjective matter. The reasons behind the selection of either of the correction methods are seldom clarified and almost never are the normalization uncertainties and limits detailed. This evidently carries the danger of employing a normalisation procedure that adds noise to the data rather than reducing it.

- It follows that the types and quality of on-board sensors rarely reflects the needs brought forward by the chosen normalisation procedure — as it should ideally be. Due to practical reasons, the opposite is often happening at the expense of the quality of the performance assessment.

- The importance of handling the large data generated with modern automatic measurement systems is underestimated in traditional deterministic methods, adding

to the reduced data quality for the analysis. An investigation on suitable raw data handling methods needs as yet to be carried out.

- Most existing SPMSs employ exclusively power-based Key Performance Indicators, whose reference baseline is often obscure and which does not provide a detailed information regarding the cause of performance loss.

- To date, a complete, published Uncertainty Analysis on a working SPMS has never been conducted.

- Applications of SPMSs pertain almost exclusively to large commercial ships. Thus, the possibilities and uncertainties related to small vessels installations are mostly unknown.

To the best knowledge of the Author, this study is the first published deterministic ship performance monitoring application that attempts to take into account all of the aspects above in the design and implementation of a working SPMS and analysis method devoted to the assessment of biofouling effect on the hull and propeller performance.

## 3.8 Summary

After a general overview, the Author presented in this Chapter a comprehensive literature review of the efforts devoted to overcome the challenges of ship performance monitoring (**Objective A** and **B**). Firstly, he considered the existing SPMSs, grouped in reason of their underpinning performance modelling methods. Secondly, he attempted to outline the recent ISO 19030, viewed as the joint effort of several parties to standardise the assessment of the hull and propeller hydrodynamic performance. A review was also given of the research devoted to the estimation of uncertainty in ship performance monitoring. Finally, he justified the choice of the traditional deterministic method as the core of the presented SPMS, underscoring the motivation of the current study under the perspective of the state-of-art technology.

# CHAPTER 4

# Methodology

## 4.1 Introduction

In this Chapter, the methodology adopted to achieve the objectives laid out in Chapter 1 and justified in Chapter 3 is presented (**Objective B**). In doing so, Section 4.2 describes the principles that must be adopted in the design of a deterministic SPMS. Methods and equations to normalise (correct) the measured in-service performance for the external disturbances are discussed in detail to define the characteristics of the SPMS.

Thereafter, a full description of the proposed deterministic SPMS follows (**Objective C**). Section 4.3 deals with the measurement system in the framework of the requirements set forth by Section 4.2. At first, the concept of vessel-specific time constant is introduced and its derivation from first principles is described. Each variable necessary or useful for the performance assessment is considered and a range of suitable sensors is examined to measure it. The general principles of on-board signal communication and data logging are also presented. At last, the concept of 'datapoint' is introduced. Section 4.4 tackles all the steps necessary to prepare the data for normalisation and performance analysis, starting with the identification of steady-state periods and of sailing in conditions suitable for performance monitoring and following with the management of data outliers and the validation of critical measurements. Section 4.5 describes the adopted normalisation process after a brief introduction of existing deterministic procedures currently validated and in use with ship performance monitoring practitioners. Finally, Section 4.6 presents the proposed long term performance analysis method with a detailed description and derivation of four novel KPIs (**Objective D**). The Section also describes a new method to estimate the frictional coefficient increase, $\Delta C_f$, from the available performance data. A summary of the findings is presented at the end of the chapter.

Figure 4.1 summarises the performance monitoring process as it will be described, showing the data flow through the complete SPMS, from the on-board measurements to the derivation of in-service performance.

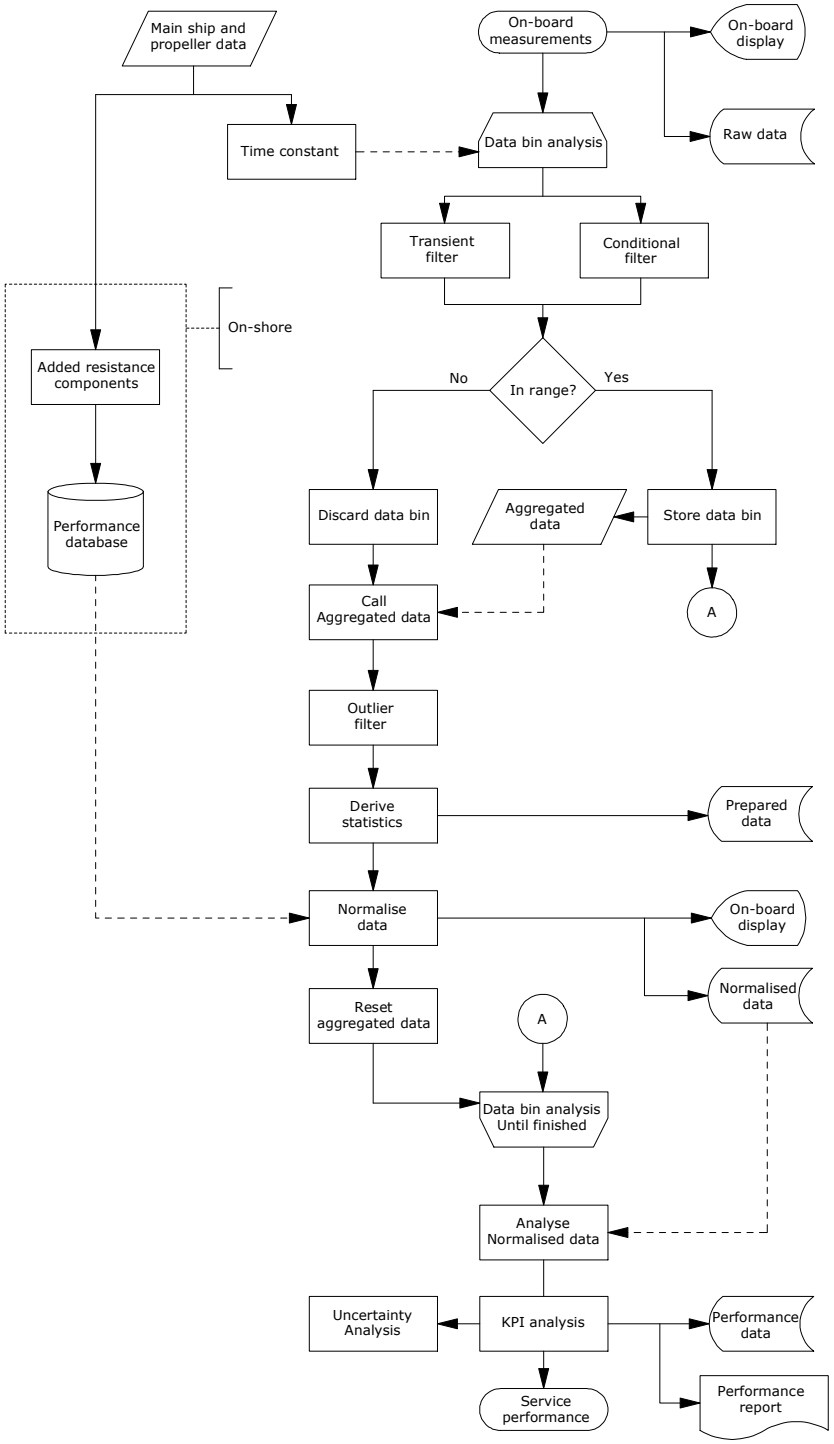


**Figure 4.1** – *Representation of the data flow through the SPMS.*

## 4.2 Design of the deterministic method

The most critical part in employing a deterministic approach for monitoring the performance of a ship is deciding upon the normalization procedure to adopt. In other words, it should be assessed which correction is worth applying to $R_{add}$ and to what extent. Corrections ought to be accurate to avoid the introduction of greater errors in the data, which happens for instance when a correction is used outside its validity. However, from a more practical point of view, corrections must also be designed to be viable and convenient at the same time. In principle, one could find accurate corrections for all possible combinations of disturbances, but it might not be practical to employ the resources required to obtain them. Certain disturbances will be corrected for or they will be sufficiently small to be ignored. Others will instead require a normalization neither accurate nor convenient, and therefore a stricter filtering criterion will need to be devised. Chapter 1 has already stressed the importance of finding the optimal balance between correcting and filtering, which should seek to reduce the data scatter without drastically reducing the sample size. The initial phase in the design of a deterministic SPMS must therefore be an assessment of the chosen normalization procedure to determine its limitations and viability.

### *4.2.1 Added resistance components*

Chapter 2 introduced the factors affecting the ship performance by describing their driving phenomena and briefly mentioning their effect on the ship. It was noted how during manoeuvres of any kind the performance equations (2.17) are altered so as to make monitoring of the ship performance inconsistent and not recommended. It was also reviewed that, apart from biofouling and roughness, those worth considering for correction in ship performance monitoring are:

- Direct wind resistance, including the effects of changes in air properties;
- Added wave resistance;
- Currents;
- Restricted waters;
- Change in water properties;
- Change of displacement;
- Change of static trim;
- Steering;
- Drift and yaw.

In the following sections, these factors and their possible corrections will be discussed.

**Winds**

Chapter 2 has already introduced the effect of winds on ship performance as causing direct and indirect resistance components. Depending on the wind direction, direct wind resistance can oppose the ship's forward motion or favour it. In the former case, it is not uncommon that wind resistance will account for even up to 20% of the total ship resistance (Kent, 1959). The time-averaged direct wind load in surge direction may be represented e.g. in the form proposed by Blendermann (1996):

$$\overline{R}_{AA} = 0.5\rho_A U_{AR}^2 C_X(\mu_{AR}) A_L \tag{4.1}$$

with $\rho_A$ being the air density, $U_{AR}$ the relative wind speed and $A_L$ is the projected lateral plane area of the vessel's superstructure. $C_X$ the wind resistance coefficient in surge direction, which is function of the relative wind bearing $\mu_{AR}$ (0 deg is head wind). Note that since this equation uses the relative wind direction, it incorporates both air and wind resistance. The air resistance can be subtracted from the calculation in a similar way, for instance:

$$\overline{R}_{AA0} = 0.5\rho_A V_g^2 C_X(0) A_L \tag{4.2}$$

Where $V_g$ is the ship's speed over ground. The wind resistance coefficients depend upon the shape of the vessel's superstructure and the size and distribution of its area exposed to the wind. Because of this, the maximum of the direct wind resistance is normally for winds coming from 20–30 degrees off the bow (Fig. 4.2). The wind speed measured on board needs to be corrected for the natural wind profile (see eq. (2.19)) according to the equation (ITTC, 2014*a*):

$$U_{AR}(Z) = U_{AR}(z)\left(\frac{Z}{z}\right)^{\frac{1}{7}} \tag{4.3}$$

where $U_{AR}(z)$ is the relative wind speed measured at the anemometer height $z$, and $Z$ is the wind reference height, which is the height at which the flow velocity is measured when obtaining $C_X$.

Assuming the air a mixture of ideal gases, its density $\rho_A$ depends upon the dry air pressure $p_d$, the vapour pressure $p_v$, the air temperature $T_a$ and the two specific gas constants for dry air and vapour $R_d$ and $R_v$ respectively. Therefore:

$$\rho_A = \frac{p_d}{R_d T_a} + \frac{p_v}{R_v T_a} \tag{4.4}$$

The vapour pressure is related to the relative humidity $RH$ by the equation:

$$p_v = RH\, p_{sat} \tag{4.5}$$

where $p_{sat}$ is the saturation vapour pressure, which is directly related to $T_a$. Because the absolute measured air pressure is defined as $p_a = p_d + p_v$, it naturally follows that $\rho_A$ can

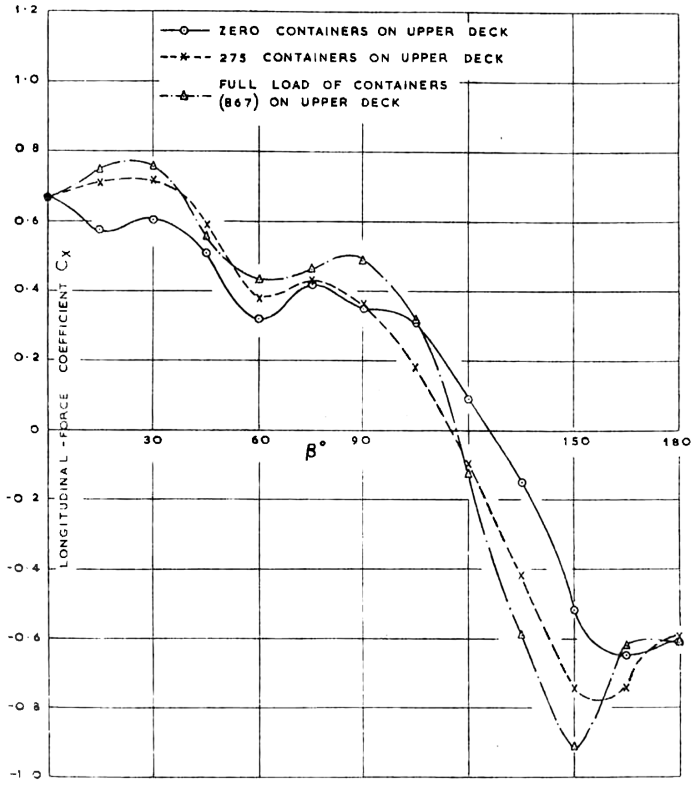


**Figure 4.2** – *Longitudinal force coefficient $C_X$ for varying relative wind direction off the bow for a container ship in different deck-loading conditions [Source:Ponsford (1978)].*

be easily calculated by measuring $p_a$, $T_a$ and $RH$. On the other hand, the impact of air density is small, which makes its calculation of secondary importance.

The wind resistance coefficient in surge direction can most accurately be derived by means of wind tunnel tests or relatively simple CFD simulations. Systematic experiments and regressions are also available in literature for certain common ship classes (e.g. Aage, 1971; Ponsford, 1978; Blendermann, 1996; van den Boom *et al.*, 2015), but their type, shape, and outfitting must be very carefully assessed against that of the database (ITTC, 2014*a*). Hasselaar (2011) stresses the importance of obtaining an accurate estimate of $C_X$, which is the principal source of uncertainty in the wind resistance estimation after the wind speed. As it can be seen in Fig. 4.2, even a different deck load configuration implies significant changes in the longitudinal force coefficient. A similar reasoning applies to the different loading condition on tankers and cargo vessels, which normally cause dramatic alterations in the above water hull shape. Usually, different $C_X$ are obtained for laden and ballast loading, where for intermediate loading conditions linear interpolation may be used (Hasselaar, 2011). Where the ship shape is unique or less common (tugs, supply vessels , etc.), it is recommended to conduct dedicated experimental or numerical wind tunnel tests.

The transverse action of the wind also induces change of heel angle and of ship course,

which forces the crew or the autopilot to the use of rudder. The water–hull interaction resulting from this effect cause the wind induced drift, yaw and steering and their relative forces which were introduced in Chapter 2. The indirect wind resistance is more difficult to evaluate particularly due to coupling with water disturbances, and it will be treated in the following paragraphs.

**Waves**

The effect of waves may well be considered the most challenging to evaluate due to two reasons — the complexity of the hydrodynamic interaction between the ship and the water and the difficulty of obtaining complete and accurate measurements of the encountered seaway.

The involuntary performance losses caused by sailing in rough seas may thus be considered formed by:

1. Added resistance.

2. Reduction of the propulsive efficiency, caused by alterations in the ship effective wake.

In addition to these effects, the seaway induces the ship to drift and yaw, forcing the use of the rudder to keep the intended course. Drifting, yawing and steering produce additional resistance that will be discussed separately.

In general, when strong non-linear forces (e.g. slamming) are absent the mean added wave resistance in irregular waves can be described by superposition of the directional wave spectrum and the mean added wave resistance in regular waves, both functions of the wave encountering frequency $\omega_e$ and the relative wave heading $\mu_R$ ($\mu_R = 180\,\text{deg}$ is head waves):

$$\overline{R}_{AW} = 2 \int_0^{2\pi} \int_0^{\infty} S_\zeta \frac{R_{AW}}{\zeta^2} \, \mathrm{d}\omega_e \mathrm{d}\mu_R \tag{4.6}$$

where $S_\zeta$ is the directional spectral density ordinate defined in eq. (2.20), $R_{AW}$ is the added wave resistance in regular waves and $\zeta$ the wave amplitude. The encountering frequency in deep waters is defined by the fundamental equation:

$$\omega_e = \omega - \frac{\omega^2 V_s}{g} \cos \mu_R \tag{4.7}$$

where $\omega$ is the wave frequency, $V_s$ the ship speed through water and $g$ the gravitational acceleration. A mean nondimensional added wave resistance transfer function in regular waves may also be defined as follows (Bhattacharyya, 1978):

$$\sigma_{AW} = \frac{R_{AW}}{\rho g \zeta^2 \frac{B^2}{Lpp}} \tag{4.8}$$

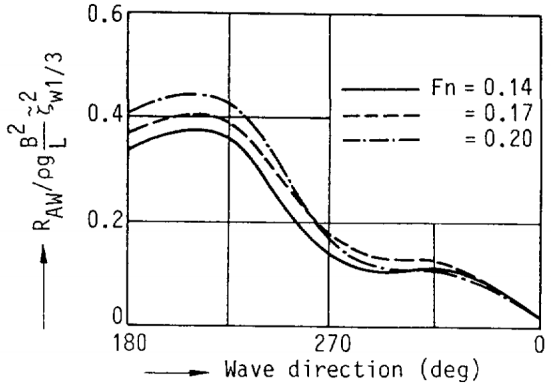


**Figure 4.3** – *Influence of wave heading on Added Wave Resistance transfer function [Source:Blok (1993)].*

where $\rho$ is the water density, $B$ and $L_{pp}$ the ship breadth and length b.p. respectively. For a general hullform, the added wave resistance is greater when the ship sails in head waves, and is maximum with waves in the bow quarter (Blok, 1993, see Fig. 4.3). Stern quartering and following seas cause smaller added resistance, but significantly affect the propeller inflow and might cause severe yaw and even broaching.

Several approximated methods exist to evaluate the added wave resistance. The ITTC proposes the two semi-empirical methods developed within the STA–JIP (van den Boom *et al.*, 2015) and the theory proposed by Maruo (1960). All three methods are quick and inexpensive to implement, but their accuracy is confined to certain hull shapes and a very limited range of Froude numbers and wave headings (Bertram, 2016). Towing tank tests certainly deliver the most accurate results and are thus employed whenever possible (ITTC, 2014*a*). Several seakeeping studies have been conducted based on towing tank tests, among which the most relevant to this study may be those by Wahab *et al.* (1971); Faltinsen and Helmers (1991); Wellicome *et al.* (1995, 1999); Fang *et al.* (1996) and Bouscasse *et al.* (2013). However, the literature witnesses that seldom the large seakeeping tanks that have the capability of testing the models with several wave directions are available. Moreover, the time and the investment required to run the full spectra of seakeeping tests (i.e. ship loading, speed, wave directions and frequencies, etc.) cannot often be justified in the framework of commercial ship performance analysis. As a consequence, the experiments are mostly conducted in head or following waves to match the capabilities of the more common towing tanks and, where they are available, they are used to assess and calibrate their numerical counterpart (see e.g. Bruzzone *et al.*, 2009).

A similar reasoning applies to complex computational techniques as the unsteady Reynolds Averaged Navier-Stokes (RANS) simulations (see e.g. Castiglione *et al.*, 2011; Tezdogan *et al.*, 2015), which are rapidly gaining popularity with the ever-increasing

availability of computational power and the resulting accuracy. However, the expertise and computational resources required for the set-up and run of systematic CFD seakeeping simulations are at the time of writing not yet commercially justifiable. Therefore CFD often serves a similar purpose to that of Experimental Fluid Dynamics (EFD).

Less demanding numerical calculations are available since the late '50s with the introduction of the strip theory (Korvin-Kroukovsky and Jacobs, 1957). In this classic method, the three-dimensional seakeeping problem is reduced to a discrete number of two-dimensional 'strips' (i.e. transverse sections) having no interaction with each other. The total forces will therefore be obtained by integration of the two-dimensional forces over the length of the hull. In analogy with earlier theories, the strip theory usefully considers $R_{AW}$ as formed by two components — wave radiation and wave diffraction. The effects of wave radiation is generally greater than that caused by diffraction. However, at the higher encountering frequencies (waves shorter than approx. half ship length) wave diffraction is the predominant component (Fig. 4.4). Steen and Faltinsen (1998) remark that the influence of small waves on slender hulls is significant down to wave-to-ship length ratios of 1%. Because ships tend to sail predominantly in waves relatively small compared to their size, the diffraction component must not be ignored. The advantages of the strip theory are down to the quickness of calculation and its applicability to a wide variety of hullforms. However, it is also known to present several shortcomings in the calculation of the diffraction effect, with consequent inaccuracies at higher Froude numbers, oblique seas and at the higher encountering frequencies (Faltinsen *et al.*, 1991; Söding, 2006; Bertram, 2016). Other more advanced methods, like 3D panel methods, Rankine Singularity methods (Park *et al.*, 2016; Shigunov, 2017) offer more accurate solutions still at affordable computational time, but care still needs to be used in interpreting predictions of the motions and added wave resistance for oblique seas and at low Froude numbers (van den Boom *et al.*, 2015; Bertram, 2016). These latter methods however appear to be the best compromise solution to compute the added wave resistance with reasonable resources and good results (Bertram, 2016), provided that for non-conventional hulls an assessment of a few conditions is made by means of EFD or CFD.

The effect of waves on the self-propulsion factors was investigated e.g. by Nakamura and Naito (1975); Faltinsen *et al.* (1980) and Ueno *et al.* (2013), who found that, whereas the thrust deduction factor isn't much affected, the wake field tends to accelerate for increasing wave height. All results identified the pitch motion as the principal responsible. However, Nakamura and Naito (1975) also showed that in irregular waves, the change in wake is not as remarkable as in regular waves and tends to the still water value. The study conducted by Taskar *et al.* (2016) combined previous wake analysis methods to estimate the change of inflow velocities at the propeller for various combinations of wave heights, periods and directions. A worst-case change in the effective wake of about 10% was estimated for stern quartering and following waves (Fig. 4.5). These studies conclude that

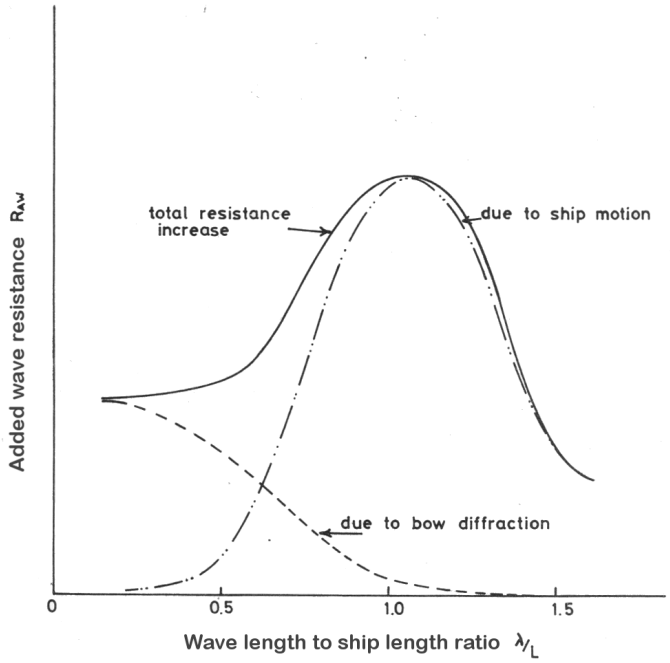


**Figure 4.4** – *Wave radiation and wave diffraction components for a general hullform, after BSRA (1981).*

the effect of ship motions and indirectly of waves on the inflow velocities at the propeller cannot be neglected. However, it is very difficult to estimate it accurately without help of CFD tools and it is therefore recommended to avoid applying any correction for it.

On the other hand, an added wave resistance estimation should be used to correct for the effect of waves — if it is of proven accuracy. The evaluation of added wave resistance in head seas for a limited number of loading conditions (e.g. full-load and ballast) is feasible and not excessively expensive. According to the Author's experience, the use of modern numerical panel methods or advanced modified strip theories to obtain head waves predictions only and the application of a directional filter is a sensible and practical choice that improves the data quality and requires limited resources. Other conditions, including those where strong non-linear effects become prominent, must be filtered out. Where other and more comprehensive means can be used, they shall be employed as per their availability.

### Currents

As discussed in Chapter 2, the consequence of a current on ship performance may be practically described as the difference between speed through water and speed over ground and a change in the ship's attitude due to the distorted water flow around the hull. In these terms, the elimination of the first effect is entrusted to the measurement system (i.e. to the speed log), whilst the second is considered separately. The drawback of this approach stands in the reliability of the speed log measurements, which has long been

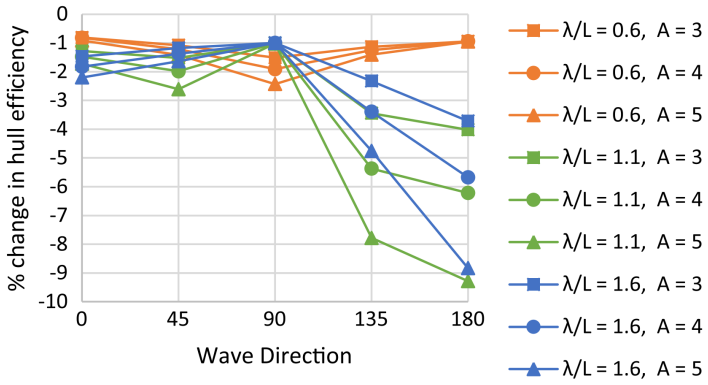


**Figure 4.5** – *Change in hull efficiency $\eta_h$ for the KVLCC2 hull due to waves with varying wave length to ship length ratio $\lambda/L$ and amplitude $A$ in m. Since the thrust deduction factor is assumed constant, the change in hull efficiency is here equal and opposite to the change in wake [Source: Taskar* et al. *(2016)].*

object of great debate amongst practitioners of ship performance monitoring (see e.g. Townsin *et al.* (1975)) and that will be treated in the next section.

### Restricted waters

It has already been discussed how shallow water affects several resistance components — namely viscous and wave resistance. It was also described how the reduced amount of water under the hull produces an accentuated sinkage that also contributes to increase the ship's resistance.

The ITTC suggests the use of the known correction method developed by Lackenby (1963) for the analysis of speed trial data (ITTC, 2014*a*). However, as Lackenby's method is based on little and obsolete experimental data, a new study was conducted by Raven (2016). In this new method, all the three components of ship resistance affected by shallow waters were analysed separately by means of RANS solvers, ensuring a better agreement with sea trials data of several ship types.

No reliable method exists however to correct for the changes occurring to self-propulsion factors. For this reason, since ships do sail in deep waters during performance monitoring, speed correction for shallow waters should be avoided as it is also implied by the ISO 19030 (ISO, 2016).

### Changes in water properties

According to the ITTC (2014*a*), the effects of changes in water density $\rho$ and kinematic viscosity $\nu$ are calculated:

$$R_\rho = R_{T0}\left(1 - \frac{\rho}{\rho_0}\right) - R_f\left(1 - \frac{C_{f0}}{C_f}\right) \tag{4.9}$$

where $C_f$ and $C_{f0}$ are the frictional resistance coefficients for actual and reference water properties respectively; $R_{T0}$ is the total resistance in ideal conditions; $R_f$ is the frictional resistance in actual waters; $\rho$ and $\rho_0$ are the water densities respectively in actual and ideal conditions (normally 15°C and density of 1025 kg/m$^3$).

The water density $\rho$ can be related to the water temperature $T_w$ and its salinity $S_A$ for instance by the one-atmosphere seawater equation of state developed by Millero and Poisson (1981), which is in the form:

$$\rho = \rho_{fw} + A\,S_A + B\,S_A^{1.5} + C\,S_A^2 \tag{4.10}$$

where $\rho_{fw}$ is the pure fresh water density and $A$, $B$ and $C$ are polynomial functions of $T_w$.

In a similar way to density, the kinematic viscosity $\nu$ can be calculated according to the regression given, for example, by Isdale *et al.* (1972):

$$\nu = \frac{\mu_{fw}}{\rho}\left(1 + A\,S_A + B\,S_A^2\right) \tag{4.11}$$

where $\mu_{fw}$ is the pure fresh water dynamic viscosity and $A$ and $B$ two polynomial functions of $T_w$.

The correction here presented is relatively accurate and easy to apply. However, the effect of changes in water quality is generally of very modest entity for ships sailing always in the same areas due to the limited variation of water density and viscosity during the year (see Chapter 2). Moreover, a relatively accurate measure of the vessel's wetted surface needs to be given. To avoid introducing further uncertainty in the data, one could restrain from correcting for the change in water density and limit the correction to the change of viscosity only (Hasselaar, 2011), e.g.:

$$R_\nu = -R_f\left(1 - \frac{C_{f0}}{C_f}\right) \tag{4.12}$$

In other cases, it may be decided to entirely discard this correction if the relative added resistance is proved to be negligible and the uncertainty of the correction would risk to be larger still.

### Change of displacement

For changes in displacement of up to 5% of the ideal value and where the waterline does not intersect areas of the hull with dramatic shape changes (e.g. in proximity of a bulbous bow), the change in the self-propulsion factors and particularly the wake field is negligible and the change in resistance can be estimated by the well-known relation (van den Boom and Hasselaar, 2014; ISO, 2016):

$$R_\Delta = \left[1 - \left(\frac{\Delta_0}{\Delta}\right)^{\frac{2}{3}}\right] R_T \tag{4.13}$$

where $R_\Delta$ is the resistance increase due to displacement change, $\Delta_0$ is the displacement in ideal conditions and $R_T$ the measured total resistance.

For displacement variations greater than 5% or when the hull shape changes greatly (e.g. between laden and ballast condition of most tankers) it is recommended to conduct dedicated EFD or CFD tests. For instance, Hasselaar (2011) and Kakuta *et al.* (2016) suggests to carry out systematic experimental or virtual towing tank tests on a range of loading conditions from which to extrapolate the resistance and self-propulsion factors for the relevant fractional displacement. In principle, this is by far the optimal solution since interpolation between a few draughts 'far' from each other (e.g. ballast and laden) can be quite risky (Krapp and Bertram, 2016; Krapp and Schmode, 2017). However, seldom will the shipowner be ready to invest much resources in such an intensive testing campaign. Depending on the operational profile of the vessel and on the available data and resources, an alternative solution would be to conduct self-propulsion tests for only one or two relevant loading conditions and use performance monitoring data only relative to such draughts. This would necessarily mean to discard all the data measured with the ship having a different draught. Whereas the data quantity may be reduced, it would still be a very good solution for ships sailing mostly with these draughts, e.g. tankers and bulk carriers.

On the other hand, a displacement change within the above limits, produces but a negligible effect on the wake fraction, as reported by Harvald (1983).

#### Change of static trim

Changes in trim greatly affect the ship performance and in proportion more than a change of displacement. An example reported by Hasselaar (2011) shows that for a 2400TEU container vessel sailing at a speed of just over 22kn, the power needed at ballast draught (5.75m) is about 31% lower than at scantling draught (11.4m), but only 11% lower than at design draught (10.1m). The author concludes that the nonlinearity of these measurements are due to the abrupt change in shape of the underwater hull, to which the trim of the ballast draught heavily contribute.

The most accurate and only means of calculating the effects of trim changes on ship performance is to carry out systematic towing tank experiments similar to those described above. To date, no alternative reliable correction exists. It is therefore recommended to avoid correcting for trim changes if systematic tests cannot be conducted (ISO, 2016; Krapp and Schmode, 2017).

#### Steering

According to many manoeuvrability models, the steering resistance can be described as a function of the normal force acting on the rudder and the helm angle. For example

the model developed by the Japanese Maneuvering Modeling Group, the so-called MMG model (Ogawa *et al.*, 1977), defines it as:

$$R_\delta = -(1 - t_R) F_N \sin\delta \tag{4.14}$$

where $F_N$ is the rudder normal force and $t_R$ the steering resistance deduction factor. The rudder force is expressed:

$$F_N = 0.5\rho A_R \left(u_R^2 + v_R^2\right) f_\alpha \sin\left[\delta - \tan^{-1}\left(\frac{v_R}{u_R}\right)\right] \tag{4.15}$$

where $A_R$ is the rudder area, $f_\alpha$ the lift coefficient, $u_R$ and $v_R$ respectively the longitudinal and transverse components of the rudder inflow velocity. The difficulty lies here in the correct estimation of the rudder inflow velocity, which involves use of several experimental constants obtained through dedicated manoeuvrability tests (Molland and Turnock, 2002). Alternatively, the constants may be very carefully selected from databases in the literature or even waived by approximating the velocities at the rudder with the forward and athwart ship velocities $u_s$ and $v_s$. It must be noted that the sensitivity of the manoeuvring derivatives dictates use of the utmost care in the choice of the derivatives.

To investigate in detail the effect of steering resistance and different methods to calculate it, a 2-Degrees Of Freedom (DOF) manoeuvrability program described in Carchen *et al.* (2016) was employed to simulate two course-keeping manoeuvres on a representative vessel. Figures 4.6 and 4.7 show the variables' history during zig-zag course-keeping manoeuvres respectively with 3 deg and 5 deg helm angles respectively. The direction of the first turn (i.e. to port or starboard) does not change significantly the overall results, thus Fig. 4.6 was chosen to show a starboard turn, Fig. 4.7 a port turn. The results show that for $\delta = 3\,\text{deg}$, the relative steering resistance $R_\delta/R_T \approx 0.01$ at most. For $\delta = 5\,\text{deg}$, the relative steering resistance is higher at $R_\delta/R_T \approx 0.03$. They also show that in the coarsest assumption (i.e. when $u_R \approx u_s$ and $v_R \approx v_s$) approximating $R_\delta$ with $R_{\delta\,proxy}$ leads to very large errors in the estimation of the steering resistance. The estimated resistance is sometimes more than 10 times greater than the real rudder resistance.

Whereas the above simulation was conducted on a representative cargo vessel, the proportion of the steering resistance does not greatly deviate, for other types of vessels, from the one shown. Considering that $R_\delta$ is quite small, the Author agrees with Hasselaar (2011) on the dubious usefulness of correcting for the steering resistance in the framework of ship performance monitoring.

### Drift and yaw

To describe the drift and yaw a detailed overview of the components of ship velocity needs to be given. Figure 4.8 shows the relations between vessel and water surface motion. The drift of the vessel over the ground may be practically considered as having two components,

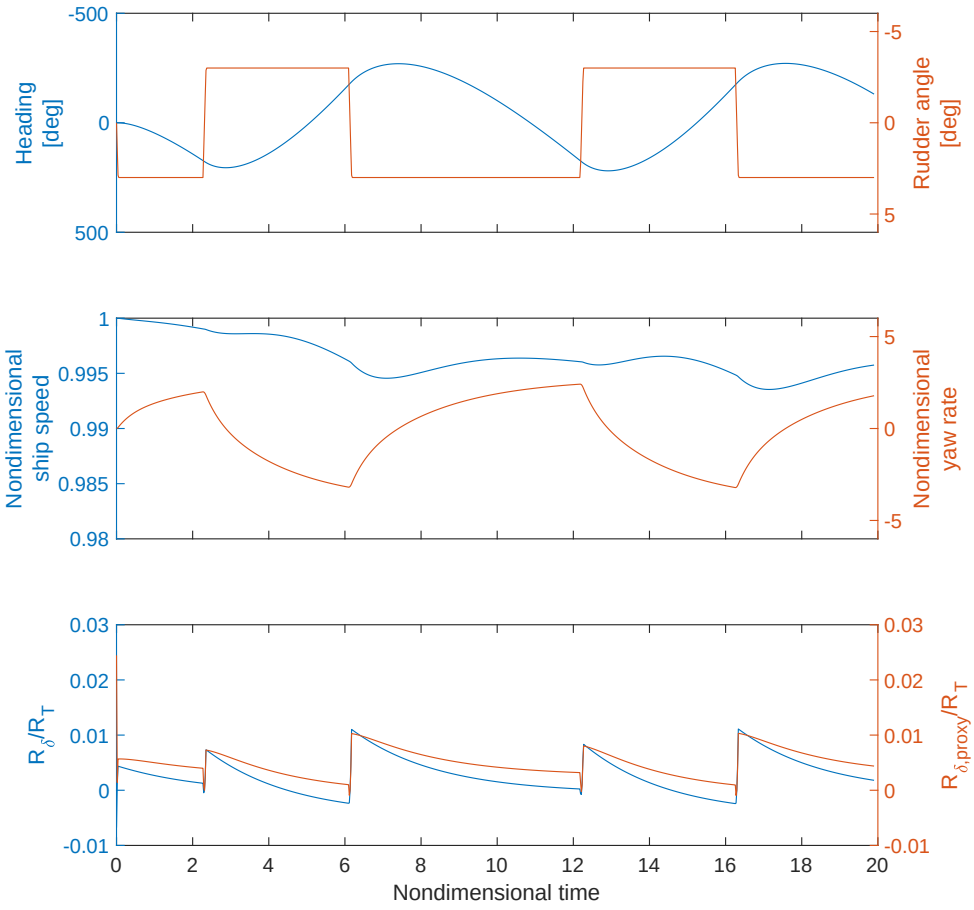


**Figure 4.6** – *Effect of a* 3deg *rudder angle in a starboard zig-zag manoeuvre on the total resistance.*

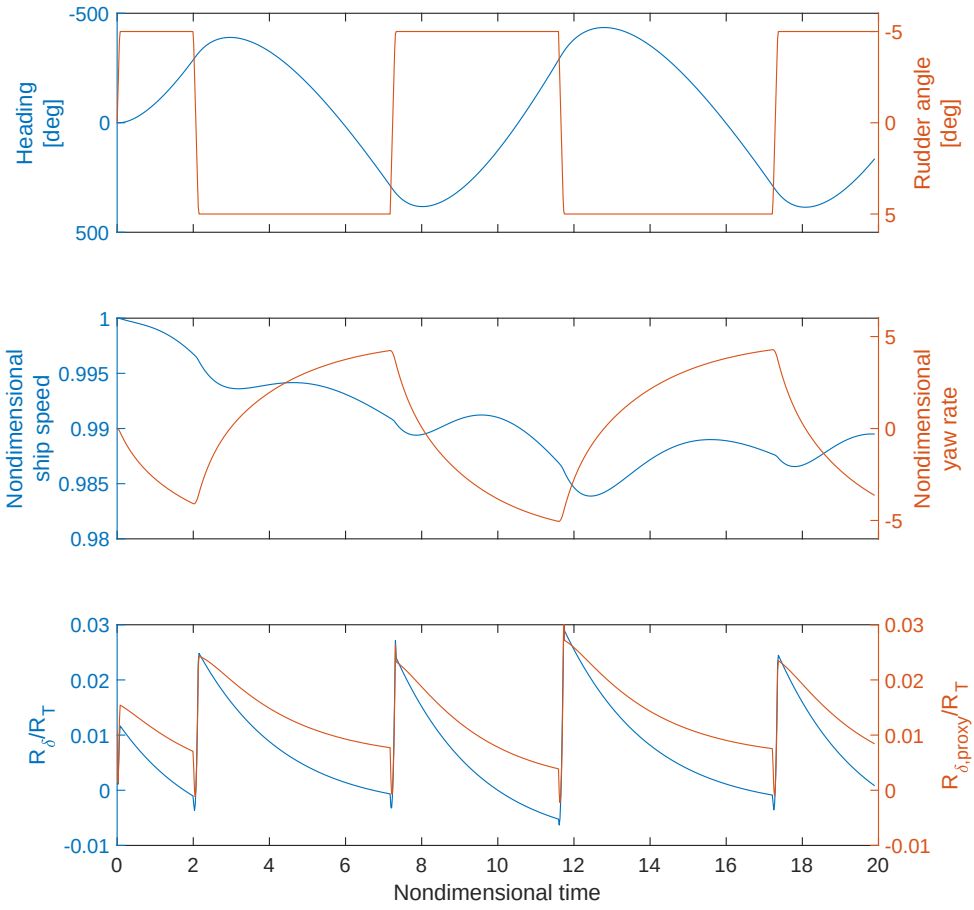


**Figure 4.7** – *Effect of a* 5deg *rudder angle in a port zig-zag manoeuvre on the total ship resistance.*

namely the drift caused by winds, waves and manoeuvring, otherwise referred to as 'leeway drift' ($a$) and the surface current drift ($b$). Provided that a good measurement of the speed through water $V_s$ is available, only $a$ is relevant because it alters the water flow around the hull and propeller. Drift motion is often complemented by yaw motions due to the unbalanced hydrodynamic side forces and steering to keep the intended course (see Chapter 2 and the Winds and Waves sections in the present chapter).

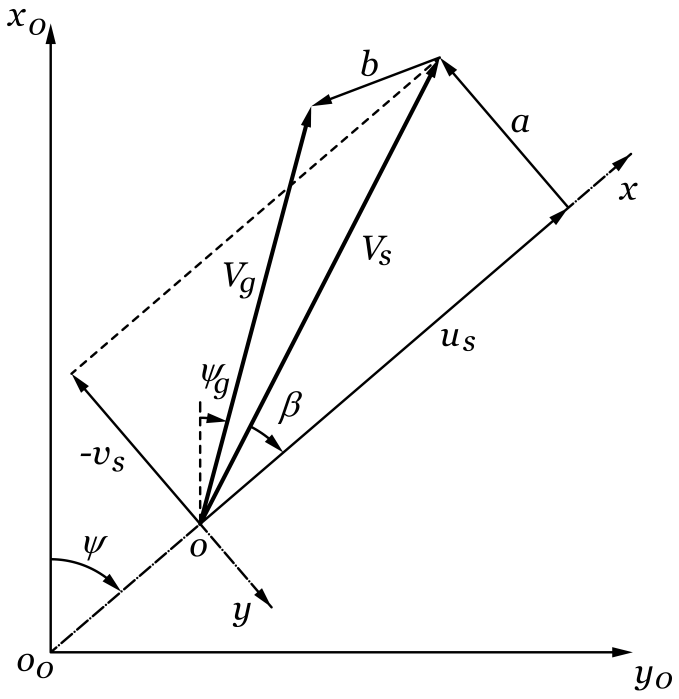


**Figure 4.8** – *Components of vessel speed: $V_s$ is the speed through water; $V_g$ the speed over ground; a ship drift; b the surface current velocity. $\beta$ the drift angle; $\psi$ the vessel heading; $\psi_g$ the course over ground.*

Drift and yaw produce coupled resistance components on the hull, which, again in the manoeuvring terms of the MMG model, can be typically expressed as:

$$R_{\beta,\dot{\psi}} = 0.5\rho L_{pp} T_M V_s^2 \left( X'_{\beta\beta}\beta^2 + X'_{\beta\dot{\psi}}\beta\dot{\psi} + X'_{\dot{\psi}\dot{\psi}}\dot{\psi}^2 + X'_{\beta\beta\beta\beta}\beta^4 \right) \tag{4.16}$$

where $T_M$ is the midship draught and $\beta$ and $\dot{\psi}$ are the drift angle and yaw rate respectively. $X'_{\beta\beta}$, $X'_{\beta\dot{\psi}}$, $X'_{\dot{\psi}\dot{\psi}}$ and $X'_{\beta\beta\beta\beta}$ are the manoeuvring hydrodynamic derivatives. The drift angle is defined as:

$$\beta = \tan^{-1}\left(-\frac{v_s}{u_s}\right) \tag{4.17}$$

and therefore requires the measurement of the transverse speed through water $v_s$. The real challenge in calculating the effect of drift and yaw on ship resistance stands in the estimation of the manoeuvring derivatives, which can be most accurately obtained by conducting manoeuvring tank tests (see e.g. Yasukawa and Yoshimura, 2015; Carchen *et al.*, 2016) or CFD simulations (e.g. He *et al.*, 2016). Semi-empirical formulas can be

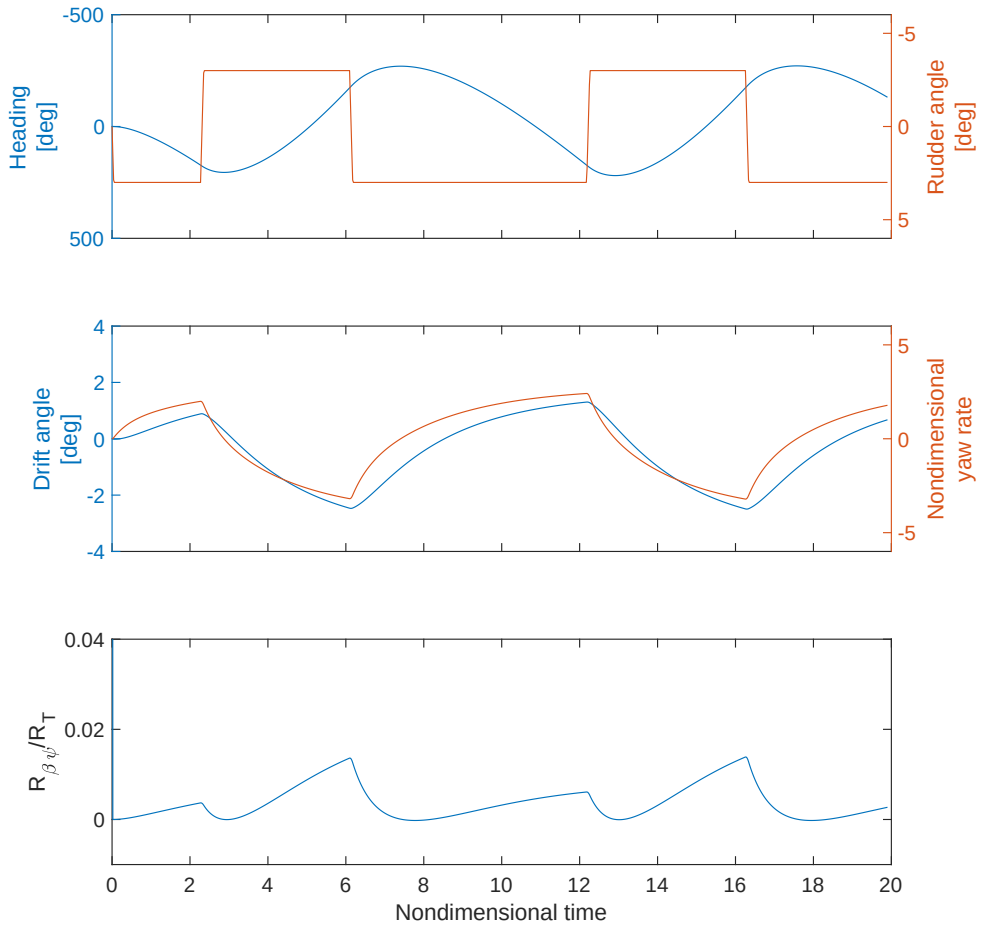


**Figure 4.9** – *Effect of drift forces and yaw moments during a 3* deg *zig-zag manoeuvre to starboard on the total resistance.*

found in literature, for example in Inoue *et al.* (1979*a*,*b*); Kijima and Tanaka (1993) and Yamaguchi *et al.* (2009), but because of the sensitivity of the derivatives the utmost care must again be taken in the use of these coefficients.

The 2-DOF earlier described can again be used to investigate the effects of leeway drift and drift and yaw motions. A quasi-steady simulation can be easily conducted with a fixed drift angle $\beta \approx 10\,\text{deg}$, resulting in $R_\beta/R_T \approx 8.5 \cdot 10^{-3}$. This is a considerably small value for a relatively large drift angle. Things do change during course keeping manoeuvres, where the influence of yaw resistance in greater. The same manoeuvres presented above yield the results shown in Fig. 4.9 and 4.10, whereby at most $R_{\beta,\dot{\psi}}/R_T \approx 0.01$ in the +3Z manoeuvre and $R_{\beta,\dot{\psi}}/R_T \approx 0.03$ in the -5Z manoeuvre.

Again, although each ship has different manoeuvrability properties, the resistance figures earlier presented are a reasonable representation of a generic case. In this perspective, given the modest entity of the impact of the combined drift and yaw forces on the ship resistance and the large uncertainty in their calculation, the Author agrees with the general practice of applying a suitable filter instead. This will be discussed later in Section 4.4. Nonetheless, in case there is availability of reliable data, drift and yaw induced resistance can be readily calculated (see e.g. Orihara and Tsujimoto, 2017).

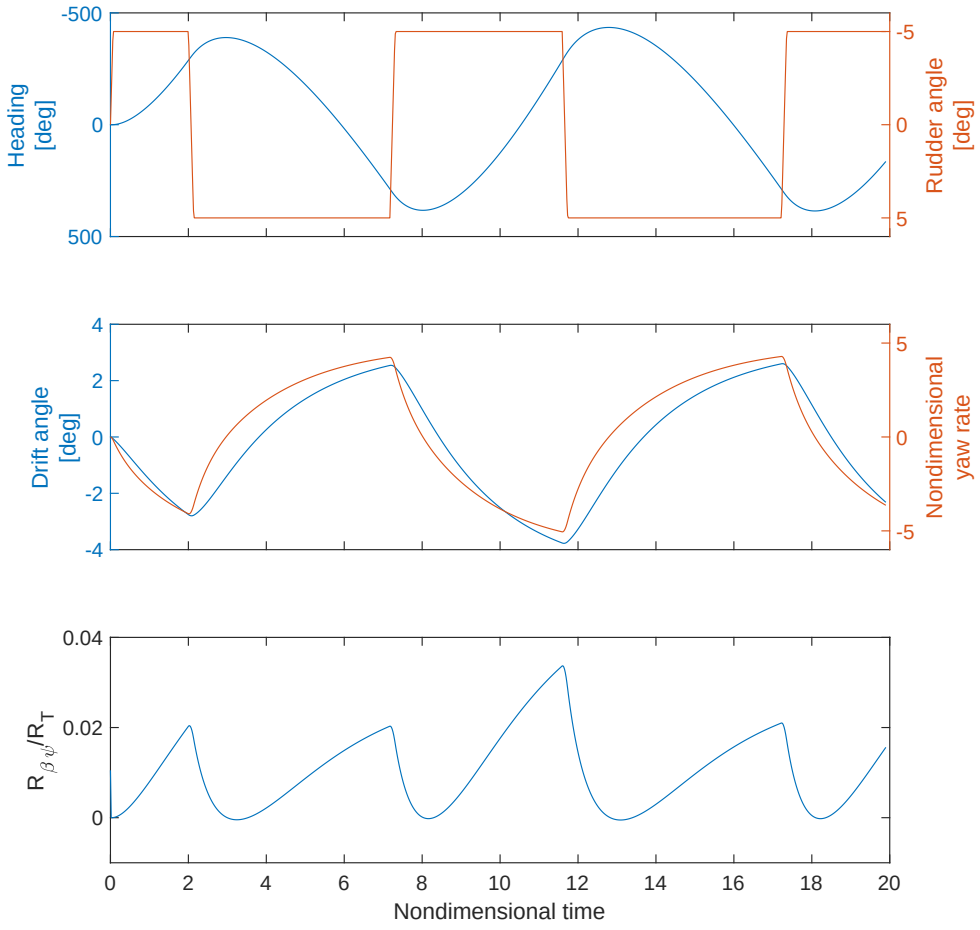


**Figure 4.10** – *Effect of drift forces and yaw moments during a 5* deg *zig-zag manoeuvre to port on the total resistance.*

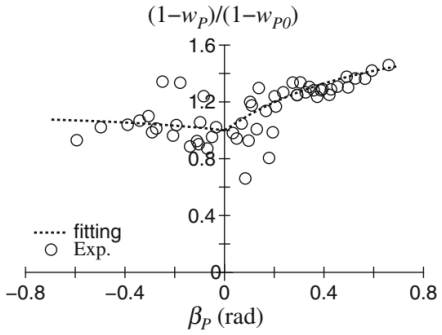


**Figure 4.11** – *Effect of drift on the effective propeller wake as fraction of the nominal value [Source: Yasukawa and Yoshimura (2015)].*

Finally, drift and yaw motions also contribute substantially to alter the wake field. Figure 4.11 shows the relative change of effective propeller wake fraction against the drift angle for the KVLCC2. For $\beta \approx 10\,\text{deg}$ for a starboard turn, the experiments showed that $(1-w)/(1-w_0) \approx 1.2$. An accurate estimation of such changes is challenging, although several empirical equations have been derived, e.g. in Hirano (1980); Inoue *et al.* (1981); Yasukawa (1992). It is felt that the effects of drift on the propeller dynamics are more constraining than those on the ship resistance. If no reliable methods can be used to evaluate $w/w_0$ or to measure $\beta$, a drift filter needs to be devised based on the generally expected alterations of the effective wake fraction.

### *4.2.2 Summary of the design principles*

The present Section investigated the possibility and requirements of a deterministic SPMS. It is concluded that for a vessel sailing in steady state condition:

- Direct wind resistance, added wave resistance and the effects of currents and changes in displacement should be corrected using measurements and suitable formulae within their limits of applicability.

- The effects of changes in water properties, steering, drift and yaw may be corrected if the necessary measurements and equations are available and reliable.

- The effects of shallow or restricted waters and of trim should not be corrected unless dedicated experiments have been carried out for the hull under scrutiny.

Based on the above, the following sections will detail the methodology proposed for the deterministic SPMS presented in this study.

## 4.3 Data acquisition

The measurement apparatus may be rightfully regarded as the backbone of an on-board SPMS. However, its characteristics should in principle be chosen so as to fulfil the needs of any subsequent data analysis method. The considerations made in Chapter 2 and in Section 4.2 helped define such needs. In the framework of ship performance monitoring, the measured variables should enable the practitioner to:

1. Obtain performance data of suitable quantity and quality to assess the hydrodynamic performance of the ship;

2. Identify periods appropriate for performance monitoring.

Both objectives are of primary importance particularly where the data acquisition is completely automated and not necessarily do all the measurements serve both purposes. The main objective of this section is therefore to summarise the variables that should be logged and the means to measure them.

The section will then introduce different types of signal transmission and data logging methods. It will finally define the concept of 'datapoint', which is the format of raw data ready for further analysis.

At first, however, the concept of ship time constant must be considered.

### *4.3.1 The time constant*

Every ship has a specific response phase to forces and moments to which she is subjected. Large tankers respond to excitations in the order of minutes, whilst small vessels in the order of a few seconds. This applies to those generated, for instance, by the propeller as well as to those generated by the action of the wind. The response time has significant implications on the data logging and the data analysis procedures, because the targeted measurement resolution will be dictated not only by the measured phenomenon (e.g. wind speed) but also by the quickness of the changes of vessel performance to it. Small vessels will therefore require a faster sampling frequency than large vessels.

A time constant $\vartheta$ may be thus defined as a ship-dependent coefficient that characterises a representative phase lag between excitation and response. Since the majority of the existing SPMSs operates on large vessels, practice has indicated that $\vartheta \approx 10$–$15$ minutes is a fair size for data analysis (ISO, 2016). This is not so for smaller vessels, whose response to disturbances can be in the order of seconds. In line with a similar principle followed by Lackenby (1952), $\vartheta$ was defined based on the ship response to acceleration and depending on the ship's design characteristics. Consider the single degree-of-freedom motion equation dependent on time $\mathbb{t}$:

$$(1-t)\,T(\mathbb{t}) - R_T(\mathbb{t}) = \Delta\,(1+m_x)\,\frac{\mathrm{d}u_s}{\mathrm{d}\mathbb{t}} \tag{4.18}$$

where $t$ is the thrust deduction factor, $T$ the propeller thrust, $R_T$ the total ship resistance, $\Delta$ the design ship mass displacement, $m_x$ the nondimensional added mass in surge direction and $u_s$ the forward component of the speed through water. The following functions are defined:

$$\mathrm{a}(\mathbb{t}) = \frac{T(\mathbb{t})}{T^*} \tag{4.19a}$$

$$\mathrm{b}(\mathbb{t}) = \frac{R_T(\mathbb{t})}{R_T^*} \tag{4.19b}$$

$$\mathrm{c}(\mathbb{t}) = \frac{u_s(\mathbb{t})}{V_s^*} \tag{4.19c}$$

where $T^*$ and $R_T^*$ are the thrust and the resistance at the design ship speed through water $V_s^*$. Using eq. (2.17) and (4.19), for small accelerations eq. (4.18) can be approximated:

$$\frac{P_S^* \eta_d \eta_s}{V_s^*} \left[\frac{\mathrm{a}(\mathbb{t}) - \mathrm{b}(\mathbb{t})}{\mathrm{c}(\mathbb{t})}\right] \approx \Delta\,(1 + m_x)\, V_s^* \frac{\mathrm{d}c(\mathbb{t})}{\mathrm{d}\mathbb{t}} \tag{4.20}$$

Integrating over time yields:

$$\int_0^{\vartheta} \mathrm{d}\mathbb{t} \approx \frac{V_s^{*2}\,\Delta}{P_S^*\, k_t} \int_0^{\vartheta} \left[\frac{\mathrm{c}(\mathbb{t})}{\mathrm{a}(\mathbb{t}) - \mathrm{b}(\mathbb{t})}\right] \frac{\mathrm{d}c(\mathbb{t})}{\mathrm{d}\mathbb{t}} \mathrm{d}\mathbb{t} \tag{4.21}$$

which by the properties of integrals can be rewritten as:

$$\vartheta \approx \frac{V_s^{*2}\,\Delta}{P_S^*\, k_t} \int_{c_{\mathrm{ini}}}^{c_{\mathrm{fin}}} \left[\frac{\mathrm{c}}{\mathrm{a}(\mathrm{c}) - \mathrm{b}(\mathrm{c})}\right] \mathrm{d}c \tag{4.22}$$

where $\eta_d$ is the propulsive efficiency, $c_{\mathrm{ini}}$ and $c_{\mathrm{fin}}$ are respectively the initial and final nondimensional velocities over which to integrate the time and $k_t$ a vessel efficiency parameter defined as:

$$k_t = \frac{\eta_d \eta_s}{(1 + m_x)}$$

which, if lacking real values, may be generally taken as 0.55 considering $\eta_d = 0.6$ and $(1 + m_x) = 1.08$.

The desired time would be long enough to encompass the slowest accelerations, which occurs when both $c_{\mathrm{ini}}$ and $c_{\mathrm{fin}}$ are small. Clearly, the expression for $\vartheta$ above is speed dependent. However, since a simple round figure is here sought, it is suggested that:

$$c_{\mathrm{ini}} = 0\,\mathrm{kn}; \quad c_{\mathrm{fin}} = c(0.1P_S^*)$$

which corresponds to a power increase of $10\%P_S^*$ from idle. This ensures that the slowest accelerations are encompassed by the time window defined by $\vartheta$. The asymptotic behaviour of $\mathrm{c}(\mathbb{t})$ can be considered to converge when it reaches within $0.01\mathrm{c}_{\mathrm{fin}}$. The time $\vartheta$ needed to dissipate the acceleration was studied with a 1-DOF manoeuvrability simulation for three different vessel types, namely a small high-speed vessel, a medium-sized chemical tanker and a VLCC.

Then, a vessel-specific parameter $\xi$ can be defined from the main design features as:

$$\xi = \frac{V_s^{*2}\,\Delta}{P_S^*\,k_t} \tag{4.23}$$

which has the dimension of seconds and can be nondimensionalised as $\xi' = \xi V_s^*/L_{pp}$. The time constant $\vartheta$ can be defined by considering its nondimensional value $\vartheta' = \vartheta V_s^*/L_{pp}$ as a function of $\xi'$. Table 4.1 shows simulated time constant values for the three vessel types. A curve fitting analysis on these data yielded:

$$\vartheta' = \frac{161\,\xi'}{48 + \xi'} \tag{4.24}$$

for $V_s$ expressed in m/s, $\Delta$ in tons and $P_S$ in kW. The accuracy of this equation is obviously limited due to the very small ship dataset considered. However, it can be easily used to provide an approximate guidance regarding the time taken by a ship to reach steady state after a low-frequency excitation. Equation (4.24) can also be expressed in terms of ship lengths travelled, which may be useful to mariners and practitioners to quantify the distance taken by the ship to reach steady state. Equation (4.20) can be rewritten as:

$$\frac{\mathrm{d}u_s(\mathbb{t})}{\mathrm{d}\mathbb{t}} \approx \frac{P_S^*\eta_d\eta_s}{V_s^*\Delta\,(1+m_x)}\left[\frac{\mathrm{a}(\mathbb{t}) - \mathrm{b}(\mathbb{t})}{\mathrm{c}(\mathbb{t})}\right] \tag{4.25}$$

which can be integrated twice over time to provide the distance travelled:

$$\iint_0^{\vartheta} \frac{\mathrm{d}u_s(\mathbb{t})}{\mathrm{d}\mathbb{t}}\mathrm{d}\mathbb{t}\mathrm{d}\mathbb{t} \approx \frac{P_S^*\,k_t}{V_s^*\,\Delta}\iint_0^{\vartheta}\left[\frac{\mathrm{a}(\mathbb{t}) - \mathrm{b}(\mathbb{t})}{\mathrm{c}(\mathbb{t})}\right]\mathrm{d}\mathbb{t}\mathrm{d}\mathbb{t} \tag{4.26}$$

Dividing by the ship length $L_{pp}$ the following is obtained:

$$\lambda \approx \frac{V_s^*}{\xi L_{pp}}\iint_0^{\vartheta}\left[\frac{\mathrm{a}(\mathbb{t}) - \mathrm{b}(\mathbb{t})}{\mathrm{c}(\mathbb{t})}\right]\mathrm{d}\mathbb{t}\mathrm{d}\mathbb{t} \tag{4.27}$$

where $\lambda$ is the ship lengths travelled. Similar to eq. (4.24), the 'space constant' was found to be as:

$$\lambda = -3.2\ln\left(\frac{V_s^*}{\xi L_{pp}}\right) - 5 \tag{4.28}$$

Equations (4.24) and (4.28) can be applied to any vessel size and type to provide a round figure of the time taken and ship lengths travelled for the slower accelerations to be dissipated by that vessel. This information will be very useful during the data preparation phase and can be used to verify the suitability of the sampling frequency. One of the first uses of the time constant is indeed to ensure that, in the time window it identifies, a good amount of data is sampled. Whereas high speed data usually contains more information than low speed data, statistically, we may consider 'good amount' a variable number between 100 and 200 data points. However, in particular cases where those numbers may be difficult to achieve, a least data sample size of 20 data points is considered to be statistically relevant. These high frequencies are of course not necessary for those slowly changing variables related to weather and ship loading conditions, where the sampling frequency may be relaxed to slower rates.

TABLE 4.1
*Simulated time constant values.*

| *Vessel type* | $\vartheta$ |
|---|---|
| High speed vessel | 21 s |
| Small tanker | 619 s |
| VLCC | 3444 s |

### *4.3.2 Variables and sensors*

A comprehensive account of the variables and sensors useful for performance monitoring was given by Hasselaar (2011), who has investigated several aspects of measurement systems in deterministic SPMSs. The present study values his findings and builds on them with the knowledge gathered during the course of the research.

According to the considerations made in Chapter 1, the primary variables to be measured are:

- Speed through water (at least the surge component)
- Propeller speed
- Propeller torque

The secondary variables identified by the investigation presented in Section 4.2 are instead:

- Speed over ground
- Course over ground
- Heading
- Rudder angle
- Midship draught
- Trim
- Wind speed
- Wind direction
- Wave spectra
- Water depth

We may also identify tertiary variables as secondary variables of lesser relevance that may be not logged without significantly affecting the overall performance analysis:

- Athwart speed through water
- Propeller thrust
- Air properties (pressure, temperature and humidity)
- Water properties (density and viscosity)
- Fuel flow

Means of measuring all the above variables and their suitable sampling frequencies will be discussed in the following paragraphs.

### Primary variables

***Speed through water.***—Speed through water is, together with propeller power, the most important parameter measured in ship performance monitoring. Besides, it is also one of the most challenging to observe due to the several conditions that induce misreadings or unexpected values.

The most important component of ship speed through water for the sake of ship performance monitoring is in the surge direction ($u_s$). This can be measured directly by means of fundamentally three types of speed logs:

1. Doppler logs (DL)
2. Electromagnetic (EM) logs
3. Acoustic-Correlation (AC) logs

Doppler logs are the most common types of speed logs and are based on the concept of frequency shift originated by the so-called Doppler effect. A single-axis sensor emits at two different angles two high energy sound waves into the water, which are reflected by the particles in the water (e.g. plankton). The received signal will present a frequency shift which can be related to the relative velocity between the sensor and the water (Fig. 4.12). The measuring depth ranges normally 1–9m below the transducer. The position of the transducer is recommended around midship at the centre line and far from propellers and similar devices (e.g. echo sounders), respectively to minimise the impact of ship motions and interference from other measurements. The sampling frequency of speed log should be such that the natural fluctuations of water speed significant for the performance of the ship are captured. As a rule of thumb, the considerations made in the previous section can be used, whereby an indicative sampling frequency of $100/\vartheta$ was fundamentally suggested. Generally, speed logs have a 1Hz sampling rate, which suits most commercial applications.

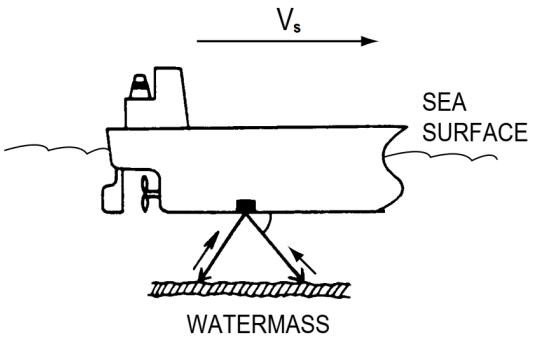


**Figure 4.12** – *Doppler log principle, after Furuno (2003).*

DLs can operate with two different modes, namely water tracking and bottom tracking. In bottom tracking mode, the sensor measures the speed relative to the seabed — in other words, it measures $V_g$ instead of $V_s$. Only water tracking mode should be used for performance monitoring.

The greatest advantage of DLs stems from their measuring outside the ship's boundary layer, which renders them unaffected by biofouling and general roughening of the wetted surface. On the other hand, often speed logs are held responsible for delivering incorrect measurements. Contrary to the vast majority of literature statements, DLs are very accurate and are insensitive to or corrected for several variations of conditions, such as pitch motions (up to $\pm 10$ deg), temperature changes and salinity change (Furuno, 2003). They are affected by extreme conditions, such as lack of particles in the water (e.g. in icy waters), very shallow waters ($<$ 3m) and very rough weather, which are however conditions were performance monitoring should be avoided. Installing the sensor close to ship elements that may interfere with the signal (e.g. propellers, echosounders etc) must be avoided to prevent misreads. DLs are also affected by water aeration, which is however a phenomenon that rarely occurs when sailing in deep waters. The majority of the errors imputed to the DL are related to disturbances to the propeller wake (as described in Section 4.2), to stratified ocean currents and to leeway drift. This was confirmed by an extensive full-scale monitoring campaign lead by MARIN within the joint industry project SPA-TOO, whose outcomes are partly presented in van den Boom and Hasselaar (2014) and Hasselaar (2015). The studies showed that if suitable detectors are used to avoid monitoring in such circumstances, DLs deliver reliable and accurate data.

Electromagnetic logs are based on the principle that a voltage is induced in a conductor by a moving magnetic field. The water is used as a conductor, whilst a sensor produces an electromagnetic field. Another sensor is used to measure the voltage in the water, which can then be related to the speed of the water (Hiam, 2003). The speed through water is therefore measured directly on the sensor surface, which makes EM logs vulnerable to changes of the boundary layer. As a consequence, EM logs are mostly unsuited for ship

performance monitoring, despite their relative robustness to other disturbances. Some companies produce EM logs mounted on fins that protrude in the water outside the boundary layer. However, the limited fin length and its fragility makes this solution unsuited for most applications. The location of the sensor is thus recommended the closest possible to the bow, where the boundary layer thickness is minimum. Sampling frequencies of EM logs are again in the order of 1Hz.

Acoustic Correlation logs are based on the measurement of the speed of sound through water. The time lag between emission and reception of two acoustic signals can be then correlated to the speed through water. AC logs have several advantages in terms of accuracy and robustness, but suffer from the same drawback of EM logs in that they only measure water velocity on the sensor surface. They are therefore less suited than DL for performance monitoring.

Alternative methods to the use of the speed log do however exist, albeit more intricate. Hasselaar (2011) reprised the use of the propeller as speed through water indicator, on the same principle developed by Telfer (1926). This method, however, is very heavily reliant on the accuracy of the torque sensor, on the effective wake and of the propeller open water curves. As biofouling starts growing on hull and propeller, wake fraction and open water diagrams need to be corrected, which is a very delicate and difficult operation. Hasselaar later outlined how this method introduces very large uncertainties in the performance data and is not recommended for performance monitoring (van den Boom and Hasselaar, 2014).

In a different perspective, Bos (2016) proposes the integration of predicted ocean current data with on-board measurements of speed over ground, such that the speed through water is obtained by subtraction of the two. A more sophisticate and interesting procedure based on the same concept is described by Antola *et al.* (2017*a*), who employ measurements of $V_g$, $V_s$ and ocean forecasts to generate a 'virtual' and more stable $V_s$ with statistical algorithms. The paper shows that the the data quality is dramatically improved by using the virtual $V_s$. It may be concluded that albeit several errors may still arise with the erroneous estimation of the current speed and direction from metocean data, this approach is an interesting alternative that should be employed when no reliable speed through water measurement is available.

***Propeller speed.***—The propeller rate of revolutions is most commonly measured by means of proximity sensors or optical encoders. In the first case, a magnetic sensor is placed close to a particular geared flange which is mounted at some point on the drive shaft. When a metal tooth of the gear comes in proximity of the magnetic sensor, a voltage is induced in the sensor's circuit producing a pulse. In the case of optical encoders, a high energy beam is transmitted between two sensors mounted at the sides of a slotted flange

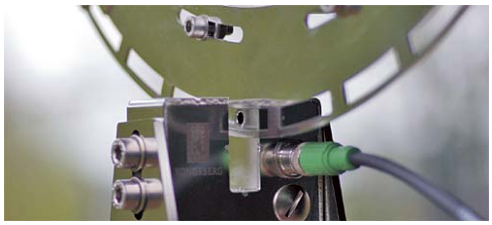

**Figure 4.13** – *Optical propeller speed sensor [Source: Kongsberg (2019)].*

(Fig. 4.13).

For both type of sensors, the shaft rate of revolution is calculated similarly:

$$n = \frac{c}{N_t T}$$

where $c$ is the number of pulses counted in the period $T$ and $N_t$ is the number of teeth or slots in the flange. It follows that the measurement is the more accurate the longer is the counting period and the higher the number of teeth or slots. In general, the simple structure and principle of operation of these sensors ensures a very high reliability and their accuracy is often better than 0.5% required by most standards (e.g. ISO, 2016).

***Propeller torque.***—Propeller torque can be measured on board by means of a variety of different methods. Currently, the most common sensors for direct shaft torque measurement are:

- Strain gauges
- Vibrating strings
- Optical

All of these are capable of delivering accurate measurements at very high sampling rates (above 500Hz) and are thus able to capture variations of ship power requirements as well as shaft vibrations.

Strain gauges are the most widely used application in virtue of their low cost, simple build and accuracy. The fundamental concept used by strain gauges is that the electrical resistance through a conductor changes if it is subject to some degree of strain. Since these resistance changes are very small compared to the supply voltage, strain gauges are usually arranged within a Wheatstone bridge circuit to improve the signal-to-noise ratio and reduce the effects of temperature changes. Depending on the target strain, the arrangement of the bridge varies accommodating from one to four strain gauges. To measure torque on a drive shaft, the arrangement is normally that of a full Wheatstone bridge, i.e. with four strain gauges (Fig. 4.14). The output voltage is then further conditioned and amplified to ensure a suitable reliability and cleanness of the signal.

The principal issues related to strain gauges arise from their incorrect installation. The alignment of the strain gauge pattern with the direction of the strain to be analysed

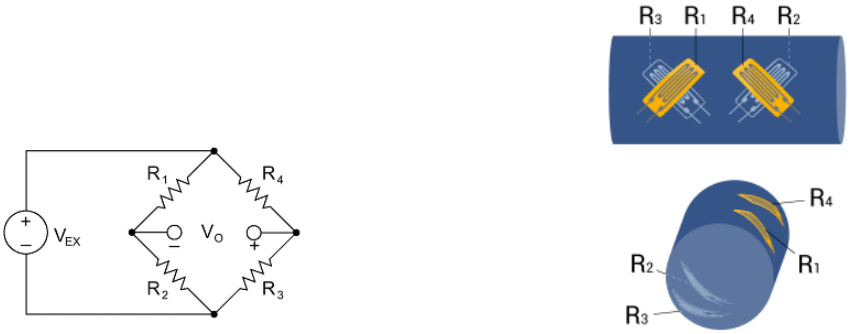


(a) (b)

**Figure 4.14** – *Wheatstone bridge. Figure* (a) *shows the typical circuit, where* $V_{EX}$ *is the excitation voltage, whilst* $V_O$ *is the output of the system. Strain gauges can replace any of the four resistances. Figure* (b) *shows the arrangement of full Wheatstone bridge on a drive shaft for the measurement of torque. This particular arrangement is designed to minimise the effects of vibration and the ensuing alternate loading [Source: HBM (2019)].*

and with the rest of the Wheatstone bridge is crucial to avoid nonlinearity between output voltage and shaft strain. Moreover, strain gauges rely on their perfect adhesion to the shaft surface. Therefore, the adhesive needs not only to be of excellent quality, but should also be properly insulated from the harsh and salty environment of the engine room.

Vibrating strings operate according to a similar principle, where the electrical resistance is replaced by acoustic vibration. When the vibrating string is stretched, it will produce a higher tone, when compressed a lower tone. The sound frequency shift can then be related to strain, delivering a measurement of high quality, robust and durable at the expense of higher pricing. This particular sensor is also relatively insensitive to external influences such as humidity, radiation and temperature.

The basic principle of optical sensors is instead the measurement of the displacement of a point along the shaft relative to another reference point on the shaft (Fig. 4.15). Several sensors exist in commerce based on this principle, delivering different levels of accuracy and robustness. Optical measurements are known for their reliability, as they are non-contact sensors, but they are relatively more delicate systems and more expensive.

In addition, propeller shaft torque can be estimated from proxy measurements of fuel consumption or mean effective cylinder pressure. Both proxies have the advantage of being relatively simple measurements, redundant and already entailed by most routine engine checks on board. However, they both heavily depend on the fuel characteristics and on the Specific Fuel Oil Consumption rates of the engine (Hasselaar, 2011). If these

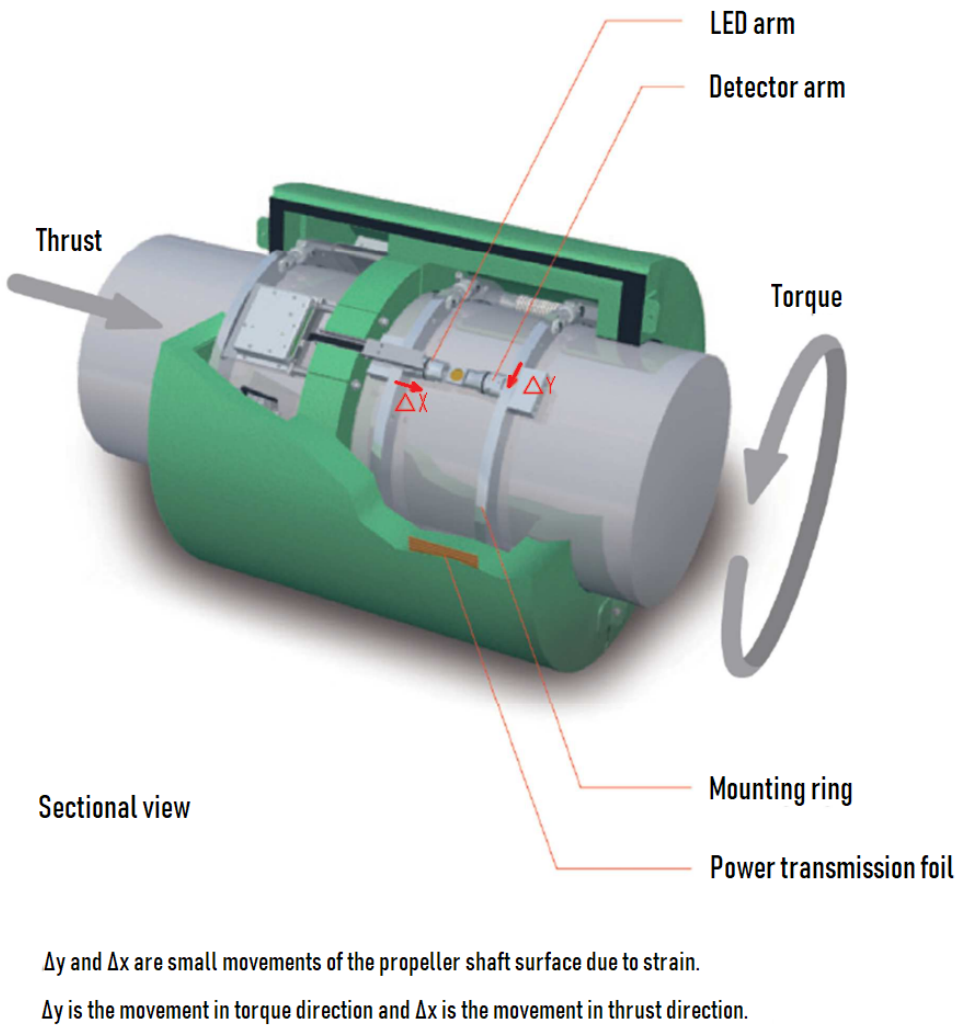


**Figure 4.15** – *A torque and thrust optic measurement system produced by VAF. This particular sensor has been conceived to be fitted on an existing shaft by means of mechanical 'jaws' [Source: van Ballegooijen* et al. *(2017)].*

factors are unknown, large uncertainties are introduced in the calculations. This consideration was embraced by the ISO 19030 following the extensive study carried out by the Ship Technology Research Association of Japan on comparing shaft power and fuel consumption of 18 ships for over 45 years (Fumi, 2016). Direct shaft power measurements are therefore to be preferred in the framework of performance monitoring.

**Secondary variables**

***Speed and course over ground.***—These two parameters are nowadays almost exclusively measured by means of Global Positioning System (GPS), which calculates the distance between the sensor and one or more satellites with known position. This information is updated with a frequency of 1Hz by the majority of navigational systems. However, provided that signal is received, GPS information is prone to errors amounting in the worst case to a positioning error of 15m. This has a negative impact in the calculation particularly of the speed over ground.

To improve the GPS signal, several correction methods were developed. The most common one is DGPS, where 'D' stands for 'differential'. Here the GPS signal is corrected (locally) by comparing the satellite positioning with the known position of a nearby ground GPS base station. The achieved accuracy improves in this case to 5m. A further enhancement was given by the introduction of the Wide-Area Augmentation System (WAAS), which extended the concept of DGPS to a wide network of base stations. A more global correction is thus calculated and distributed to GPS receivers by purpose-launched satellites. The accuracy when using WAAS correction is about 2m.

Despite the above listed differences, either measurement is very stable, does not require particular calibration and depends primarily on the availability of satellite signals or 'fixes'.

***Heading.***—A gyrocompass is probably the most accurate and common instrument to obtain ship heading. It works based on the natural precession of a fast-spinning disc (gyroscope) with respect to the Earth's rotational axis. Whereas common magnetic compasses are also employed in navigation, the advantage of a gyrocompass stems from it indicating the true North (as opposed to magnetic) and from being uninfluenced by proximity with magnetic sources. For this reason it is regarded as a very accurate and robust measurement. Measures of heading are normally sampled at 1Hz.

***Rudder angle.***—To measure rudder angle, a potentiometer connected to the rudder stock is normally employed. Apart from providing valuable performance monitoring data, the signal is used by the autopilot to control the course of the vessel.

Rudder angle data is very reliable and robust and, although it can be sampled at relatively high frequencies, a 1Hz sampling frequency is common and sufficient for most installations.

***Draught.***—Draught is an essential parameter for ship performance monitoring, as it can be related to displacement, wetted surface area and trim. The most reliable and used method to measure draught is by visual observation. However, a measurement of this kind can be only conducted when at rest in harbour with the departing load. Moreover, draught measurements are inherently sensible and difficult to carry out. For instance, a 5cm misreading would produce an error of about 100t in a 12'000t ship. It is therefore necessary to conduct the visual measurement with appropriate training.

Alternatively, pressure draught gauges may be used, which still deliver accuracy sufficient for performance monitoring purposes. These consist of pressure transducers located at suitable points on the hull of the vessel and provide a measurement of the static head. Although they allow remote draught measurements, pressure transducers are known for their poor long term stability, which needs to be regularly checked against visual reads.

Draught may be read at very low frequency (even once-per-voyage would suffice). Coherently, pressure transducers should only be used when sailing at very low speeds and in calm waters to prevent readings from including effects of sinkage and dynamic head from waves (Hasselaar, 2011).

***Trim.***—Any of the above measure of draught can be used to derive trim by differentiating fore and aft measurements. At times, on-board inclinometers may be used, though they are less common.

***Wind speed and direction.***—Accurate wind measurements must be ensured by a good anemometer and its wise location on the ship. Given that visual wind observations are too inaccurate for performance monitoring, we shall therefore focus on suitable anemometer types and their location.

Cup anemometers and rotating vane anemometers are by far the most common types found on board. The formers are usually supplemented by vanes for the measurement of wind direction (Fig. 4.16). The spinning cups generate a voltage which can be directly related to the wind speed, whilst the vane acts on a potentiometer that is related to the wind direction. Cup anemometers and vanes benefit from low pricing and robust measurements, although they suffer in accuracy and require more maintenance.

Ultrasonic anemometers are slightly superior, as they require very little maintenance and deliver accurate measurements with long term stability. They are capable of operating effectively in very harsh and turbulent environments and are for this preferred in oceanographic campaigns. Their basic principle is the change of sound speed resulting from wind flow between a transmitting and a receiving transducer. Owing to their particular shape, ultrasonic anemometers are usually calibrated in wind tunnels by the manufacturer to account for the wind flow distortion from the structure supporting the transducers.

Of more recent development are the acoustic anemometers, which measure the phase


(a) (b)

**Figure 4.16** – *Anemometers:* (a) *cup anemometer with vane;* (b) *ultrasonic anemometer for marine applications. [Source: R.M. Young Company (2019)].*

shift of a high-energy sound wave as it is trespassed by a wind flow. This type of anemometer, albeit smaller, shares similar quality features with the ultrasonic anemometer and is therefore suited for performance monitoring.

Whereas all the above sensors deliver relatively accurate and high speed data (in the order of 1Hz), it has to be questioned whether their sampling frequency is necessary or sufficient for the ship they are mounted on. Different ships react differently to the same wind gust in virtue of the damping and restoring forces they produce. Again, $\vartheta/100$ may be used as an indicative value of a minimum sampling frequency.

A major issue for wind measurement, however, is the sensor location. The National Oceanographic Centre together with Southampton University have conducted a comprehensive study on the positioning of anemometers on tankers and bulk carriers (Moat *et al.*, 2006*a*,*b*), finding that the best position for an anemometer is as high as feasible in proximity of (but not at) the forward edge of the supporting ship structure (e.g. bridge top). At this location, the wind inflow distortion is minimal, though not totally eliminated, as shown by Fig. 4.17. Eventually, a check on the calculated true wind speed over reciprocal runs during sea trials can serve the purpose of estimating the impact of shadowing from superstructures.

***Wave amplitude and spectrum.*** —The solution to eq. (4.6), requires knowledge of the directional wave spectrum $S_\zeta$. This parameter is particularly important to prevent that additional uncertainty and noise are gained by the data. Bos (2018) corroborated this principle by showing how the relatively small error in wave height and distribution estimation leads to added wave resistance errors in excess of 250%. An accurate wave spectrum measurement system must therefore be employed if added wave resistance is to

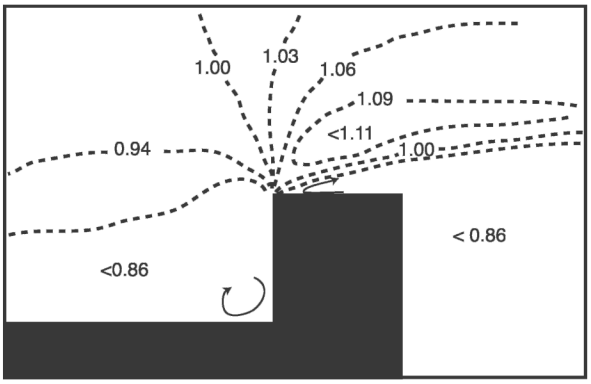


**Figure 4.17** – *Wind speed gradients as a fraction of the free-stream velocity for a head (i.e. left-to-right) flow on a generic ship superstructure [Source: Moat* et al. *(2006*b*)].*

be corrected for (Hasselaar, 2011).

On-board wave radars are probably the best choice to obtain directional wave spectra measurements and typically provide high sampling frequencies. All of these devices work based on the emission of radio waves and the analysis of their 'echo' after hitting at a certain angle the water surface. Grønlie (2004) provides a very insightful review of the recent state-of-the-art, reporting that although several types of sensors and techniques exist, only a few wave sensing technologies are suited to ship performance monitoring. Among these are the X-band radars and the Doppler radars. The post-processing of the image provided by conventional navigation radars has found a wide consensus and scope of application in recent times (Hasselaar, 2011). Conventional or, as they are called, X-band radars exploit the backscattering generated from hitting the surface ripples (Bragg waves) at low-grazing angles (Grønlie, 2004). As a consequence, a wind with minimum speed of 2–3 m/s needs to be present for a signal to be generated (Gangeskar *et al.*, 2018). Figure 4.18 shows the typical Cartesian reference grid of an X-band radar. The directional spectrum thus measured needs however to be scaled to the true wave energy. A calibration of some sort is therefore necessary, which may be carried out empirically or by means of redundant wave energy measurements. Using these types of calibration, such wave radars have been shown to provide very good measurements of the seaway (Gangeskar *et al.*, 2018). Another type of accurate on-board wave radar is the range-gated pulsed Doppler Microwave radar. These exploit the Doppler shift of moving wave particles observed at a distance from the observing platform, allowing a measurement of an almost undisturbed wave field (Grønlie, 2004). At the same time, however, they make use of several sensing antennas, which renders their installation and maintenance more expensive than their counterparts.

Finally, a possible solution is presented by an array of vertical Doppler radars, which would be able to triangulate the wave field in proximity of the measurement platform reconstructing the wave field. This solution is not to be recommended since the wave

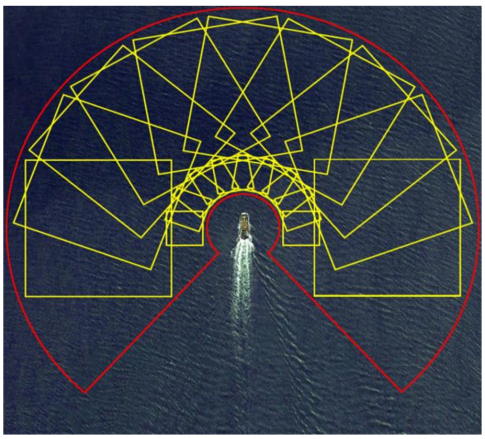

**Figure 4.18** – *Measurement grid of an X-band radar [Source:Gangeskar* et al. *(2018)].*

spectrum measurement can only be conducted on one side of the vessel (e.g. at the bow).

An interesting and cheaper alternative to the employment of wave radars is given by the measurement of ship responses. Nielsen (2005, 2006) shows how ship motion responses in a seaway can be efficiently analysed to reproduce the full directional spectrum encountered by the ship at a given speed. His work compares the performance of two methods, namely the parametric and non-parametric. The former assumes the actual seaway to be formed by parametrised wave spectra (see Chapter 2), whilst the latter derives it by a complete discretization of the measurements in the frequency-directional domain without an *a priori* assumption on the spectrum shape. The two methods are shown to perform similarly. The full-scale implementation of the two concepts provided estimations in reasonable agreement with the measurement given by an on-board wave radar, but unfortunately lacks a robust verification from an external sea spectrum measurement (Nielsen, 2005). Hinostroza and Guedes Soares (2016) confirmed the feasibility of the parametric method using a genetic algorithm code to obtain the best estimation of wave parameters. The full-scale application, however, again failed to provide a strong proof of the concept.
The available studies regarding wave spectra estimates through the measurement of ship responses show that a reasonable mapping of the seaway is attainable. Some difficulties do however arise in presence of following waves (Nielsen, 2006; Hinostroza and Guedes Soares, 2016) and in tuning the statistical parameters of non-parametric methods.

A practical alternative to several of the issues encountered with on-board measurements of the seaway is given by nowcast and hindcast weather data. A significant number of wave buoys have been deployed along the shores of several countries in the effort to monitor the behaviour of coastal waters. These derive the full-directional wave spectrum much in a similar way as the previous paragraph has presented. The network of wave buoys provides a good coverage of coastal national waters and is an good source of nowcast wave data. However, when the wave buoy is located in particular locations (e.g. in proximity of a bay or in relatively shallow waters) the waves might be distorted and their

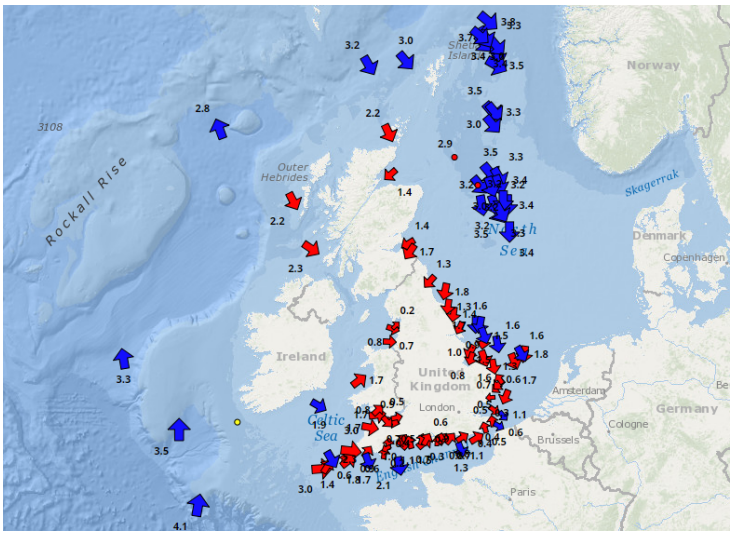


**Figure 4.19** – *WaveNet wave buoy network along the coast of UK [Source: CEFAS (2019)].*

measurements will have restricted validity. Figure 4.19 shows the wave buoy network (WaveNet) coverage in UK. Hindcast wave measurements are possible using numerical simulations at global and local scales, also known as MetOcean data. Bos (2016, 2018) presented a detailed study of how this type of data can improve significantly the quality of ship monitoring data, particularly when combined with on-board weather measurements.

Either of the three alternatives above presented would deliver a good measurement of the seaway. In addition, wave spectra do not need to be sampled at very high speed due to the slowly varying weather circumstances. Sampling speeds of 1 sample/hour is acceptable. According to the Author's research, an X-band radar would be the best solution, despite the relatively higher investment. If a vessel is operated within the catchment area of a wave buoy network, nowcast data is also a valid alternative.

***Water depth.***—Water depth can be measured with great accuracy using a Doppler echo-sounder, which, in analogy with Doppler speed logs, usually samples at a speed of 1Hz.

***Athwart speed through water.***—The transverse component of speed through water ($v_s$) can be measured by employing a dual-axis speed log retaining sampling characteristic similar to single-axis logs. Although this type of sensor is not common on small craft, it has become increasingly popular on larger vessel to aid port manoeuvring and dynamic positioning.

***Propeller thrust.***—As mentioned earlier in Chapter 1 and 2, the availability of thrust measurements would permit the separation of the effects of hull fouling and propeller fouling. The measurement of propeller thrust can be carried in much the same way as torque measurement. The most popular sensor is still the strain gauge, but optical

measurements are a very valid (yet more expensive) alternative. The main issue with thrust measurement stems from the higher stiffness opposed by the shaft to an axial stress. The Young's modulus of common marine steel is about three times larger than the shear modulus, so that the axial stress (thrust) will produce a much smaller strain than that generated by a torsional stress (more than 10 times smaller). Consequently, thrust measurements exhibit a higher sensitivity with respect to torque measurements, they have a lower signal-to-noise ratio and require significant amplification of the output signal (ITTC, 1993). Temperature changes in the engine room, residual stresses caused by the shaft resting on journal bearings, poor lubrication, shaft vibration and misalignment are all causes of the scatter and inconsistency that is so often observed in thrust measurements (Hasselaar, 2011). Furthermore, the minimal misalignment of the thrust sensor with the shaft axis would produce what is commonly referred to as a 'parasitic load', which is essentially a virtual axial stress produced by the torsional strain. To account for it, a shaft calibration should be carried out over the full scale of the measurement, which is obviously impossible in the majority of the cases. As a result, either the amount of parasitic load is unknown or it is calibrated over a limited thrust range.

***Air properties.***—Although of lesser significance to performance monitoring, the air pressure, temperature and humidity are related to the air density, which affects the wind resistance, see Section 4.2. These air properties are easily measured by means of on-board weather stations or stand-alone barometer, thermometer and hygrometer.

***Water properties.***—Local sea water density $\rho$ and kinematic viscosity $\nu$ can be calculated knowing the water temperature and salinity. The most accurate data can be conducted by means of an on-board thermometer and an electrical conductivity meter, which measure respectively the temperature and salinity of the sea water drawn inside engine room sea chests. The sea surface temperature may alternatively be measured by means of hindcast satellite date (Bos, 2016).

### Calibration

A great concern in ship performance monitoring is sensor drift. In his acclaimed paper, Telfer stated that

> "instruments are governed by no moral laws." Telfer (1926)

Their failure is largely unpredictable in entity and timing and is known to affect important on-board sensors, namely speed logs, strain gauges, pressure sensors and echo-sounders. Procedure to identify and correct for sensor drift are limited and not well established, so that even the ISO 19030 implicitly urges the identification of standardised procedures (ISO, 2016). A relatively simple way of inspecting the measurement quality is by comparison with other similar variables or with reference values. Some of these methods will

be later presented in Section 4.4.

The corrective measure for a sensor's drift is obviously its recalibration, which should ideally happen regularly during the year. However, this is most of the times not viable, either because of the time needed to carry out the calibration (e.g. speed log) or due to the large loads that would be needed for in-situ tests (e.g. shaft strain gauges). As a consequence, corrective factors are applied if the entity of the sensor drift can be determined with reasonable accuracy (Sasaki and Carchen, 2015).

### *4.3.3 Signal communication*

Another relevant part of a SPMS is the signal transmission from the sensor to the monitoring unit. Since the signal may travel long distances and be subjected to various interferences during its path, data quality must be assured in two ways:

1. Cabling through the ship should be arranged such that electrical noise and interference is kept to a minimum. This can be achieved by good cable shielding, segregating different voltages, using twisted pairs cables and employing differential (grounded) voltage measurements (Hasselaar, 2011).

2. A signal quality inspection must be carried out after connection with the sensor is established.

There are fundamentally two types of signal communication, namely analogue and digital. An automated SPMS must be designed to accommodate both type of signals irrespectively.

Analogue signals are the simplest to obtain as they employ low-level communication (voltage or current). However, since the signal is very often transmitted as-is from the transducer to the monitoring unit, it becomes more vulnerable to magnetic interference from the external environment. Receiving a high speed signal is in this case of great importance since it allows a better quality analysis. Figure 4.20 shows a small sample of raw torque signal sampled at high rate as it is received by the monitoring unit on a fast vessel. The interpretation of the time series of a raw signal is difficult and may be misleading at times. A better representation of the characteristics of the signal is in the frequency domain (Fig. 4.20 below). In this particular case, a few low frequency (below 40Hz) peaks can be observed. Electrical noise shows normally a peak around 50Hz, which can be seen in Fig. 4.20. Higher frequencies are also present. Comparing the non-electrical frequency peaks with the propeller rate of revolution (about 6Hz), the number of cylinders of the engine (6) and the engine type (4-stroke Diesel engine) it can be easily understood that the higher peak (about 36Hz) represents the torque produced by the firing of all the cylinders. The lower frequencies show characteristics of the firing of each cylinder, with the middle frequency (about 18Hz) adding to the 1/2 torsional harmonic typical of 4-stroke engines. At the higher frequencies a few other harmonics can

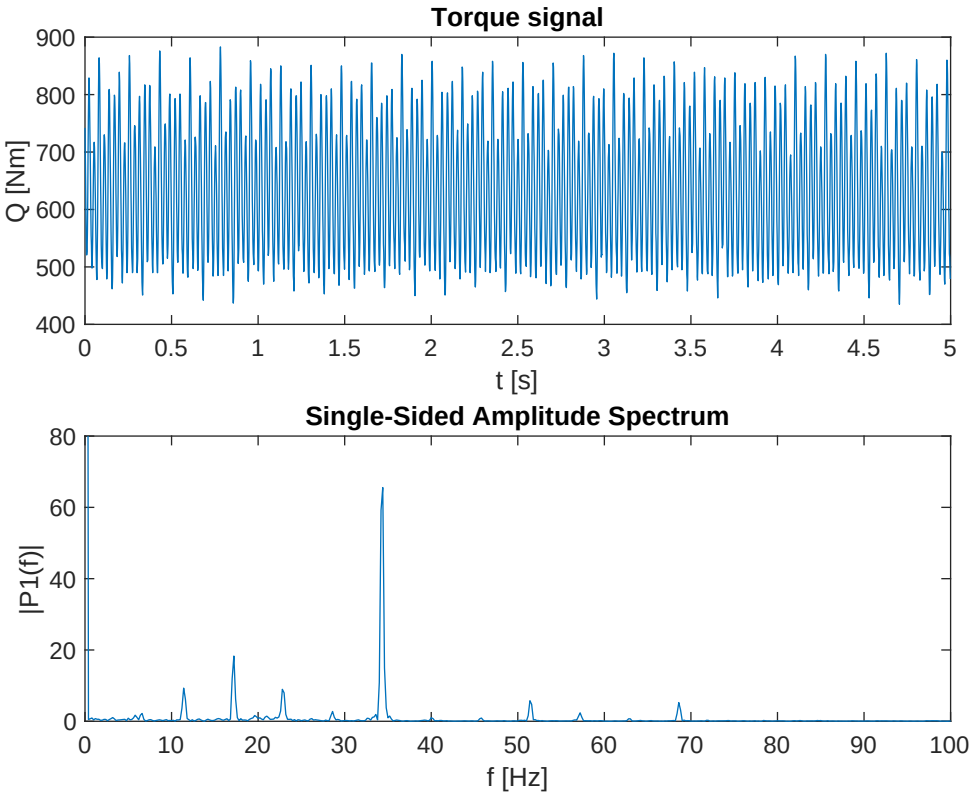


**Figure 4.20** – *Above: raw torque signal recorded at a sampling frequency of 565Hz on a small high-speed vessel. Below: signal analysis in the frequency domain using an FFT with Hanning window.*

be identified. This simple analysis ensures that the signal is of good quality, it does not suffer from contamination and may safely be used for subsequent analysis.

The introduction of digital signal transmission was a decisive step forward in the improvement of measurement reliability and signal-to-noise ratio. In a typical configuration, the signal from the transducer is immediately converted to a digital transmission protocol that conveys the measurement and additional information in a standard binary *sentence* (e.g. a string of ASCII characters). This particular format allows the immediate identification and rejection of a broken and corrupted signal, greatly improving the final data quality. Examples of typical protocols are NMEA 0183, MODBUS TCP/IP and UDP (vom Baur, 2016).

The most used digital protocol is the NMEA 0183, which was first commercialised by the National Marine Electronics Association (NMEA) in 1983 in the effort to standardise the electrical interface and data communication protocol between marine instrumentation (Betke, 2001). The devices compatible with the standard are classified as either *talkers* or *listeners*. The formers are all devices that produce sentences (e.g. an echo-sounder), whilst the latter are receivers (e.g. a chart plotter). The typical NMEA 0183 sentence is structured as follows:

```
$ttsss,d1,d2,....<CR><LF>
```

where `$` denotes the start of the NMEA sentence, `tt` identifies the talker type and `sss` distinguishes the sentence. The identification pattern is followed by a set number of data fields (`d1, d2` etc.) containing the measurements and associated values (e.g. number of satellites in a GPS fix). The sentence terminates in an optional checksum character and a carriage return+line feed pair. More recently, the NMEA has developed a more complete and complex standard, the NMEA 2000, whose aim is to increase the data communication speed, its reliability and most of all the smart connectivity between all on-board devices. It was conceived as a bi-directional, multi-talker and multi-listener network without a central controlling unit (Betke, 2001). It has currently been adopted by several manufacturers.

### *4.3.4 Data logging*

The crew boarding the majority of merchant ships are required to manually record a number of navigational and machinery variables. These are normally combined in daily noon reports forming what are referred to as 'abstract logs'. Despite most primary parameters such as ship speed and power are common to the majority of seagoing ships, logging of secondary parameters depends on the available sensors, the crew training and motivation and the needs of the ship operator (Hasselaar, 2011). In the past, performance monitoring measurements were exclusively extracted from noon reports, which are however prone to several inaccuracies from part of the crew members in addition to those of the sensors.

In general, data quality is to be preferred to data quantity; however, when both are insufficient the overall quality of the outcomes of the performance analysis are clearly jeopardised. This leads to a preference for automatic monitoring systems to manual logging, despite particular circumstances may force the performance monitoring practitioner to the analysis of manual noon reports (Antola *et al.*, 2017*b*). The great advantages of modern automated acquisition systems has been experienced by the Author and is proven in the literature by several studies, e.g. Aldous *et al.* (2013, 2015) and Dückert *et al.* (2016). There are many advantages in the use of an automated system, among which:

- Reduced measurement uncertainty owing to much larger sample sizes and faster sampling frequencies;
- More robust statistical analysis, which allows detailed quality auditing of raw data, clear detection of outliers and steady-state identification;
- Real-time data analysis and feedback to the crew, leading also to immediate error tracking;
- Avoidance of human error in the data acquisition process.

It should be also noted that while in the past automated systems were mostly a benefit resulting from the installation of a SPMS, most ships are now bound to adopt automatic measurement systems by the international regulations (IMO, 2002). In an automated SPMS under regime of continuous monitoring, all the measurements are transmitted to a central monitoring unit with the task to acquire and store raw data and preferably to prepare and store/transmit it for performance analysis.

### *4.3.5 The datapoint*

When the measurements are received by the central logging unit, all the measurements are combined in what will be herein termed *datapoint*. The raw data contained in the datapoint must be in the same format and with the same sampling frequency. As emphasised by Section 4.2, in case two or more signals are sampled at different frequencies, the priority must be given to the primary variables. Data sampled at high frequency between two subsequent lower-frequency acquisitions of primary variables must be averaged to 'align' it with the primary frequency. Conversely, measurements logged at a lower frequency than the primary variables must be duplicated (ISO, 2016). In the datapoint, four different data types can be identified, namely date-time, geographical, Cartesian and circular type.

***Date-time variables.***—Data time stamp is of great importance in ship performance monitoring and can be effectively stored either as a datetime string or a fractional number indicating the number of seconds elapsed since a reference point in time. A numeric time stamp can effectively be used as a datapoint unique identifier for fast database access and can be easily analysed.

***Geographical variables.***—The vessel location is important meta-data that complements the primary and secondary variables allowing retrieval of hindcast data, route analysis and troubleshooting of data errors. Geographical coordinates are most efficiently formatted in decimal degrees to allow easier data analysis. Similarly to the degree-minute-seconds notation, latitude and longitude have domain -90°–90° and -180°–180° respectively.

***Cartesian variables.***—Most of the measurements of interest to ship performance monitoring can be identified with Cartesian variables, whereby their analysis follows the common arithmetic rules.

***Circular variables.***—Directional measurements (e.g. Course Over Ground, wind direction, etc.) share a similar format with Cartesian variables, but are limited to the positive circular range 0–360 deg. This requires the use of different equations for the calculation, for instance, of the location and spread of a set of data. In general, mean and standard deviation of a dataset with size $n$ are calculated for a random circular variable

$\theta$ as follows (Fisher, 1993). The *circular sample mean* $\overline{\theta}$ is defined:

$$\overline{\theta} = \begin{cases} \arctan\left(\frac{S}{C}\right) & \text{if } S > 0,\, C > 0 \\ \arctan\left(\frac{S}{C}\right) + \pi & \text{if } C < 0 \\ \arctan\left(\frac{S}{C}\right) + 2\pi & \text{if } S < 0,\, C < 0 \end{cases}$$

where

$$S = \sum_{i=1}^{n} \sin\theta_i; \quad C = \sum_{i=1}^{n} \cos\theta_i$$

The *circular standard deviation* $\nu$ is approximated according to the following:

$$\nu = \sqrt{-2\log\left(\hat{\rho}\right)}$$

where $\hat{\rho}$ is termed *mean resultant length* and is defined as

$$\hat{\rho} = \frac{\sqrt{C^2 + S^2}}{n}$$

## 4.4 Data preparation

The result of the data acquisition process is therefore an aggregated *dataset* of raw datapoints which needs to be prepared for further analysis. During this process, data binning might be necessary and bins must be defined having size:

$$N = f\vartheta \tag{4.29}$$

where $f$ is the sampling frequency of a primary variable and $\vartheta$ the time constant of the specific vessel.

In brief, the objective of data preparation stage is to:

1. Identify sailing periods suitable for performance monitoring, encompassing:
   - Identification of steady-state navigation periods (see e.g. eq. (2.22)) and
   - Filtering of measurement periods where the external disturbances can be either corrected for or neglected.
2. Clean the dataset from outlying values;
3. Detect data acquisition issues;
4. Build time averages from aggregated 'clean' datapoints.

The general principle behind data preparation is that one should seek a good balance between filtering the data and correcting it for the disturbances. As already stressed in Section 1.3, the key concept of data filtering is the reduction of the impact of the disturbances ($R_{add}$) at the expense of a drastic reduction of the dataset (Logan, 2011).

Another hugely underrated aspect of data preparation regards the choice of the tools to carry out the analysis. If the SPMS is to be implemented on-line, the computational burden and time lag of the data analysis should be kept to a minimum. Moreover, the greatest issue lies in the fact that the raw data might be neither normally distributed nor devoid of outliers. It follows that a Steady State Identification (SSI) strategy needs to be devised secure from the influence of outliers. On the other hand, the identification of outliers cannot be carried out using an assumption of normality if the measurements do not belong to a steady-state period. Therefore, one of two possibilities must be adopted:

A. The steady-state identification is devised secure from the influence of outliers, or

B. The outlier-detection method should be chosen not based on the assumption of data normality.

Because of the great potential of normal distributions, the first option is better in a generic case. A detailed statistical analysis is given in this Section to justify this choice and clarify this aspect of performance monitoring.

### *4.4.1 Steady-State Identification*

A Steady-State Identification (SSI) technique must be at first used to exclude transient periods from the data analysis. The following variables should be used as indicators:

- Vessel speed, better if ship speed through water $V_s$;
- Propeller speed;
- Shaft torque;
- Vessel heading or alternatively Course Over Ground.

In the literature, mainly two SSI techniques can be found:

**Spread-based SSI** implements dynamic or pre-determined thresholds as the criteria against which a local measure of dispersion is assessed and, if found in excess, rejected. The data may thus be subdivided in data bins or by other more complex means. Dynamic thresholds may be for instance the natural spread of the steady-state signal, whilst the most used dispersion parameters are the range and the standard deviation. Among these methods is the one proposed by the ISO (2016).

**Regression-based SSI** compares the parameters (e.g. slope) of a curve fitted to a time series bin to pre-determined values. Curve fitting up to the 2nd order are common. This method, despite being very intuitive and simple, is however both computationally intense and poorly performing in several cases, for example in the middle of a low frequency oscillation (Rhinehart, 2013).

Because of the unfavourable characteristics and poor performance of regression-based SSI, only spread-based SSI shall be herein discussed.

Since in a SPMS the data normalization is carried out with time-averaged corrections, ship monitoring data usually exhibits a high variability due to the small time-dependent fluctuations in the disturbances. The candidate SSI should therefore be able to allow a certain degree of variation in the data and at the same time be insensitive to outliers. This is achieved either by complementing it with data filtering of some sort or by employing measures of dispersion that *accommodate* for outliers. In the literature, large use is made of high-threshold Low Pass Filters (LPFs), which maintain the measurement's general trends whilst damping the high frequency fluctuations due to noise or outlying values. On the other hand, some statistical devices are able to calculate the statistical properties of a data sample (e.g. location, spread etc.) without being influenced by the presence of outliers. This property is termed accommodation of the outlier. A simple example of a measure of location with such characteristic is the sample median (Barnett and Lewis, 1994).

The most used LPFs are the exponential filter, the moving average and the moving median (or median filter). Since the sample median is *per se* a robust estimation of location, the moving median is the only LPF among the ones above having accommodation properties and was thus chosen to be assessed in this research. The median filter of a sample $X = x_1, x_2, \cdots x_i \cdots x_{n-1}, x_n$ is a $1^{\text{st}}$ order LPF defined:

$$y_i = \tilde{S}_i \tag{4.30}$$

where $Y = y_1, y_2, \cdots y_i \cdots y_{n-1}, y_n$ is the filtered sample, $\tilde{S}_i$ is the median of $S_i$, which is a subset of $X$ centred on $x_i$ and having extremes $x_{i-lr}$ and $x_{i+rr}$. $S_i$ is defined:

$$S_i = x_{i-lr}, x_{i-lr+1}, \cdots x_{i-1}, x_i, x_{i+1}, \cdots x_{i+rr-1}, x_{i+rr}$$

where $lr$ and $rr$ are termed *left rank* and *right rank* respectively. The interval $(lr, rr)$ is termed *window*. Note that the purpose of the median filter is not merely to smooth the data sample, but rather to protect further analysis from strong anomalies in the data, e.g. glitches in the electrical system. Data smoothing is a practice that has little meaning if time averages are thereafter taken.

In the following paragraphs, the steady-state identifiers investigated in this study are described.

***Range.***—The range identifier is the simplest means of testing for a transient state. The data is initially filtered with a median filter having $lr = rr = 4$ (symmetrical windowing). This is a high-threshold LPF which leaves intact the data variability apart from extreme values. The allowable data variation or range may be pre-defined based on experience from on-board measurements specific to the vessel. Table 4.2 shows such

TABLE 4.2

*Allowable variability in the range filter developed for a small fast catamaran.*

| *Variable* | *Variation* |
|---|---|
| $V_s$ | 0.5kn |
| $n$ | 0.0875Hz |
| $Q$ | 27.5Nm |
| $\psi_g$ | 2deg |

TABLE 4.3

*Allowable scaled variability from the local mean for a normalised range identifier.*

| *Variable* | *Variation* |
|---|---|
| $V_s$ | 5% |
| $n$ | 1% |
| $Q$ | 5% |
| $\psi_g$ | 2deg |

values defined for a small high-speed catamaran. Range identifiers are computationally lightweight and if combined with an LPF are robust against strongly outlying values like electrical glitches. Their main problems stems from their inability to scale noise, the need to define pre-determined values and their strong dependence on the LPF gating and data bin size. The crude fashion of this identifier therefore doesn't make it very suitable for performance monitoring and was investigated for comparison with more complete identifiers.

***Normalised range.***—It shares similar features to the range identifier, but the range of the Cartesian variables is normalised by the local mean of the filtered variable, making it able to scale the data noise. Suitable normalised range values are reported in Table 4.3. Because these thresholds are normalised they can be used on vessels on any dimension.

***Normalised standard deviation.***—A LPF equal to those used for range and normalised range SSI is used to secure the normalised standard deviation from outliers. This identifier is still computationally lightweight, scales the noise and is less affected by the LPF window size. The same intuitive values presented in Table 4.3 can be used if the local sample standard deviation is expanded to encompass at least 90% of the data of a hypothetical normally distributed steady-state period:

$$s_E = 3s \tag{4.31}$$

where $s$ is the local sample standard deviation and $s_E$ is the sample expanded standard deviation. It is then normalised by the mean of the filtered data bin to be assessed against the threshold values.

***Normalised IQR.***—The Inter-Quartile Range ($IQR$) is a powerful statistic that can be used as a steady-state identifier. It is a *trimmed* estimator at 0.25, which practically means that it is insensitive to the higher and lower 25% of the ordered dataset. It is therefore a measure of dispersion that accommodates outliers and does not require pre-filtering. On the other hand, it needs to be standardized to be a consistent estimator of the sample standard deviation $s$ of the hypothesised normal distribution. The $IQR$ is standardised according to the following:

$$\hat{s}_{IQR} = \frac{IQR}{2\sqrt{2}\,\mathrm{erf}\,(1/2)} \tag{4.32}$$

where $\hat{s}_{IQR}$ is the standard deviation estimated by the $IQR$ and erf is the Gaussian error function (Huber, 1981). Hence, the standardised $IQR$ is expanded as shown by eq. (4.31) and then scaled by the local median.

The normalised $IQR$ identifier is computationally lightweight and scales noise. Its high trim ratio however makes it 'overprotective' and dull to tail end scatter. As a consequence, it might not recognise the onset or ending of a transient state located at the end or the beginning of the data bin.

***Normalised trimmed standard deviation.***—Another powerful statistic is the $\alpha$-trimmed standard deviation, $\overset{T}{s}_\alpha$, which can be defined as the standard deviation of an $\alpha$-trimmed sample. Similarly to the $IQR$, the higher and lower $\alpha$-fraction of the ordered dataset have no influence on the statistic. $\alpha$ is chosen according to the amount of outliers expected in the data bin and the statistical power of the statistic. According to the detailed studies reported by Barnett and Lewis (1994), a trimmed standard deviation with $\alpha = 0.05$ (5%) has in general a superior performance against other robust measures of dispersion and it was found to provide excellent results when applied to a SPMS. The $\overset{T}{s}_\alpha$ is standardised according to the following:

$$\hat{s}_T = \frac{\overset{T}{s}_\alpha}{\gamma(\alpha)} \tag{4.33}$$

where:

$$\gamma(\alpha) = 1 - 2\alpha - 2\Phi^{-1}(1-\alpha)\varphi\left[\Phi^{-1}(1-\alpha)\right]$$

where $\Phi$ and $\varphi$ are respectively the standard normal cumulative distribution and density functions (Huber, 1981). $\hat{s}_T$ can be then expanded and normalised as explained earlier. The normalised trimmed standard deviation is a robust steady-state identifier, it does not require pre-filtering, it preserves the natural spread of the measurements and is computationally undemanding.

***F-Type statistic.***—Slightly different methods are those based on F-test type statistics, which assess the ratio of sequential to local dispersion of filtered data. F-Type statistics were first introduced by Crowe *et al.* (1955) and then improved by Dr. Rhinehart (Cao and Rhinehart, 1995*b*,*a*). In the latest study, the data is initially filtered using a $1^{st}$ order exponential filter:

$$y_i = \lambda_1 x_i + (1 - \lambda_1)\, y_{i-1}$$

where $y_i$ is the i-th filtered measurement, $x_i$ the i-th raw measurement of the variable under steady-state assessment and $\lambda_1$ a filter factor. The local measure of dispersion is again exponentially filtered and is defined as:

$$v_i^2 = \lambda_2 \left(x_i - y_{i-1}\right)^2 + (1 - \lambda_2)\, v_{i-1}^2$$

The sequential measure of dispersion is similarly defined:

$$\delta_i^2 = \lambda_3 \left(x_i - x_{i-1}\right)^2 + (1 - \lambda_3)\, \delta_{i-1}^2$$

The steady-state identifier, called R-statistic, is then calculated:

$$R = \frac{(2 - \lambda_1)\, v_i^2}{\delta_i^2} \tag{4.34}$$

Fundamentally, when the process is at steady state the sequential dispersion will approximate the local dispersion, thereby making $R \approx 1$. As a transient state is triggered, the filtered data $Y$ will lag behind the data and the local dispersion will be much larger than the sequential dispersion, making $R \gg 1$ (Rhinehart, 2013). $R$ must therefore be assessed against critical values to determine steady-state. Cao and Rhinehart (1995*a*) suggest the following values for the tuning parameters:

$$\lambda_1 = 0.2$$
$$\lambda_2 = 0.1$$
$$\lambda_3 = 0.1$$
$$R_{\text{crit}} = 2.5$$

F-Type statistics have several good properties, such as they do not require data binning, they scale noise, they only require four parameters and need low computational resources when used on-line (i.e. in 'real time').

However, the performance of the R-statistic applied to on-board ship data was found to be poor using the suggested parameters. The likely cause is the high variability of the ship data, which 'confuses' the statistic. To improve the SSI consistency, the parameters

TABLE 4.4

*Computational time of different SSIs relative to the Range identifier in an off-line application* .

| *SSI* | *Performance* |
|---|---|
| Range | 1 |
| Norm. Range | 1.30 |
| Norm. SD | 1.23 |
| Norm. trimmed SD | 0.92 |
| Norm. $IQR$ | 0.77 |
| F-Type | 3.77 |

were changed as follows:

$$\lambda_1 = 0.2$$
$$\lambda_2 = 0.2$$
$$\lambda_3 = 0.1$$
$$R_{\text{crit}} = 6$$

In short, the increase in $\lambda_2$ decreases the damping of $v^2$ and improves the resolution of the local dispersion. As a consequence, the variability of $R$ is increased, thereby requiring to increase the critical value. To compensate for this, the steady-state value is also increased from 1 to 2. In addition, since a lot of the data variability is given by the fluctuation of water motion, the on-board measurements are sequentially autocorrelated. Therefore, an autocorrelation time $\mathbb{t}_{\text{AC}}$ was chosen as:

$$\mathbb{t}_{\text{AC}} = \vartheta/4$$

where $\vartheta$ is the ship time constant. This means that if $X$ is the variable used to determine steady-state (e.g. $V_s$), then only the $x_{k\vartheta/4}$ are used to calculate $R$, with $k = 1, 2, 3 \ldots$.

To compare the six identifiers described so far, a brief section of real sea-trial data measured onboard a high-speed catamaran was used as a test dataset. The dataset includes three steady-state periods, an acceleration and a route inversion at constant propeller speed (Fig. 4.21). The SSI was carried out off-line, i.e. analysing the whole test dataset at once. Figure 4.22 shows the performance of the different SSIs, whilst Table 4.4 compares the required computational effort relative to the basic Range identifier.

Figure 4.22 shows that the best-performing SSIs are the normalised range and the normalised trimmed standard deviation. Unexpectedly, the normalised $IQR$ performs

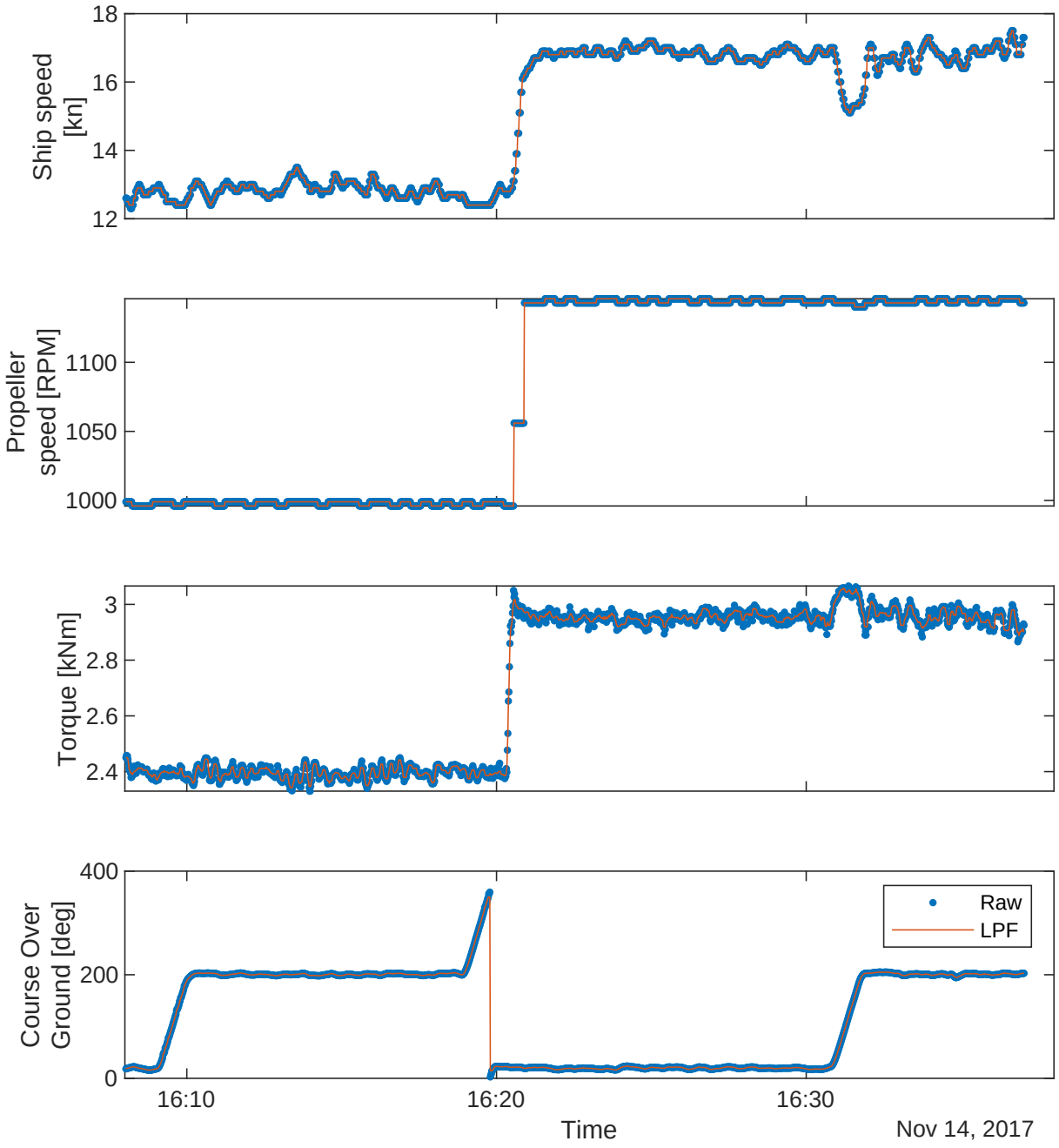


**Figure 4.21** – *Test measurements for SSI. The steady-state indicators are $V_s$, $n$, $Q$ and $\psi_g$.*

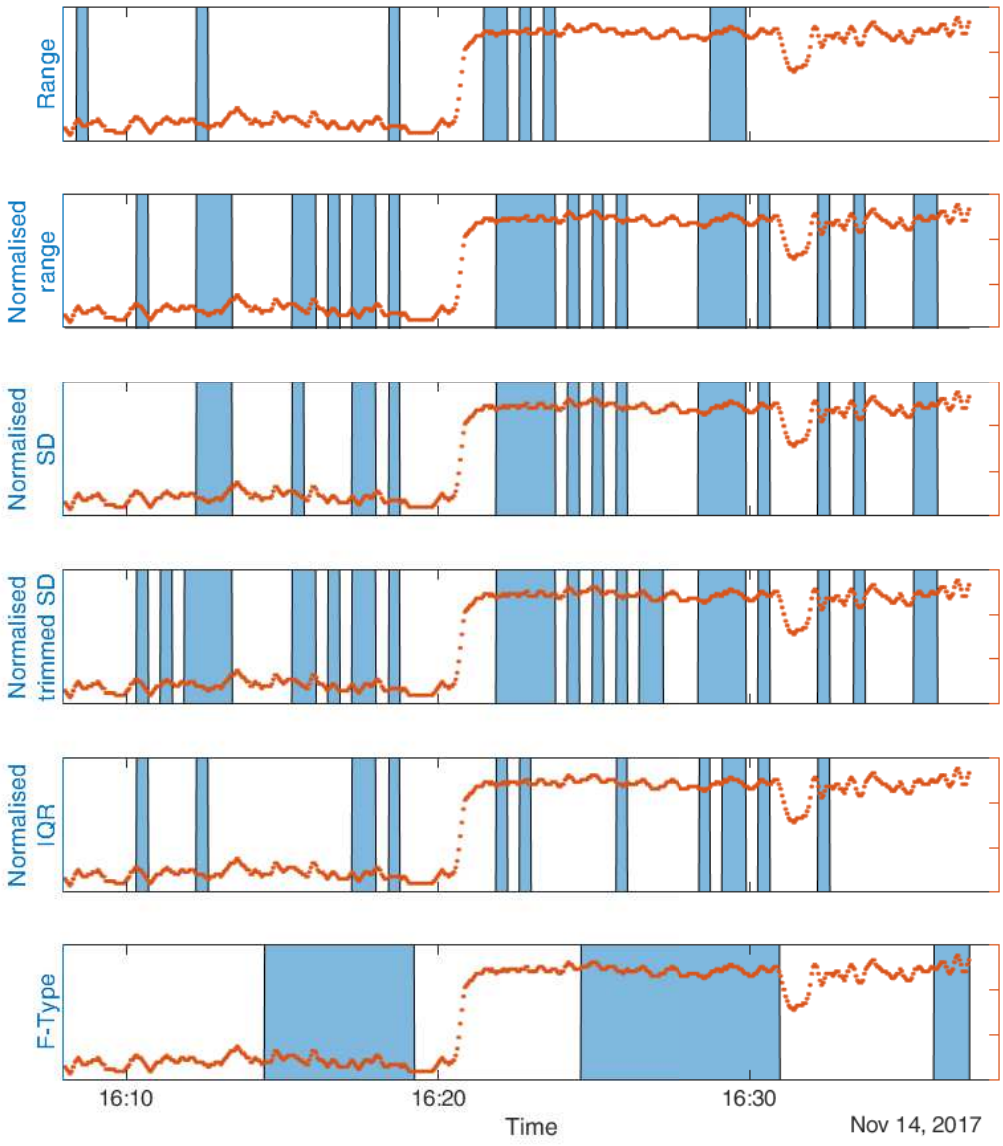


**Figure 4.22** – *Performance comparison of different SSI techniques.*

very poorly, most likely because of the high trimming ratio. The F-Type statistic is the most stable identifier, although it appears to have a large lag before detecting the steady-state condition. The major drawbacks of F-Type statistics are however the weak protection against strong outlying values and the greater computational time needed when running on off-line applications. Moreover, tuning the parameters is not banal and further study is necessary to find the optimal combination in the application to SPMSs. For this reason, a normalised trimmed standard deviation with $\alpha = 0.05$ was selected as the steady-state identifier.

### *4.4.2 Conditional filters*

Making reference to Section 4.2, the objective of conditional filters is to ensure that the normalization of external disturbances is applied within their limits of validity or that the effect of the disturbances on ship performance can be ignored. Since the data is not yet free from the outliers, the conditional filters must be applied either to filtered data or to trimmed samples, depending on the SSI used. In this research, the normalised $\alpha$-trimmed standard deviation is employed and the conditional filters are thus applied to the $\alpha$-trimmed sample.

#### Waves

According to Section 4.2, following, stern quartering and bow quartering seas need stricter filtering, whilst beam seas can be allowed more relaxed thresholds. To reflect this, a simple directional filtering criterion can be devised in the form:

$$H_{S_\zeta} \leq \begin{cases} H & \text{if } \mu_{Rp} < \mu_R < \mu_{Rs} \\ H\left[1 + \gamma \cos^2(\mu_R)\right]^{-1} & \text{Elsewhere} \end{cases} \tag{4.35}$$

where $H$ can be the ITTC total significant wave height threshold ($2.25\sqrt{L_{pp}/100}$ in case the encountered wave spectrum is measured); $\mu_{Rp}$ and $\mu_{Rs}$ are respectively the port and starboard side angular limits of applicability of the wave correction. For instance, if only head seas experiments are available, $\mu_{Rp} = 150\,\text{deg}$ and $\mu_{Rs} = 210\,\text{deg}$; $\gamma$ is the directional filter strictness parameter. The suggested value for $\gamma$ is:

$$\gamma = 0.5 \tag{4.36}$$

This reduces the bow and stern allowed wave height by a third and the added wave resistance and the wake fraction change by about half according to the results in Taskar *et al.* (2016).

**Winds**

The wave threshold set in eq. (4.35) will be constraining on the wind in the majority of the weather conditions. However, at the onset of a strong wind waves may not have formed yet to produce a reasonable monitoring threshold for wind. Therefore, the ITTC (2014*c*) wind threshold shall be used as an upper wind speed limit, whereby:

$$U_{AR} \leq \begin{cases} 10\text{m/s} & \text{if } L_{pp} \leq 100\text{m} \\ 14\text{m/s} & \text{if } L_{pp} > 100\text{m} \end{cases} \tag{4.37}$$

**Currents**

To avoid excessive effects of ocean currents on the ship performance, the following threshold can be suggested:

$$|V_s - V_g| \leq 2\text{kn} \tag{4.38}$$

As remarked in Section 4.2, this filter is reliable if complemented by a good vessel drift filter and if a good, calibrated speed log is used.

**Restricted waters**

A water depth threshold like the one developed by the ITTC (2014*c*) may be implemented by discarding all measurement conducted in areas where the water depth is less than:

$$h = \max\left\{3\sqrt{BT},\ 2.75\frac{V_s^2}{g}\right\} \tag{4.39}$$

where $B$ and $T$ are the ship's breadth and draught respectively and $V_s$ and $g$ the speed through water and gravitational acceleration.

**Water properties**

Following the recommendation of the ISO 19030, a water temperature threshold is suggested to prevent monitoring in icy waters (ISO, 2016):

$$T_w \geq 2°C \tag{4.40}$$

**Displacement and trim**

For eq. (4.13) to be valid, the displacement variation must be limited to:

$$\frac{|\Delta - \Delta_0|}{\Delta_0} \leq 0.05 \tag{4.41}$$

where $\Delta$ is the actual displacement and $\Delta_0$ the displacement in ideal conditions (ITTC, 2014*a*).

If systematic trim tests are not available to correct for trim effect, the trim must comply with the following criterion:

$$|\theta_L| \leq \arctan\left(0.01\frac{T_M}{L_{pp}}\right) \tag{4.42}$$

where $\theta_L$ is the trim angle and $T_M$ the midship draught (ITTC, 2014*c*).

**Steering**

As shown in Section 4.2, the steering resistance is shown to have negligible values when $\delta \leq 3\,\text{deg}$. However it still produces an effect ship resistance of acceptable proportions even when $\delta \leq 5\,\text{deg}$, provided that the steering is occasional and due to small course-keeping adjustments rather than to continuous usage. Therefore:

$$\max|\delta| \leq 5\,\text{deg} \tag{4.43a}$$

$$\frac{\sum_{i=1}^{N}\delta_i}{N} \approx 0\,\text{deg} \tag{4.43b}$$

where $N$ is the size of the data bin defined by eq. (4.29).

**Drift and yaw**

Since correction methods for drift and yaw are difficult, it is necessary to filter their effect. The drifting motion of the vessel can be approximately detected in this case by looking at the over-ground drift angle and the rudder usage (Hasselaar, 2011). Equation (4.43) should already prevent the typical drifting 'into' the current counteracted by the rudder usage.

According to Fig. 4.10 in Section 4.2, the drift forces start to have relevant effects when $\beta \approx 3\,\text{deg}$. Therefore, according to eq. (4.17), the lateral speed through water $v_s$ can be given threshold:

$$|v_s| \leq 0.052u_s \tag{4.44}$$

It has to be remembered that $v_s$ can be measured only with a dual axis speed log. Where this is not available, the ISO 19030 filtering criteria can be used to limit the impact of drift and yaw (ISO, 2016):

$$|\psi - \psi_g| \leq 3\,\text{deg} \tag{4.45}$$

If the heading measurement is not available either, a yaw rate threshold alone can be applied based on the course over ground $\psi_g$:

$$\left|\dot{\psi}_g\right| \leq 4\frac{V_s}{L_{pp}} \tag{4.46}$$

This value is based on the findings presented by Fig. 4.10 and on the definition of nondimensional yaw rate as $\dot{\psi}_g{}' = \dot{\psi}_g L_{pp}/V_s$. Of course, this threshold is less accurate than the other two.

### 4.4.3 Outlier filtering

The steady-state data bins obtained from after SSI and the application of conditional filters can be assumed to be normally distributed and irrespective of their time-dependent nature. Therefore, several statistic tools can be used to finalise the data for the normalization by dealing with the eventual outliers. Outliers arise for several different reasons. Barnett and Lewis (1994) identify two main sources:

**Measurement errors** which are caused by sensors misreading, inadequacy of the measuring equipment and rounding of wrong values. Electrical signal transmission of automatic SPMS also pertains to this category.

**Execution errors** which may arise from collecting a biased data sample that may not be representative of the entire population that needs to be sampled. Although this error may be reduced by taking larger samples, it is often a possibility in automatic measurement systems.

Two statistical methods exist to deal with the outliers — *rejection* and *accommodation*. The former is historically the oldest method (e.g. Peirce, 1852; Chauvenet, 1863) and tests the outlier to verify its fitness within the assumed distribution of the sample. If found statistically unreasonable, i.e. *discordant*, the outlier is rejected from the sample (Barnett and Lewis, 1994).

On the other hand, the accommodation of outliers is conceived to derive valid statistics about a sample without being significantly affected by the presence of outliers. Such statistics are called *robust* against outliers (Huber, 1981).

***Outlier rejection.*** —In the literature relevant to ship performance, outliers are mostly rejected using the Chauvenet's criterion, which has however a high probability of rejecting non-outlying values. It can be shown that for large samples the Chauvenet's criterion has a chance of rejecting a non-outlying measurement of approximately $1 - e^{-1/2}$, which is about 40% (Barnett and Lewis, 1994).

There are different types of discordancy test. Most are ratios of a certain sample property to the sample spread, such as range/spread, deviation/spread, etc. One issue in ship performance monitoring, however, is that a data sample may contain more than one outlier. Therefore, a technique that analyses more than one datapoint is necessary, either by recursive application of a single-value test or by block tests. The most effective multi-outlier detection techniques appear to be the recursive applications of two renowned tests — the Grubb's test and the sample kurtosis. In an extensive research, Jain (1981*a*,*b*) tested the statistical power of recursive discordancy tests, attributing the highest performance to the recursive Grubb's test, commonly called generalised Extreme Studentized Deviate (ESD) (Rosner, 1975).

Given the random data sample $X = x_1, x_2, \cdots x_{n-1}, x_n$, the aim of the ESD is to test the null hypothesis that the sample has no outliers against the alternative that it contains at most $k$ outliers. Then $k$ Grubb's two-tailed statistics are calculated, where:

$$G_j = \frac{\max\{|x - \overline{x}_j|\}}{s_j} \qquad \forall\, x \in X_j$$

where $j = 1, 2, \cdots k$, $\overline{x}_j$ and $s_j$ are respectively the sample mean and sample standard deviation of $X_j = X_{j-1} - \{x_{j-1}\}$, with $x_{j-1}$ that maximises:

$$|x - \overline{x}_{j-1}| \qquad \forall\, x \in X_{j-1}$$

Each $G_j$ is then tested for discordancy against the critical value:

$$G_{j,\text{crit}} = \frac{(n-j)t_{j,\text{crit}}}{\sqrt{(n-j+1)\left(n-j-1+t^2_{j,\text{crit}}\right)}}$$

where $t_{j,\text{crit}}$ is the critical value of the $t$ distribution $T(n-j-1)$ at the significance level $\alpha/(2(n-j+1))$. If $G_j > G_{j,\text{crit}}$, then the null hypothesis is rejected and the tested value marked as an outlier (Barnett and Lewis, 1994). The only caveat of the ESD is having to specify at the onset the maximum expected number of outliers $k$. Thereafter, the recursive test will 'stop' if both $G_j < G_{j,\text{crit}}$ and $G_{j+1} < G_{j,\text{crit}}$. $k$ must be chosen according to engineering judgement. The Author suggests $k = N/5$, where $N$ is the data bin size.

***Outlier accommodation.***—Alternatively to outlier rejection, the more sophisticated accommodation techniques can be used to estimate the statistical properties of a measured sample. Several are the measures that can be used. Huber (1972) reports the results of a detailed investigation regarding the performance of a large selection of location estimators, concluding that the $\alpha$-trimmed mean and standard deviation with $\alpha = 5\%$ present the highest statistical power in most cases. Therefore, if these two estimators are computed within the two filtering stages of SSI and conditional filtering, outliers would be immediately accommodated without the need for further calculations.

In this research, the Author chose to align to the ISO 19030 practice of outlier rejection, but employing the better-performing ESD test. Further study would be needed to compare the performance of the SPMS using the trimmed mean and standard deviation as SSI and outlier accommodation method.

### *4.4.4 Data validation*

Data validation should be periodically carried out to ensure consistency in the measuring equipment. Differently from the other data preparation stages, data validation can be carried out off-line. Although simple in principle, several of these procedures cannot

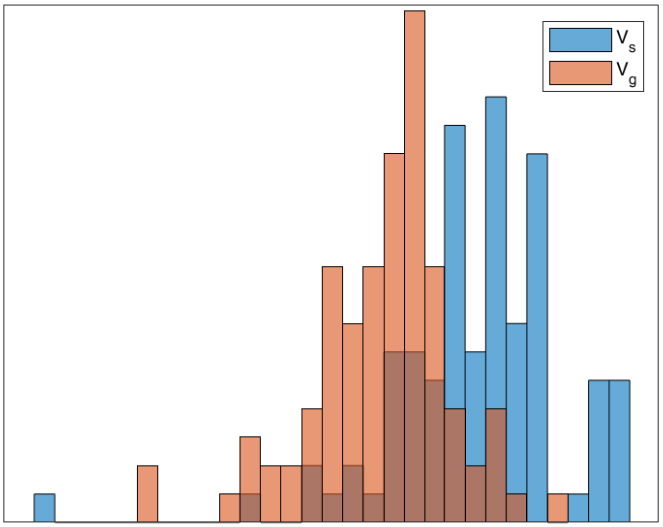


**Figure 4.23** – *Comparison of the distributions of $V_s$ and $V_g$ of a large vessel over a period of a few years [Source: confidential].*

be carried out during the normal operation of commercial vessels, either due to time limitations or to the lack of instrumentation. This section aims at providing a few practical examples of data validation techniques for the most important on-board measurements.

***Speed through water.***—Speed logs are sensors subjected to ageing and to measurement drift. It is thus appropriate to assess their consistency over a certain period of time. The best solution would be to conduct dedicated sea trials to re-assess the speed log calibration. However, this option is unlikely to find many supporters among the ship operators due to the time losses it involves. An alternative way is to analyse the distribution of $V_s$ against the distribution of speed over ground $V_g$ over a long period of time, e.g. one year. (Hasselaar, 2011; Antola *et al.*, 2017*a*; Orihara and Tsujimoto, 2017). Of course, the data must have before passed the filtering process presented earlier. With a consistent dataset, the $V_s$ and $V_g$ distributions will approximate the normal distribution and by the central limit theorem, the two means should ideally be coincident. The underlying assumption is that the data is not biased, i.e. it is randomly acquired and distributed throughout all the period of time. Figure 4.23 shows the comparison of the $V_s$ and $V_g$ distributions for a large ship over a period of a few years. However, data has here a very low sampling frequency. In this case, the analysis should trigger a recalibration of the speed-log.

***Propeller torque and thrust.***—Shaft torque sensors are also subjected to drift, most of the times following the partial detachment of the electrical foil (strain gauges) or misalignment of rotating wheels (e.g. optical sensors). In such cases, the torque measurements may display significantly altered values. In general, however, it would be

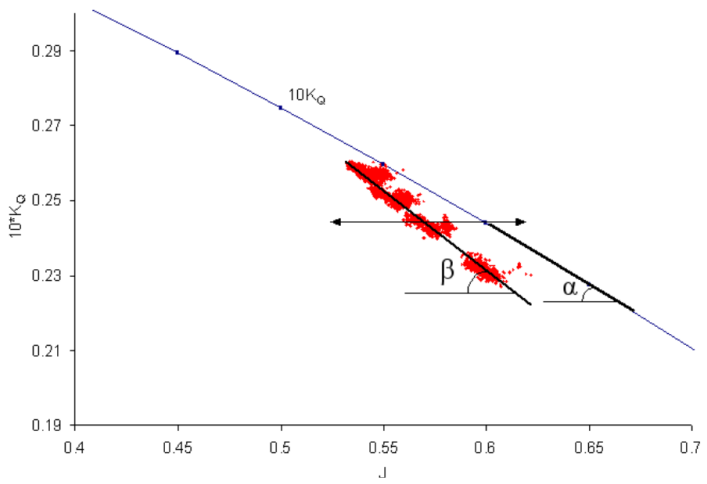


**Figure 4.24** – *Comparison of measured torque against propeller open water curves in Hasselaar (2011).*

recommended to regularly assess the torque measurement, for instance by comparing the derived shaft power with the engine brake power calculated from the fuel consumption (Hasselaar, 2011).

Alternatively, if the propeller open water curves are available, they can also most effectively be used to examine the propeller torque and thrust. $K_T$ and $10K_Q$ coefficients, eq. (2.18a) and (2.18b), are initially calculated from short-term monitoring data. To enter the propeller open water curves, the advance coefficient $J$ (eq. (2.6) and (2.18c)) is calculated using a wake fraction $w$ evaluated in the same short-term period according to the procedure shown in Section 4.5. Figure 4.24 shows the $10K_Q$ values measured on-board the R/V *Bernicia* by Hasselaar against the propeller open water torque curve. In his case, the propeller open water curves were incorrect and made the performance analysis very difficult (Hasselaar, 2011). The resulting effect is similar to what would happen in case of torque sensor drift. Chapter 5 will show the same procedure applied to the case study of this research. Another aspect of torque sensor calibration is related to the presence of residual shaft stresses. When resting on the journal bearings for a relatively long time after sailing (e.g. in port during loading/unloading operations), shafts can develop torsional stresses that severely affect early readings after the vessel's departure (Sasaki and Carchen, 2015). The stresses are released only after abundant lubrication in the stern gland. This usually happens after a few hours of navigation or after 'manual' shaft lubrication, which can be carried out by turning the shaft ahead and astern before departure (ITTC, 2014*c*).

***Wind speed and direction.***—Wind speed and direction should be checked for consistency against shadowing from the superstructure. This can be done during acceptance trials or by conducting a single double run and comparing the calculated true wind speed

and direction as shown in Fig. 4.25. In this case, the shadowing of the sensor from the vessel superstructure can be estimated from the high differences of true wind speed and direction during reciprocal runs.

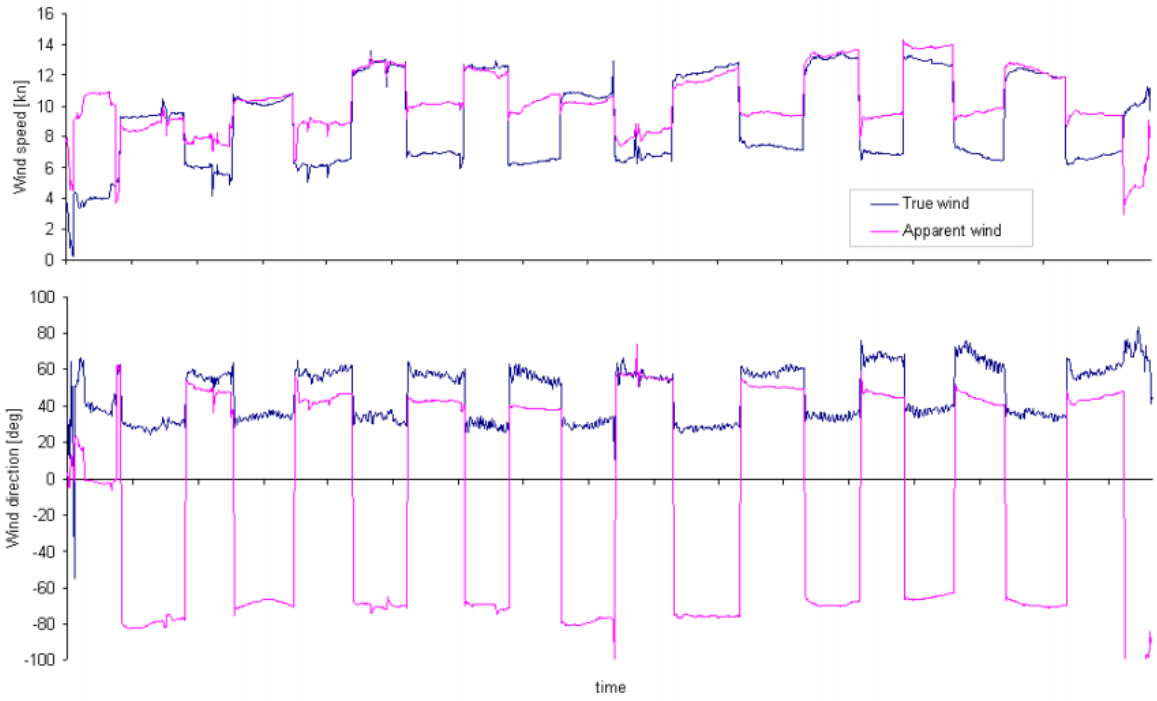


**Figure 4.25** – *Time history assessment of wind measurement consistency on a small research vessel, after Hasselaar (2011).*

### *4.4.5 Performance data*

At the end of the data preparation process, consecutive data bins measured during the same steady-state period are aggregated and the mean, standard deviation and sample size of every variable and for each period are calculated and stored. The datapoints hence obtained are centred at the mid of the period they describe and are ready to be normalised.

## 4.5 Data normalization

In this section, the method used to normalise the effects of disturbances on ship performance are presented under the steady-state assumption identified in Section 4.4. In the data normalisation stage, the added resistance components due to external disturbances are estimated following the equations defined in Section 4.2 and are subtracted from the measured service performance (see eq. (1.3)). In the deterministic normalization process, the principle of superposition is adopted since the correlation between disturbances can be neglected as their effects are not large (ITTC, 2014*a*). It should also be noted that, since

the datapoints obtained after the data *preparation* are essentially averages over a steady-state period, each added resistance component will be evaluated in a similar fashion as the average added resistance over that same steady-state period.

In the following sections, the adopted deterministic normalization method is described in detail after a more general introduction of similar methods.

### *4.5.1 Common normalization methods*

At the time of writing, two methods can essentially be applied to normalise the ship performance data retrieved on board. These are the so-called Taniguchi–Tamura method and the Direct Power method commonly used in the analysis of Sea Trials data. Both take into account a prominent aspect of ship performance monitoring, which is the effect of disturbances on the propulsive efficiency.

Comparing several methods in use in the early 2000, the ITTC (2002*a*) fostered the adoption of the ISO TC8/SC9 method, later ISO 15016:2002 (ISO, 2002), which was essentially a comprehensive revision of the earlier Taniguchi–Tamura method (Taniguchi and Tamura, 1966). This is a speed and torque identity method based on the balance of the propulsive forces at the propeller loading point using the open water performance. The change in propulsive efficiency is derived from the change of the propeller loading point, assuming unaltered thrust deduction factor.

The Direct Power method was devised in a joint effort by the ITTC, the ISO and industry partners to substitute the former ISO 15016:2002 (ITTC, 2014*a*; ISO, 2015*a*). The effect of the added resistance components on vessel powering is calculated similarly to the Taniguchi–Tamura method, but the effect on the propulsive efficiency is instead based on the full-scale wake fraction and the results of load variation tests that have to be conducted beforehand in a towing tank.

Despite the Direct Power method is of more recent conception, the normalization procedure used in this research is based on the Taniguchi–Tamura method (Taniguchi and Tamura, 1966) due to the unavailability of load variation tests. The difference in the two different methods is expected to be negligible for small added resistance components.

### *4.5.2 Normalization procedure*

The main assumption of the Tanguchi–Tamura method is that in steady state conditions, at ship speed $V_s$ the full-scale propeller operating in a velocity field with effective wake fraction $w$ delivers the same thrust as in open water condition under speed $V_s(1-w)$. The open water characteristics of the propeller relate the propeller thrust with torque, which is a more accurate measurement, and provide propeller efficiency estimates — see Section 4.3. Where physical open water tests wouldn't be possible, reliable analytical methods or numerical simulations (e.g. Greeley and Kerwin, 1982) can be used to calculate the

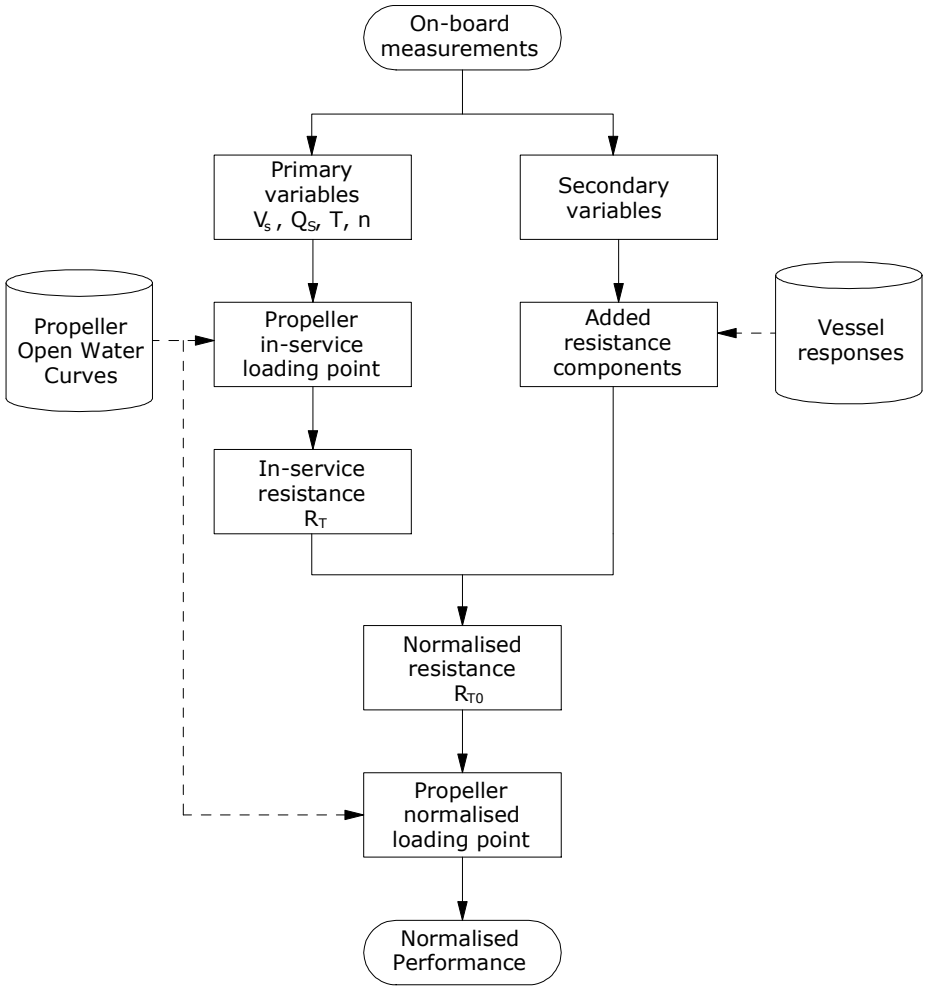


**Figure 4.26** – *Flowchart of the proposed normalisation procedure.*

propeller's open water characteristics based on its geometry. Coherently, an estimate of the thrust deduction factor also needs to be made by means of towing tank tests or empirical formulations. The thrust deduction factor is assumed to be solely dependent on ship speed, neglecting the influence of disturbances. Within the limits described in Section 4.4, this assumption is satisfactory. The normalization procedure is at first represented in the flowchart of Fig. 4.26 and described in the following paragraphs.

The measured propeller coefficients are firstly calculated from:

$$K_Q = \frac{Q_S}{\rho n^2 D^5} \eta_r \eta_s \tag{4.47a}$$

$$K_T = \frac{T}{\rho n^2 D^4} \eta_r \eta_s \tag{4.47b}$$

where $Q_S$ and $n$ are the measured propeller shaft torque and speed respectively. For convenience, both coefficients are expressed as second-order polynomials of the propeller

coefficient of advance $J = V_a/nD$:

$$K_Q = \mathrm{f}(J) = a_0 + a_1 J + a_2 J^2 \tag{4.48a}$$

$$K_T = \mathrm{g}(J) = b_0 + b_1 J + b_2 J^2 \tag{4.48b}$$

As already mentioned, fouling affects the propeller torque and only negligibly its thrust (Mosaad, 1986). On the other hand, thrust measurements are more difficult to obtain and display a scatter larger than torque's (Section 4.3). For this reason, the measured thrust is suggested for use in later stage analysis only and torque be instead the primary performance measurement. This will be further explained in Section 4.6. Therefore, two separate $J$ numbers are calculated, one based on measured torque and the other on thrust:

$$J_Q = \mathrm{f}^{-1}(K_Q) \tag{4.49a}$$

$$J_T = \mathrm{g}^{-1}(K_T) \tag{4.49b}$$

The thrust coefficient is recalculated from $J_Q$ using eqs. (4.48) as:

$$K_{T_{KQ}} = \mathrm{g}(J_Q) \tag{4.50}$$

It should be noted that in standard conditions and with no propeller fouling $K_T = K_{T_{KQ}}$, but not necessarily so in other cases. This is explained in Fig. 4.27, which makes reference to Fig. 2.17 in Chapter 2. The subfigure (a) shows the derivation of $J$ from $K_T$ and $K_Q$ measurements in case of a clean propeller. Subfigure (b) shows instead the case of a fouled propeller, where the $10K_Q$ curve is higher (dash-dot line) due to the fouling build-up. In the current methodology, the propeller open water curve is not corrected for fouling. Hence, when the propeller is fouled and the $10K_Q$ curve increases, $J_Q$ will be underestimated as a consequence of using a 'clean' open water curve for a fouled propeller. In this case, the $J_T$ and $J_Q$ values would be different. It should be noted that the overestimation of the real $J$ does not affect the goodness of the analysis significantly since the evaluation of the vessel's performance is relative to another measurement. The full-scale effective wake fraction is calculated according to both advance coefficients of eqs. (4.49), obtaining a torque identity wake fraction ($w_Q$) and a thrust identity wake fraction ($w_T$):

$$w_Q = 1 - \frac{nDJ_Q}{V_s} \tag{4.51a}$$

$$w_T = 1 - \frac{nDJ_T}{V_s} \tag{4.51b}$$

An apparent wake fraction can be therefore defined as:

$$w_{app} = w_Q - w_T \tag{4.52}$$

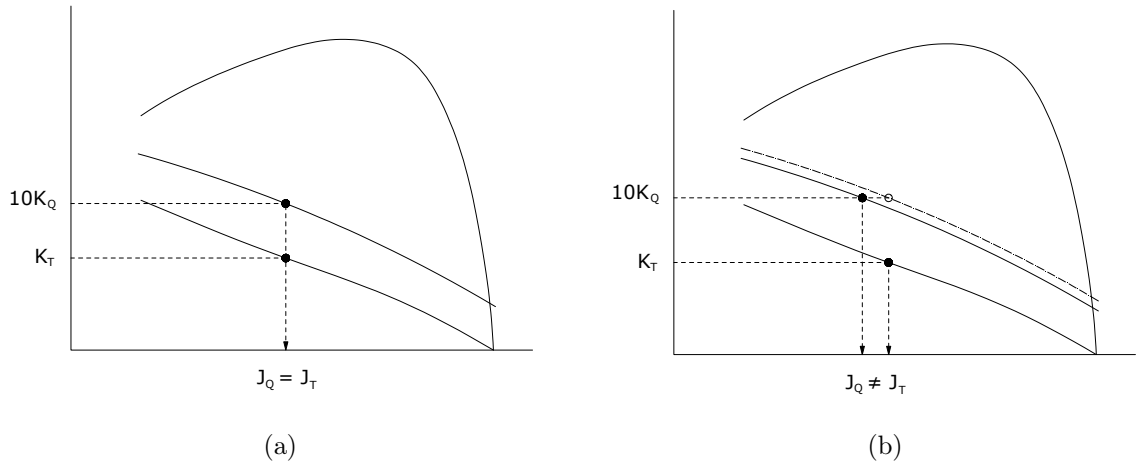


(a) (b)

**Figure 4.27** – *Estimation of J number from $K_T$ and $K_Q$ measurements from the propeller open water curves in* (a) *clean and (*b*) fouled propeller condition.*

As thrust is negligibly affected by fouling, the true effective wake fraction $w$ is well approximated by the thrust identity wake fraction defined in eq. (4.51):

$$w \approx w_T \tag{4.53}$$

According to eq. (4.52) and (4.53), we can thus consider the torque identity wake fraction as:

$$w_Q = w + w_{app} \tag{4.54}$$

$w_{app}$ is a fictitious wake component resulting from using the torque of a propeller with rough blades to enter 'smooth' open water curves. $w_{app}$ is therefore an indirect indicator of the amount of fouling on the propeller and its function will be described in Section 4.6.

The propeller loading point is calculated based on the torque-identity variables, defined by:

$$\tau = \frac{K_{T_{KQ}}}{J_Q^2} \tag{4.55}$$

In the Taniguchi–Tamura method, the propeller loading point is used to calculate the balance of forces. The total measured resistance is therefore estimated as:

$$R_T = \rho D^2 V_s^2 \left(1 - t\right) \left(1 - w_Q\right)^2 \tau \tag{4.56}$$

where $\rho$ is the water density, $D$ the propeller diameter, $V_s$ the ship speed through water, $t$ is the thrust deduction factor and $w_Q$ the torque-identity wake fraction. The total added resistance of eq. (1.3) is therefore calculated from the following equation:

$$R_{add} = \overline{R}_{AA} - \overline{R}_{AA0} + \overline{R}_{AW} + R_\rho + R_\Delta + R_\delta + R_{\beta,\psi} \tag{4.57}$$

where $\overline{R}_{AA0}$ is the time-averaged air resistance due to the ship motion, defined in eq. (4.2), and the added resistance components are those defined in Section 4.2. Nevertheless,

recalling the design principles in Section 4.2, the manoeuvring resistance $R_{\beta,\psi}$ and the steering resistance $R_\delta$ can be neglected and omitted from the equation. The normalised service resistance (i.e. in ideal conditions) can be estimated from the equation:

$$R_{T0} = R_T - R_{add} \tag{4.58}$$

The correction of the propeller loading condition is thus carried out accordingly:

$$\tau_0 = \tau - \Delta\tau \tag{4.59}$$

with

$$\Delta\tau = \frac{R_{add}}{R_T}\tau \tag{4.60}$$

The normalised propeller advance coefficient and torque coefficient are calculated from:

$$J_{Q0} = \frac{-b_1 - \sqrt{b_1^2 - 4b_0\left(b_2 - \tau_0\right)}}{2\left(b_2 - \tau_0\right)} \tag{4.61}$$

and

$$K_{Q0} = \mathrm{f}\left(J_{Q0}\right) \tag{4.62}$$

Accordingly, the corrected propeller speed can be recalculated from:

$$n_0 = \frac{J_Q}{J_{Q0}}n \tag{4.63}$$

and the corrected effective wake fraction:

$$w_{Q0} = 1 - \frac{J_{Q0}n_0D}{V_s} \tag{4.64}$$

The normalised delivered power is finally evaluated by the following equation:

$$P_{D0} = 2\pi\rho D^5 K_{Q0} n_0^3 \eta_s \tag{4.65}$$

The dataset obtained after the normalisation process in principle contains information regarding the vessel performance in the *ideal* service conditions defined in Section 1.3, i.e. with calm weather, defined loading condition and steady-state sailing. Moreover, several other variables are derived within the algorithm, such as the wake fraction indicators and other propeller-related variables. These will be employed in the final stage of data analysis presented in the next section.

## 4.6 Performance analysis

Once the data is normalised, the vessel performance against fouling can be assessed observing the variability of parameters commonly termed Key Performance Indicators (KPI). Existing deterministic and non-deterministic SPMSs use very different KPIs, based on

the available data and the data treatment used. For instance, the ISO 19030 (ISO, 2016) employs a speed-loss KPI calculated over an evaluation period at a fixed power. Hasselaar (2011) and Orihara and Tsujimoto (2017) define a KPI based on power increase, which indicates the instantaneous influence of external conditions over the short term, whilst if observed over the long term it indicates the developing effect of fouling on ship performance. Since Hasselaar's method corrects the propeller open water curves for propeller fouling, the power KPI he proposes reflects the sole influence of hull fouling. Hunsucker (2016) again develops a power-based KPI, however subtracting from the measured in-service powering the effect of viscous forces.

According to the Author's research, the above presented KPIs are not sufficient to provide a clear perspective of the hydrodynamic performance of a vessel. Power increase is a very basic, low-uncertainty and robust indicator, but it is however not specific and precise in identifying the source of power increase, particularly over the short term. Hasselaar's method is the sole that modifies the propeller open water curves by periodically measuring propeller roughness and applying Mosaad's correction (1986). However, such procedure has proven in the past to be rather unwieldy due to the involvement of the measurement of propeller roughness. The Author believes that comparison of different KPIs may provide a clearer insight in the vessel' hydrodynamic performance.

### *4.6.1 Proposed method*

Broadly speaking, most KPIs are derived by torque-identity and may thus include the effect of propeller fouling. Their interpretation must be therefore carefully considered. In case the KPI is influenced by propeller fouling, it will be here represented in its 'fouled' form denoted by a circumflex. In this section, four KPIs are suggested.

The first KPI is based on shaft power and describes the change in normalised power over time $\mathbb{t}$ with respect to a reference period $\mathbb{t}_{\text{ref}}$. The reference period is identified as the length of time during which the vessel performance is obtained for *reference* conditions. The baseline value calculated during the reference period can be obtained, for instance, by curve fitting. Care must be taken in carrying out such operation to avoid overfitting whilst at the same time capturing the trend of the variable. For every given $V_s$, this KPI can be defined as follows:

$$P_K(\mathbb{t}, V_s) = \frac{P_{D0}(\mathbb{t}, V_s)}{P_{D0\,\text{ref}}(\mathbb{t}_{\text{ref}}, V_s)} - 1 \tag{4.66}$$

where $P_{D0}$ is the normalised delivered power defined in eq. (4.65). Power-based KPIs are robust, easy to interpret and encompass the effect of propeller fouling on the total performance. However, they can be somewhat blunt when used to analyse the effect of fouling.

In this respect, KPIs derived from the analysis of the measured effective wake fraction are more indicative despite their higher sensitivity to other external disturbances. Since

it represents a measure of the mean inflow to the propeller, the wake fraction is directly related to the thickness of the hull's boundary layer. It is therefore very sensitive to changes of hull roughness and less sensitive than $P_{D0}$ to several external disturbances. Furthermore, the analysis of wake-based KPIs is simplified by the almost linear dependence of the wake fraction from the ship speed — at displacing speeds. Therefore, in a similar fashion the second KPI is based on the effective wake measurement and is defined as the relative change in effective wake fraction, described as follows:

$$\hat{w_K}(\mathbb{t}, V_s) = \frac{w_Q(\mathbb{t}, V_s)}{w_{Q\,\mathrm{ref}}(\mathbb{t}_{\mathrm{ref}}, V_s)} - 1 \tag{4.67}$$

This KPI is referred to as wake fraction gain and it attempts to describe the increase of wake fraction (or the decrease in propeller inflow) due to hull fouling, $w_\phi$, as set forth in the aims of this research — see eq. (1.4). However, it must be noted that eq. (4.67) depends on the propeller open water characteristics and the measured propeller torque $Q$, which can significantly be affected by fouling. Therefore, in case of a fouled propeller, $w_Q$ will be an overestimation of the true wake fraction as a consequence of the increased drag characteristics of the propeller blades and the reduced open water efficiency. Consequently, $\hat{w_K}$ will overestimate $w_\phi$ and shouldn't therefore be interpreted in its absolute meaning but, rather, as a relative indicator of the combined effect of hull and propeller fouling on vessel performance. In any case, such combined effect is usually of interest to the ship operator.

The distinction between hull and propeller contributions to the increase in propeller torque is possible if thrust measurement are available or regular propeller roughness measurements are conducted with which to correct the open water curves for fouling effect (Atlar *et al.*, 2002; Seo *et al.*, 2016). Thrust measurements are, as mentioned, quite uncertain for primary use but can provide a good indication of propeller fouling. However, because the thrust measurement can be quite unstable and may include a parasitic load, a calibration of some sort is necessary. A robust way of doing this is to employ the apparent wake fraction, $w_{app}$, presented in eq. (4.52). $w_{app}$ can be calibrated during the reference period against the vessel speed through water. If properly carried out, the baseline apparent wake fraction can be evaluated secure from most non-linear effects of thrust measurements.

The third KPI can be therefore defined as the ratio between the apparent wake fraction increase and the reference torque-identity wake fraction:

$$w_{app\,K}(\mathbb{t}, V_s) = \frac{w_{app}(\mathbb{t}, V_s) - w_{app\,\mathrm{ref}}(\mathbb{t}_{\mathrm{ref}}, V_s)}{w_{Q\,\mathrm{ref}}(\mathbb{t}_{\mathrm{ref}}, V_s)} \tag{4.68}$$

$w_{app\,K}$ is an indicator of the accumulation of propeller fouling over time and it represents the proportion of $w_Q$ caused by propeller fouling. The reader may find it useful to refer to Fig. 4.27. Thus, $w_{app\,K}$ will be zero with a clean propeller and increase its value as biofouling builds up on the propeller blades.

The fourth and last KPI is related to the increase of hull viscous drag. As expressed by eq. (1.3), the only component of ship resistance significantly affected by hull fouling relates to the viscous forces. In nondimensional terms:

$$C_T = (1 + \phi)C_v + C_w \tag{4.69}$$

where $\phi$ was termed fouling coefficient and defined in Chapter 1. $\phi$ represents the effect of fouling on the hull's viscous drag. The viscous drag coefficient is defined as in eq. (2.3):

$$C_v = (1 + k)C_f \tag{4.70}$$

where $C_f$ is the frictional coefficient of the equivalent flat plate and $k$ is the form factor. The total resistance coefficient, $C_T$, can be calculated from eq. (4.56). Since $R_T$ is estimated from $Q$, it may be a slight overestimation of the real $R_T$ due to the effect of the eventual propeller fouling. It shall therefore be written in its spurious form $\hat{C_T}$. The reference wave pressure coefficient can be assessed for the clean hull and propeller as $C_{w\,\mathrm{ref}} = C_{T\,\mathrm{ref}} - C_{v\,\mathrm{ref}}$. Since $C_w$ remains practically unchanged with fouling, the fouling coefficient $\phi$ can be used as a KPI:

$$\hat{\phi}(\mathbb{t}, V_s) = \frac{\hat{C_v}(\mathbb{t}, V_s)}{C_{v\,\mathrm{ref}}(\mathbb{t}_{\mathrm{ref}}, V_s)} - 1 \tag{4.71}$$

with $\hat{C_v}(\mathbb{t}, V_s) = \hat{C_T}(\mathbb{t}, V_s) - C_{w\,\mathrm{ref}}(V_s)$.

Although $\hat{\phi}$ includes the effect of propeller fouling on the calculated resistance, it gives a more detailed indication of the effect of fouling growth on viscous and total resistance. If the effect of propeller fouling needs to be separated from that of the hull, the thrust measurements may be used as in the following description. With reference to eq. (4.49), (4.50) and (4.52):

$$J_Q - J_T = -\frac{V_s}{nD}\, w_{app} \tag{4.72}$$

$$\therefore K_{T_{KQ}} - K_T = -\frac{V_s}{nD}\, \frac{\mathrm{d}K_T}{\mathrm{d}J}\, w_{app} \tag{4.73}$$

where $\mathrm{d}K_T/\mathrm{d}J$ is calculated in the operational range. Using eq. (4.56), the eq. (4.73) can be rewritten as:

$$C_{v\,app} = -\frac{2nD^3(1-t)}{SV_s}\, \frac{\mathrm{d}K_T}{\mathrm{d}J}\, w_{app} \tag{4.74}$$

where $S$ is the hull's wetted surface area. $C_{v\,app}$ is the effect of propeller fouling on the estimation of the viscous resistance and can be defined as:

$$C_{v\,app} = \hat{C_v} - C_v \tag{4.75}$$

with $C_v$ being the real viscous drag coefficient. For a fouled hull, $C_v$ may be expressed as:

$$C_v = C_{v\,\mathrm{ref}} + \Delta C_f \tag{4.76}$$

or

$$C_v = C_f(1+k) + \Delta C_f \tag{4.77}$$

where $\Delta C_f$ is the frictional coefficient increase caused by hull roughness change as defined by the ITTC '78 (2011$a$). From eq. (4.71) and (4.77) it follows that:

$$\Delta C_f = \hat{\phi}(1+k)C_f - C_{v\,app} \tag{4.78}$$

or

$$\Delta C_f = \hat{\phi}(1+k)C_f + \frac{2nD^3(1-t)}{SV_s}\,\frac{\mathrm{d}K_T}{\mathrm{d}J}\,w_{app} \tag{4.79}$$

Several studies are nowadays involved with the estimation of the effect of hull fouling on vessel performance from the knowledge of the elemental surface roughness (e.g Schultz, 2007; Demirel *et al.*, 2017$a$). These methods were defined 'bottom-up' approaches in Section 2.4. The $\Delta C_f$ derived in eq. (4.79) can therefore be compared with $\Delta C_f$ estimations obtained in 'bottom-up' studies. These will inevitably show some differences, due to three-dimensional flow effects and approximations of the theory. However, the proposed methodology in this perspective contributes to Telfer's long-sought reconciliation of the small-scale measurements and predictions with full-scale trials and monitoring (1972).

## 4.7 Summary

The chapter described in detail the deterministic methodology proposed in this study in accordance with **Objective B** and **C**. At first, it was shown that the design of a deterministic SPMS revolves around the adopted normalisation method. Much discussion was devoted to examine not only the feasibility of each correction (e.g. wind, waves, etc.), but also its convenience in view of the kind of measurements it requires, the complexity of the correction and its impact on the overall vessel performance. It was shown that direct wind resistance, added wave resistance, the effect of currents and of changes in displacement should be corrected for. It was also shown that the effects of changes in water properties, steering, drift and yaw may be corrected only if the necessary means are available and reliable, since their effect is small and difficult to evaluate. Conversely, the effects of shallow or restricted waters and of trim should not be corrected unless dedicated experiments have been carried out for the hull under scrutiny.

In Section 4.3, an equation for the time constant was derived with the scope of obtaining a vessel-specific time scale with which to calibrate the whole data analysis — such as data binning, sampling frequency, etc. Hence, several sensor types were described with their common issues and advantages. A major consideration was made with respect to Doppler speed logs, deemed unreliable by the vast majority of the literature. Following the extensive work of MARIN (van den Boom and Hasselaar, 2014; Hasselaar, 2015),

Doppler logs were verified to deliver reliable measurements, often confused by the presence of currents or drift. The proposed methodology embraced these findings, enacting a series of filters to limit the impact of both above factors. The principles of data communication and logging were then discussed, with particular attention to the quality inspection of analogue signals and the importance of continuous automatic measurement systems. The section then presented the different types of data contained in the datapoint and the general approach to their analysis.

Section 4.4 described the raw data handling techniques. Several Steady-State Identifiers were compared in underlying principles and performance. It was concluded that the standardised trimmed standard deviation at the 5% compared against dynamic thresholds is the most suitable choice in ship performance monitoring. A particular F-Type statistic was also identified to deliver interesting results, which shall be further investigated in future study. Conditional filters were then defined to complement the normalisation procedure identified earlier. In particular a new directional filter was proposed for added wave resistance and conditional filters for drift and yaw motions were derived from manoeuvring simulations. The section then tackled the management of outliers, distinguishing two radically different approaches, namely outlier rejection and accommodation. The adoption of the generalised Extreme Studentized Deviate is proposed in replacement of the obsolete Chauvenet's criterion based on exhaustive research. Data validation techniques were at last proposed for speed through water, propeller torque and thrust, wind speed and wind direction.

In Section 4.5, the Taniguchi–Tamura sea trials correction principles were adopted and described. The method avoids correcting the propeller open water curves for propeller fouling, taking advantage of the discrepancy between torque-identity and thrust-identity variables. The concept of apparent wake fraction was therefore introduced.

Finally, in pursuit of **Objective D** Section 4.6 derived four KPIs, three of which are of novel concept in modern ship performance monitoring. These are based on the wake fraction increase due to biofouling, the apparent wake fraction increase due to propeller fouling and the increase of fouling coefficient, which represents the impact of biofouling on the vessel's viscous drag. Most importantly, it was considered that if the source of power increase is to be assessed, the use and comparison of multiple KPIs is radically more beneficial than observing a single parameter. Finally, in the effort to contribute to the reconciliation of full-scale measurements with small-scale experiments and simulations, a novel derivation of $\Delta C_f$ from the above KPIs is proposed.

The final two chapters of this thesis will present the application of the proposed methodology to Newcastle University's R/V *The Princess Royal* and a detailed estimation of the uncertainty related to the final performance assessment.

# CHAPTER 5

# Case study: *The Princess Royal*

## 5.1 Introduction

In accordance with **Aim 2** and **Objectives E F** and **G**, this chapter describes how the methodology laid out in Chapter 4 was applied by the Author to Newcastle University's R/V *The Princess Royal*. A complete, working SPMS was designed and implemented on-board the vessel with the capability of on-line operation, i.e. to carry out data acquisition, preparation and normalization and long-term performance analysis directly on the vessel without the need to communicating data onshore.

To facilitate the reader in following the method laid out earlier, this chapter follows closely the structure of Chapter 4. In doing so, Section 5.2 presents *The Princess Royal* characteristics and main features. Section 5.3 details the methods used to normalise the measurements for the disturbances in order to define the characteristics of the SPMS. Section 5.4 then describes the 'physical' monitoring system, with a detailed insight into the sensors and their capabilities. A brief description of the data acquisition software module is also given. In addition, the timeline of the sea trials and monitoring campaign is provided. Next, Section 5.5 and 5.6 describe respectively the procedures adopted to prepare the data for the performance analysis and the normalization carried out on the sea trials data conducted after the implementation of the final SPMS (January 2017). Descriptions of the data preparation and data normalization software modules are also given. Finally, the service performance of *The Princess Royal* is analysed and widely discussed in Section 5.7. Here, at first the method employed to derive the baselines for the reference performance is presented. Then, the service performance of the R/V is discussed by analysing the four proposed KPIs and $\Delta C_f$. At the light of the hull and propeller surveys presented, the outcomes of this SPMS are discussed. Eventually, a brief comment on the fouling control strategy is included as a result from this performance analysis.

## 5.2 Vessel description

With the 1973 R/V *Bernicia* nearing the end of her service life, the School of Marine Science and Technology of Newcastle University took on the challenge to design an innovative replacement vessel to fulfil the needs of an increasing demand for field research (Atlar *et al.*, 2010). The efforts of a team of marine technology final year students, doctoral candidates and academics resulted in the design of a novel 18m semi-displacement type aluminium alloy catamaran, which was eventually built in Blyth by Alnmaritec Ltd (Fig. 5.1). The vessel's hullform was based on the catamaran application of the displacement type Deep-V hull form with an anti-slamming bulbous bow and a stern tunnel (Atlar *et al.*, 2013*b*), shown in Fig. 5.2. Both features are inherited from the *coble*, a typical Northumberland fishing vessel. Although the seakeeping properties of catamarans are generally worse compared to monohulls, the Deep-V form gives *The Princess Royal* a superior seakeeping performance, allowing to sail at cruising speed up to sea state 4 (Atlar *et al.*, 2013*a*). On the other hand, the relatively small waterplane area results in lower damping and smoother restoring forces, which translate in significant motions also at lower speeds. Since motions largely impact the added wave resistance, such feature of the R/V must be taken into consideration in the design of the SPMS. In addition to the seakeeping characteristics, the vessel was refitted with a pair of manually controlled interceptors to correct for the large dynamic trim angles at speed. These provided about 5% power savings at 12 kn (Atlar *et al.*, 2013*a*).

Beside the above sailing features, the R/V boasts the wide working deck area typical of catamarans, which is additionally fitted with a moon pool facility for Remotely Operated Vehicles (ROV) deployment and modular research equipment (e.g. Atlar *et al.*, 2015). The moon pool is complemented by a wide range of hydraulic cranes and by a hydrographic winch (Atlar *et al.*, 2013*a*; Atlar, 2014). A wildlife observational tower was also built above the wheelhouse deck to support marine science research and chartering. *The Princess Royal* thus lends itself to be used as a multi-purpose science and technology platform with a flexible speed range for a wide variety of full-scale marine measurements and observations. Her main duties include conventional trawling, sampling, dredging, marine wild life observation, wind farm/renewable device support, performance monitoring, coating/fouling inspection, cavitation and noise research. Table 5.1 reports all the main characteristics of *The Princess Royal*, whilst Fig. 5.3 presents the front and side view from the General Arrangement drawings.

The R/V is fitted with a pair of fixed pitch propellers designed to provide good efficiency over the unusually wide operating range of the vessel. In fact, depending on the mission profile, *The Princess Royal* may be required to operate at extremely low speed for trawling (∼3kn) or at high speeds for Search And Rescue (SAR) operations (∼20kn) as well as at a cruise speed of 15kn (Atlar *et al.*, 2013*a*). The original propellers were designed


(a)

(b)

**Figure 5.1** – The Princess Royal *sailing to her berth in Blyth* (a) *and in the drydock, September 2016* (b).

(a)

(b)

**Figure 5.2** – *Particulars of the* The Princess Royal*'s hull design.* (a) *shows the anti-slamming bulbous bow and* (b) *the stern tunnel with the arc-shaped interceptor.*

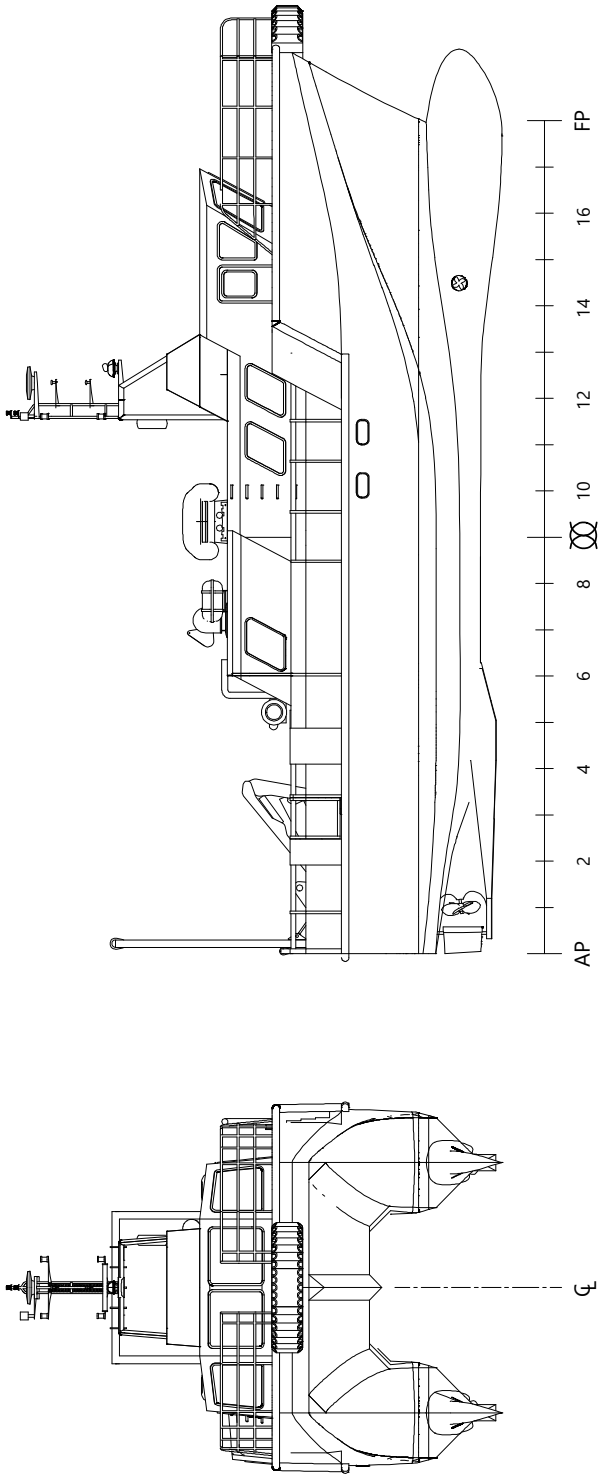


**Figure 5.3** – The Princess Royal *front and side view from the General Arrangement drawings.*

TABLE 5.1
The Princess Royal's *main characteristics.*

| *Characteristic* | *Symbol* | *Value* |
|---|---|---|
| Length Overall | $L_{oa}$ | 18.88m |
| Length B. P. | $L_{pp}$ | 16.45m |
| Breadth, moulded | $B$ | 7.3m |
| Demi-hull separation ($C_L$ to $C_L$) | | 4.9m |
| Light Load Displacement | $\Delta$ | 45.5t |
| Average midship draft | $T$ | 1.86m |
| Wetted Surface | $S$ | 118.52m$^2$ |
| Block Coeffcient | $C_b$ | 0.362 |
| Prismatic Coefficient | $C_p$ | 0.737 |
| Max Speed | | 22kn |
| Time constant | $\vartheta$ | 23s |

and manufactured according to the above principles. However, during the construction of the vessel, various late specification changes and the poor weight control policy of the yard resulted in a lightship displacement increase of more than 18%. Because of these reasons, the performance of the vessel was reassessed a few years later (2015) through a series of speed-power trials and, based on this review, the propellers were redesigned (Carchen *et al.*, 2015). The propeller replacement work was conducted in collaboration with Stone Marine Propulsion Ltd., resulting in a pair of propellers based on the 'New Profile Technology' (NPT), which had been successfully applied to medium and large size ships. The project demonstrated that the NPT design is also suitable for small size vessels. The NPT propellers were fitted to *The Princess Royal* in late June 2015. They boast a larger sweep angle to enhance the effect of skewness on the tip cavitation development and a much smaller blade area ratio, resulting from a particular blade section design that minimises the cavitation inception (Carchen *et al.*, 2015). To allow propeller cavitation observation in full scale, the R/V is fitted with two pairs of bespoke propeller observation windows in the hull just above the propeller plane (Fig. 5.4).

Finally, based on the manoeuvrability simulations mentioned in Section 4.3, the time constant of *The Princess Royal* was calculated as $\vartheta = 23s$.

Table 5.2 reports the principal characteristics of the R/V NPT propellers, whilst Table 5.3 describes the characteristics of the two main engines.

**Figure 5.4** – *Stern view of the port side NPT propeller. The two observation windows can be seen above the propeller.*

TABLE 5.2

*Full-scale propeller main characteristics.*

| *Characteristic* | *Symbol* | *Value* |
|---|---|---|
| Number of propellers | | 2 |
| Propeller diameter | $D$ | 0.75m |
| Pitch to diameter ratio @0.7R | $P/D$ | 0.845 |
| Expanded Blade Area Ratio | $EAR$ | 0.83 |
| Number of blades | $Z_p$ | 5 |
| Rake angle | $\theta_{ip}$ | 0deg |
| Skew angle | $\theta_{sp}$ | 30deg |
| Hub to propeller diameter ratio | $D_h/D$ | 0.18 |
| Chord length @0.7R | $c_{0.7}$ | 0.286m |
| Thickness to chord ratio @0.7R | $t_p/c$ | 0.0414 |
| Thickness @0.7R | $t_p$ | 81.7mm |

TABLE 5.3
*Engine and gear main characteristics.*

| | |
|---|---|
| Number of main engines | 2 |
| Maximum output | 2x537 kW |
| Rated speed | 2300 RPM |
| Absolute fuel consumption | 2x142 l/h |
| Operation mode | 4-stroke Diesel engine |
| Cooling | Watercooled with heat exchanger |
| Turbocharging | Turbocharger with intercooler and waste gate |
| Fuel system | Common Rail EC direct injection |
| Reduction gears | 2xQuickShift TwinDisc MGX 5114 A |
| Reduction ratio | 1.75:1 |

### *5.2.1 Propulsive characteristics*

The vessel's features which are most relevant in view of the application of the ship performance analysis method proposed in this study are those related to the propulsion. Following the discussion made in Chapter 1 to eq. (1.1), the backbone to the normalization method is embodied by the propeller Open Water performance. The second propulsive parameter necessary for the analysis is the thrust deduction factor.

#### Propeller Open Water curves

The Open Water (OW) tests for *The Princess Royal*'s propellers were conducted at Newcastle University's Emerson Cavitation Tunnel (Fig. 5.5) as reported by Carchen (2015*a*); Carchen *et al.* (2015). The experimental campaign included OW tests for both the old (ECT-TPR-001) and new propeller (ECT-TPR-002) models for comparison and to allow for a better assessment of the experimental consistency with previous measurements. Both models had scale parameter of 1:3.5 and hence a diameter of 214 mm (Fig. 5.6). The propellers were tested on a Kempf & Remmers H33 dynamometer according to the test matrix in Table 5.4 with advance coefficient increments of 0.05. This has provided a blade Reynolds number variation between $0.78 \times 10^6$ and $1.74 \times 10^6$. The blade Reynolds number $Rn_{0.7}$ is described based on the chord length at the radius $0.7R$ ($R = D/2$) as follows:

$$Rn_{0.7} = \frac{c_{0.7} + \sqrt{V_a^2 + (0.7\pi nD)^2}}{\nu_{fw}}$$

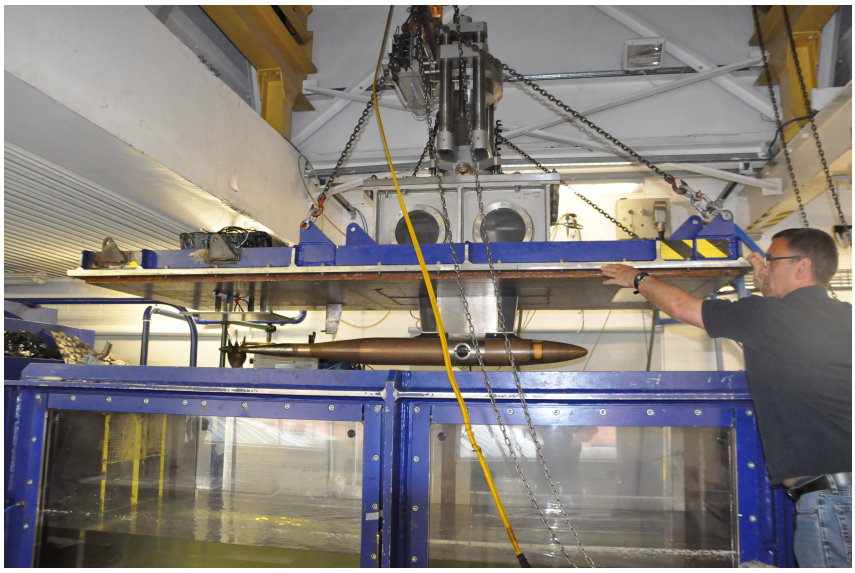

**Figure 5.5** – *A test of the ECT-TPR-002 at Newcastle University's Emerson Cavitation Tunnel.*

TABLE 5.4
*Open Water test matrix.*

| Test condition | Water speed [m/s] | Propeller speed [Hz] |
|---|---|---|
| 1 | 2 | varying |
| 2 | 3 | varying |
| 3 | 4 | varying |
| 4 | varying | 20 |

where $c_{0.7}$ is the blade chord length at $0.7R$, $V_a$ is the advance speed, $n$ is the propeller rate of revolution, $D$ is the propeller diameter and $\nu_{fw}$ is the kinematic viscosity of fresh water in standard conditions. Each test was repeated 4 times to ensure measurement repeatability. Figure 5.7 reports the ECT-TPR-002 OW curves in model scale together with the full-scale extrapolation.

### Thrust deduction factor

Self-propulsion tests for the R/V were carried out at Istanbul Technical University (Korkut and Takinaci, 2013; Atlar *et al.*, 2013*a*). Two model propellers were mounted on a pair of Kempf & Remmers R25 dynamometers to propel the 1:5 scale vessel model in the towing tank. The model was tested with full appendages in light load departure condition. Table 5.6 reports the results of the tests for reference. It must however be borne in mind that the results reported in the table belong to a loading condition (light load departure) which eventually increased of 18% by the time the vessel was delivered. Consequently, the wake

**Figure 5.6** – *Model propellers of the starboard NPT ECT-TPR-002 (left) and the original ECT-TPR-001 (right).*

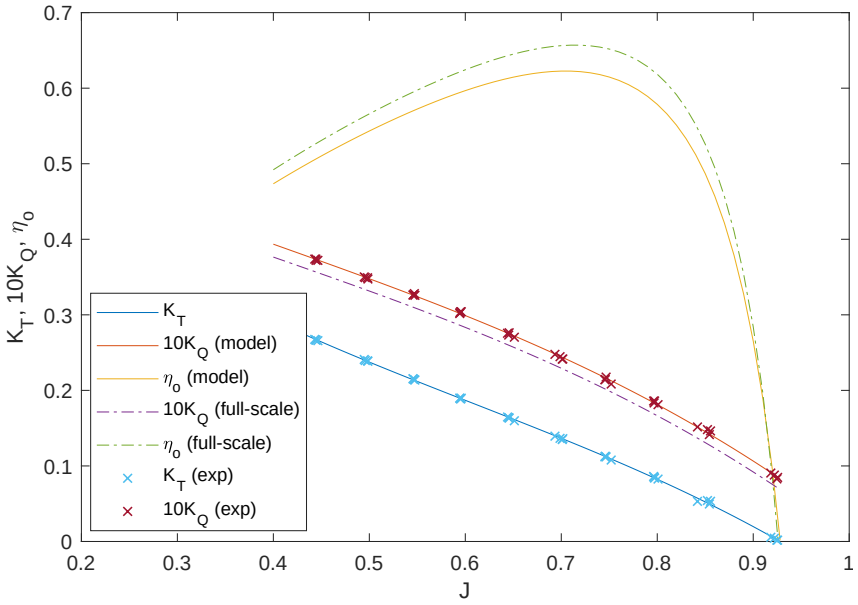


**Figure 5.7** – *Propeller Open Water curves of the ECT-TPR-002 with full-scale extrapolation.*

TABLE 5.5

*Full-scale propeller Open Water performance.*

| $J$ | $K_T$ | $10K_Q$ | $\eta_o$ |
|---|---|---|---|
| 0.40 | 0.29 | 0.38 | 0.49 |
| 0.50 | 0.24 | 0.33 | 0.57 |
| 0.60 | 0.19 | 0.28 | 0.62 |
| 0.70 | 0.14 | 0.23 | 0.66 |
| 0.80 | 0.08 | 0.17 | 0.62 |
| 0.90 | 0.02 | 0.09 | 0.28 |
| 0.93 | 0.00 | 0.07 | -0.03 |

TABLE 5.6
*Self propulsion coefficients of* The Princess Royal.

| $V_s$ [kn] | $1-w$ [-] | $1-t$ [-] | $\eta_h$ [-] | $\eta_r$ [-] |
|---|---|---|---|---|
| 6.0 | 0.890 | 0.887 | 0.996 | 0.989 |
| 7.0 | 0.895 | 0.890 | 0.994 | 0.989 |
| 8.0 | 0.897 | 0.893 | 0.996 | 0.989 |
| 9.0 | 0.903 | 0.890 | 0.986 | 0.989 |
| 10.0 | 0.906 | 0.885 | 0.976 | 0.989 |
| 11.0 | 0.910 | 0.886 | 0.974 | 0.989 |
| 12.0 | 0.914 | 0.890 | 0.974 | 0.989 |
| 13.0 | 0.918 | 0.891 | 0.971 | 0.989 |
| 14.0 | 0.921 | 0.899 | 0.977 | 0.989 |
| 15.0 | 0.924 | 0.892 | 0.966 | 0.989 |
| 16.0 | 0.927 | 0.891 | 0.962 | 0.989 |
| 17.0 | 0.929 | 0.898 | 0.966 | 0.989 |
| 18.0 | 0.932 | 0.894 | 0.959 | 0.989 |
| 19.0 | 0.934 | 0.900 | 0.963 | 0.989 |
| 20.0 | 0.936 | 0.890 | 0.950 | 0.989 |

fraction and thrust deduction values are not accurate estimation of the actual. Whereas this consideration is relevant with respect to the wake fraction, it follows from the method presented in Chapter 4 that the accuracy of the thrust deduction factor has a secondary importance.

### *5.2.2* The Princess Royal *SPMS software*

In order to efficiently measure, log visualise and analyse the hydrodynamic performance of *The Princess Royal*, a SPMS software was developed by the Author in a LabView environment. LabView was chosen due to its native ease of communication with hardware and instrumentation and its availability among the University's IT services.

In the description of the software, the reader might find useful to refer to Fig. 4.1, which represents the data flow through the SPMS developed in this research. The software is composed of four independent modules that loosely follow the main headlines of this research, namely:

1. Onboard monitoring
2. Data preparation
3. Data normalization
4. Performance analysis

When run, each module allows to save the data measured or analysed in the session for later use or export. The system is designed such that the output of a module can be directly analysed by the subsequent software chain. Modules 2, 3 and 4 were conceived to be run on-line in semi-real time to provide periodical feedback to the crew during normal navigation. Since the R/V however is operational only during normal office time (9am–5pm), these three modules were almost exclusively run off-line in the shore office. Each module of the SPMS software will be briefly described in the relevant section of this chapter.

## 5.3 Design of the deterministic method

Following the principles presented in Chapter 4, the normalization procedure is at first assessed by investigating the correction of each resistance component identified in Section 4.2 and for which a normalization method is available. Since no dedicated systematic experiments were conducted to investigate the effects of trim and restricted waters, the relevant disturbances here treated will be:

- Direct wind resistance;
- Added wave resistance;
- Effect of changes in water properties;
- Effect of changes of displacement;
- Steering resistance;
- Drift and yaw induced resistance.

### *5.3.1 Added resistance components*

**Winds**

Direct wind resistance was identified in the previous chapter as a significant disturbance, whose effect must not be ignored for the sake of ship performance monitoring. Owing to the unique shape of *The Princess Royal*'s superstructure, the wind resistance coefficients

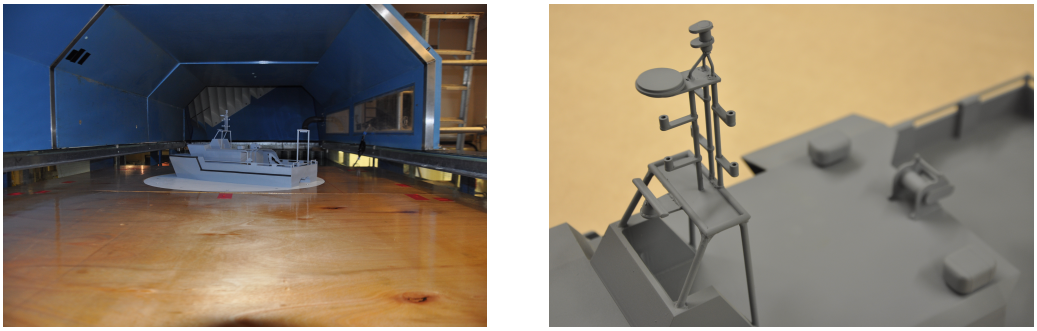

**Figure 5.8** – *Wind tunnel setup, looking downstream (left) and close look on a detail of the R/V model (right).*

were derived by wind tunnel tests (Vranakis, 2016; Vranakis *et al.*, 2017) — see recommendations in Section 4.2. The wind tunnel tests were conducted at Newcastle University's Wind Wave Current tank, which required the design and manufacture of a bespoke 'false floor' structure to adapt it for the experiment. A detailed 1:25.5 scale model was manufactured by Hobson Design of Morpeth to match the exact actual full-scale shape in light load departure condition. Figure 5.8 shows a view of the R/V model on the false floor structure in the Wind Wave Current tank opened during the setup and a detail of the model. The time-averaged direct wind resistance was defined:

$$\overline{R}_{AA} = 0.5\rho_A U_{AR}^2 C_X(\mu_{AR}) L_{oa}^2 \tag{5.1}$$

with $\rho_A$ being the air density, $U_{AR}$ the relative wind speed and $C_X$ the wind resistance coefficient in surge direction, function of the relative wind direction $\mu_{AR}$. The vessel length over all $L_{oa}$ was used instead of the more common lateral area. This was dictated purely by the ease of obtaining $L_{oa}$ for the R/V in view of future projects (Vranakis, 2016). Hence, in analogy with eq. (4.2) the air resistance can be calculated as:

$$\overline{R}_{AA0} = 0.5\rho_A V_g^2 C_X(0) L_{oa}^2 \tag{5.2}$$

Figure 5.9 and Table 5.7 report the wind resistance coefficients evaluated from the wind tunnel tests. The experimental results were also successfully compared with full-scale CFD simulations (Axiotis, 2016).

In accordance with the practice established e.g. by Blendermann (1996), no correction was applied to the air flow velocity distribution in the tunnel to mimic the full scale wind profile. It is thereby assumed that the natural air flow gradients in the tunnel approximate the real condition. The wind reference height to be used in the full scale correction (eq. (4.3)) was calculated during the wind tunnel tests as 3 m (Vranakis, 2016).

The effect of changes in air density were calculated during several sea trials to verify its entity. It was found that the variation of air density is itself negligible in the area of operation of the R/V and its effect can therefore be neglected.

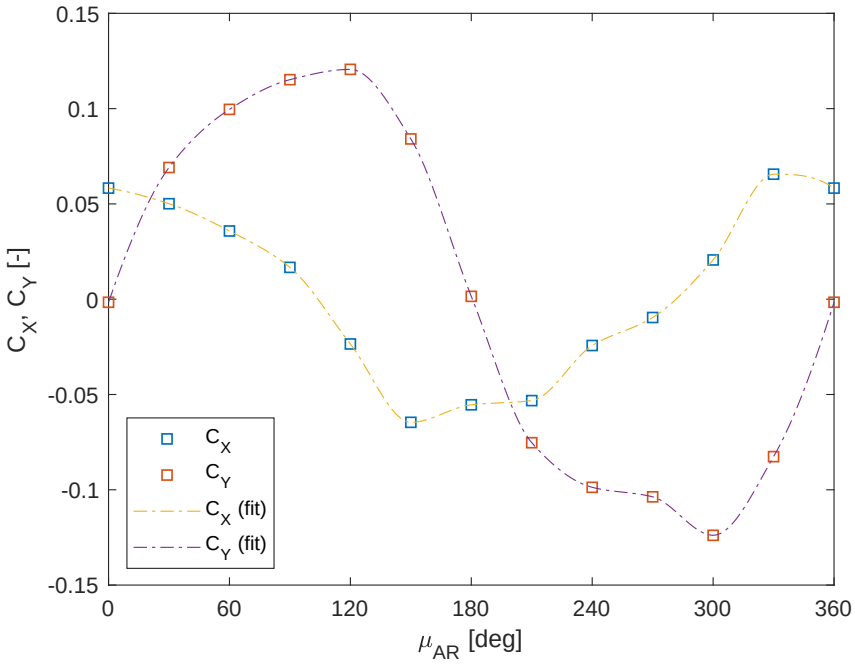


**Figure 5.9** – *Direct wind resistance curves of* The Princess Royal*, after Vranakis* et al. *(2017).*

TABLE 5.7

*Direct wind resistance coefficients [after Vranakis* et al. *(2017)].*

| *Bearing [deg]* | $C_X$ [-] | $C_Y$ [-] |
|---|---|---|
| 0 | 0.058 | -0.002 |
| 30 | 0.050 | 0.069 |
| 60 | 0.036 | 0.100 |
| 90 | 0.017 | 0.115 |
| 120 | -0.024 | 0.121 |
| 150 | -0.065 | 0.084 |
| 180 | -0.055 | 0.002 |
| 210 | -0.053 | -0.075 |
| 240 | -0.024 | -0.099 |
| 270 | -0.010 | -0.104 |
| 300 | 0.021 | -0.124 |
| 330 | 0.066 | -0.083 |
| 360 | 0.058 | -0.002 |

As anticipated in Chapter 4, the above presented direct wind resistance correction requires the measurement of wind speed, direction and density.

**Waves**

The evaluation of the added wave resistance transfer function of *The Princess Royal* was carefully considered due to the peculiarities of the case. The bespoke hullform of the R/V requires the use of either EFD or CFD techniques to calculate its seakeeping performance, which cannot be simply neglected according to the previous chapter. With respect to numerical calculations, the vessel presents several unconventional features, among which the following can be listed:

- Operation at high Froude numbers: some numerical theories don't include an adequate method to account for the three-dimensional effect that is prominent at higher speeds.

- Transom stern: dealing with a transom stern at low Froude numbers is difficult in case the added wave resistance is evaluated from direct pressure integration over the hull.

- Deep-V hull shape: the smaller damping forces derived from the narrow demi-hulls result in small waves inducing larger motions. In combination with a low wetdeck height (see Fig. 5.3), this easily leads to non-linear motions (e.g. slamming) even at modest speed. Moreover, the strip theory tends to be inaccurate for wave lengths roughly below 40% of the hull length (Söding, 2006).

- Multihull: several numerical methods cannot accommodate for multihulls or correctly estimate the hull interaction factors.

After an extensive investigation, which attempted to overcome the above problems as well as benefiting from the available resources, the commercial code ShipX (Fathi and Hoff, 2016) was selected for use in this research. The option of conducting multi-directional seakeeping tank tests or CFD simulations was ruled out due to the resources they required. On the other hand, ShipX allows multihull calculations and employs, among others, Faltinsen and Zhao's $2\frac{1}{2}$D high-speed theory (Faltinsen *et al.*, 1991), which takes into account the flow correlation between subsequent stations and is therefore more suited to analyse fast craft. Moreover, ShipX allows calculation of the added wave resistance by direct pressure integration over the hull, which is regarded as one of the most accurate methods (Faltinsen *et al.*, 1980; Fathi and Hoff, 2016). Coincidentally, since *The Princess Royal* often operates at Froude numbers greater than 0.2, dealing with the transom stern is relatively easier and doesn't significantly affect the accuracy of the method (Faltinsen *et al.*, 1980). The wave height issue has to be dealt with at first by applying a stricter

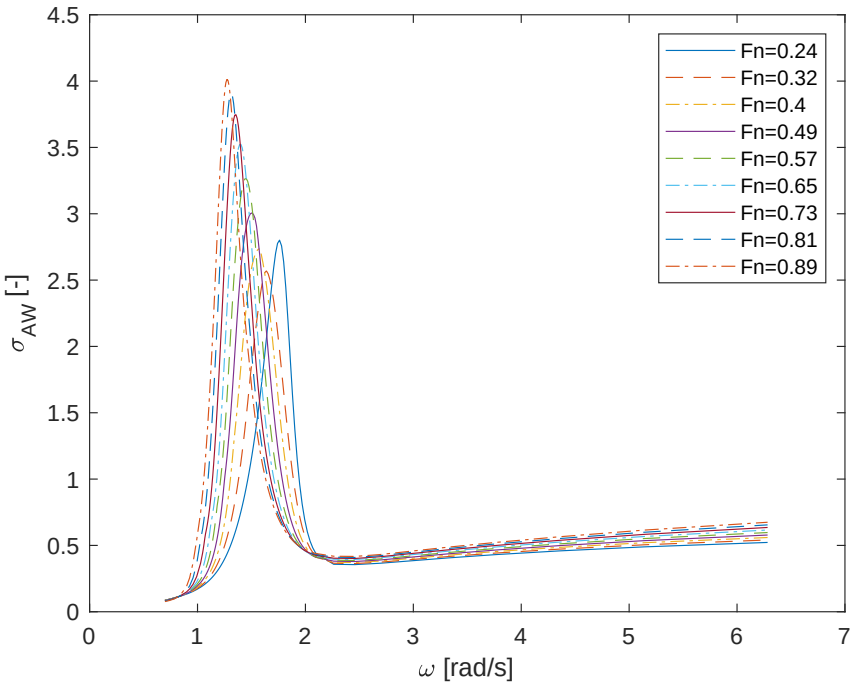


**Figure 5.10** – *Added Wave Resistance transfer function of* The Princess Royal *for the design draft.*

filter to deny wave heights when slamming begins to occur. Secondly, ShipX's simulations must be validated to ensure a sufficient accuracy of the prediction.

In general, it was mentioned in Chapter 4 about the convenience of carrying out added resistance calculations for a limited number of loading conditions. Owing to her typical mission profile, the displacement of the R/V varies very slightly. Therefore, the added wave resistance transfer functions were calculated only for Light Load Departure displacement, which was identified as the most frequent loading condition. Figure 5.10 shows *The Princess Royal*'s nondimensional added wave resistance transfer functions calculated with ShipX for the useful range of Froude numbers and plotted against the full-scale wave frequency $\omega$. In summary, here is implemented an added wave resistance correction that covers all the speed range of the R/V operation, head waves and for one loading condition (fundamentally the only one for *The Princess Royal*). Although the limits of such correction are apparent, the cost implications of implementing it in a real case scenario are deemed to be low whilst certainly providing an improvement of data quality and quantity. A directional wave height filtering criterion as the one presented in eq. (4.35) was coherently applied, which will be discussed in the following sections.

It is also clear that such correction method requires the availability of either the sea spectra or the mean parameters (e.g. significant wave height, average zero-crossing period etc.) to reconstruct them. This will need to be dealt with in the next section during the 'data acquisition' discussion.

An experimental validation was conducted to calibrate the numerical prediction as it

TABLE 5.8
*Seakeeping test matrix, after Sfakianos (2016).*

| Wave/ship length ratios | Froude numbers | | |
|---|---|---|---|
| | 0.398 | 0.495 | 0.597 |
| | 0.477 | 0.477 | 0.477 |
| | 0.953 | 0.953 | 0.953 |
| | 1.430 | 1.430 | 1.430 |
| | 1.907 | 1.907 | 1.907 |
| | 2.384 | 2.384 | 2.384 |
| | 2.860 | 2.860 | 2.860 |
| | 3.337 | 3.337 | 3.337 |

is described in the next paragraph.

***Experimental validation.***—Towing tank tests in regular waves were conducted by Sfakianos (2016) at Newcastle University using a 1:12 scale model of the vessel. Due to the availability of a normal towing tank instead of a seakeeping tank, only head seas condition (180deg) could be tested, using the test matrix shown in Table 5.8 and a fixed wave height of 0.03m. Testing in following waves was avoided since the useful measurement length would have been too small to produce significant results.

As already noticed by Hasselaar (2011), the signal-to-noise ratio at Newcastle University tank is relatively low, although it was higher in the *The Princess Royal* case due to the higher Froude numbers. A frequency domain analysis of the raw measurement data and a calibration check of the load cell eventually confirmed the reliability of the experimental data (Sfakianos, 2016). Figure 5.11 shows the ShipX validation with the experimental measurements in model scale, plotted against the wave encountering frequency — see eq. (4.7).

### Changes in water properties

Because of the limited variation of water quality in the North Sea, the effect of a change in water properties is generally small and accounts for up to 0.5% of the total resistance of *The Princess Royal*, calculated using the ITTC eq. (4.9). Figure 5.12 shows the relative resistance increase due to the change in water properties that resulted from an increase in water temperature of 9°C during a winter trial — about the temperature change expected in the North Sea between winter and summer.

The effect of changes of water properties was corrected for during several sea trials.

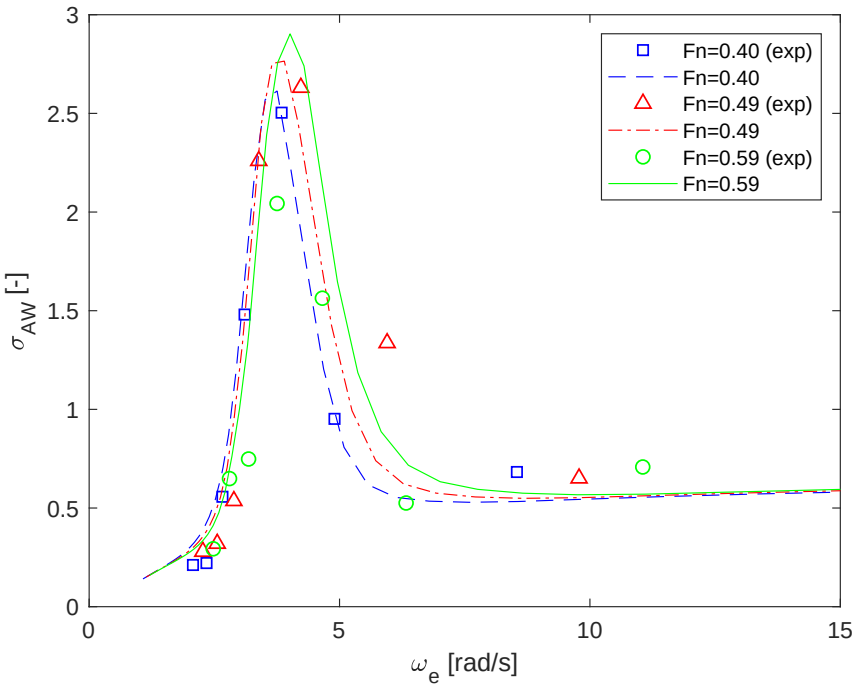


**Figure 5.11** – *Validation of the nondimensional added wave resistance transfer function $\sigma_{AW}$ by means of towing tank tests.*

However, the correction was not implemented in the automated SPMS because of its modest impact and after unexpected issues encountered in the connection to the sensor on board.

#### Change of displacement

The maximum deviation in displacement during normal operation of *The Princess Royal* corresponds to about 2 tonnes (about 4%), which affects the powering of the R/V by about 3% according to the ITTC eq. (4.13). The application of this correction requires therefore a measurement of draught.

#### Steering, drift and yaw

In accordance with the conclusions drawn in Section 4.2, since *The Princess Royal*'s experimental constants related to the rudder performance and the hydrodynamic derivatives couldn't be obtained, no correction was applied for either of the three resistance components. Suitable filters were therefore implemented to limit their impact on the propulsive performance of the vessel. These will be presented in Section 5.4.

### *5.3.2 Summary of the SPMS design*

The present section has investigated the possible correction methods to be used in the deterministic SPMS implemented on-board *The Princess Royal*. Table 5.9 summarises all

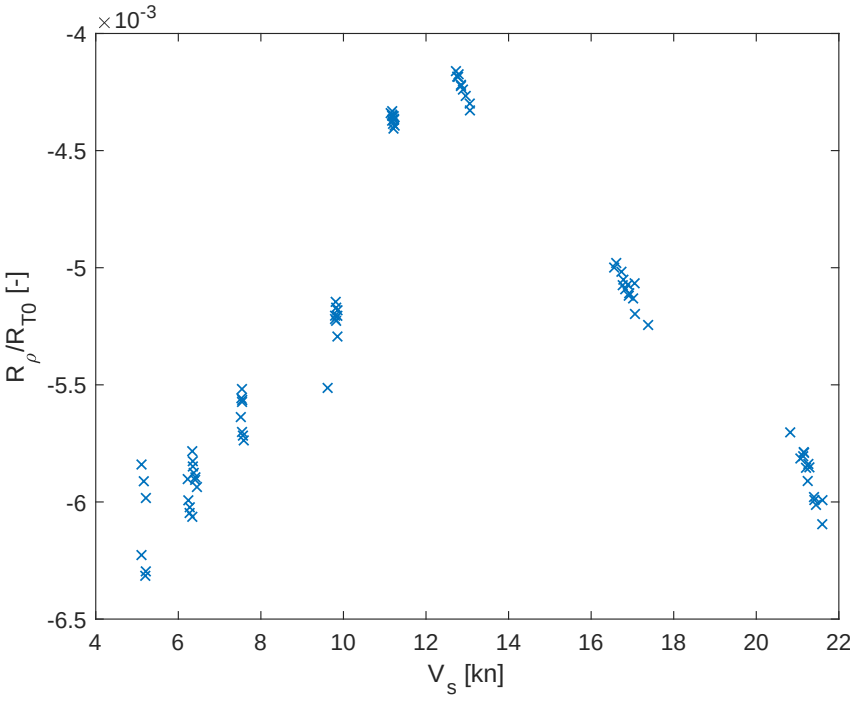


**Figure 5.12** – *Effect of a 9°C change in water temperature on* The Princess Royal*'s resistance.*

the resistance components here considered and the adopted correction method.

## 5.4 Data acquisition

### *5.4.1 Sensors description*

As described in Section 5.2, *The Princess Royal* was by design supplied with substantial measuring equipment. A good part of the work related to the setup of the on-board

TABLE 5.9

*Summary of resistance components and methods used in the normalization.*

| *Component* | *Symbol* | *Correction method* |
|---|---|---|
| Direct wind resistance | $\overline{R}_{AA}$ | Wind tunnel tests |
| Added wave resistance | $\overline{R}_{AW}$ | $2\frac{1}{2}$D strip theory w/ pressure integration |
| Effect of change in water properties | $R_\rho$ | ITTC method |
| Effect of change in displacement | $R_\Delta$ | Admiralty coefficient (ITTC method) |
| Steering resistance | $R_\delta$ | Neglected |
| Drift and yaw added resistance | $R_{\beta,\dot{\psi}}$ | Neglected |

monitoring system was therefore devoted to inspect the existing sensors verifying their compliance with the needs of the deterministic method described in Section 5.3. Specifically, the following variables need to be measured:

- Speed through water (surge component $u_s$)
- Propeller speed $n$
- Propeller torque $Q$
- Speed over ground $V_g$
- Course over ground $\psi_g$
- Heading $\psi$
- Rudder angle $\delta$
- Draught $T$
- Trim $\theta_L$
- Wind speed $U_{AR}$
- Wind direction $\mu_{AR}$
- Directional wave spectra $S_\zeta(\mu_R)$
- Water depth $h$
- Propeller thrust $T$
- Air properties (pressure $p_a$, temperature $T_a$ and humidity $RH$)
- Water properties (density $\rho$ and viscosity $\nu$)

This section presents the measurement system on-board *The Princess Royal* by describing each sensor and the variables it collecting. Figure 5.13 presents an impression of the SPMS developed on-board Newcastle University' R/V, with labels to the most important sensors. In the following paragraphs, each sensor will be defined by make and model, the symbols of the measured variables with rated factory accuracy in brackets, the sampling frequency, the communication protocol and its location on the vessel. Where available, a picture of the instrument is given.

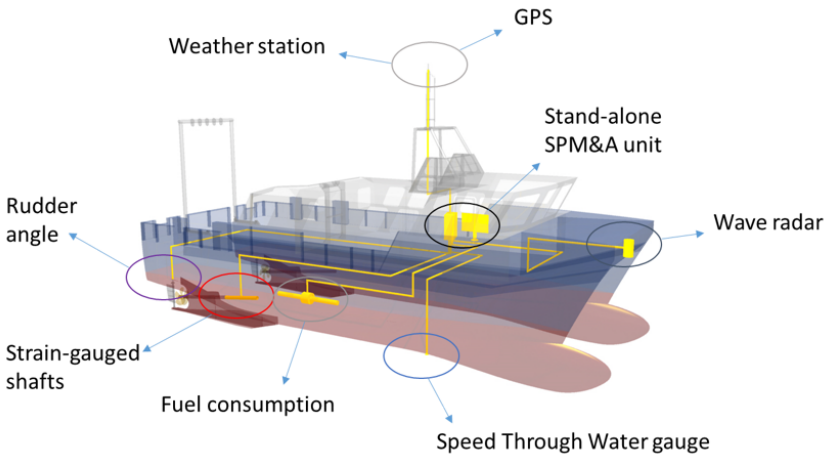


**Figure 5.13** – *Ship Performance Monitoring System on* The Princess Royal.

### GPS

*Make*: Furuno.
*Model*: GP33.
*Variables*: $\updownarrow$, $V_g$, $\psi_g$ ($\pm 0.9$ deg).
*Sampling frequency*: 1Hz.
*Com. protocol*: NMEA 0183.
*Location*: Mast.

### Satellite Compass

*Make*: Furuno.
*Model*: SC-50.
*Variables*: $\psi$ ($\pm 0.5$ deg).
*Sampling frequency*: 1Hz.
*Com. protocol*: NMEA 0183.
*Location*: Mast.

### Doppler Speed Log

*Make*: Furuno.
*Model*: DS-80.
*Variables*: $u_s$ ($\pm 1\%$ or $\pm 0.1$kn).
*Sampling frequency*: 1Hz.
*Com. protocol*: NMEA 0183.
*Location*: Hull bottom at $L_{pp}/2$.

In Chapter 4 it was shown how a dual axis log is useful in providing information about the effective drift motion (see eqs. (4.16) and (4.14)) by measuring both $u_s$ and $v_s$ components of $V_s$. It was however decided that due to the small vessel size and the mission profile of the R/V a single-axis Doppler Log (DL) was to be sufficient. The speed log was installed in June 2015 during the Dry-Docking (DD) to substitute the lesser reliable Electro-Magnetic log (see below). The location of the transducer was carefully chosen according to the principles presented in Section 4.3 (see also Furuno, 2003). The DL was installed on the port side demi-hull at midship, far from the interferences of the Echo-Sounder and propellers, whilst sufficiently close to the centre of gravity to keep the motions to a low level. The DL calibration was carried out shortly after running a dedicated speed-power trial in calm weather. By principle, the DL can measure the speed through water outside the vessel's boundary layer. This feature can be benefited from by setting the 'track depth' to a suitable distance from the sensor's surface in 'water track' mode. The track depth was set to 2 m on the R/V.

**Electro-Magnetic Speed Log**

*Make*: Agilog.
*Model*: EM-2000.
*Variables*: Standby $u_s$.
*Sampling frequency*: 1Hz.
*Com. protocol*: Manual logging.
*Location*: Outer hull plating on the forebody.

This Electro-Magnetic (EM) log had been installed on delivery of the vessel. However, the sensor was found not compliant with the SPMS's needs and was supplemented by the more accurate Doppler Log. The EM log has been since used as comparative sensor.

**Instrumented shafts**

*Make*: Design Unit.
*Model*: -.
*Variables*: $n$ ($\pm 0.5\%$), $Q$ ($\pm 0.16\%$), $T$ ($\pm 0.6\%$).
*Sampling frequency*: 565Hz.
*Com. protocol*: RS-232.
*Location*: Abaft the gearboxes.

Two purpose built intermediate hollow shafts were designed, manufactured and shop-calibrated by Newcastle University spin-off company Design Unit (Hamer, 2015). The shafts replace a section of the main shaft between the stern gland and the gearbox and can be easily removed for maintenance and inspection.

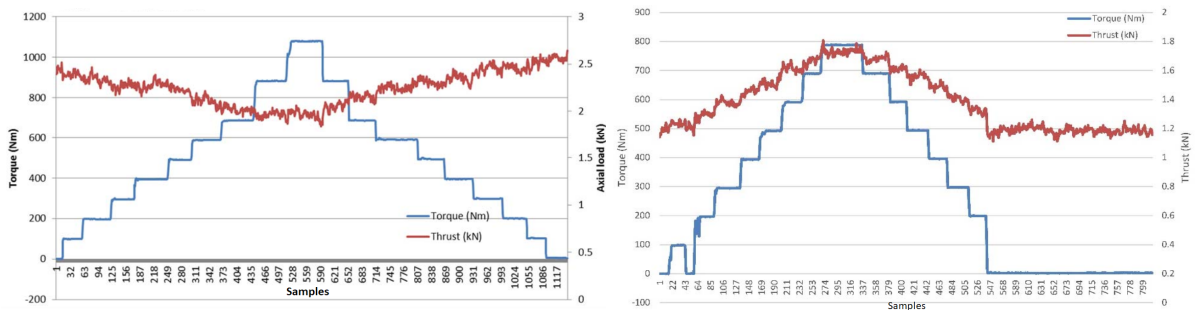


(a) (b)

**Figure 5.14** – *Parasitic thrust measured during shop calibration of the starboard (*a*) and port (*b*) shafts [Source: Hamer (2015, 2016)].*

Torque and thrust measurements are accomplished by means of two separate full Wheatstone bridge strain gauge rosettes (see Section 4.3). Both shafts had their outer diameter reduced in the area of application of the rosettes so as to increase the local strain and improve the sensitivity of the thrust and torque readings. During the shop calibration of the torque measurement of both shafts, an axial load was measured. This is commonly referred to as 'parasitic load' and can be generated by the Poisson effect or especially by misalignment of the Wheatstone bridge with the direction of the measured strain (Hamer, 2015, 2016). Figure 5.14 shows the parasitic thrust of both shafts in the form of an almost constant $\mathrm{d}T_{parasitic}/\mathrm{d}Q$. If the parasitic loads are extrapolated to full-scale values, the following results are obtained:

$$\text{Starboard: } \frac{\mathrm{d}T_{parasitic}}{\mathrm{d}Q} = 0.565 \text{ m}^{-1}$$

$$\text{Port: } \frac{\mathrm{d}T_{parasitic}}{\mathrm{d}Q} = 0.400 \text{ m}^{-1}$$

The parasitic load is corrected during the analysis on the entire data bin. This was decided based on the manufacturer's suggestion that little certainty existed over the nature of the parasitic loads and it was therefore not advisable to correct a time series. It must however be noted that the shop tests were carried out over a limited measurement range and thus the process of extrapolation to full scale values cannot account for the likely non-linearity of the parasitic load. Therefore, it is expected that a correction based on the full-scale extrapolation won't be able to entirely correct the thrust measurement.

A considerable investigation was also carried out on the effects of the residual stresses of the shafts accumulated after resting on the journal bearings for a prolonged period (Sasaki and Carchen, 2015). It was initially suggested that prior to any measurement, the propellers should be operated ahead and astern to improve the shaft lubrication and that any residual torque or thrust reading should be zeroed. This practice was however later on rejected in consideration of the accuracy of the shop calibration and upon discovering that a significant amount of the residual stresses came from the misalignment of the

shafts. The constant torque that the misalignment produced on both shafts, led the torque measurements obtained at low shaft speed to be inconsistent and scattered.

By default, the measurement of propeller speed is obtained by a once-per-rev pulse measured over a period of 5 s. This is a relatively low frequency measurement for a shaft speed sensor and it was thus decided to increase the period to 23 s to obtain a target measurement resolution of ±0.5% at a low shaft speed (8.57 Hz). Although the period is unconventionally long, it was deemed sufficient for an application were mainly steady-state monitoring was to be performed.

**Rudder potentiometer**

*Make*: Furuno.
*Model*: NavPilot 700.
*Variables*: $\delta$ (±2%).
*Sampling frequency*: 1Hz.
*Com. protocol*: NMEA 0183.
*Location*: Rudder stock.

**Anemometer and weather station**

*Make*: Coastal Environmental Systems.
*Model*: Weatherpak Marine.
*Variables*: $U_{AR}$ (±2%), $\mu_{AR}$ (±2 deg), $\rho_A$ (±0.05%).
*Sampling frequency*: 0.33Hz.
*Com. protocol*: RS-232.
*Location*: Mast top.

The location of the anemometer is fundamental to obtain accurate data, as mentioned in Section 4.3. On *The Princess Royal*, the ultrasonic anemometer is installed on the highest point of the mast to limit the flow deformation from the surrounding structures.

**Wave radar**

*Make*: Radac.
*Model*: WaveGuide On-Board.
*Variables*: $\zeta$ (±10mm).
*Sampling frequency*: 2.6Hz.
*Com. protocol*: TCP/IP.
*Location*: Bow gunwale.

At the time this research started, the uni-directional WaveGuide wave radar was fitted

to *The Princess Royal*. This sensor is capable of providing an accurate measurement of the wave surface elevation by subtracting the vessel motion from the measurement of the distance between the water surface and the transducer. However, this sensor cannot provide any information regarding direction, spreading and true mean period of the waves. After careful consideration, the installation of a complex wave radar measurement system was deemed not necessary. Owing to the area of operation of the R/V, it was instead decided to take advantage of the nearby wave buoys network to retrieve an accurate sea state hindcast.

**Thermosalinograph**

*Make*: Seabird.
*Model*: SBE 21 SeaCAT.
*Variables*: $T_w$ ($\pm 0.01$°C), $S_A$ ($\pm 0.02\%$).
*Sampling frequency*: 16Hz.
*Com. protocol*: RS-232.
*Location*: Sea chest on the bottom plating.

Although this instrument could be connected to the SPMS, several issues were encountered in the communication with the transducer, which often wouldn't respond to data acquisition queries. In such occasions, a hand-held device was used in its replacement. However, the variation of water properties long the North East coast during the year was measured to be sufficiently little to justify neglecting it.

**Fuel flow meters**

*Make*: Royston.
*Model*: MKII.
*Variables*: Fuel consumption.
*Sampling frequency*: 1/60Hz.
*Com. protocol*: TCP/IP.
*Location*: Fuel line.

As part of a project running in parallel to this research, four volumetric fuel flow meters were installed on *The Princess Royal*, two on the fuel supply pipeline and two on the return pipeline on the port and starboard engines. The meters could be included in the monitoring system as a power measurement proxy. However, due to the low accuracy of the calculated brake power, the fuel flow measurements were never included in the analysis and were simply kept as a backup estimation of propulsive power. This was due to mainly three reasons. Firstly, volumetric flow meters are by nature less accurate than, for instance, mass flow meters because the mass of a volume of fuel decreases with

increasing oil temperature. Moreover, to damp the oscillations of the injector pump, the flow readings were averaged over 1 minute, making the sampling frequency too low for an accurate comparison. Lastly, the engine Specific Fuel Oil Consumption (SFOC) characteristic, necessary to convert fuel consumption into power, were kept confidential by the manufacturer, forcing the use of the few values calculated over the standard propeller matching curve given in the engine manual.

The Monitoring System software was however built to accommodate the fuel flow signal for the eventual use in future projects.

### *5.4.2 Complementary measurements*

**Draught measurements**

The installation of draught gauges was considered to be not necessary due to the ease of conducting more accurate visual draught measurement and the little displacement variation of *The Princess Royal*. During the DD in 2018, it was fortuitously discovered that the draught marks have about 5cm offset with respect to the real draught. For instance, the visual measurement of 1.80m draught corresponds in reality to 1.75m. A discrepancy had already been observed between the weight of the vessel measured by the lifting crane and that given by the stability booklet at the measured draught. Therefore, a built-in correction for the draught mark error was implemented within the SPMS, so that it is sufficient to enter the draught reading in the user interface.

**Wave buoy**

The National Network of Regional Coastal Monitoring Programmes of England was developed in 2011 to unify and standardise the local coastal monitoring schemes (CCO, 2017). In the North East England, wave and tidal data are measured through a network of three wave buoys. Since the monitoring on board *The Princess Royal* was conducted almost exclusively between Tynemouth and Amble, the closest measurement site is located off the shore of Newbiggin and it is managed by the North East Coastal Observatory (NECO). The wave parameters and full directional wave spectra are logged roughly every 30 minutes by means of a Datawell Directional WaveRider Mk III buoy (Fig. 5.15). The buoy had been deployed in June 2013 at the exact location 55° 11.11' N 001° 28.69' W — about 5km away from the area where performance monitoring of the R/V was conducted.

### *5.4.3 On-board monitoring software module*

The on-board monitoring module is composed of a Graphic User Interface (GUI) and five main subroutines, each handling the communication and logging with a sensor or family of

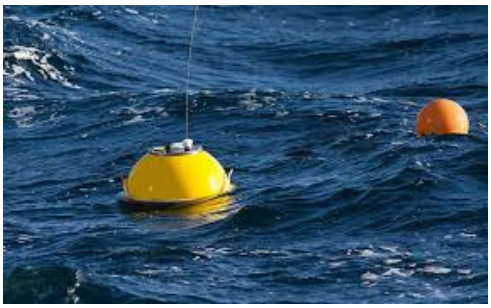

**Figure 5.15** – *A Datawell Directional WaveRider Mk III.*

sensors. Since the speed through water and several other parameters are sampled at 1Hz, all the other sampling frequencies were converted to obtain one datapoint every second. This frequency preparation is carried out at subroutine level before logging and storing the raw data (see ISO, 2016). The five subroutines can be described as follows:

**Subroutine 1:** handles communication, parsing and logging with the NMEA 0183 COM port from all the sensors attached to the NMEA network (i.e. GPS, Compass, DL and rudder potentiometer).

**Subroutine 2:** handles communication, signal parsing and logging with the Starboard instrumented shaft using a custom communication protocol. Torque and thrust signals are averaged over the second to align to a 1Hz sampling frequency. Since the shaft speed measurement is instead carried out at a virtual sampling frequency of 1/23Hz, its value is replicated over the second.

**Subroutine 3:** same as above with the Port instrumented shaft.

**Subroutine 4:** handles communication, parsing and logging of the Weatherpak weather station through a RS-232 communication protocol. Since the sampling speed is lower than 1Hz, the datum is replicated over the second.

**Subroutine 5:** handles communication, parsing and logging of the fuel flow meters signals.

The raw data is stored in the monitoring PC as a tab-separated file of datapoints sampled at 1Hz. The raw data log can then be manually or remotely retrieved for onshore analysis or can be directly analysed in-situ. Figure 5.16 shows two of the three tabs found in the GUI of the Monitoring software module. The first picture shows the main monitor and data input tab, where instantaneous measurements can be visualised and monitored through a clear and intuitive layout. The tab also accepts a few manual inputs, namely the vessel draught and the water temperature and salinity, which are assigned default values at the start of the software. The second tab allows the user to visualise the measurement history in two self-updating charts — one for NMEA data and

the second for instrumented shafts data. The third tab shown by subfigure (b) gives access to data communication settings and low-level monitoring, where the user may change the COM port settings as well as inspect the incoming raw digital signals and the eventual communication errors. Finally, the tab also provides the calibration values for the instrumented shafts.

### 5.4.4 Sea trials and Drydockings

The development of the SPMS on board *The Princess Royal* was carried out with the aid of several sea trials. These were conducted according to the most recent ITTC Recommended Guidelines (2014*a*; 2014*c*) off the shore of Blyth, Northumberland (Fig. 5.17). Normally, the trials were conducted as multiple straight runs in reciprocal directions to cancel out the current effect. Double or triple runs were used, where the first run is followed by a return run in the exact opposite course and eventually by a third having same direction and settings as the first one. All runs of the same 'engine set' shall have same engine speed. Each run is set to last a fixed amount of time of 5 minutes, whereas in the original ITTC recommendation the time is 10 minutes. However, the small size of *The Princess Royal* allows the use of a shorter measurement period. Since the North Sea is subjected to very high currents and winds, the direction of the runs was chosen to head the vessel into or following the 'most severe' environmental force — whether the waves or the North–South tidal currents.

Employing dedicated speed-power trials had the advantage of maintaining a certain degree of control (or 'manual' filtering) over some of the parameters involved in vessel performance monitoring — e.g. location, engine speed, weather, etc.. At the same time, it allowed to obtain a reasonably sized data set with large variability in a reduced amount of time. It must also be borne in mind that the normal duties of the R/V often hamper the monitoring of performance — for instance during trawling or navigation in shallow waters. Therefore, since *The Princess Royal* is operational on average 15% of her time, conducting dedicated trials was more of a necessity rather than an option.

Figure 5.18 shows the timeline of the relevant events during the course of this research. At first, it is noted that *The Princess Royal* undergoes a yearly DD approximately every summer. Within this constraint, the sea trials campaign began soon after the start of the project in support of the propeller refitting process, which ended in June 2015 (see Section 5.2). At that time, the measurements were carried out mostly manually (apart from the shaft power) since the SPMS had yet to be developed. An engine breakdown occurred during the trials in July 2015 led to a long downtime which, in turn, made the vessel unavailable for almost a year due to the accumulated backlog. During this period, the vessel crew altered the loading plan of *The Princess Royal* in the attempt to reduce wetdeck slamming in rough weather. The vessel's light load displacement was at the time

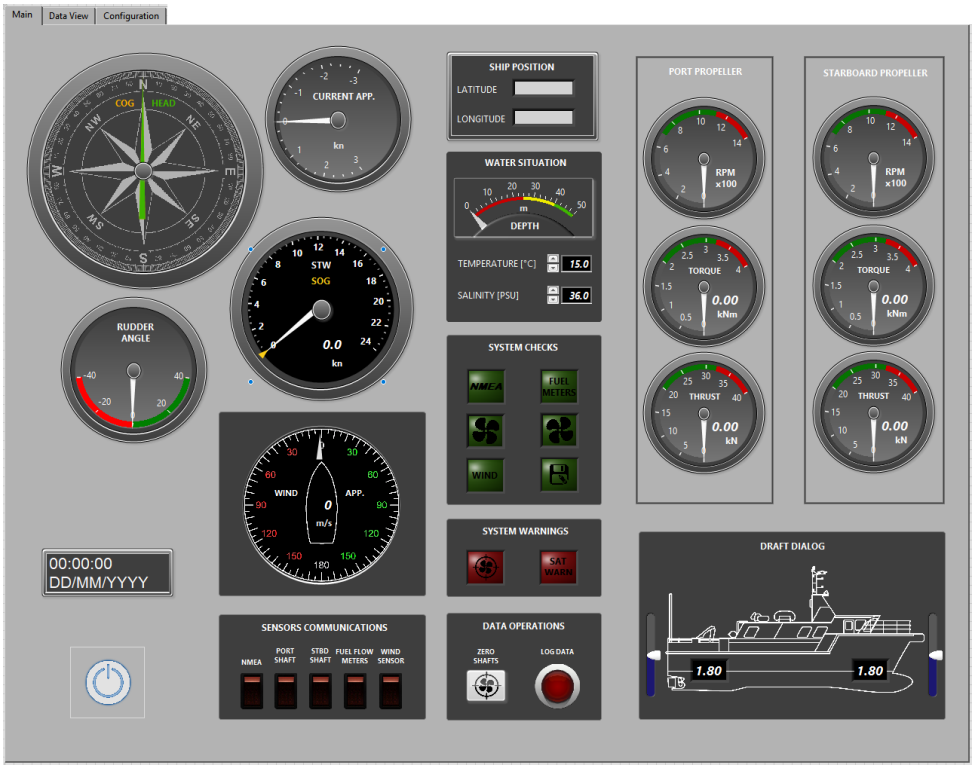


(a)


(b)

**Figure 5.16** – *Two of the three GUI panels of the SPMS data acquisition module:* (a) *main control panel and* (b) *sensor communications and other settings panel.*

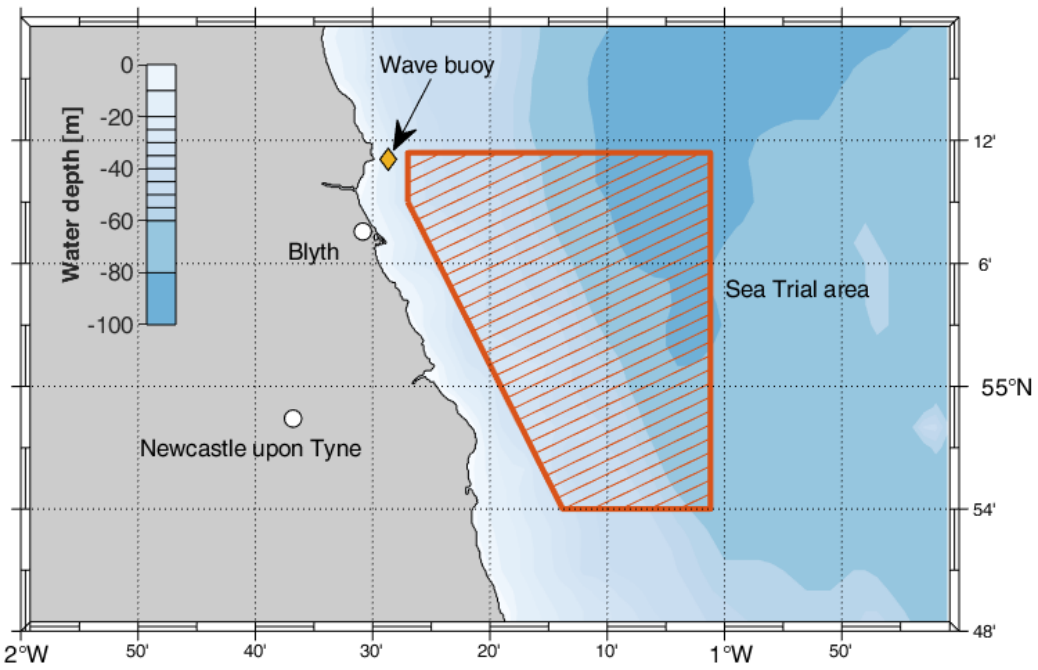


**Figure 5.17** – *Location of the sea trials and performance monitoring on* The Princess Royal, *also showing bathymetry and position of the NECO wave buoy.*

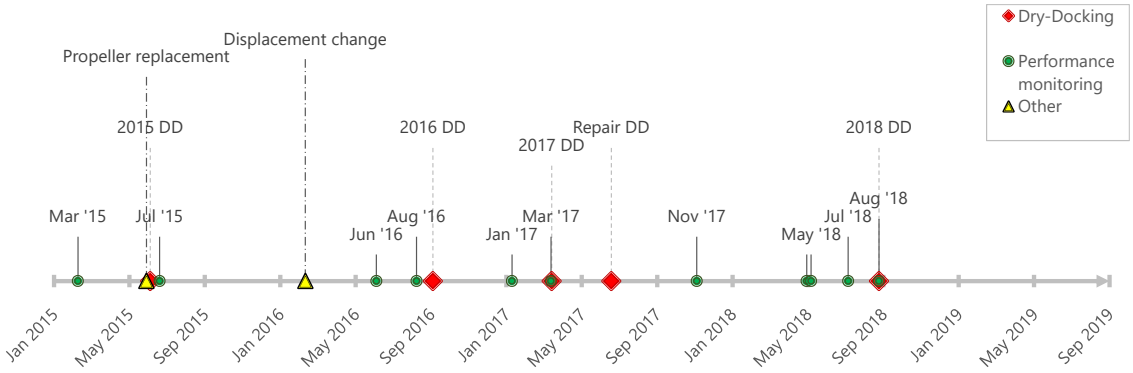


**Figure 5.18** – *Event timeline of the performance monitoring on* The Princess Royal.

increased to roughly 45t by loading 1t of sand bags in the fore peak tanks. It must be noted that the measurements obtained during the development trials couldn't benefit from the accuracy of the final monitoring system and it was therefore decided not to include them in this research to avoid unnecessary confusion.

### *5.4.5 Summary*

This section has presented the data acquisition system by describing the sensors installed on board *The Princess Royal*, the data collection alternatives that complement the on-board sensors, the general functions of the monitoring software and the data collection location and routine. Table 5.10 summarises the variables measured on board *The Princess Royal* and their reliability ranking based on the preliminary factory information.

## 5.5 Data preparation

The preparation of the data acquired on board *The Princess Royal* is carried out by applying the method presented in Section 4.4. This section will therefore focus on the threshold values adopted to carry out the SSI, weather filtering and outlier filtering. Finally, it will present the outcomes of the validation of some of the most critical variables.

### *5.5.1 Steady-State Identification*

SSI was implemented on *The Princess Royal* using an $\alpha$-trimmed standard deviation identifier with $\alpha = 0.05$ — see eq. (4.33). The threshold values for the allowable variability of the indicators around the local mean are reported in Table 5.11.

TABLE 5.10
*Variable reliability.*

| *Type* | *Variable* | *Symbol* | *Reliability* |
|---|---|---|---|
| Primary variables | Forward Speed Through Water | $u_s$ | ●● |
| | Propeller speed | $n$ | ●●● |
| | Propeller Torque | $Q$ | ●● |
| Secondary variables | Time | $s$ | ●●● |
| | Speed Over ground | $V_g$ | ●●● |
| | Course Over Ground | $\psi_g$ | ●●● |
| | Heading | $\psi$ | ●●● |
| | Propeller Thrust | $T$ | ● |
| | Rudder angle | $\delta$ | ●●● |
| | Midship draught | $T_M$ | ●●● |
| | Trim | $\theta_L$ | ●●● |
| | Wind speed | $U_{AR}$ | ●● |
| | Wind direction | $\mu_{AR}$ | ●● |
| | Air properties | $p_a, T_a, RH$ | ●●● |
| | Wave amplitude | $\zeta$ | ●● |
| | Wave spectrum | $S_\zeta$ | ●● |
| | Water properties | $\rho, \nu$ | ●●● |

TABLE 5.11

*Allowable scaled variability from the local mean.*

| *Variable* | *Variation* |
|---|---|
| $u_s$ | 5% |
| $n$ | 1% |
| $Q$ | 5% |
| $\psi_g$ | 2deg |

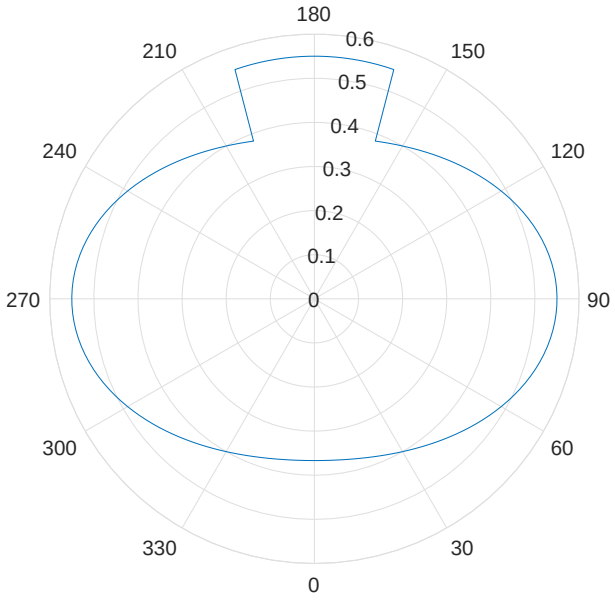


**Figure 5.19** – *Significant wave height threshold $H$ as a function of the relative wave direction $\mu_R$.*

### *5.5.2 Conditional filters*

The thresholds to filter out undesired weather and operational conditions were defined for *The Princess Royal* based on the findings and considerations of Section 4.4. However, since her size and hullform are significantly different from those of large commercial ships, a special wave height threshold had to be devised. Table 5.12 presents all the conditional filter thresholds and provides details where necessary. Figure 5.19 shows the significant wave height threshold developed for *The Princess Royal* in function of the relative wave direction, $\mu_R$. Head waves with $\mu_R = 180\,\text{deg}$.

In addition to the values presented in Table 5.12, extremely low speeds and propeller operating points are excluded from the analysis by imposing a minimum speed over ground and propeller speed of 4kn and 330RPM (idle speed) respectively.

It was anticipated in Section 4.4 that strict filtering criteria heavily influence the quantity of data that is retained for analysis. As already shown in Section 5.4, this

TABLE 5.12
*List of conditional filter thresholds for* The Princess Royal.

| *Parameter* | *Symbol* | *Value* | *Ref. equation* |
|---|---|---|---|
| Significant wave height (max) | $H$ | 0.55m | See note (1) |
| Directional wave strictness parameter | $\gamma$ | 0.5 | Eq. (4.36) |
| Wind speed (max) | $U_{AR}$ | 10m/s | Eq. (4.37) |
| Current (max) | $\lvert u_s - V_g \rvert$ | 2kn | Eq. (4.38) |
| Water depth (min) | $h$ | 28m | Eq. (4.39) |
| Displacement variation (max) | $\lvert\Delta - \Delta_0\rvert/\Delta_0$ | 0.05 | See note (2) |
| Trim (max) | $\lvert\theta_L\rvert$ | 0.001deg | See note (3) |
| Rudder angle (max) | $\delta$ | 5deg | Eq. (4.43) |
| Apparent drift (max) | $\lvert\psi - \psi_g\rvert$ | 3deg | Eq. (4.45) |

Notes:

(1) Defined by eq. (4.35) in function of the bearing of the regular wave component. Due to her seakeeping characteristics, to avoid wetdeck slamming and the consequent nonlinear motions *The Princess Royal*'s significant wave height threshold $H$ is reduced to $H = 0.55$m. The value was assigned based on the Author's experience on board.

(2) Corresponds to a maximum draught variation of about 4cm, eq. (4.41)

(3) Corresponds to an aft–fore draught difference of about 2cm, see eq. (4.42).

necessarily had to happen with *The Princess Royal*, since her small size and seakeeping characteristics are not well in accord with the harshness of the North Sea where she operates. In particular, the very strict wave height parameter is responsible for discarding the vast majority of the data acquired when she was available for monitoring. Despite the negative impact on the R/V, the performance monitoring and analysis method here presented is expected to yield less drastic results if applied to a larger vessel, since the effect of weather would then be much less felt.

### *5.5.3 Outlier filtering*

The SPMS implemented on board *The Princess Royal* employed the generalised Extreme Studentized Deviate (ESD) already presented in Section 4.4. This ensured an efficient detection and rejection of several signal glitches occurring particularly during the development phase of the SPMS. Nevertheless, in general the number of outliers detected by

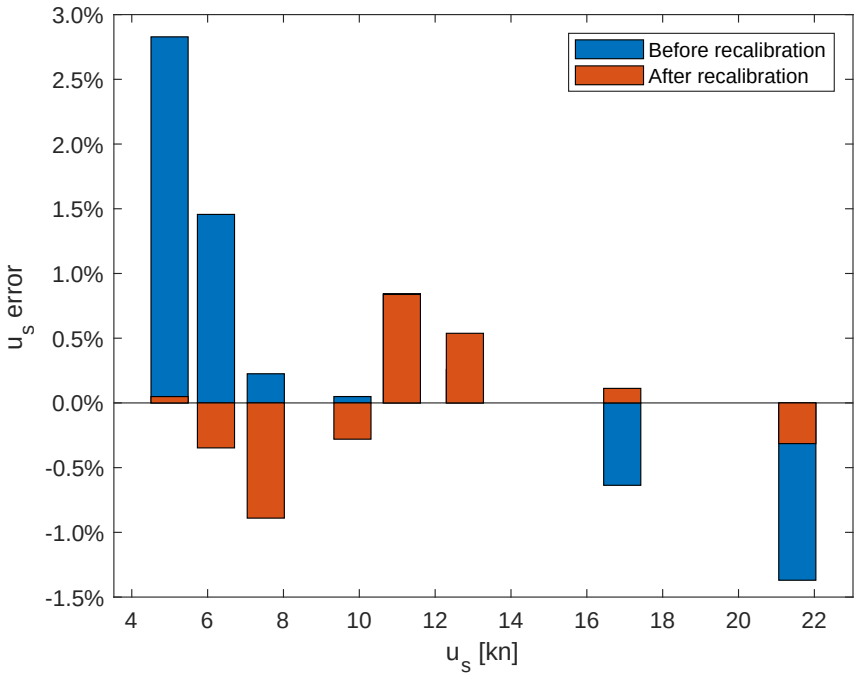


**Figure 5.20** – *Validation of speed through water measurement conducted by means of dedicated speed trials. Estimation of measurement bias before and after recalibration of the DL.*

the algorithm was less than 1% of the total data.

### *5.5.4 Data validation*

Certain on-board sensors have a greater tendency than others to drift over time, hence distorting the measurements by the introduction of a bias. In Section 4.4, the Author mentioned the good practice of validating or cross-checking the data acquired through these sensors on a periodical basis.

Owing to the short operational time of the R/V, validation was carried only once in November 2017 to ensure a consistency of the measured data. The following paragraphs show the results of these validations.

***Speed through water.***—The analysis of a speed-power trial conducted to ITTC standards, allows the speed through water, $u_s$, to be calculated from the GPS speed by calculating the effect of tidal currents on the speed over reciprocal runs (ITTC, 2014*a*; ISO, 2015*a*; Strasser *et al.*, 2015). This can be used to recalibrate the speed log. Figure 5.20 shows the relative estimated error (bias) between $u_s$ calculated from the sea trial analysis (i.e. derived from the GPS) and that measured by the on-board DL over the range 4–22kn. Despite the error is moderate (about 1% at higher speeds and 2.5% at the lower speeds), the graph shows a clear downward trend in the error, which leads to consider it a likely bad calibration of the sensor or a measurement drift. A linear fit to the absolute error values was used to recalculate the linear calibration parameters or the

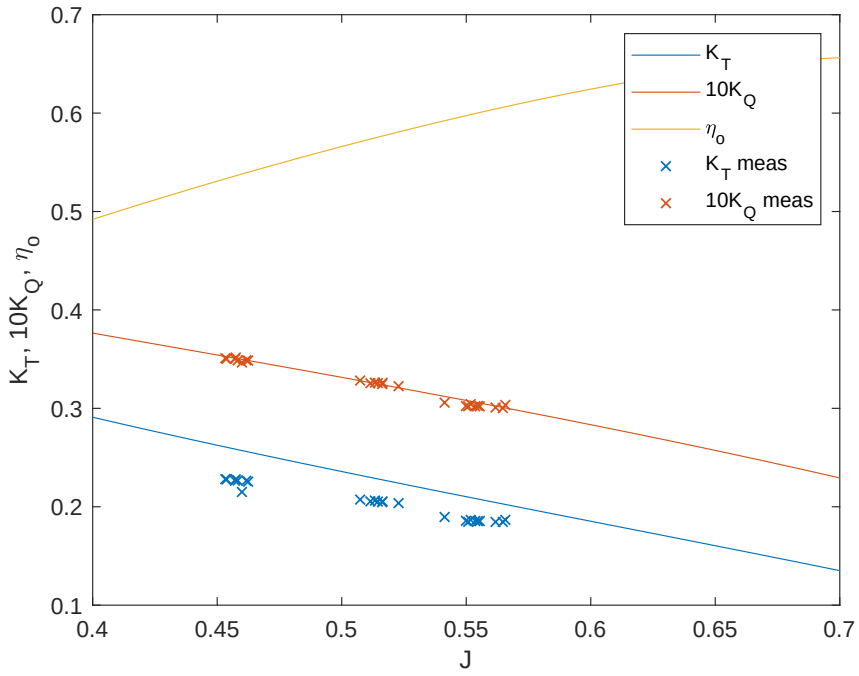


**Figure 5.21** – *Assessment of* The Princess Royal*'s shaft torque and thrust measurement consistency using the propeller open water curves.*

following speed correction:

$$\Delta u_s = p_1 u_s + p_2$$

where $p_1 = -0.0227$ and $p_2 = 0.2556$. The error after recalibration of the sensor is shown in Fig. 5.20 and is acceptable as within 1

***Propeller torque and thrust.***—Figure 5.21 shows the $K_T$ and $10K_Q$ values against the propeller open water curves, calculated from filtered data measured on-board *The Princess Royal* by the Author. Propeller torque measurements correctly fall on the open water values, whilst thrust shows a trend that is both lower than the open water curve and having a slightly different slope. This was attributed to the expected non-linear behaviour of the parasitic thrust already mentioned in Section 5.4. To account for this effect, the thrust measurements are 'calibrated' with the wake fraction during the performance analysis as explained in Section 5.7.

***Wind speed and direction.***—The accuracy of the on-board anemometer can be assessed by analysing the true wind speed and direction measurements conducted over reciprocal runs during a speed-power trial. Figure 5.22 shows the distributions of the calculated true wind speed and direction derived from the analysis of eight double runs. Every double run was composed by a 5min run with heading $\psi = 0\,\text{deg}$ immediately followed by a reciprocal run with $\psi = 180\,\text{deg}$. Both graphs show different distributions for the first and reciprocal run. This can also be confirmed by a Two-Sample t-test, which rejects the equality of their mean values with a probability of about 98% for both wind speed and direction. The mean difference of true wind speed between the two reciprocal

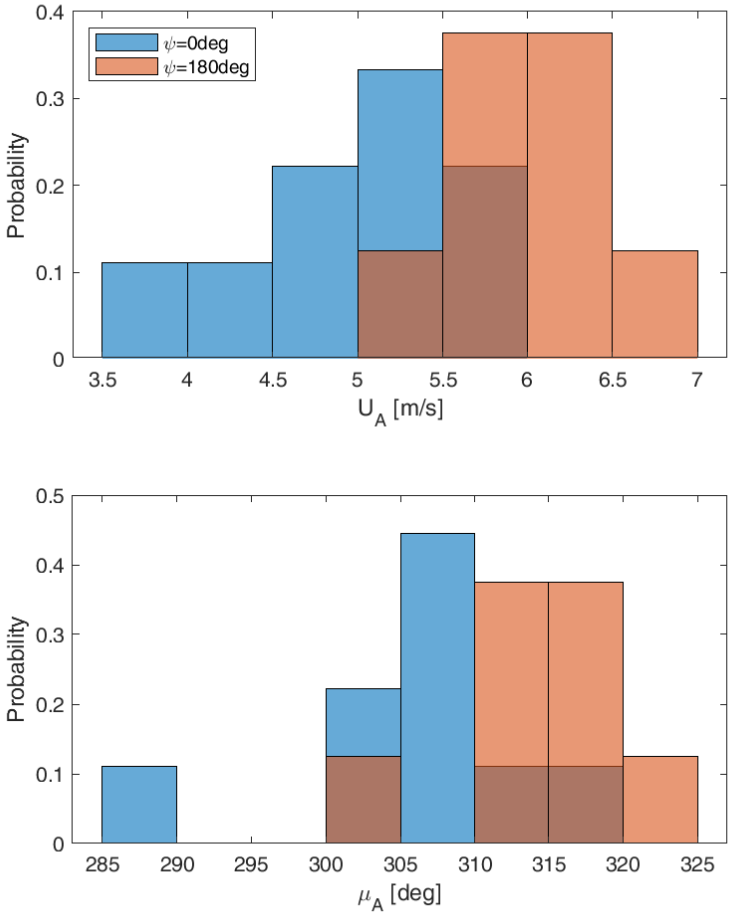


**Figure 5.22** – *Validation of* The Princess Royal*'s true wind speed and true direction measurement acquired during a speed–power trial with eight double runs.*

runs is 1m/s while the mean difference of true wind direction is just less than 10deg. These values show that the wind inflow to the anemometer is probably lightly distorted by the surrounding superstructure, despite the efforts to locate the ultrasonic anemometer on the vessel's highest position. The differences (especially for wind speed) are not insignificant, although they are generally quite reasonable for an on-board anemometer (Hasselaar, 2011). It may be speculated that the circumstance here presented is a rather a 'worst case'. Firstly, since the wind came from almost behind the mast during the northbound run, secondly because following winds having speed of the same order of the vessel speed often promote the generation of unsteady flows around the anemometers. In this perspective, the measurement of wind speed and direction is expected to be better with other wind bearings. Nonetheless, wind flow distortion is a known phenomenon that cannot be entirely avoided with an on-board measurement, although it must be limited by correct positioning of the anemometer.

### *5.5.5 Data preparation software module*

This module of the SPMS software is designed to work in on-line and off-line mode. The difference between the two stands in how the raw data is handled. In the first case, the live raw data are aggregated in data bins, which according to eq. 4.24 have size:

$$N = 23 \tag{5.3}$$

In the second case the raw data is read from the log file(s) and subdivided in data bins having the same size of the above eq. (5.3). Thereafter, the analysis is conducted in the same manner. The off-line version will here be described.

The data bin is initially passed to the Steady-State Identification subroutine. Successive data bins belonging to the same steady-state are aggregated in a subset and treated as a whole. Within the same subroutine, the conditional filters are applied to ensure the suitability of weather and navigational conditions. The eventual outliers in each steady-state subset are then searched and rejected using the generalised ESD test. Finally, the statistics of the steady-state subset are calculated (mean, standard deviation, etc.). The analysis loops until all the datapoints are analysed. At this point, the prepared data can either be saved for a later session, or directly sent to the data normalization module. It should be noted that in case of on-line application, one analysed datapoint is calculated every $\vartheta = 23$s.

Figure 5.23 shows the main panel of the software module GUI. Two charts allow to visualise every measured variable as a time series (top chart) and in dependence from any other variable (bottom chart). On the left hand side, the user is asked to select the log file to analyse and the folder where to save the prepared datapoints. The user may also decide to change the sample trimming parameter, by default set to $\alpha = 0.05$

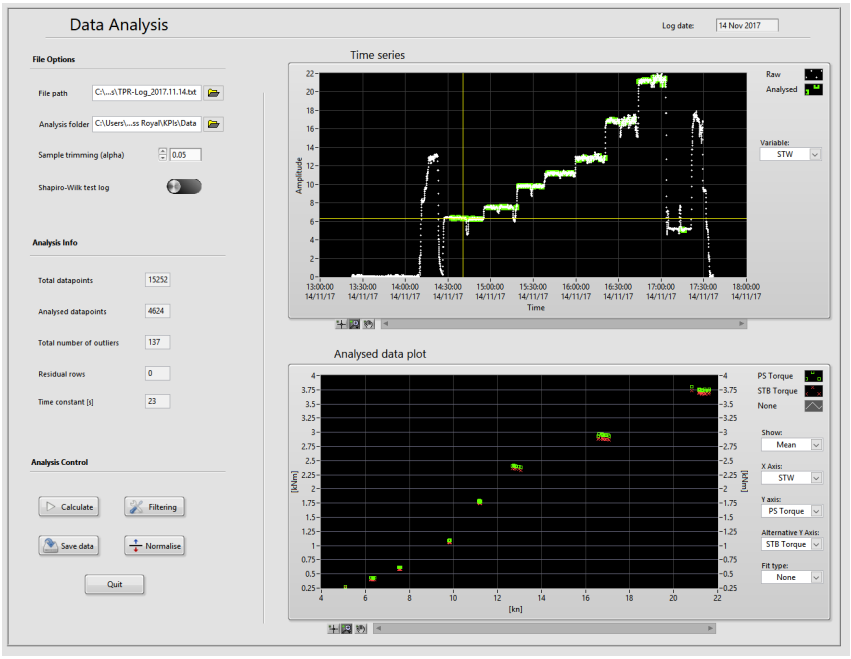


**Figure 5.23** – *Panel of the SPMS data preparation module.*

(see eq. (4.33)). Additionally, there is the possibility to run and log the results of a Shapiro-Wilk algorithm (Barnett and Lewis, 1994) to test the data bin for normality on the Cartesian and circular variables. The interface provides a few info regarding the analysis (e.g. analysed datapoints, total number of outliers, etc.), which are however not stored after the session. Finally, interactive buttons can be used by the user to start the data preparation analysis, modify the default filtering parameters, save the prepared data and initiate the data normalization (described in the following section).

## 5.6 Normalization

The normalization to ideal conditions of the prepared data was carried out following the deterministic method laid out in Section 4.5. The data necessary to conduct the normalization analysis were introduced in Chapter 4 in the details of the normalization algorithm. Table 5.13 summarises all the input data used for *The Princess Royal*'s case study with the respective source. It shall however be recalled that whereas the Author made extensive use of experimental data, it need not be so. Some parameters can be derived by means of empirical formulations (e.g. the thrust deduction factor) or database data (e.g. wind resistance coefficients) without necessarily jeopardising the accuracy of the method. In addition to the above, the shafting and relative rotative efficiencies used in the normalization were assumed respectively as:

$$\eta_s = 0.98 \tag{5.4a}$$

$$\eta_r = 1 \tag{5.4b}$$

TABLE 5.13

*Summary of* The Princess Royal*'s data necessary for the normalization and their source .*

| *Item* | *Symbol* | *Source* |
|---|---|---|
| Length b.p. | $L_{pp}$ | Vessel drawings |
| Length overall | $L_{oa}$ | Vessel drawings |
| Breadth | $B$ | Vessel drawings |
| Reference draught | $T_{M\text{ref}}$ | Statistics |
| Hydrostatics | | Stability booklet |
| Thrust deduction factor | $t$ | Self propulsion tests |
| Anemometer height | $z$ | Vessel drawings |
| Propeller diameter | $D$ | Propeller description |
| Propeller pitch/diameter ratio @0.7R | $P/D$ | Propeller description |
| Propeller Open Water Curves | | Cavitation tunnel tests |
| Wind resistance coefficients | $C_X$ | See Table 5.9 |
| Reference wind height | $Z$ | Wind tunnel tests |
| Added wave resistance transfer functions | $\sigma_{AW}$ | See Table 5.9 |

### *5.6.1 Sea trials data*

Figures 5.24 to 5.26 show respectively the direct wind resistance, the added wave resistance and the resistance due to displacement change as a fraction of $R_T$ calculated from the R/V's full-scale service trials and monitoring conducted after January 2017 (see Section 5.4.4). All the weather data here presented is within the limits imposed by the conditional filters of Table 5.12. It must then be borne in mind that the added wave resistance correction was evaluated exclusively for head and bow seas up to 20deg off the bow. Therefore, a $R_{AW} = 0$ on the graph doesn't necessarily mean that the R/V was navigating in calm waters, but may indicate that the added wave resistance was in that circumstance not calculated. Figure 5.27 shows the total added wave resistance as a percentage of $R_T$. It will be noticed that at slower speeds, the impact on the vessel performance of winds and waves in particular is higher than at higher speed. This has in turn a significant impact on the scatter of the measurements as it will be seen in the next paragraphs. Overall, the figures show that the weather state was reasonable throughout the trials and that $R_{add}$ had a limited impact on the total resistance — a maximum 8% influence was recorded on

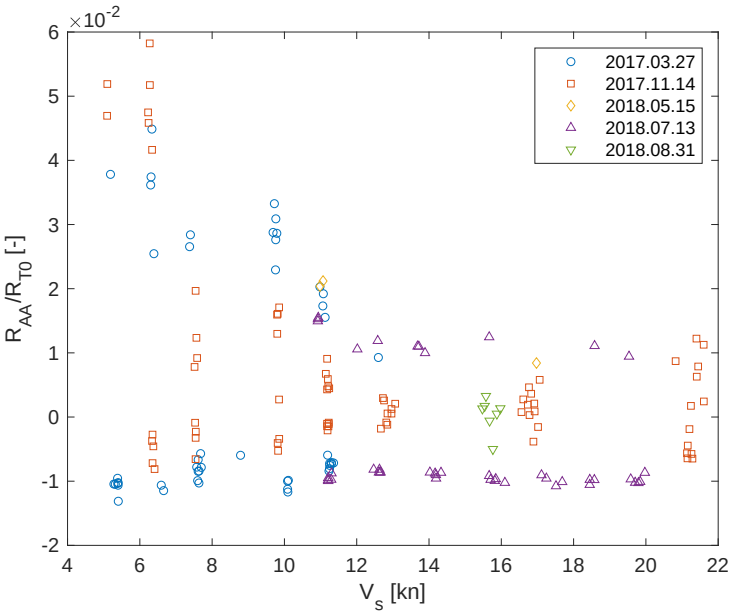


**Figure 5.24** – *Direct wind resistance during the performance trials and monitoring.*

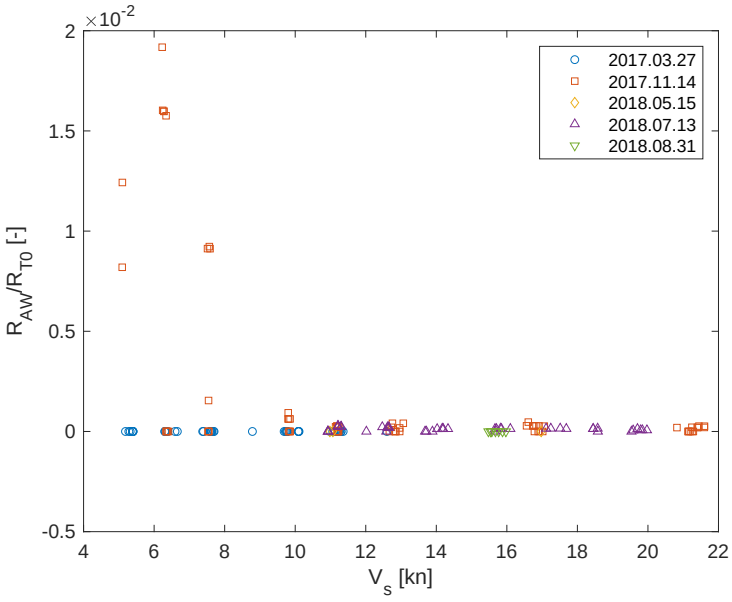


**Figure 5.25** – *Added wave resistance during the performance trials and monitoring.*

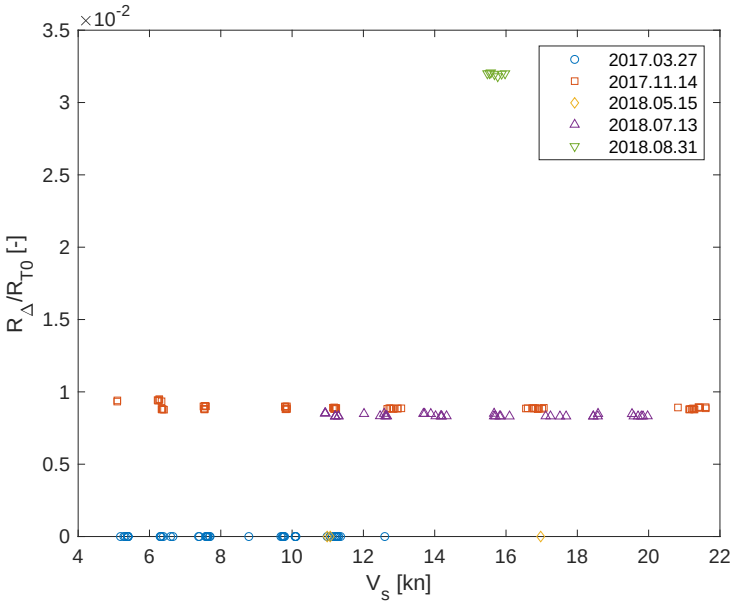


**Figure 5.26** – *Added resistance due to displacement change during the performance trials and monitoring.*

the 14th November 2017 at speeds around 6kn.

Figure 5.28 shows the normalised delivered power against the speed through water measured and analysed during all the monitoring/trials conducted since January 2017. The data show very good agreement among them, with the power curve being well defined throughout. The curve shows clearly the three speed ranges peculiar to the behaviour of high-speed vessels, i.e. the displacing region ($Fn <\approx 0.3$), the transition region ($Fn \approx 0.3 - 0.5$) and the semi-planing region ($Fn >\approx 0.5 - 1$). The delivered power curve starts growing visibly at speeds nearer the 'hump' region (i.e. $\approx 11 - 14$kn) as the date of the trial gets further from the DD. At the higher speeds, the power increase can be noticed to become much clearer. It may be here recalled that the two DDs relevant to this monitoring campaign had been carried out in Semptember 2016 and July 2017 — see also Fig. 5.18. The power reaches its maximum increase on the 31st of August 2018 (11 months after DD).

Similar trends are shown in Fig. 5.29, which presents the normalised total resistance coefficient $C_{T0}$ — see eq. (2.2). Again, a resistance increase is apparent at the higher $Fn$, whereas it becomes slightly more confused at transition speeds. In this particular graph, the differences between measurements conducted on different days are much more evident even at the lower speeds. This suggests that nondimensional coefficients can be more insightful than dimensional variables. A slightly larger spread can be seen at low speeds in the data logged on the 27th of March 2017.

So far, the figures have concerned exclusively the effect of disturbances on the resistance and they haven't provided information of their impact on the effective wake fraction. According to the dissertation made in Section 4.2, the change of wake fraction induced by

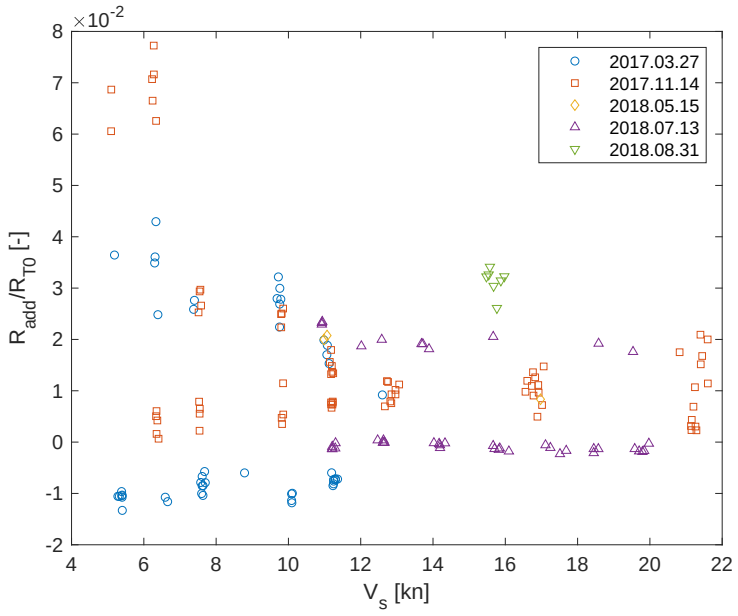


**Figure 5.27** – *Total added resistance during the R/V's performance trials and monitoring.*

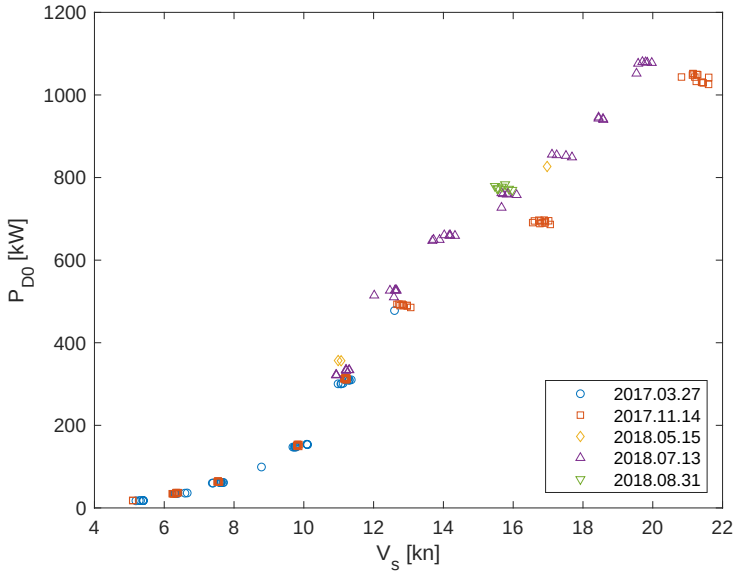


**Figure 5.28** – *Normalised delivered power for all performance trials and monitoring.*

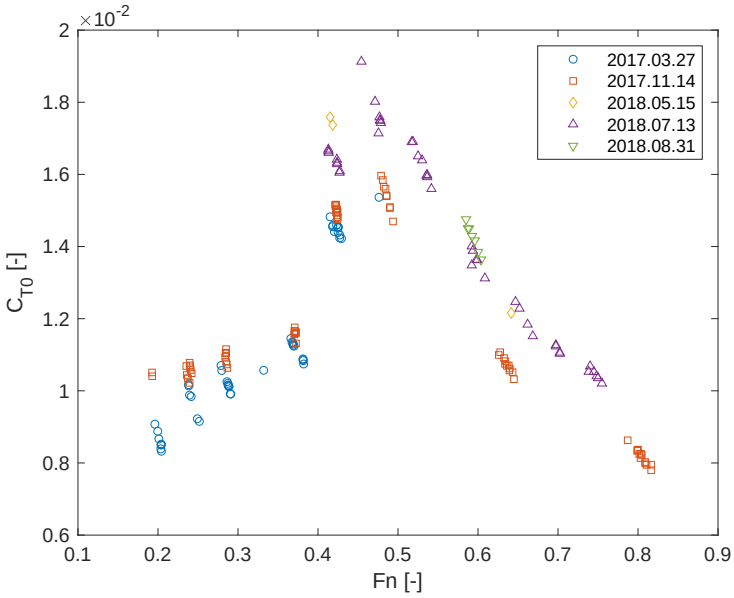


**Figure 5.29** – *Normalised total resistance coefficient for all performance trials and monitoring.*

the disturbances is unfortunately difficult to estimate. A general insight on goodness of the wake measurements can however be given by observing the behaviour of the effective wake fraction. Figure 5.30, shows the normalised wake fraction 'felt' by the port and starboard side propellers — refer to eq. (4.64). The port measurements are amiss due to a failure of the port shaft gauges that will be expanded upon in the following sections. The trends shown in the figure appear to confirm those seen in Fig. 5.28 and 5.29. Specifically, the wake fraction $w_Q$ increases over time, which is particularly clear at the high $Fn$. It can also be noticed a difference in the two wake fractions, especially at $Fn$ below 0.5. The data recorded on the 13th of July 2018 particularly shows a wider scatter at transition speeds. At the same speeds, the data from the same trials show an interesting drop of the starboard wake, which is also generally lower than the port side's.

### *5.6.2 Data normalization software module*

As for the data preparation, the normalization module was conceived to be operated both in on-line and off-line mode. The GUI is composed by the simple interface shown in Fig. 5.31, which shows information regarding the vessel and the analysis. Two charts at all similar to those presented in Section 5.5.5 are placed at the centre and are tailored to display the normalised variables. The software code is mainly composed of a script that executes the normalization algorithm accepting as input the output of the data preparation module or other pre-saved files. The analysis is carried out in a completely automated way and when started it fetches all the data necessary for the analysis from the vessel database. The normalization procedure is triggered and saved by means of purpose-made buttons placed on the lower left corner of the GUI.

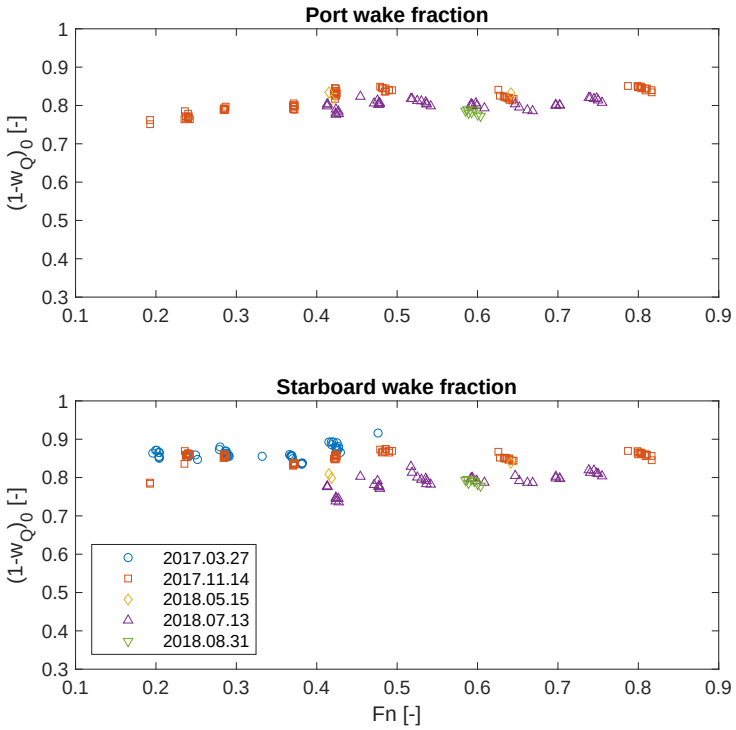


**Figure 5.30** – *Normalised effective wake fraction derived from torque-identity for all performance trials and monitoring.*

## 5.7 Performance analysis

The service performance analysis here presented was carried out with the purpose of assessing the impact of biofouling growth and the suitability of the fouling control strategy adopted on *The Princess Royal*. The results of the normalization laid out in the previous section, indicate that the performance of the R/V had been deteriorating since the DD. They also suggest that the disturbances didn't play a dominant role in this, but they had rather limited impact. It is the scope of this performance analysis to attempt to better understand the cause behind such performance deterioration.

Owing to the discontinuity of the on-board measurements, this analysis ended up being conducted exclusively off-line and no GUI was thus developed for it. This section therefore describes the derivation and analysis of the KPIs introduced in Section 4.6 for *The Princess Royal*. These are:

- $\hat{P_K}$, eq. (4.66)
- $\hat{w_K}$, eq. (4.67)
- $w_{appK}$, eq. (4.68)
- $\hat{\phi}$, eq. (4.71)

The derivation of $\Delta C_f$ from $\hat{\phi}$ and the thrust measurement will also be here shown.

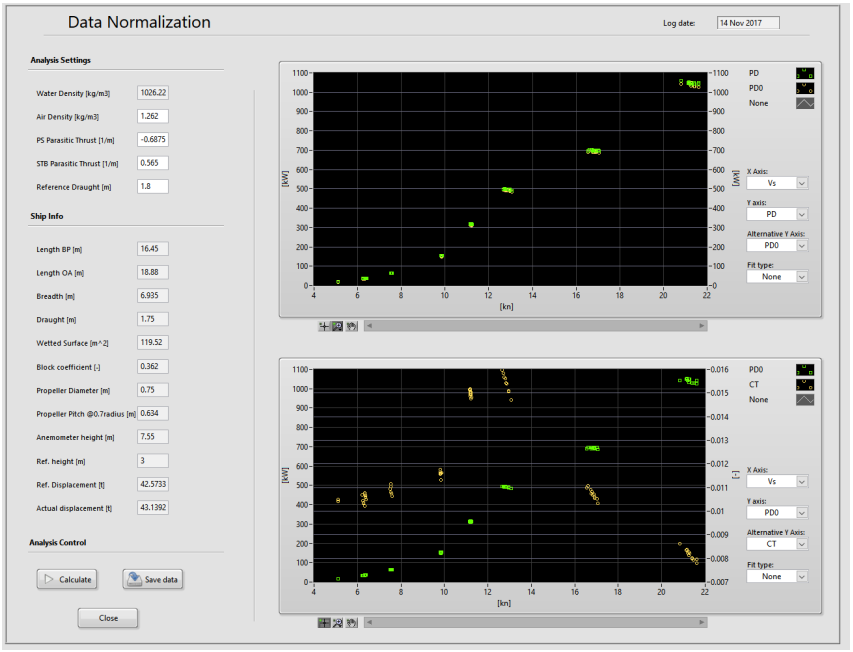


**Figure 5.31** – *GUI of the SPMS data normalization software module.*

The section will at first present the method adopted to derive the *reference* baseline performance. The change of hydrodynamic performance from the reference will then be investigated and discussed through the presentation of the KPIs. A paragraph is also dedicated to the observation of fouling on the Princess Royal.

### *5.7.1 Reference performance*

In accordance with the method adopted in this research, the reference performance of *The Princess Royal* was determined from full-scale speed-power trials. The trial data had to be chosen such that the following requirements were satisfied:

- A sufficient range of speeds was covered
- A fair weather was encountered throughout the trials
- The trial was conducted with sufficiently clean hulls and propellers

The speed-power trials conducted on the 14th November 2017 were found to satisfy these requirements. The mild fouling state on the hull had been ensured by only four months out of DD, during which the vessel had been kept relatively busy by teaching, research and chartering jobs alike. Since at the time the vessel was coated with a FR coating, continuous operation at speed helped maintaining the hulls and propellers sufficiently clean. At the time of the trials, *The Princess Royal* was found having diffused hard slime over the hull and clean propellers. This feature was complemented by the goodness of the weather and the extent of the speed range (the largest during all the years of research).

As wisely expressed by Munk (2006), a part of underrated importance in ship performance analysis is the determination of the reference baselines. The choice of the model to fit the reference performance from sea trials data is indeed one of the riskiest operations of the traditional deterministic approach. The model must not only be a good descriptor of the input data, but should also have a reasonable physical meaning. Since a KPI is fundamentally a measure of distance from a reference line, the choice of a wrong baseline fit may completely obfuscate the information the KPI intends to convey. In the case study here presented, the choice of baseline fit is made rather difficult by the large range of Froude numbers covered by the R/V. As most catamarans, *The Princess Royal* mostly behaves as a displacing vessel up until $Fn <\approx 0.35$, where a first resistance hump is observed (see also Molland *et al.*, 1994). In the range $Fn \approx 0.4 - 0.5$, the largest resistance hump marks the transition from displacing to semi-planing behaviour (Larsson and Raven, 2010). In this speed range, the dynamic trim finds its peak and the lifting forces assume increasing significance. Above $Fn > 0.6$, the vessel assumes a steady behaviour and no resistance hump occurs (see also Faltinsen, 2005). At these speeds, the viscous resistance component returns to be dominant as it was at the lower speeds (Molland *et al.*, 1994). It will be clear that most, if not all, parameters linked to the vessel performance will display a different behaviour at least before and after the transition speed. Within the transition speed range $Fn \approx 0.35 - 0.5$, the shape of most variables presented as functions of $Fn$ is obviously extremely difficult to model with accuracy, particularly if disposing of a limited dataset. It was therefore decided that to avoid jeopardising the KPIs by choosing a meaningless baseline fit, only the displacing and semi-planing speed ranges were to be studied.

The power increase KPI was defined by eq. (4.66) as:

$$P_K(\mathbb{t}, V_s) = \frac{P_{D0}(\mathbb{t}, V_s)}{P_{D0\,\mathrm{ref}}(\mathbb{t}_{\mathrm{ref}}, V_s)} - 1$$

Figure 5.32 shows the reference curve extrapolated from the normalised delivered power measured during the sea trials. For both $0 \leq Fn \leq 0.35$ and $0.5 \leq Fn \leq 0.9$ ranges a power type equation was used.

The second KPI is the wake fraction gain, eq. (4.67):

$$\hat{w_K}(\mathbb{t}, V_s) = \frac{w_Q(\mathbb{t}, V_s)}{w_{Q\,\mathrm{ref}}(\mathbb{t}_{\mathrm{ref}}, V_s)} - 1$$

The reference baselines for the starboard and port wake fractions were thus derived as shown in Fig. 5.33. Since the wake fraction is almost in linear relationship with speed at displacing speeds, a linear fit was chosen for $Fn < 0.35$. At the higher $Fn$, a second-order polynomial was considered to be a better descriptor.

Similarly, the apparent wake gain was defined in eq. (4.68):

$$w_{app\,K}(\mathbb{t}, V_s) = \frac{w_{app}(\mathbb{t}, V_s) - w_{app\,\mathrm{ref}}(\mathbb{t}_{\mathrm{ref}}, V_s)}{w_{Q\,\mathrm{ref}}(\mathbb{t}_{\mathrm{ref}}, V_s)}$$

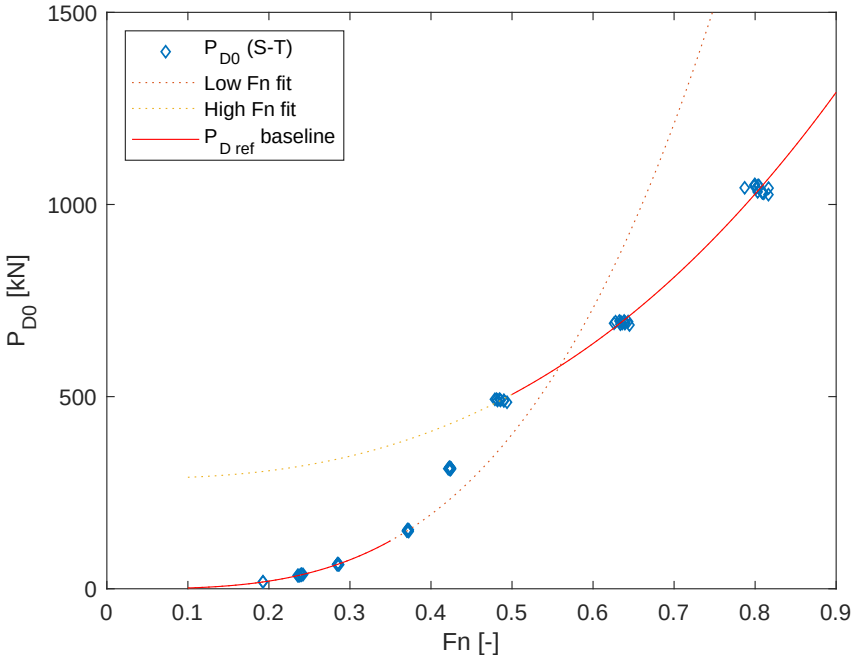


**Figure 5.32** – *Derivation of the reference $P_{D0}$ curve.*

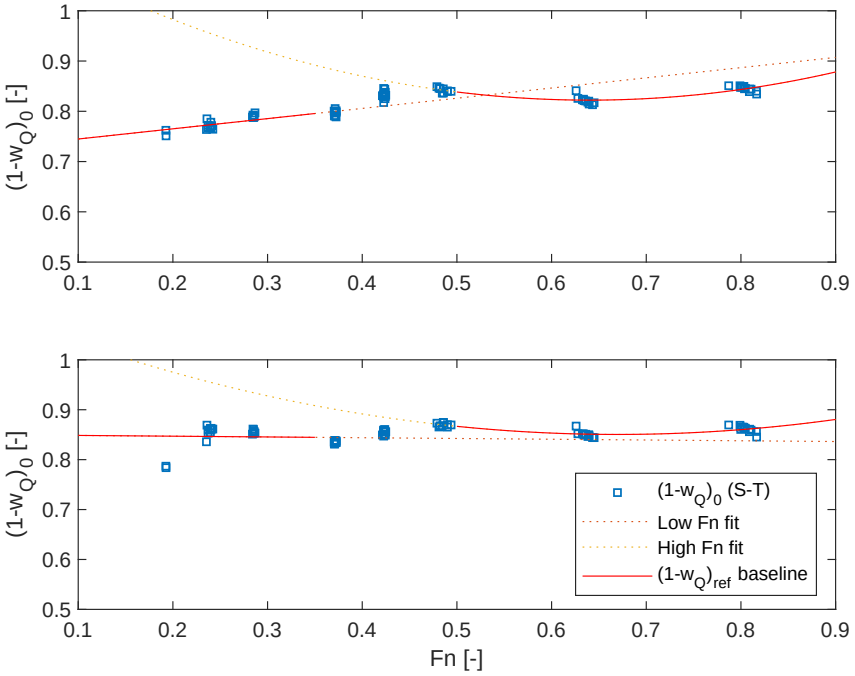


**Figure 5.33** – *Derivation of the reference $(1 - w_Q)_0$ curve.*

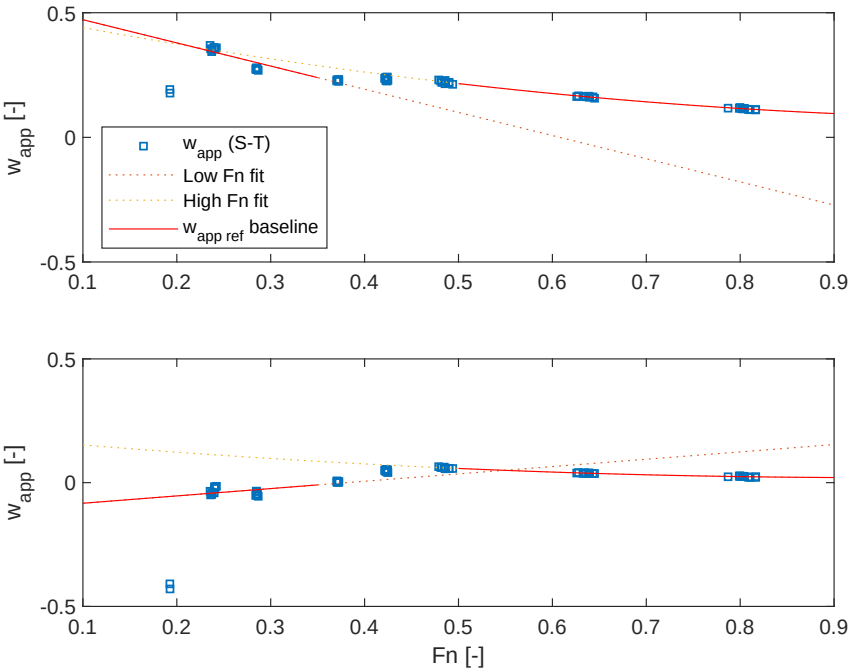


**Figure 5.34** – *Derivation of the reference $w_{app}$ curve.*

In Fig. 5.34, the reference curve for the apparent wake fraction is presented. In this particular case, the greatest concern was to capture the non-linearity of the parasitic thrust. It was found that a linear fit and a second-order polynomial could describe reasonably well its behaviour at low and high $Fn$ respectively.

Lastly, the estimation of the viscous drag increase is observed from the change of $\hat{\phi}$, eq. (4.71):

$$\hat{\phi}(\mathbb{t}, V_s) = \frac{\hat{C}_v(\mathbb{t}, V_s)}{C_{v\,\mathrm{ref}}(\mathbb{t}_{\mathrm{ref}}, V_s)} - 1$$

where $\hat{C}_v(\mathbb{t}, V_s) = \hat{C}_T(\mathbb{t}, V_s) - C_{w\,\mathrm{ref}}(V_s)$. Therefore, the reference curves of $C_{v\,\mathrm{ref}}$, $C_{w\,\mathrm{ref}}$ and consequently $C_{T\,\mathrm{ref}}$ are needed. For fast catamarans, both the inception of planing lift forces at $F_n \approx 0.4$ and the interaction between demi-hulls introduce additional viscous forces. In accordance with the work of the Molland group (1994), a modification to the standard viscous drag of eq. (4.70) can be proposed as:

$$C_v = (1 + \varkappa k)C_f \tag{5.5}$$

$\varkappa$ is termed viscous resistance interference factor and includes both the change of pressure field around the demi-hull and the increase of flow velocity between the two demi-hulls. $\varkappa k$ was initially estimated from Holtrop's (1984) regression. According to the Molland group method, it was then calibrated at the higher $F_n$ where the stable planing lift forces in this region define a clearer resistance trend. This yielded:

$$\varkappa k = 0.7765 \tag{5.6}$$

The ITTC '57 formulation was used for the skin friction coefficient. The static wetted surface area was preferred, since estimating the running wetted surface area is both difficult

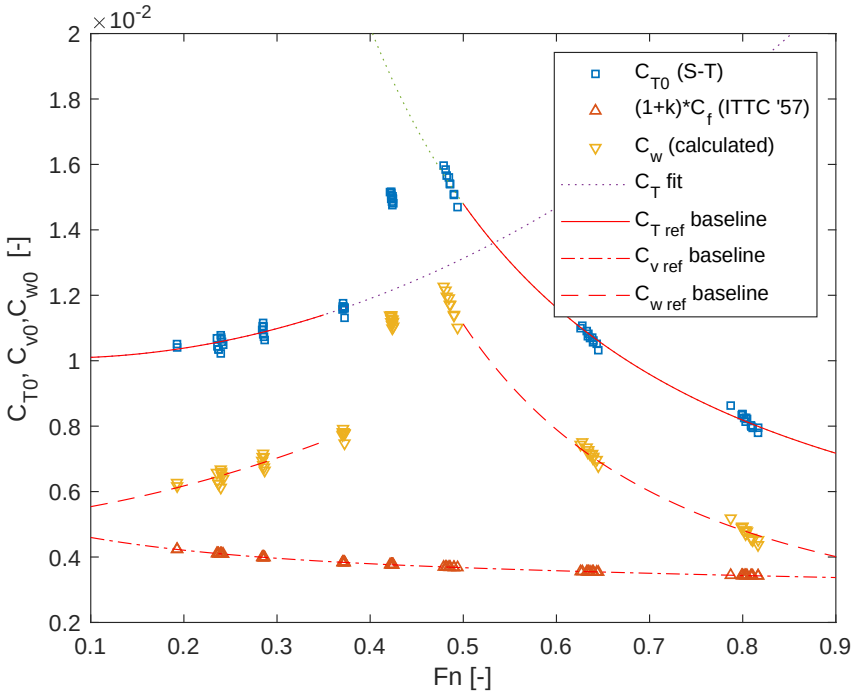


**Figure 5.35** – *Derivation of the reference curves for the nondimensional resistance coefficients.*

and not significantly influential (Molland *et al.*, 1994). It should be borne in mind that an erroneous estimation of $\varkappa k$ has the effect of introducing a small bias in the calculation of $\hat{\phi}$, but it doesn't affect the overall meaning of the KPI. Figure 5.35 shows the reference curves obtained for the resistance coefficients. For $C_T$, a second-order polynomial was used for $Fn < 0.35$ whereas a power function was used for $Fn > 0.5$.

### 5.7.2 Service performance

The application of the four KPIs and $\Delta C_f$ to *The Princess Royal*'s case study is described in this section. Because the analysis was conducted separately in the two ranges $Fn < 0.35$ and $Fn > 0.5$, these will be presented on separate graphs.

Firstly, it is relevant to prefigure what it is to be expected from the analysis. According to **Assumption 1** given in Section 1.3, the effect of fouling (or more generically of an increased roughness) affects only the viscous-related components of ship resistance. The derivative of the viscous resistance coefficient as a function of $Fn$ (Fig. 5.35) is strictly monotonic over the whole speed range, whilst the derivative of the wave resistance is not. As a consequence, $P_K$ will not be expected to be monotonic. Conversely, as fouling increases, $\hat{\phi}$ will have a shape at all similar to the $C_f$ function, because it is a ratio of two monotonically decreasing functions — both behave as $1/\log_{10}$. Similarly, the frictional coefficient increase $\Delta C_f$ will be a monotonic function, strictly decreasing over the whole speed range as the fouling builds up. On the other hand, the behaviour of the effective wake fraction is different at displacing and semi-planing speeds. For $Fn < 0.35$ the wake

largely depends on viscous phenomena and hence on the thickness of the hull boundary layer. This leads to expect that the wake will have an approximately constant offset depending on the fouling accumulation on the hull. For $Fn > 0.6$, the wave and potential wake components will have higher impact and thus a speed-dependent behaviour will be expected. It must however be noted that the reference performance was obtained with a hull covered with hard slime. If a measurement is taken with milder fouling state (as it will be shown), the monotonic functions will obviously switch from nonincreasing to nondecreasing. According to **Assumption 3**, the fouled propeller will show an increased torque resulting from the higher sectional foil drag. Since the foil drag is totally dependent on viscous forces, $w_{app\,K}$ is expected to be a nondecreasing function of the blade Reynolds number.

Figure 5.36 shows the change of $P_k$ respectively at the displacing and semi-planing speeds. At displacing speeds, measurements were available only from one-day worth of monitoring. The data shows that the power absorption in March 2017 is generally lower than the baseline, although displaying a relatively large scatter. A clear increasing trend in the range $Fn \approx 0.2 - 0.3$ can be seen. It is also noticed a bias in the measurements, indicated by the regular 'diagonal' distribution of the scatter. This is a direct consequence of the variability of the $u_s$ measurement on the baseline fit, which could be clearly seen in Fig. 5.32. In general, the observations conducted on *The Princess Royal* confirmed that the speed log measurements fluctuate more than the other primary variables — about 1.5% variation against 0.7% of both $Q$ and $n$. The high sensitivity of the KPIs makes such small differences very apparent. Therefore, this 'bias' shown by the KPIs is an unwanted and yet unavoidable by-product of the KPI definition itself. As of the higher $Fn$ range, it can be seen that already in May a significant power variation from the baseline is present, which gradually increases over time and reaches its peak in August. The data spread is much less pronounced though still noticeable, particularly for data acquired on the 13th of July. The KPI appears to have a convex behaviour in the range $0.5 < Fn < 0.8$. These results can also be considered in terms of resistance, by defining:

$$\hat{C}_{T0\,K}(\mathbb{t}, V_s) = \frac{C_{T0}(\mathbb{t}, V_s)}{C_{T0\,\mathrm{ref}}(\mathbb{t}_{\mathrm{ref}}, V_s)} - 1 \tag{5.7}$$

This is not the exact calculation of the increase of total resistance coefficient, since its derivation may be contaminated by the propeller fouling. It is thus denoted by the circumflex. Figure 5.37 shows the total resistance increase. Trends similar to those seen for $P_K$ are seen also for $\hat{C}_{T0\,K}$.

Both $P_K$ and $\hat{C}_{T0\,K}$ show a significant deterioration of *The Princess Royal*'s hydrodynamic performance over time. However, neither provides any insight regarding the cause of such deterioration. The other KPIs can be used to complement this information. Under the assumption that the demi-hulls and propellers have similar fouling state, the

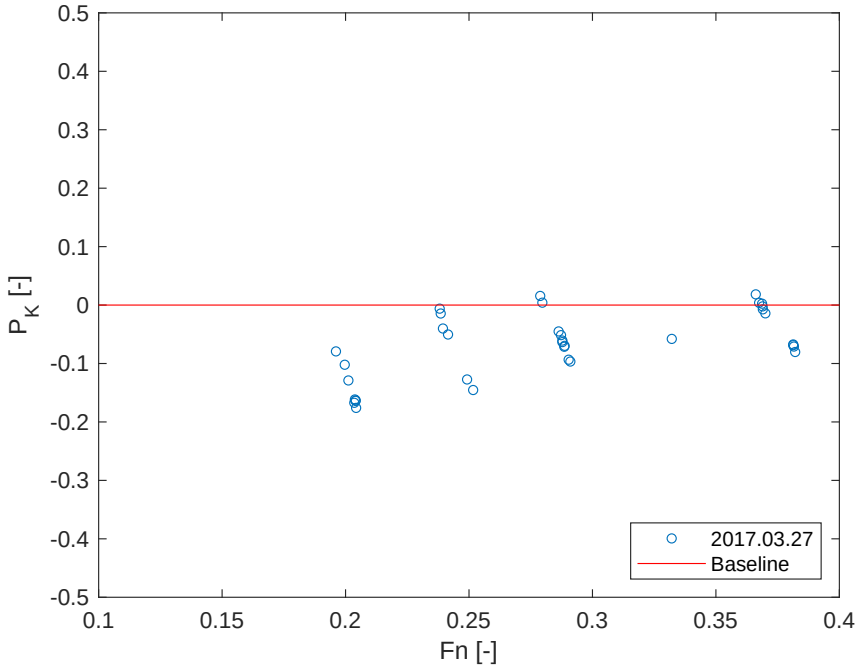


(a)

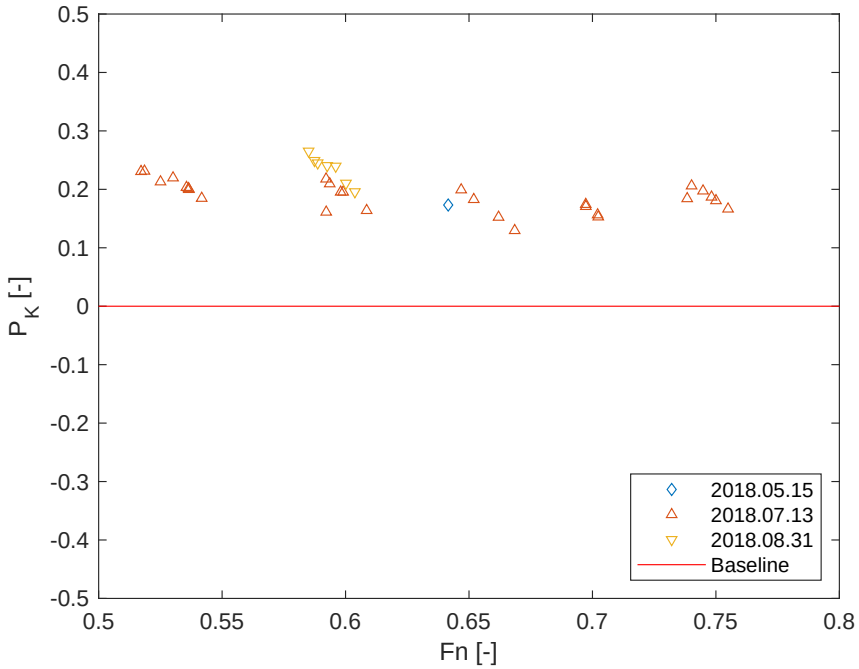


(b)

**Figure 5.36** – *Normalised power increase $P_k$ for* (a) *the range $Fn < 0.4$ and* (b) *the range $Fn > 0.5$.*

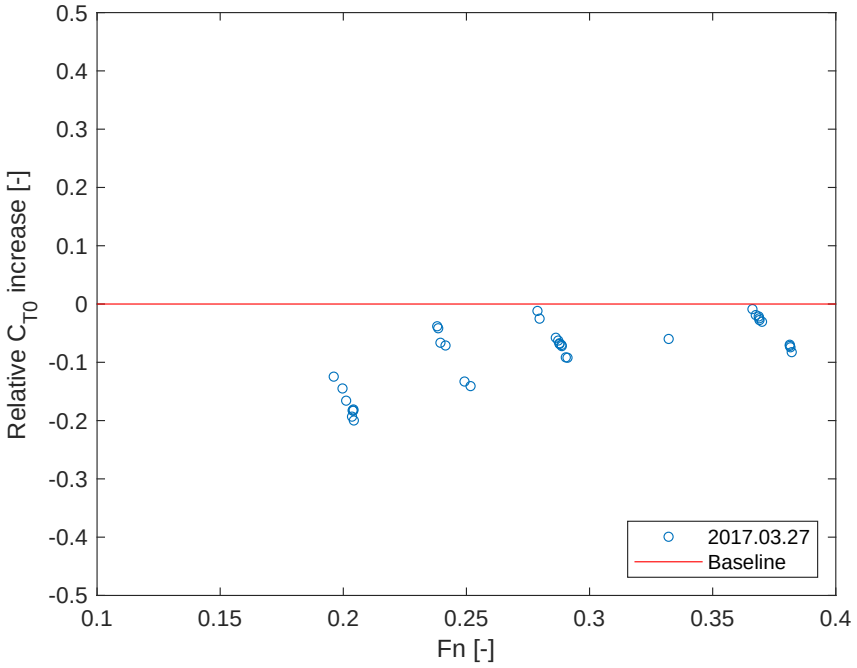


(a)

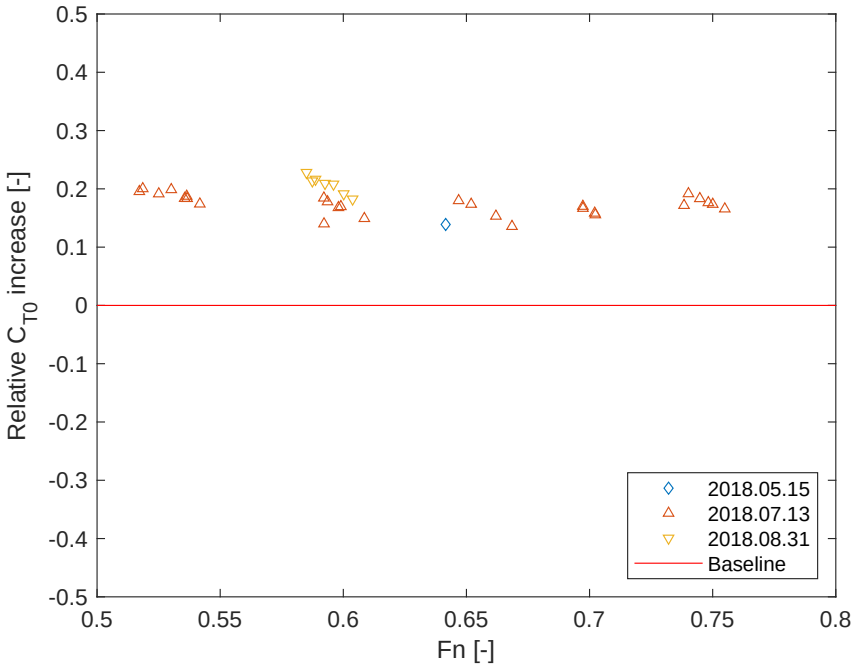


(b)

**Figure 5.37** – *Fractional increase of the normalised total resistance coefficient for* (a) *the range* $Fn < 0.4$ *and* (b) *the range* $Fn > 0.5$.

wake-based KPIs of starboard and port side were averaged in a single value. This is a fair assumption, also considering that their combined effect is under scrutiny. In Fig. 5.38a, the wake fraction gain $\hat{w}_K$ shows again a lower value than the reference, estimating a flow averagely 7.7% faster at the propeller. It can be noted that in the strictly displacing range ($0 < Fn < 0.35$) $w_K$ has an approximately constant value. Figure 5.38b shows $\hat{w}_K$ at semi-planing speed. The KPI has one value (May 2018) very close to the baseline, whilst significantly departs from it with the data acquired in July and August. In these dates, the wake fraction gain estimates a consistent drop of the propeller inflow speed. In this speed range, the KPI shows a clear nonincreasing behaviour. In July, $w_K$ ranges from 31% at $Fn \approx 0.53$ to 18% at $Fn \approx 0.75$, whilst in August $w_K = 0.33$ on average at $Fn \approx 0.6$. The advantage of the wake fraction gain KPI over $P_K$ stands in its ability to distinguish between the power needed to push the vessel at a certain speed and that needed to rotate the propeller in a certain flow field. Therefore, since the wake fraction is an indication of what the propeller perceives in terms of inflow and is strongly dependent on the viscous forces, 5.38a seems to confirm that the better performance of March 2017 is caused by a milder hull fouling. Similarly, Fig. 5.38b corroborates the suggestion that the increase of $P_K$ is strictly related to the roughening of the hull surface. In addition, the effect of disturbances on the wake was shown to be sufficiently small to not influence the analysis within the constraints defined in Section 4.5. Under these conditions, $\hat{w}_K$ warns about the growth of the hull's boundary layer, or of the presence of propeller fouling, or (more likely) of both. The merit of the wake fraction gain KPI stands in its greater sensitivity, which is however repaid with a larger data scatter.

To separate the effect of hull fouling from that of propeller fouling the measurement of thrust is employed to derive the apparent wake fraction gain. This KPI is shown in Fig. 5.39 and indicates the apparent proportion of the torque-identity effective wake fraction (refer to eq. (4.52)). Indirectly, it is therefore a potential indicator of propeller fouling. In Fig. 5.39a, $w_{app\,K}$ shows a neat positive value, being 16% on average. This suggests that in March 2017 the roughness of the propeller blades was significantly higher than the baseline. In perspective, this result is rather striking, considering the short time elapsed since the previous DD and the expected cleanness of the propeller. Whereas the data spread is very high and is of the same order of the mean value, the KPI is however convincing given the relatively high number of datapoints. At the higher speeds, in July $w_{app\,K}$ stands at about 25% at $Fn \approx 0.52$, then drops at about 2% to increase monotonically up to 10% at $Fn \approx 0.75$. The high initial value is likely originated from a wake fraction distortion, caused perhaps by a tidal current. Since this KPI is very sensitive, the effect is magnified. In August, $w_{app\,K}$ shows an average value of 38%. These values indicate that the propeller roughness was almost unaltered in July, while it exhibited a significant deterioration by August. In other words, $w_{app\,K}$ indicates that by the end of summer almost 40% of the effective wake fraction 'felt' by the propeller

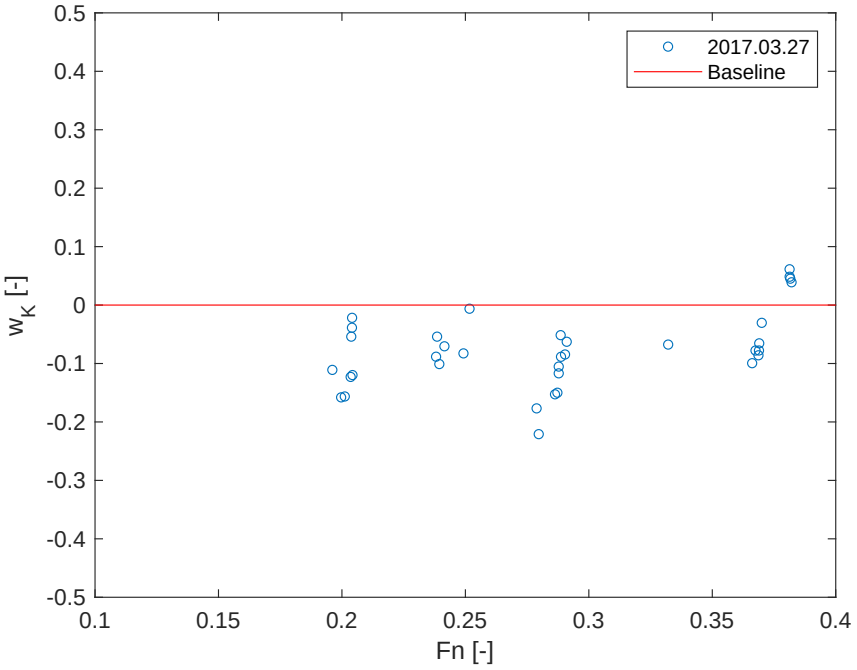


(a)

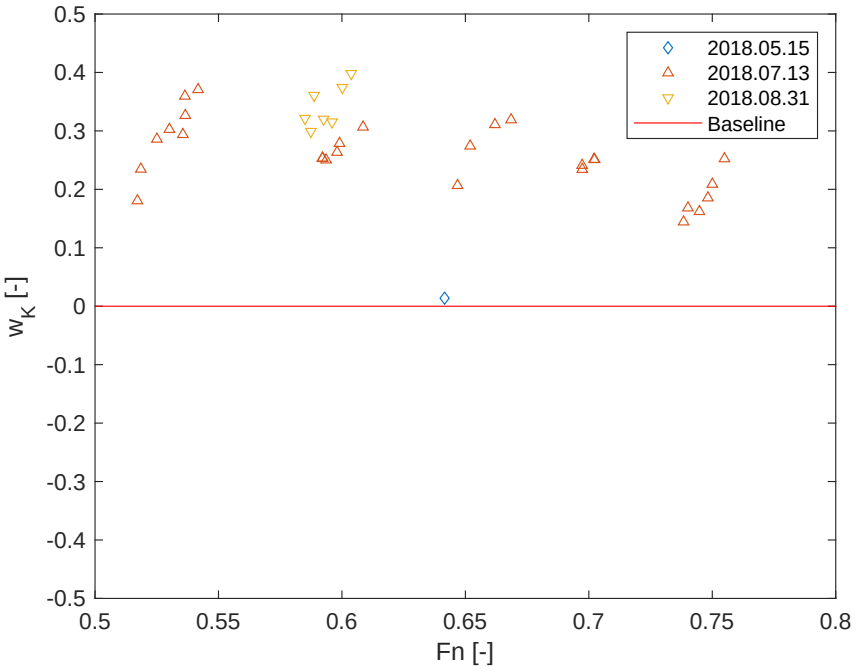


(b)

**Figure 5.38** – *Effective wake fraction gain for* (a) *the range* $Fn < 0.4$ *and* (b) *the range* $Fn > 0.5$.

is caused by a roughening of the propeller blades. The value recorded in May (17%) is instead quite bewildering considering the other KPIs recorded on the same day. It should however be considered that for this date a single value is available, from which it is difficult to draw definitive conclusions. Again, it might be possible that some strong currents were causing severe wake distortions, whose effect would be amplified by this KPI. The relatively higher scatter displayed by $w_{app\,K}$ with respect to the other KPIs is then partly justified by the high sensitivity of this parameter — a small part of the wake fraction. In part however, it is also caused by the notable uncertainty of thrust measurements, which is further complicated in this case by the presence of the parasitic thrust. Nevertheless, the overall data distribution indicates that the baseline fits describe reasonably well the KPI.

The fouling coefficient presented in Fig. 5.40 eventually estimates the impact of hull fouling on the viscous resistance. At the lower $Fn$, $\hat{\phi}$ demonstrates that the viscous drag measured in March 2017 was generally lower than the baseline. The KPI is clearly a nondecreasing function of $Fn$ similar to what shown by Fig. 5.36 and 5.37. At this point, these increasing trends would confirm the expected effect of a lesser fouling accumulation in March. On the other hand, the spread exhibited by the KPI is large and is again in the same order of the average value. Figure 5.40b shows a neatly nonincreasing behaviour of $\hat{\phi}$ against speed, again confirming the dependency of frictional drag from the Reynolds number. Considering that these latter data were collected about 6 months after the reference period and the operational profile of *The Princess Royal*, the estimation of viscous drag increase is quite sensible.

The fouling coefficient was explained in Section 4.6 to include the effect of propeller roughening which, if present, would result in an overestimation of the viscous drag increase. Owing to the availability of the thrust measurement and according to eq. (4.78) and (4.79), it was possible to separate the effect of propeller and hull roughness from $\hat{\phi}$ and to derive the full-scale frictional coefficient increase $\Delta C_f$ *with respect to the reference fouling state* — heavy slime. Figure 5.41a demonstrates overall a $\Delta C_f$ lower than the baseline, with the nondecreasing behaviour in the region $Fn \approx 0.2 - 0.3$ already seen in Fig. 5.36 and 5.37 much more evident. Again, in this date the spread of the data is relatively large. However, this value globally indicates a smoother hull surface compared to the baseline. In Fig. 5.41b, $\Delta C_f$ behaves as a nonincreasing function of $Fn$, which again meets the expectations. At $Fn = 0.6$, the average $\Delta C_f$ values are of $2.0 \times 10^{-3}$ and $2.1 \times 10^{-3}$ respectively in July and August 2018. Very interestingly, the behaviour of $\Delta C_f$ reflects what expected comparing the trends of all the other KPIs, particularly of $\hat{\phi}$ and $w_{app\,K}$. It will be noticed that where $w_{app\,K}$ had larger values (August 2018), $\hat{\phi}$ is corrected to deliver very similar $\Delta C_f$ values to those of the previous month. This suggests that the hull fouling severity did not greatly increase from July to August. On the other hand, it appears that the roughening of the propeller blades is the chief reason

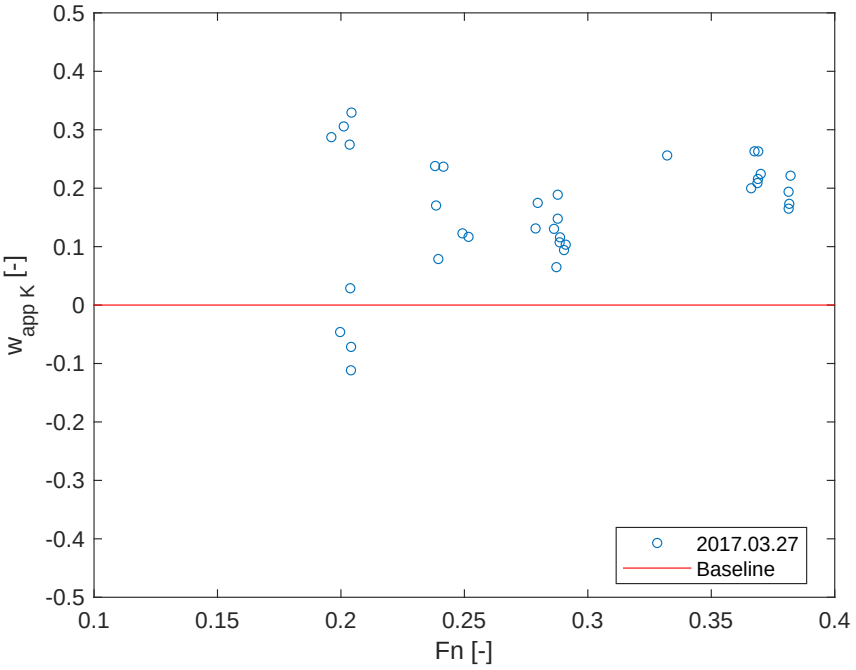


(a)

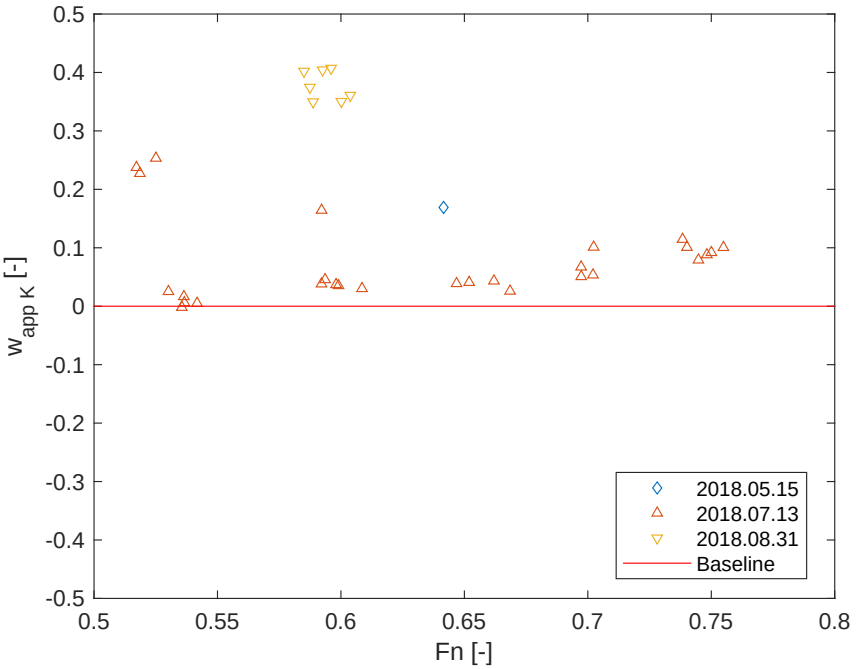


(b)

**Figure 5.39** – *Apparent wake fraction gain for* (a) *the range* $Fn < 0.4$ *and* (b) *the range* $Fn > 0.5$.

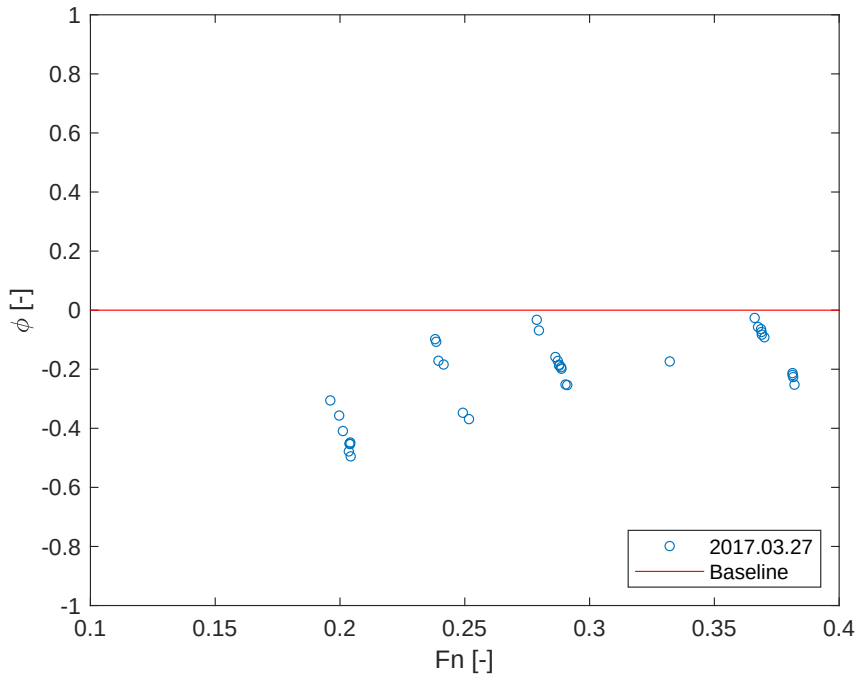


(a)

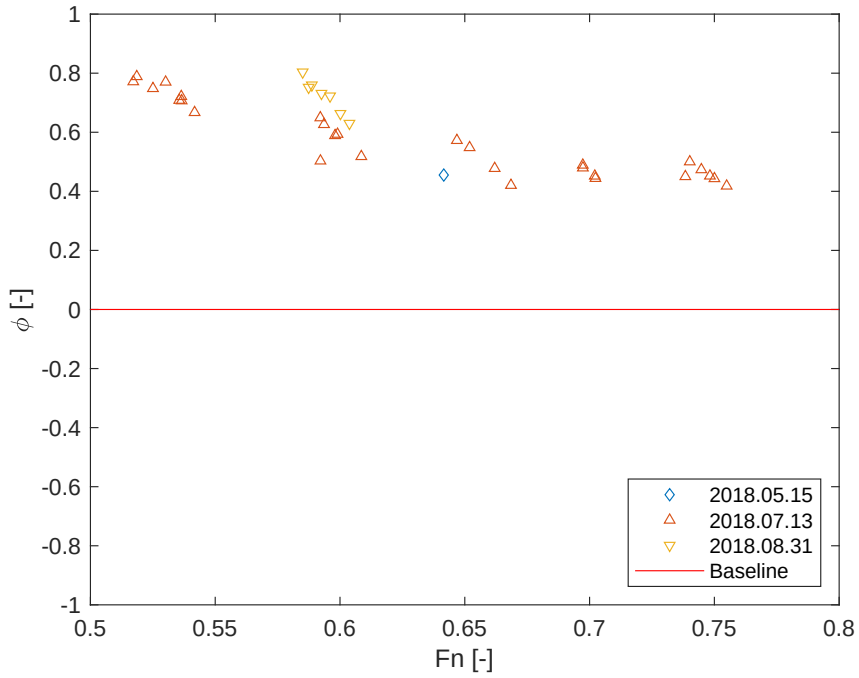


(b)

**Figure 5.40** – *Estimated fouling coefficient for* (a) *the range* $Fn < 0.4$ *and* (b) *the range* $Fn > 0.5$.

TABLE 5.14

*KPI values estimated by linear interpolation @$Fn = 0.287$ and referred to the heavy slime reference condition* .

| | $P_K$ | $\hat{C}_{T0\,K}$ | $\hat{\phi}$ | $\hat{w}_K$ | $W_{app\,K}$ | $\Delta C_f$ |
|---|---|---|---|---|---|---|
| *March-17* | -0.053 | -0.062 | -0.170 | -0.121 | 0.126 | -0.821e-03 |

TABLE 5.15

*KPI values estimated by linear interpolation @$Fn = 0.607$ and referred to the heavy slime reference condition* .

| | $P_K$ | $\hat{C}_{T0\,K}$ | $\hat{\phi}$ | $\hat{w}_K$ | $W_{app\,K}$ | $\Delta C_f$ |
|---|---|---|---|---|---|---|
| *May-17* | 0.186 | 0.148 | 0.522 | 0.015 | 0.191 | 1.63e-03 |
| *Jul-18* | 0.184 | 0.168 | 0.580 | 0.281 | 0.054 | 2.02e-03 |
| *Aug-18* | 0.230 | 0.203 | 0.696 | 0.341 | 0.369 | 2.02e-03 |

for the August performance loss witnessed in Fig. 5.36b and 5.37b.

The direct comparison between the KPIs estimated in different dates is not possible, given the different speeds at which they were measured. Using a localised linear interpolation, all KPIs were estimated for a cruising speed of 7kn and the design speed of 15kn, corresponding respectively to $Fn = 0.287$ and $Fn = 0.607$. Tables 5.14 and 5.15 summarise these estimations for the four KPIs, the increase of total resistance coefficient and $\Delta C_f$. In addition, Fig. 5.42 shows the evolution over time of the estimated values at $Fn = 0.607$ for the four KPIs, $\hat{C}_{T0\,K}$ and $\Delta C_f$. The estimations for the range $Fn < 0.4$ was not here included since only one day worth of data was available and a time series would not be meaningful. The graphs clearly show the consistency of the increasing trends of the indicators, let alone the May measurements that, having just one datapoint, are not able to grant a sufficient certainty over the estimation. Therefore, to help the reader to better follow the discussion, the KPIs measured in May 2018 are plotted with a transparent shade.

According to the findings reported in this section, it might be concluded that:

- In March 2017 (5.5 months out of DD) the performance of the R/V was generally slightly better than the reference (4 months out of DD). This was probably due to a smoother wetted surface, itself a likely consequence of a lesser fouling accumulation. Despite having spent more time out of dock than in the reference period, the hull condition could be justified by the very different season and activity of the vessel. From late September 2016 to March 2017 the vessel was highly active in very cold

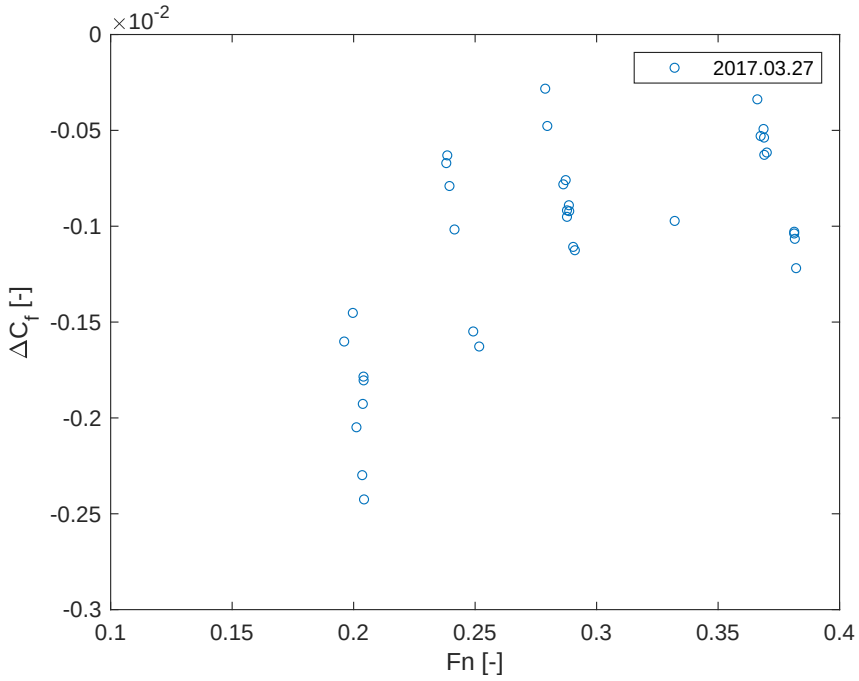


(a)

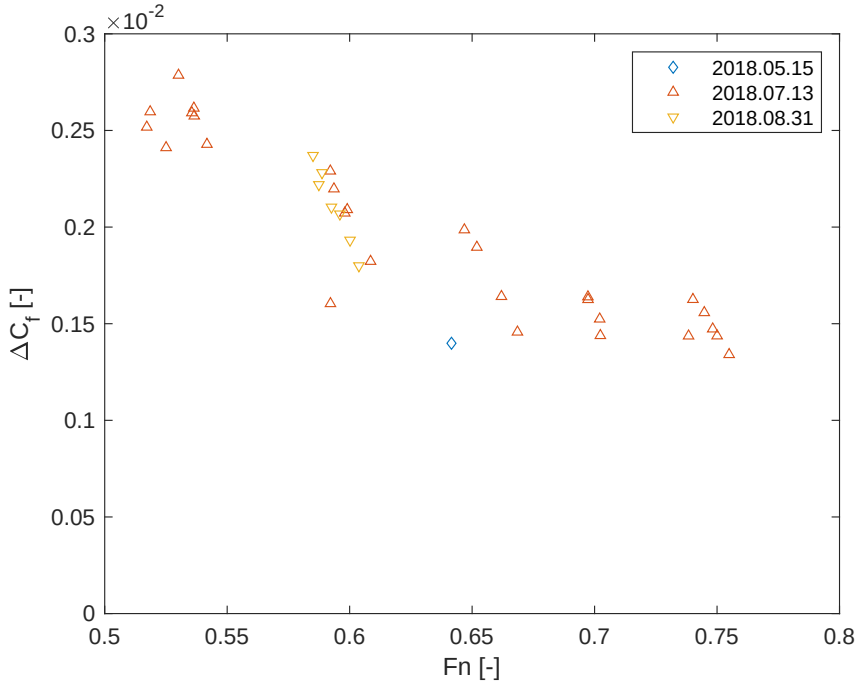


(b)

**Figure 5.41** – $\Delta C_f$ *values for* (a) *the range* $Fn < 0.4$ *and* (b) *the range* $Fn > 0.5$ *referred to a heavy slime baseline.*

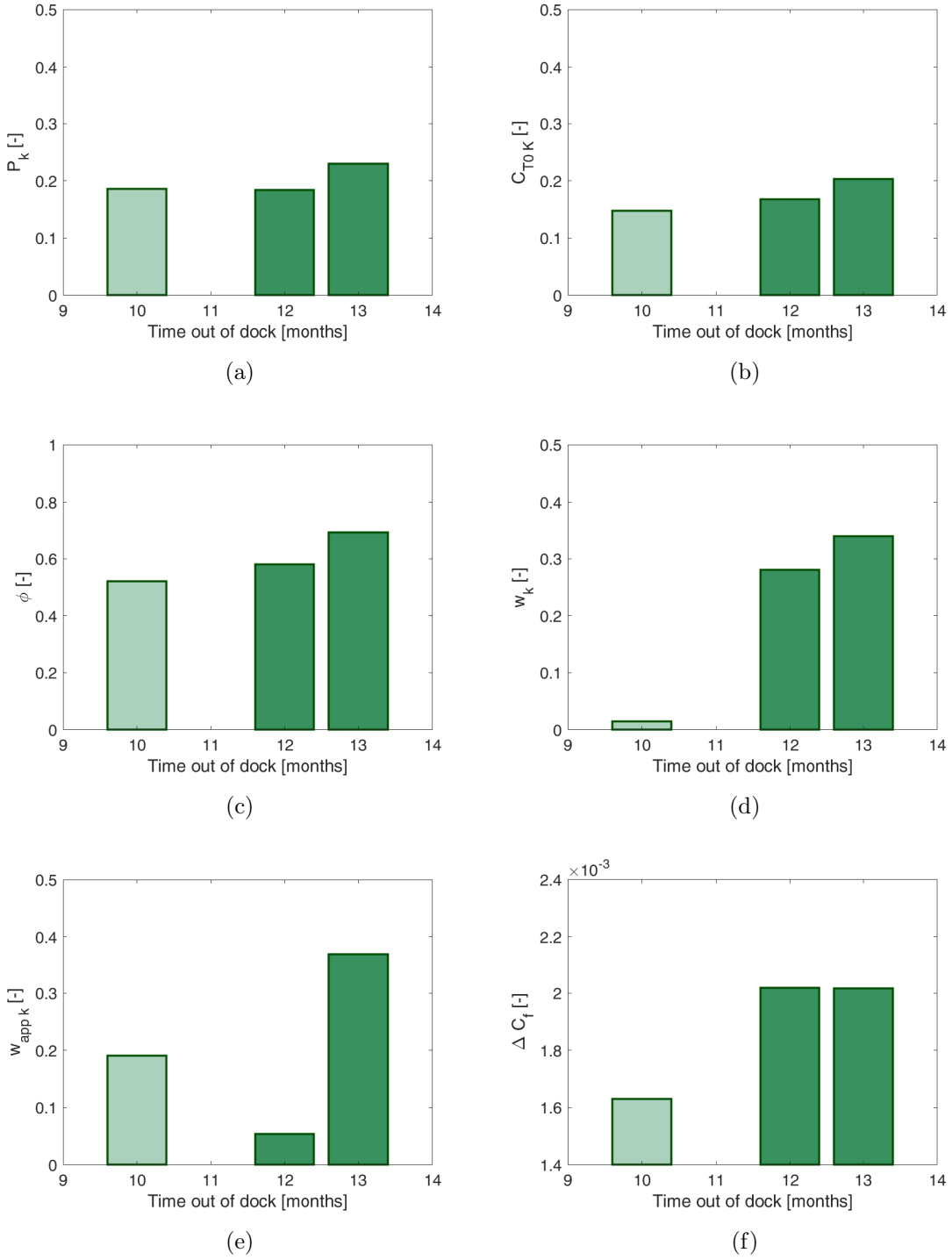


**Figure 5.42** – *Time series of the values estimated @$Fn = 0.607$ for* (a) $P_K$, (b) *increase of* $C_{T0}$, (c) $\hat{\phi}$, (d) $w_K$, (e) $w_{app\,K}$ *and* (f) $\Delta C_f$ *referred to the baseline 'heavy slime' condition, as function of the time out of dock. The lighter shade bar refers to the single datapoint available in May 2018.*

weather. From late June to November the vessel was still active (despite being laid-up during the earlier period), but the weather was much warmer and suitable for the growth of biofouling — see Section 2.3.

- In discordance with the above findings, in March 2017 the propellers resulted to deliver a much worse performance than the baseline, likely caused by the roughening of the propeller blades. However, from the considerations made so far, propeller fouling appears to be an unlikely cause given the activity of the vessel and the season of the year.

- Since the reference period, *The Princess Royal*'s performance had been deteriorating, resulting in an increase in power demand of about 25% at the higher speeds after 13 months out of dock. The causes of this performance loss are identified in an increase of hull roughness and, lately, in a roughening of the propeller blades. It is plausible to attribute both roughness cases to fouling given the timing, weather and operational circumstances of the development.

- The measurements conducted in May 2018 result pretty much in line with the above, apart from the low $w_K$ and the anomalously high $w_{app\,K}$. If a sudden smoothing of the propeller blades appears unlikely, on the other hand drawing conclusions from a single normalised datapoint is risky.

- To a limited extent, some effects of the disturbances possibly could not be entirely corrected in the normalization process. These may contribute to the scatter observed in the KPIs. It should however be borne in mind that most KPIs and particularly $w_{app\,K}$, $\hat{\phi}$ and $\Delta C_f$ are highly sensitive and hence by nature they amplify the normal spread of the data.

- Overall, the KPIs seem to meet the initial expected behaviours, which supports the assumptions of this research.

### *5.7.3 Hull and propeller surveys on* The Princess Royal

One of the great benefits of employing a proprietary R/V for this research was the possibility to inspect her conditions. Hull and propeller surveys could be carried out as part of a Dry-Docking (DD) or during an In-Water Survey (IWS) conducted by the Performance Monitoring Team of Newcastle University. Figures 5.43, 5.44 and 5.45 show pictures of the observations made on *The Princess Royal* during these surveys.

From the pictures shown in Fig. 5.43, it can be seen that in March 2017 *The Princess Royal* was subjected to a mild fouling state — mainly soft slime. However, the propellers show evident signs of damage. Figure 5.43c in particular displays a significant erosion on the suction side of the blades and on the leading edges, as if caused by heavy sheet and

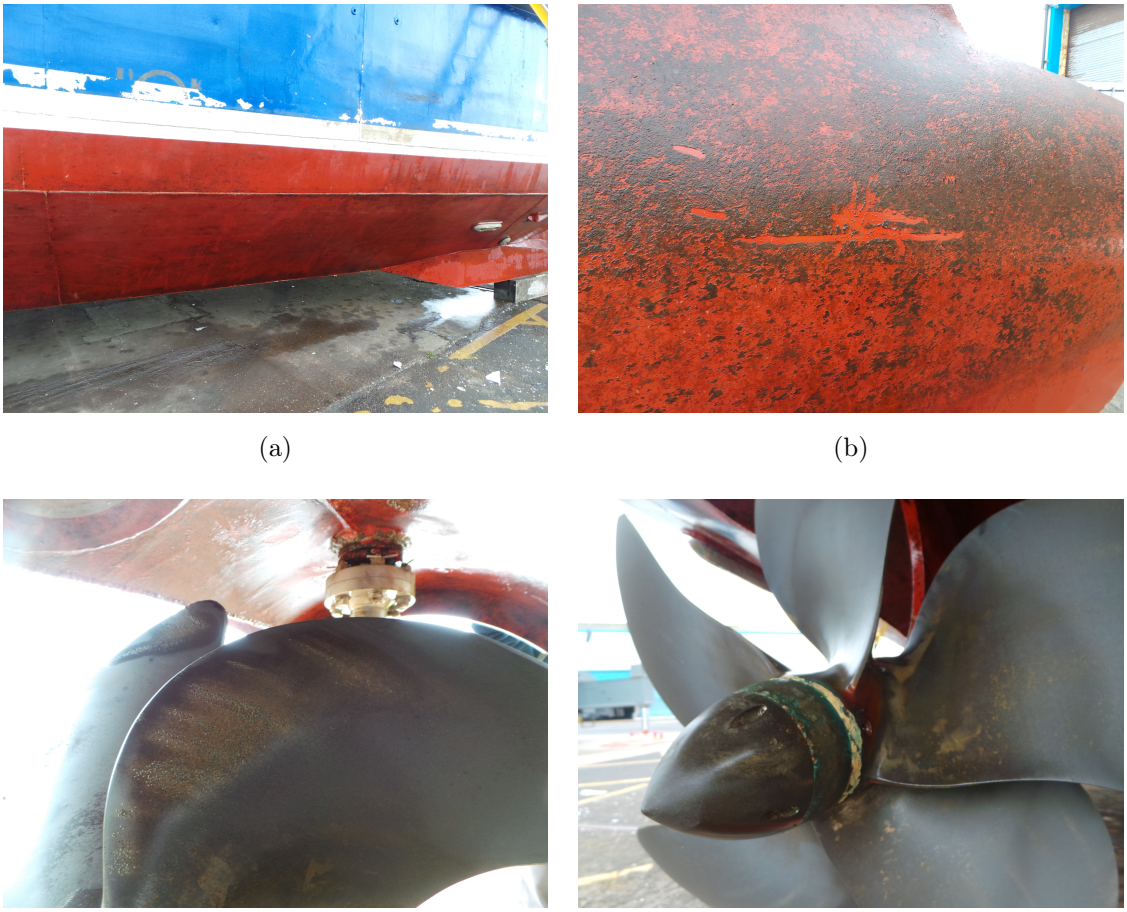

(a) (b)

(c) (d)

**Figure 5.43** – *Hull and propeller fouling at the early April 2017 DD.* (a)*: view of the port side outer demi-hull.* (b)*: detail of the starboard side bulbous bow.* (c)*: detail of the starboard propeller.* (d)*: view of the port propeller.*

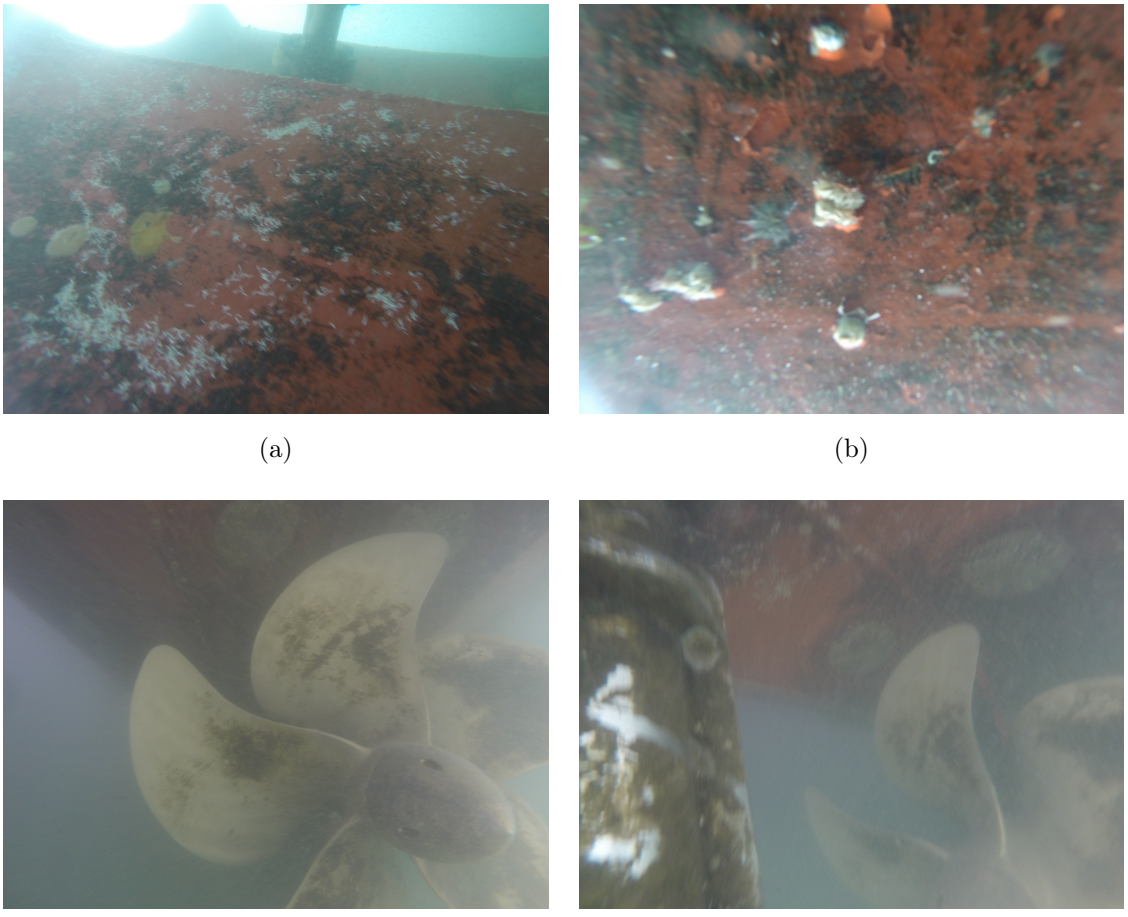

(a) (b)

(c) (d)

**Figure 5.44** – *Hull and propeller fouling at the July 2018 IWS.* (a) *and* (b)*: details of the port side outer demi-hull.* (c) *and* (d)*: details of the port propeller.*

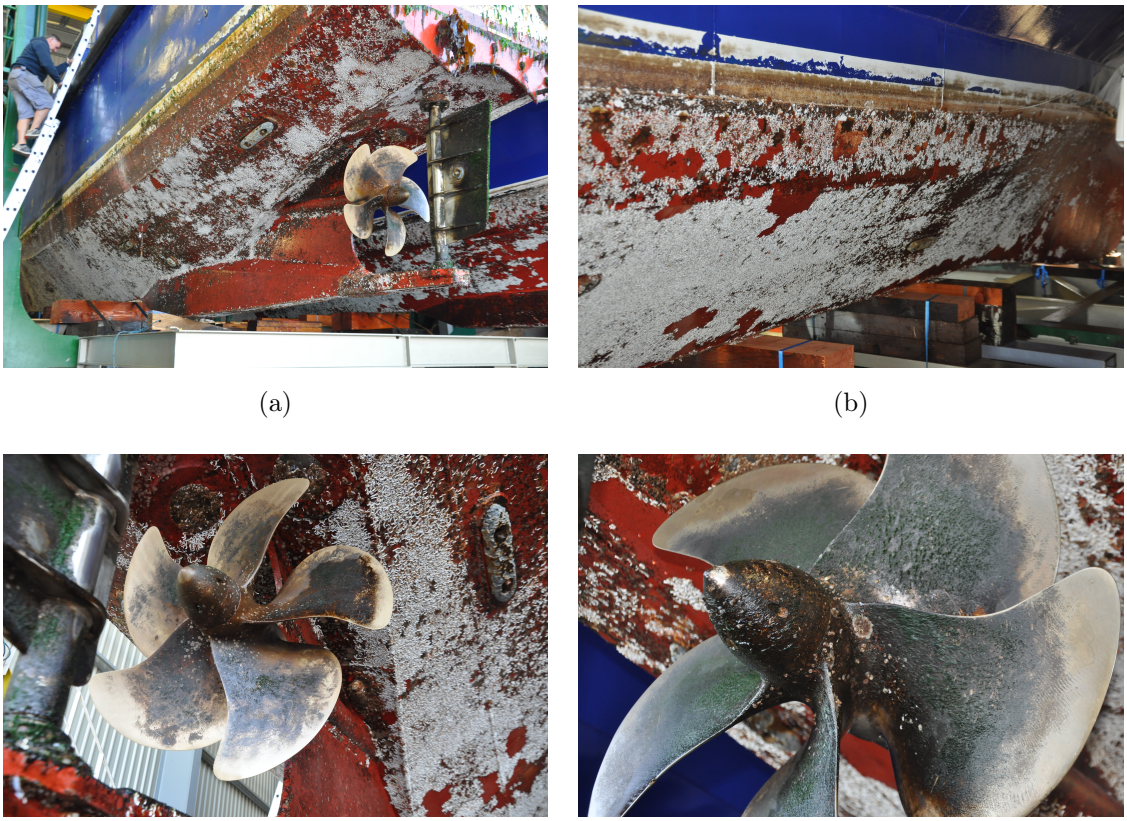

(a) (b)

(c) (d)

**Figure 5.45** – *Hull and propeller fouling at the late August 2018 DD.* (a)*: view of the port side demi-hull.* (b)*: detail of the starboard side demi-hull.* (c)*: view of the port propeller.* (d)*: detail of the starboard propeller.*

tip vortex cavitation. The propellers also display an unnatural dark colour, accompanied by clear signs of galvanic corrosion at the hub (5.43d). At this DD it was discovered that during the previous DD the engineering service had not refitted the cathodic protection anodes and the shaft earthing systems. This had led the propellers to act as anodes in the water, initiating a corrosion process that somewhat facilitated the cavitation erosion. After this finding, the propellers had to undergo significant repair.

Figure 5.44 displays pictures of the IWS carried out using a submersible camera manually deployed from the deck of the R/V or from the quay. Due to the constraints imposed by such device and by the underwater visibility, the extent of the pictures is limited to the close proximity of the vessel. The pictures document a significant growth of fouling on the underwater hull, which is covered with widespread heavy slime, weed fouling and calcareous fouling (mainly tubeworms). The propeller blades appear affected by a light slime layer, mainly at the inner radii region.

The pictures taken during the subsequent DD (31st August 2018) are shown in Fig. 5.45. Widespread medium-heavy calcareous fouling (tubeworms) can be seen to cover both demi-hulls apart from the bow and skeg region. On the other hand, abundant algal fouling affected the propellers, particularly the starboard one (Fig. 5.45d).

### *5.7.4 Further remarks on the service performance analysis*

The comparison between the hull and propeller surveys and the estimations made by analysing the KPIs allows some further considerations to be drawn regarding the SPMS developed in this research. Considering the fouling state of the R/V shown in Section 5.7.3, the results of the service performance analysis indicate a fouling state of the vessel which is very close to the real case.

The anomaly observed in the data acquired in March 2017 ($w_{app\,K}$ in particular) is fully justified by the mild fouling state of the hull and the severe propeller damage. Particularly, the latter induced an increase of the blade surface roughness, which in turn resulted in the higher $w_Q$ estimation. Having in mind the nature of the shaftline fault occurred in late March 2017, it is also probable that the unusual data spread observed during the March trials was caused by the critical shaft vibrations. Therefore, the SPMS installed on board *The Princess Royal* was in this case capable of identifying an anomaly in the shaftline and the unusual propeller performance.

The data obtained from the sea trials carried out after the reference period also match the real case. In particular, the variation of hull fouling was observed to be small between July and August, whereas the propellers showed an intense growth between the two months. This condition is confirmed by a cross-comparison between all KPIs. Those that include both effects of hull and propeller fouling ($P_K$, $w_K$ and $\hat{\phi}$) exhibit an increase from July to August. The only KPI referring to the sole propeller fouling ($w_{app\,K}$) boasts

instead a drastic increase in August, whereas $\Delta C_f$, which is in theory only affected by hull fouling, has very similar values over both months. This suggests that hull fouling had not changed significantly its impact from July to August.

Considering the fouling state of the R/V hull, the estimations of viscous drag increase and $\Delta C_f$ seem very reasonable according to the relevant literature (see e.g. Schultz, 2007; Demirel *et al.*, 2017*b*). For instance, Demirel *et al.* (2019) employed CFD simulations to derive $\Delta C_f$ with respect to a hydraulically smooth surface for several ship dimensions and speeds using a flat plate assumption. For *The Princess Royal*'s case, at $Fn = 0.6$ $\Delta C_f$ stands at $0.12 \times 10^{-2}$, $0.3 \times 10^{-2}$ and $0.46 \times 10^{-2}$ respectively for the conditions of heavy slime, medium calcareous fouling and heavy calcareous fouling. These values compare really well with what obtained in the service performance analysis of *The Princess Royal*, considering that the latter have to be referred to (i.e. deducted of) the heavy slime $\Delta C_f$.

On the other hand, all KPIs are calculated from the measured shaft torque and, as such, they rely on the quality of the measurement and normalization process. Chapter 4 concluded that correcting for all disturbances is not feasible in several practical applications. Some weather or operational effect will thus often contribute to a limited extent to the noise in performance data, where waves are usually the greater contributor. It must here be noted that at lower $Fn$ the data scatter is much larger than at higher speeds. This reflects the greater uncertainty caused by the relatively heavier impact that disturbances and shaft residual stresses have on the displacing performance (Carchen *et al.*, 2017). Measurements above $Fn > 0.6$ are therefore to be held more reliable. At the same time, over the long term the high frequency noise caused by such disturbances becomes less relevant with respect to the slower evolving trend of the KPIs.

Finally, it should be stated that the significance of the analysis here presented is somewhat weakened by the limited sample size, which could ideally be improved by the acquisition of more data. In this respect, some limitations were identified. Firstly, monitoring the biofouling growth was constrained between subsequent yearly DD. Whereas the vessel operation allowed much fouling to grow, the number of monitoring days was obviously reduced. Secondly, the vessel duties often included trawling, manoeuvring or sailing in shallow waters, which are conditions outside of the defined filtering criteria. Another aspect that needs to be considered is the weather factor in relation to this specific vessel. Two elements came here into play that were independent from the Author's will — namely the local weather and the small size of the R/V. The North Sea weather is known to be troublesome and historical records show that very seldom does it get sufficiently calm to consider the trials in 'ideal conditions'. This is even more so considering the small vessel size, whereby even the smaller waves cannot be neglected and the sea considered 'calm'. In this respect, installing and testing the SPMS on a larger vessel would make the performance analysis easier and its uncertainty lower. Conversely, larger vessels are more difficult to manage and an eventual SPMS installation would normally require longer

times (e.g. Hasselaar, 2011). The Author therefore feels that whereas the implementation of the SPMS on board *The Princess Royal* was facilitated by the small vessel size, the performance analysis was instead made more challenging.

Overall, it can be concluded that within the above limitations, *The Princess Royal* service performance analysis yielded notable results. In particular, the cross-comparison of the KPIs can be used as a hull/propeller cleaning trigger which can be employed to identify the best DD period — *at least* on a qualitative basis. In addition, $\Delta C_f$ estimates were showed to be very much in line with the results of the relevant literature.

### *5.7.5 Quality assessment of the fouling control strategy*

In September 2016, a Foul Release (FR) coating was applied on *The Princess Royal*. This choice appears to have been driven mainly by the fast speeds at which the vessel is customary to sail. However, given the above analysis, the fouling control strategy adopted on *The Princess Royal* is deemed inadequate for her operational profile. Her total sailing time was in fact estimated to cover on average only 15% of her time. In a period of just over a year, widespread calcareous fouling was allowed to grow on all the wetted surface and significant algal fouling populated the propellers. This is a direct consequence of the inability of the FR coating to inhibit the fouling settlement given the averagely low wall shear stresses to which the hull is subjected. In this framework, biocidal coatings would be a better choice.

## 5.8 Summary

According to **Aim 2** and **Objectives E**, **F** and **G**, the ship performance monitoring and analysis methodology presented in Chapter 4 was applied to the case study R/V *The Princess Royal* owned by Newcastle University. In doing so, a real, working SPMS was designed, developed and installed on the vessel and tested at sea. The R/V and the SPMS were at first described in their characteristics starting from Section 5.2, where a description of *The Princess Royal* and her general performance features was detailed.

Following the structure of Chapter 4, Section 5.3 dealt with the design of the deterministic normalization method used on the R/V, discussing each disturbance and the means that were put in place to correct the raw data for it. Wind tunnel testing was used to derive the wind resistance coefficients, whilst a potential code running a $2^{1/2}$D strip theory provided the added wave resistance transfer functions in head waves. The resistance increase due to displacement change was calculated using the Admiralty coefficient, whilst the ITTC procedure was employed to estimate the effect of the change of water properties. The other disturbances were not corrected for and instead suitable filters were later on developed.

Section 5.4 described in detail the data acquisition system installed and where necessary complemented by the Author on-board *The Princess Royal*. Each sensor used on the vessel is presented and where necessary brief notes are given. Two auxiliary measurement practices were also described — namely the visual draught measurements and the wave buoy used to hindcast the local wave energy spectra. A description is also provided about the on-board monitoring software module. Finally, a section is devoted to detailing the storyline of the on-board SPMS development and the full-scale measurements.

Section 5.5 described the means and parameters adopted to prepare the raw measurements for normalization according to the method proposed in Section 4.4. A subsection is devoted to the validation of speed through water, wind speed and direction and torque and thrust measurements. The speed log data were found to have a small bias, which was corrected. Wind measurements instead showed some contamination from the turbulences that develop around the vessel mast, but well within acceptable ranges. Torque measurements showed no evident drift or miscalibration, whereas the effect of parasitic loads was evident on the thrust. A paragraph was finally devoted to describe the data preparation software module.

Next, Section 5.6 summarises the data used for the normalization algorithm and their sources. Thereafter, the results of the full-scale measurements are presented. The results showed that overall the effect of disturbances during the performance monitoring period was small. At the same time, some performance variations between days were apparent already from the simple 'normalised' plots.

These changes of performance were further analysed by means of the four proposed KPIs ($P_K$, $\hat{w}_K$, $w_{app\,K}$ and $\hat{\phi}$) and the frictional coefficient increase $\Delta C_f$ in Section 5.7. At first, a subsection is devoted to detail the method used to derive the reference performance baselines. It was stressed the importance of choosing meaningful baselines, which was described as a difficult task owing to the wide $Fn$ range covered by *The Princess Royal*— particularly in the transition 'hump' region. It was therefore decided to analyse the vessel performance for the ranges $Fn < 0.35$ and $Fn > 0.5$ separately. The full-scale measurements and monitoring on-board *The Princess Royal* proved consistent with the expectations and gave promising results. The analysed performance indicators indicate fouling states that match the observations made during hull and propeller surveys. In one case, the SPMS and performance analysis were capable of detecting a propeller fault.

The outcomes of this chapter suggest that the adopted methodology is correct and the proposed KPIs are suitable for a long-term analysis of fouling and fouling control strategies. It was also demonstrated how the ship service performance analysis largely benefits from the cross-comparison of all the KPIs to validate and strengthen the evaluation of the effects of fouling. Moreover, the data demonstrated the effectiveness of the proposed estimation of the full-scale $\Delta C_f$.

On the other hand, the limitations of this study were recognised mainly in the vessel operational profile and maintenance schedule and in the weather factor related to the vessel size. It is expected that if installed on a larger vessel operating under constant regime and for longer time, the SPMS data quality and quantity would largely improve. Nevertheless, even with a limited dataset the SPMS implemented on board *The Princess Royal* was shown to deliver very interesting results, which can be used either as docking triggers or to validate other fouling studies (e.g. Schultz, 2007; Demirel *et al.*, 2017*a*, 2019; Li, 2019). Finally, in this application the effect of DD polishing could not be observed due to various circumstances. The reader will notice that it is in general easier to estimate the impact of a DD and hull and propeller cleaning. One of the merits of this research stands in the development of a SPMS capable of distinguishing the performance losses due to biofouling in service.

# CHAPTER 6

# Uncertainty Analysis

## 6.1 Introduction

A SPMS retains the characteristics of a common experimental setup, whereby a measurement and a mathematical model are employed to yield a result. As such, the quality of the whole process needs to be verified in a scientific manner by assessing the 'goodness' of all the information used and ultimately of the result (JCGM, 2008*a*). Failure to do so, makes any result the more arbitrary the higher is the targeted resolution of the measurement.

In fulfilment of **Aim 3** and **Objective H**, this chapter presents the results of the Uncertainty Analysis (UA) of vessel performance data obtained on-board Newcastle University's R/V *The Princess Royal* from in-service monitoring and periodical dedicated service trials. Generally speaking, the uncertainty of a measurement is better estimated from a larger number of observations. Given the restricted dataset of sea trials and monitoring days, this chapter could not aim at exhausting the uncertainty assessment of the proposed SPMS. Instead, it provides the reader with an estimation of the uncertainty sufficient to appreciate the 'degree of goodness' of the results (Coleman and Steele, 1989). In pursuit of this, Section 6.2 outlines the generalities of the UA. Section 6.3 presents the Uncertainty Analysis method that was adopted in the current study and analyses in detail the considered uncertainty components. Conclusions will be drawn in Section 6.4.

## 6.2 Uncertainty Analysis background

Every measurement conducted to observe or study a phenomenon retains a degree of error, a certain distance from the true value of the measurement. The estimation of such error is termed uncertainty (Coleman and Steele, 1989). Over the years, different definitions have been used to address the measurement uncertainty, each corresponding to a slightly different method to estimate it: traditionally, an error is described as formed by a systematic component, or bias, and a random component, sometimes referred to as precision error (see e.g. ASME, 1998). The bias produces a displacement of the measured value, whilst the random error is responsible for the variability across multiple measurements.

The total uncertainty of a measurement may be calculated for example as:

$$U = \sqrt{B^2 + P^2} \tag{6.1}$$

where $B$ and $P$ are respectively the estimations of the bias and precision errors. After the '80s, extensive work was carried out in the attempt to standardise the procedure for the evaluation of the uncertainty (see e.g. Coleman and Steele, 1989), resulting in the development of the Guide to the Expression of Uncertainty in Measurements, often referred to as GUM (JCGM, 2008*a*). This is the method currently adopted by the AIAA (American Institute of Aeronautics and Astronautics) and the ITTC (2014*b*).

According to the GUM, the uncertainty components are subdivided in two different categories named Type A and Type B, depending on their calculation method. A Type A standard uncertainty, $u$, of a variable is calculated as the standard deviation of a set of measurements. A Type B standard uncertainty is calculated as the standard deviation of an assumed distribution based on other *a priori* knowledge (e.g. manufacturer specifications, engineering judgement, etc.). A variable $Y$ may however be a function $f$ of $N$ multiple other quantities $X_i$. If $Y$ is estimated from the measurement of the $N$ $x_i$ quantities, the following holds:

$$y = f(x_1, x_2 \dots x_i \dots x_N) \tag{6.2}$$

where the lower case $y$ and $x$ denote respectively the estimation of $Y$ and $X$. The uncertainty of $y$ is evaluated by accounting for the weights and correlations of all those quantities through the law of propagation of uncertainty (JCGM, 2008*a*) and is termed combined standard uncertainty. The general equation for the combined standard uncertainty of $N$ uncorrelated variables is:

$$u_c(y) = \sum_{1}^{N} c_i u(x_i) \tag{6.3}$$

where $u(x_i)$ is the standard uncertainty of the $x_i$ variable and $c_i$ is termed sensitivity coefficient, defined:

$$c_i = \frac{\partial f}{\partial x_i} \tag{6.4}$$

where $f$ is the function of eq. (6.2). The GUM also accounts for the need of a consistent part of the industry to express the uncertainty as an interval about the measurement. Such interval is expected to cover a large portion of the possible observations. In this case, the GUM proposes the use of the expanded uncertainty:

$$U = k u_c \tag{6.5}$$

where $k$ is called the coverage factor and depends on the required Confidence Interval (e.g. $k = 2$ corresponds to $\sim$95% Confidence Interval in most of the cases).

It must be noted that the GUM framework is exact or close to exact in cases of linear relationship among the variables, or where linearities aren't significant. Also, the *Guide* is based on the assumption that

> "a measurement can be modelled mathematically to the degree imposed by the required accuracy of the measurement. (JCGM, 2008*a*)"

Where strong nonlinearities or complex correlations exist between the variables involved in the measurement, the application of the law of propagation of uncertainty outlined by the GUM becomes cumbersome and often violates its limits of applicability (JCGM, 2008*b*). In such cases, Monte Carlo Methods (MCMs) have proven of great value to propagate the uncertainties by evading the limitations of the GUM.

The MCMs propagate the uncertainties through the model by observing the effect that the uncertainties of the input variables have on the output variables. This is achieved by random sampling from probability distributions assigned to the input variables for a specified number of iterations. For this reason, Monte Carlo Methods are never exact. Nonetheless, if the number of iterations is large enough, they yield excellent approximations and are valid in a larger set of cases than the GUM (JCGM, 2008*b*). The MCM may be described as follows. Let $x_i$ be the estimation of the $X_i$ measurement (e.g. the speed through water $V_s$), $y$ the estimation of the measurand $Y$ (e.g. the normalised power $P_{D0}$), with $y = f(x_1, x_2 \dots x_i \dots x_n)$. Then the MCM procedure is as follows:

1. Identify the Probability Density Functions (PDFs) of the uncertainty of each $x_i$.
2. Select the number of Monte Carlo iterations, $M$.
3. Sample a random value for every $x_i$ from its PDF.
4. Calculate $y = f(x_1, x_2 \dots x_i \dots x_n)$.
5. Iterate step 3 and 4 $M$ times to obtain $M$ estimations of $y$.
6. Evaluate the standard uncertainty of the measurand $u(y)$ as the standard deviation of its resulting distribution.
7. Evaluate the expanded uncertainty $U(y)$ by choosing a suitable coverage interval.

According to the JCGM (2008*b*), the expanded uncertainty of $M$ Monte Carlo simulations that is expected to encompass 95% of the cases is taken as:

$$U(x_i) = \bar{x} - x_{0.025M} \tag{6.6}$$

where $\bar{x}$ is the mean and $x_{0.025M}$ is the 2.5th percentile of the $M$ measurements of $x_i$.

The normalization procedure presented in Section 4.5 exhibits strong nonlinearities that relate the on-board measurements (e.g. $V_s$, $Q$, etc.) with the final normalised

variables (e.g. $P_{D0}$). Because of this, MCMs have been successfully applied in recent years to solve the complexity of full scale experimental uncertainty. It is recalled that Insel (2008) showed how the overall uncertainty in the speed–power relationship varies between 8% and 10% of the total power by analysing data from the sea trials of 12 sister ships. In general, it is notable that the majority of the literature identifies in the speed measurement the most sensitive parameter for the final performance assessment, immediately followed by draught and power.

## 6.3 Uncertainty Analysis of *The Princess Royal*'s SPMS

Broadly speaking, the uncertainties in a ship performance monitoring and analysis process arise from three sources:

I. Measurement system.

II. Data preparation and normalization.

III. Variability of weather and operational conditions within the imposed filtering limits.

Ideally, the uncertainties related to all these sources would be evaluated altogether by observing the variability of the measurements and/or combining correlated error sources. However, due to the limited data set available from *The Princess Royal*'s SPMS a different approach had to be chosen. The uncertainty sources were distinguished into two components — systematic and a random errors. The uncertainty derived from sources I and II may be regarded as arising from systematic errors of the SPMS and the performance analysis process. In fact, the errors of the measurement system, of the data preparation and normalization procedures are virtually the same for every performance monitoring and analysis session. In analogy with the traditional UA methods, this component will be here assigned symbol $B$. On the other hand, the uncertainty generated by source III, i.e. by the different conditions (weather and operational) that are encountered at sea, may be considered to be a random error. In every ship performance monitoring session, such error will be different and will therefore affect the repeatability of the performance monitoring. Similarly to the above, this uncertainty component will be assigned symbol $P$. The two components can be combined to derive the standard combined uncertainty of the performance assessment. For instance, the total (combined) uncertainty of the normalised delivered power $P_{D0}$ will be thus:

$$u_c(P_{D0}) = \sqrt{B^2(P_{D0}) + P^2(P_{D0})} \tag{6.7}$$

This approach is fundamentally equivalent to the Multiple Test procedure proposed by Coleman and Steele (1989) and it was first applied by Insel (2008) in the marine field.

TABLE 6.1
*Engine speed settings during the ST-1 trials on board* The Princess Royal .

| *Triple Run* | *Engine speed* |
|---|---|
| 1 | 650 |
| 2 | 700 |
| 3 | 900 |
| 4 | 1200 |
| 5 | 1500 |
| 6 | 1750 |

### 6.3.1 Estimation of B

The uncertainties arising from sources I and II can be derived by analysing how the uncertainty propagates through the performance monitoring process by employing the MCM. The data used in this analysis was obtained during the March 2017 sea trial (here called ST-1), which was conducted according to the ITTC recommendations (2014*c*). For each engine set speed, three speed runs were conducted, with the second run having opposite heading than the other two. The engine speeds used in the ST-1 are summarised in Table 6.1.

**Assignment of elemental uncertainties**

According to the JCGM (2008*b*), the MCM input uncertainties, $u_c(x_i)$, should be taken as the most elemental possible. Alternatively, the uncertainty of the single measurement is calculated by combining the elemental sources according to the law of propagation of the uncertainty. Whereas both Type A and Type B uncertainty components may be used, two important principles have been considered, according to the GUM (2008*a*):

1. Quantitative data should be used to the maximum extent possible in the evaluation of uncertainty values, i.e. a Type A uncertainty is generally to be preferred to a Type B.

2. Each uncertainty component must be counted only once.

Keeping these principles in mind, the elemental uncertainties of the variables used in *The Princess Royal*'s SPMS and analysis were derived as follows.

***Vessel and propeller parameters.*** —The uncertainty of the vessel main dimensions was estimated of 0.1%. An uncertainty of 0.02m (height of a draught mark) was assigned

to the vessel visual draught measurement (Insel, 2008). Propeller pitch and diameter were assigned uncertainties respectively of 0.75% and 0.3% (ISO, 2015*b*). The thrust deduction factor was estimated by ITTC (2002*c*) as having an uncertainty of 0.15. All the above uncertainties have been applied uniform distributions.

***Wind speed and direction.***—The uncertainties in wind speed $U_{AR}$ and direction $\mu_{AR}$ stated by the manufacturer of the ultrasonic anemometer on-board *The Princess Royal* are 2% and 2deg respectively. However, a Type A uncertainty was used, which was derived from the trial measurements.

***Wind resistance parameters.***—The height of the anemometer is considered as bringing uncertainty in the wind speed correction for reference height. Its uncertainty was estimated as being equal to the uncertainty of the vessel draught with a rectangular distribution. The uncertainty in the calculation of the *The Princess Royal*'s wind resistance coefficients derived from wind tunnel tests was evaluated by Vranakis (2016). He employed the law of propagation of the uncertainty proposed by the GUM to estimate a combined uncertainty of $C_X$ of $7.4 \times 10^{-3}$.

***Water and air properties.***—The uncertainty in water density measurement arises from three sources — namely the water conductivity, its temperature and its salinity. By using the GUM procedure, Type B uncertainties were evaluated for each of the three sources from the technical specifications of the sensors. The resulting combined uncertainty of the water density measurement was however deemed to be unlikely small ($\sim 2.1 \times 10^{-4}$). Since the water quality sensors are also located in a sea chest within the engine room, a larger uncertainty would be more plausible. The uncertainty calculated by the ITTC (2002*b*) was therefore used for both water density and viscosity, which is about $2.1 \times 10^{-2}$. The uncertainty of the air density measurement was calculated to be negligible ($\sim 0.05\%$).

***Waves and added wave resistance parameters.***—The estimation of the estimation error of wave measurements is subject of discussion (see e.g. Bertram, 2016; Bos, 2016). To the best knowledge of the Author, an UA has never been conducted on the Datawell wave buoy which is used in this research for the derivation of the real sea wave energy spectra. It may be though speculated that the accuracy is sufficient for the purpose of this work. Wang and Freise (1997) estimated that the Root Mean Square (RMS) error given by a wave buoy deployed off the US coast was less than 30% of the total RMS spectral energy for the majority of the measurements. Under these conditions, the wave measurement can be considered sufficiently accurate.

It will be recalled that the added wave resistance transfer function $\sigma_{AW}$ was obtained by means of an advanced strip theory formulation. The calculation of the uncertainty of numerical computations is object of current study, e.g. by the ITTC. However, an

estimation of the random error may be obtained from the standard deviation of the differences between the towing tank measurements and the simulation values. Such value would then be combined with the uncertainty of the experimental results. Unfortunately, an UA wasn't provided with the seakeeping tests results conducted by Sfakianos (2016). As suggested by the ASME (1998), the uncertainty of $\sigma_{AW}$ was therefore obtained simply by analysing the Standard Error of Estimate (SEE), hence holding as accurate the seakeeping experiments. Considering the generic polynomial function $\varphi = f(\kappa)$ used to estimate $N$ observations, the SEE can be calculated according to the following equation:

$$\text{SEE} = \sqrt{\frac{1}{N-O}\sum_{i=1}^{N}\left(\varphi_i - f(\kappa_i)\right)^2} \tag{6.8}$$

where $O$ is the number of coefficients of $f$. Although the SEE is not conceived for this type of application, it is here assumed for simplicity that $f$ is locally quadratic, and hence $O = 3$. The estimation error of $\sigma_{AW}$ based on the towing tank experiments was therefore calculated to be SEE= 0.388 on average, equivalent to 38%. This value is relatively large, although common for numerical simulations.

It is noted, however, that because of the wave filtering criteria defined earlier in Table 5.12, the added wave resistance was not calculated for the sea trials included in this chapter for analysis. Therefore, the uncertainty of added wave resistance didn't have influence on the UA calculations presented in this work.

***Speed Over Ground.***—In general, $V_g$ can be expected to have a minimal uncertainty, as reported in ITTC (2011*b*). A Type A uncertainty was derived from each single run and resulted 0.10% on average.

***Speed Through Water.***—The stated accuracy of the Furuno Doppler speed log is 1% or 0.1kn, whichever greater. Again, since full-scale measurements were available, a Type A uncertainty was calculated from each single run, averaging 0.08% over the six triple runs.

***Propeller speed.***—Ideally, a Type A uncertainty would have been used. However, since the SPMS employs a relatively long averaging time to calculate the shaft RPM (23s), the used of a Type B uncertainty was a forced choice. The propeller speed uncertainty was thus calculated in line with the ITTC (2008). When the shaft speed is measured by means of a shaft marker, it is defined as:

$$n = \frac{\mathfrak{n}}{\mathfrak{p}\,\mathfrak{t}} \tag{6.9}$$

where $\mathfrak{n}$ is the number of measured pulses during the time $\mathfrak{t}$ and $\mathfrak{p}$ is the number of pulses per revolution. According to eq. (6.3) and (6.4) and ignoring the negligible uncertainty of $\mathfrak{p}$ and $\mathfrak{t}$, the relative combined uncertainty of the propeller speed measurement can be

expressed as:

$$\frac{u_c(n)}{n} = \frac{u(\mathfrak{n})}{\mathfrak{n}} \tag{6.10}$$

The error of shaft speed reading is at most one pulse per rotation, which means an equal probability of incurring or not in the error. The standard deviation of a rectangular distribution is estimated as $a/\sqrt{3}$, where $a$ is the error interval, equal to one (pulse). Since on *The Princess Royal* $\mathfrak{p} = 1$ and $\mathfrak{t} = 23$s, it follows:

$$u_c(n) = \frac{1}{23\sqrt{3}} \tag{6.11}$$

***Propeller torque and thrust.***—Torque and thrust sensors were directly shop-calibrated on the shafts in laboratory conditions. This means that the variability of the observed data and the calibration values already encompass the uncertainties related to gauge, amplifier system, measurement system and installation. Therefore, the uncertainty is considered a combination of two components, the first coming from the lab calibration (Type B), the second calculated directly from ST-1 as a Type A standard uncertainty. The calibration uncertainty can be again evaluated from the SEE. The combined uncertainty resulting from the Type A and Type B uncertainties were calculated to be about 0.15% for both torque and thrust.

***Propeller Open Water coefficients.***—SEE was again used to evaluate the uncertainties in the R/V propeller Open Water curves. It was then combined with the ITTC estimated uncertainties for cavitation tunnel tests. The combined uncertainty of the advance, torque and thrust coefficients were thus estimated at $4.95 \times 10^{-2}$, $4.89 \times 10^{-3}$ and $4.11 \times 10^{-4}$ respectively.

Table 6.2 summarises the elemental uncertainties evaluated from Type A uncertainties or from a combination of Type A and Type B uncertainties for each triple run. These values were used in combination with the assumed distributions as inputs for the MCM.

### Number of iterations

The choice of the correct number of Monte Carlo iterations M to obtain stable results is open to study. The JCGM suggests conducting $10^6$ iterations to achieve a safe result. Insel used $5 \cdot 10^4$ iterations instead. The present study further compared partial results obtained from $5 \cdot 10^4$ and $10^5$ iterations, finding that the uncertainty calculations, in the worst-case scenario, differ for as much as 0.4%. This suggest that probably a higher number of iterations must be chosen. A value of $M = 1.5 \times 10^5$ was deemed sufficient for this research.

TABLE 6.2

*Relative uncertainties calculated by Type A only or by combination of Type A and B elemental uncertainties* .

| Triple run | $n$ | $V_g$ | $V_s$ | $Q$ | $T$ | $U_{AR}$ | $\mu_{AR}$ |
|---|---|---|---|---|---|---|---|
| 1 | 4.38e-03 | 5.95e-04 | 6.07e-04 | 1.48e-03 | 1.53e-03 | 4.06e-03 | 1.34e-03 |
| 2 | 3.50e-03 | 7.52e-04 | 1.15e-03 | 1.48e-03 | 1.53e-03 | 5.16e-03 | 1.12e-03 |
| 3 | 2.94e-03 | 9.50e-04 | 1.25e-03 | 1.48e-03 | 1.53e-03 | 4.86e-03 | 1.53e-03 |
| 4 | 2.19e-03 | 1.50e-03 | 6.44e-04 | 1.48e-03 | 1.53e-03 | 3.12e-03 | 1.03e-03 |
| 5 | 1.76e-03 | 1.61e-03 | 1.12e-03 | 1.48e-03 | 1.53e-03 | 3.44e-03 | 2.75e-03 |
| 6 | 1.51e-03 | 5.75e-04 | 5.22e-04 | 1.48e-03 | 1.53e-03 | 2.31e-03 | 7.42e-04 |

**MCM results**

Figure 6.1 shows the distributions of the normalised power and normalised propeller speed resulting from the MCM. In general, the graphs show a uniform distribution of the uncertainties. The results of the Monte Carlo simulations show a generally low measurement uncertainty (B) for both $n$ and $P_{D0}$, with the standard uncertainties $u(P_{D0}) \approx 1.3\%$ and $u(n) \approx 0.27\%$. The other primary parameter, $V_s$, is not shown here since the analysis is conducted in speed identity. $u(V_s)$ was already reported in Table 6.2. In summary, the observed variability of the variables here presented is caused by the uncertainty of the SPMS itself, comprehensive of data acquisition, preparation and normalization.

### *6.3.2 Estimation of P*

The uncertainty arising from the variability of the weather state (III) was derived by calculating the standard deviation of performance data obtained with the vessel having a similar fouling condition. A set of two speed–power trials with 4 different weather and operational conditions and comparable fouling state was chosen. This speed-power data set will here be called ST-A. The trials were both conducted in the same manner and with the same engine speed settings of Table 6.3. This procedure accounts for the effects on the performance uncertainty of weather and operational changes that are not corrected for. In other words, the data scatter of dataset ST-A represents the repeatability error P under the different sailing conditions within the filtering criteria.

### *6.3.3 Combined uncertainty*

The uncertainties of normalised power resulting from the MCM and the repeatability analysis were combined according to eq. 6.7. In a similar fashion, the speed through

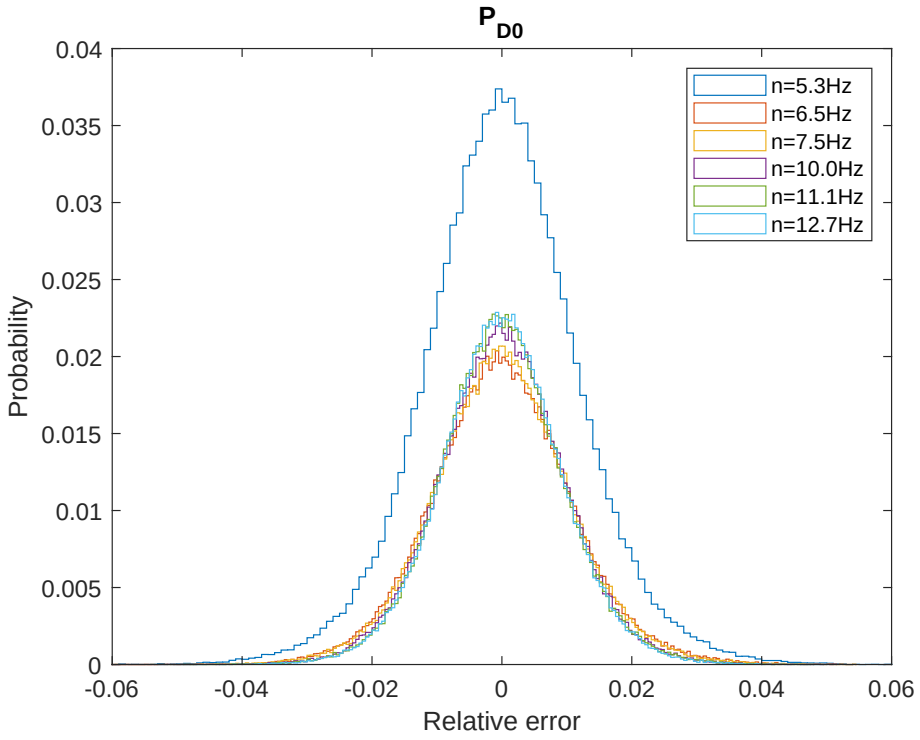


(a)

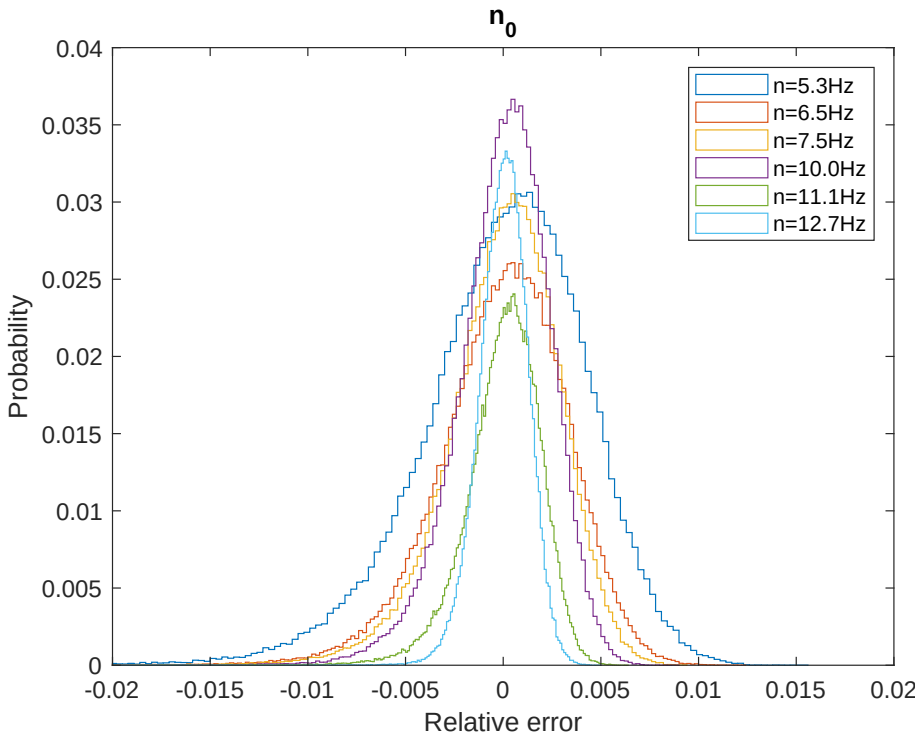


(b)

**Figure 6.1** – *Distribution of the normalized power* $P_{D0}$ (a) *and normalized propeller speed* $n$ (b) *obtained from the MCM and presented against the propeller speed (i.e. triple run set)* .

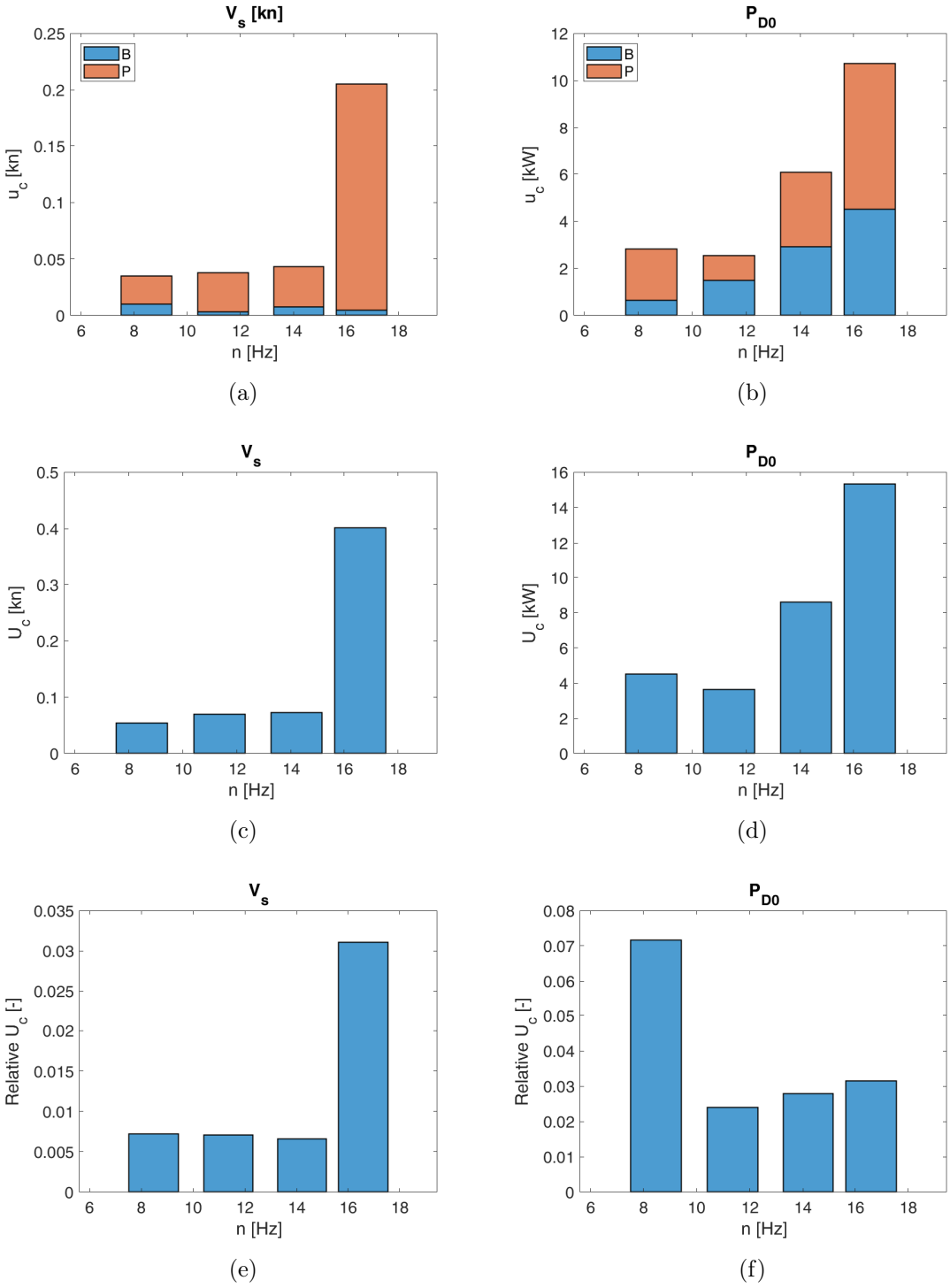


**Figure 6.2** – *Combined uncertainty values. Respectively for $V_s$ and $P_{D0}$, the graphs show:* (a) *and* (b) *the combined standard uncertainty with the fractional contributions of B and P errors;* (c) *and* (d) *the expanded uncertainty;* (e) *and* (f) *the relative expanded uncertainty.*

TABLE 6.3
*Engine speed settings during the ST-A trials on board* The Princess Royal .

| *Triple Run* | *Engine speed* |
|---|---|
| 1 | 900 |
| 2 | 1200 |
| 3 | 1500 |
| 4 | 1750 |

water uncertainty was obtained by combining the Type A uncertainty employed as an input in the MCM and that derived from the repeatability analysis. Figure 6.2 illustrates the uncertainty values of the speed through water and the normalised power as a function of the engine speed. The uncertainty in speed through water is low at the low engine speeds and stays well below 1% until it soars at 3% at $n = 13$Hz. This might be due to the inception of a strong tide current during one of the trials. The uncertainty, however, is still at very low values. The normalised power uncertainty follows the opposite trend. It is generally lower for higher speeds both for B and P uncertainties and it varies from about 7% at 8Hz to a minimum of 2.5% at 10Hz. This could be due to the higher effect the environment has on the vessel at lower speeds and to the higher impact of the shaft residual stresses.

As already observed by Insel (2008), the uncertainty in repeatability is much larger than the measurement uncertainty, reflecting the impact that the variability of environmental and operational conditions has on the final uncertainty. It is however noted that the uncertainties are relatively lower than expected. This is very likely the consequence of having very few data to obtain a realistic distribution of the repeatability error, which is therefore underestimated particularly at the lower speeds. The merit of this UA is however to have applied an existing method to a working SPMS for the first time and to have showed, within the limitations, a good agreement with the literature (e.g. Insel, 2008).

### *6.3.4 KPI uncertainty*

The uncertainty of the KPIs described in Section 4.6 and applied to *The Princess Royal* in Section 5.7 may then be evaluated. In principle, a procedure similar to that used earlier may be applied to analyse the systematic and random components of the errors of estimation of the KPIs. However, since all the KPIs are parameters relative to a baseline, the systematic error is eliminated under the assumption of absence of sensor drift. If the random error is to be observed, the variability of the KPI is to be studied. Using the data

presented in Chapter 5, the standard deviation of each KPI could be derived as a function of speed. Therefore, it is hereby assumed that the baselines are correct. To identify sets of KPI values measured at the same $V_s$, a Density-Based Spatial Clustering of Applications with Noise (DBSCAN) algorithm was used to automatically identify the clustered data measured within a $V_s$ range of $\pm 0.15$kn (mean of the expanded uncertainty of $V_s$).

Figure 6.3 shows the expanded uncertainties for the four KPIs. Such uncertainties are caused by the variability of the KPIs during the performance monitoring period described in Section 5.7. The graphs show in greater detail what was already apparent from the graphs reported in Chapter 5. The power increase KPI exhibits a high uncertainty peak at the lower speeds, where the absolute value of the uncertainty is shown as 0.12 — i.e. 12% since $P_K$ is a relative parameter. Averagely, the uncertainty is however lower, decreasing at the higher speeds to just above 0.02 (2%). A very similar pattern is followed by $\hat{\phi}$. However, since $\hat{\phi}$ is a much more sensitive parameter, its uncertainty is higher, reaching a peak 24% at displacing speeds and averaging about 8% at semi-displacing speeds. The wake fraction gain appears to have slightly better robustness, having an average uncertainty of $\sim 7\%$. This datum seems to confirm $\hat{w}_K$ a very important and strong KPI, which has uncertainty comparable to that of $P_K$. Finally, $w_{app\,K}$ is the KPI that, as expected, delivers a worse performance, reaching a peak of almost 40% and averaging almost 20%. The high variability of $w_{app\,K}$ may be attributed to both its sensitivity and its dependence on thrust measurements.

### *6.3.5 Review of The Princess Royal's performance analysis*

The performance of *The Princess Royal* presented and analysed in Section 5.7.2 should be reviewed in light of the UA above conducted. Yet, the scarce data on which the UA is based does not allow a safe estimation of the error of the KPIs. Turning a blind eye to this might unduly hamper or favour the results of the vessel performance analysis. However, for the sake of completeness a brief discussion is here included based on the time series of the KPIs presented in Fig. 5.42.

Figure 6.4 shows the four KPIs estimated in Fig. 5.42 with the expanded uncertainty error bars calculated by linear fit at $Fn = 0.607$. The figure shows that the entity of the uncertainty is rather proportional to the values of the different KPIs for $P_K$, $\hat{\phi}$ and $w_K$. On the other hand, $w_{app\,K}$ exhibits a much larger uncertainty relatively to its values, confirming the earlier remarks on the weakness of this KPI. Considering the uncertainty bands, the values of the first three KPIs can be safely considered significant *with respect to the reference*. The significance of their variation over the period of a few months results instead rather weakened for all KPIs but $w_{app\,K}$, thanks to its sudden rise between July and August. Whereas the observation of more than one KPI certainly increases the confidence of the performance analysis, the limited UA here reported thus seems to not

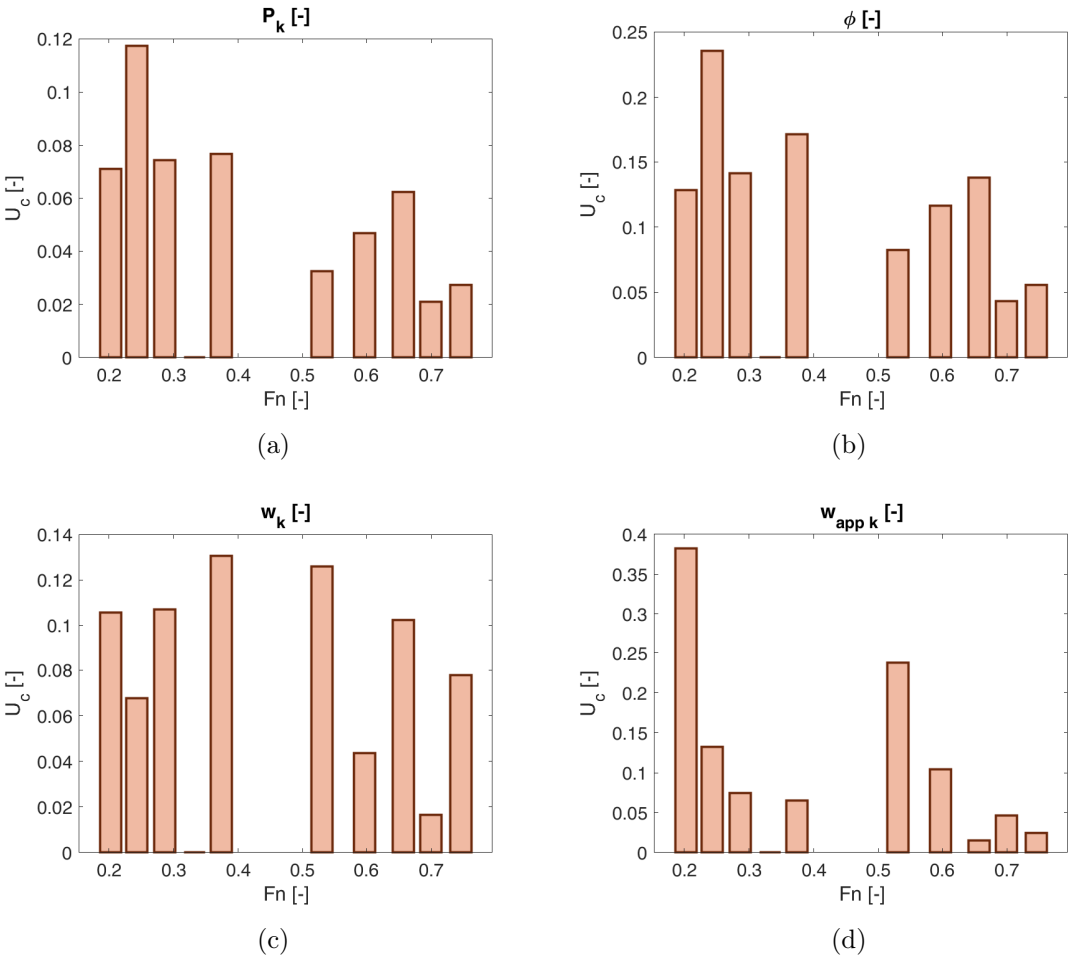


**Figure 6.3** – *Expanded uncertainty values respectively for* (a) $P_K$, (b) $\hat{\phi}$, (c) $\hat{w}_K$ *and* (d) $w_{appa,K}$ *as functions of the speed through water.*

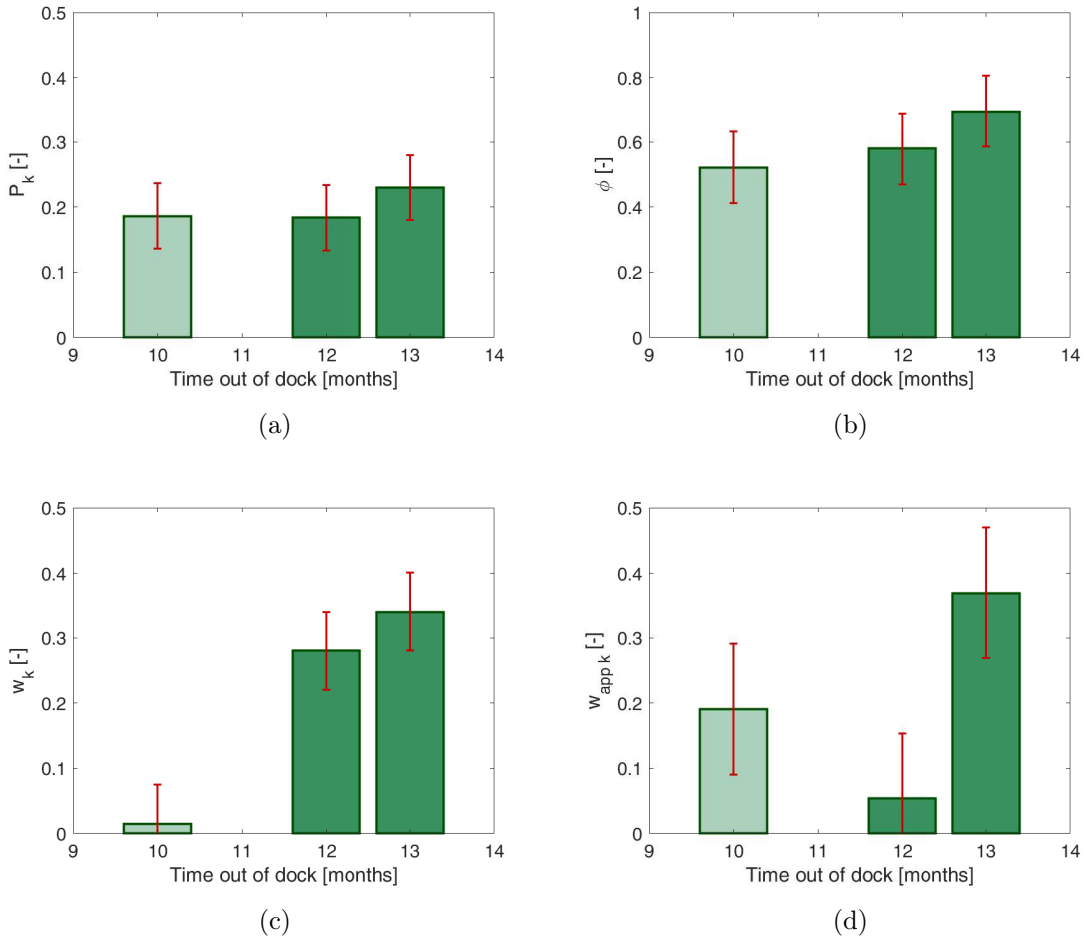


**Figure 6.4** – *Time series of the values estimated @*$Fn = 0.607$ *for* (a) $P_K$, (b) $\hat{\phi}$, (c) $w_K$, *and* (d) $w_{app\,K}$ *with expanded uncertainty bars. Again, the lighter shade bar refers to the single datapoint available in May 2018..*

confirm the significance of the variation of the KPIs over the short term.

It may be concluded that the UA conducted on the KPIs demonstrated that they can be employed for an evaluation of the fouling state of the hull and propeller *at least* qualitatively. On the other hand, it must be remarked that the same UA is based on a very limited dataset, which does not allow safe conclusions to be drawn.

## 6.4 Summary

In pursuit of **Aim 3** and **Objective H** an UA was carried out for a series of full-scale measurements of vessel performance. In doing so, Section 6.2 provided the reader with a background of UA theory and history. In Section 6.3, the UA of *The Princess Royal*'s SPMS was attempted by analysing the uncertainty of the speed and power variables. The uncertainty of these variables was considered to be originated from three sources — namely the measurement system, the data preparation and normalization phase and the variability of the weather. These uncertainty sources were grouped under two typologies of errors, a systematic (B) and a random (B) error. At first, MCMs were adopted to obtain the PDFs of the normalised performance parameters (i.e. $n$ and $P_{D0}$), which were used to estimate the B error (i.e. measurement, data preparation and normalization). The observed variability of the performance data in different sailing conditions then allowed the evaluation of the repeatability error (P) that was combined with the measurement uncertainty to provide the total error estimate. The following were found:

- The expanded uncertainty of the normalized power at 95% CI was estimated as fluctuating between 2.5%–7%, with the repeatability component being the heavier factor.

- The expanded uncertainty of the speed through water was found to be relatively low, reaching at most 3%. The uncertainty peak is found at the highest speed and is almost six times larger that the next-in-line value. This sudden change in uncertainty may be caused by the inception of a strong tidal current at the time of the runs.

- An effort has been made to quantify the random error of the four KPIs derived in Section 5.7. It was found that $P_K$ and $\hat{w}_K$ have a relatively low uncertainty compared to the other KPIs, which in general makes them more robust parameters. $\hat{\phi}$ is a more sensitive parameter and boasts an uncertainty which is slightly higher than that of $P_K$. The worst scenario is presented by $w_{app\,K}$, which suffers from the double problem of high sensitivity and dependence from the thrust measurement.

- The limitation of this study certainly stems from the small number of explored conditions and by the restricted engine settings used. This probably led to an un-

derestimation of the uncertainties, which should be recalculated as a larger dataset becomes available.

- However, within these limitations, the results were found in very good agreement with those in literature.
- It is also reckoned that the UA is an ultimate instrument in the development of a SPMS, since it provides feedback on the suitability of the ensemble of sensors, algorithms and vessel data for the assessment of its performance.

# CHAPTER 7

# Conclusions

## 7.1 Introduction

This chapter presents a general review and the main outcomes of this research in Section 7.2. The principal contributions of this work to the field of Ship Performance Monitoring identified throughout the thesis are reprised in Section 7.3. Recommendations for future work are lastly advanced in Section 7.4.

## 7.2 Philosophical review

Monitoring the performance of a seagoing vessel has always been paramount in shipping ever since the very beginning of structured shipping trades. In more recent years, the fluctuation of fuel prices together with the ever stricter environmental regulations on Green House Gases emissions bolstered a renewed interest in the performance of ships. Fine improvements of a ship's efficiency within its operational profile has rapidly become the backbone of the new ship designs and the driver of diverse fuel saving strategies and energy saving retrofits.

As a vessel enters into the water the structural condition of its hull begins to deteriorate particularly due to the growth of biofouling on the hull and propeller surfaces. This degradation produces an increase in the boundary layer at the hull and propeller surfaces, which translates into a greater viscous drag. Since the viscous forces can account for well over 80% of the total resistance of a ship, a significant amount of research was catalysed on understanding, monitoring and controlling the growth of fouling on ships. Ship Performance Monitoring Systems (SPMSs) estimate the power penalties by analysing full-scale measurements and are generally regarded as the most rational and accurate means of estimating the effect of biofouling on the performance of a seagoing ship.

The power penalties caused by biofouling are however not directly measurable in full-scale and must be related to the change over time of the speed–power curve of the vessel. Such analysis is complicated by the fact that not only all the environment a ship sails into, but even her operational profile contributes to alter its power absorption. The vessel

performance data are therefore contaminated by many factors or so-called 'disturbances'. Isolating the sole effect of biofouling is an arduous task, attainable at least if sufficient operational data is collected at a suitable sampling frequency over a suitable period of time. Therefore, a SPMS capable of estimating the effect of biofouling on ship performance has in general two main features:

1. Speed through water and shaft power are regarded as the two primary parameters
2. A method to exclude the contribution of external factors (e.g. wind, waves, etc.) needs to be implemented. This may be statistical, deterministic or based on conditional filtering of the measurements. It may also be a combination of the three. To achieve this, suitable secondary parameters (e.g. wind speed, direction etc.) also need to be measured.

In order to improve the measurement quality, the majority of the state-of-the-art SPMSs employ automatic continuous measurement system, which generally deliver superior data quality. The methods to deal with the disturbances are however very diverse. The deterministic approach fundamentally makes use of physical relationships between variables to calculate the vessel performance. Deterministic SPMSs have several good qualities, among which transparency and short-term accuracy are prominent and span very diverse applications, such as short-term retrofit analysis, validation of performance prediction methods, trim optimization and vessel mission profiling. The key aspect of a deterministic SPMS compared to SPMSs based on other principles, is the normalization method, i.e. the procedure used to correct the measured performance for the presence of disturbances.

It can be deduced from the literature that the choice of such normalization methods is often based on weak assumptions, where the limits of applicability of the corrections are not explicitly stated or are not investigated. In addition, several SPMSs are built on top of an existing ensemble of on-board sensors, whereas the choice of the measurement system should follow from the needs of the normalization method. Not only automated measurements should be implemented, but also having an accuracy in compliance with the requirements of the target performance assessment. Also, the near totality of the SPMSs presented in the open literature underestimates the importance of raw data handling or 'data preparation' techniques, which are fundamental in the reduction of measurement noise to improve the data quality in general. Little attention is also devoted, especially in the modern literature, to the selection of KPIs capable not only of estimating the change of propulsive power but also to provide a deeper insight regarding multiple aspects of the degradation of the vessel performance. At the same time, the uncertainty of the performance estimation is rarely calculated or stated.

Within the framework of the above review, the main aim of this thesis was therefore to

develop a deterministic (i.e. physics-based) SPMS dedicated to the analysis of the effect of biofouling and of fouling control strategies on the vessel performance within scrutinised uncertainty levels. To achieve this, two further aims were set. Firstly, to develop and install a working SPMS based on the proposed methodology on board Newcastle University's Research Vessel (R/V) *The Princess Royal*. Secondly, to assess the uncertainty of the system following the modern international standards of Uncertainty Analysis. These aims were attained by achieving a series of objectives. The main assumptions behind this research are that fouling affects exclusively the hull viscous drag, the wake fraction and the propeller torque.

In this thesis, a scientific background was at first given which, after defining the basic theoretical principles of ship performance, provided the reader with a characterisation of the factors that have an effect on it. These were distinguished between disturbances due to the environment and those due to the ship operation. It was acknowledged that, in accordance with the fundamental steady-state performance equations, a vessel's hydrodynamic performance should be evaluated exclusively during steady-state sailing. It was also stressed that the performance of the engine does not influence the assessment of the vessel hydrodynamic behaviour as long as the power measurement is taken from the propeller shaft.

Through a description of the biological characteristics of biofouling, the critical aspects of fouling control strategies were identified and discussed in Chapter 2. The wide spectrum of possible fouling control solutions was recognised to be often bewildering for the ship owner or operator willing to limit the fouling penalties. In support of the importance of biofouling for the performance of ships, an overview of the effects of biofouling growth on the hull and propeller was provided.

Ship performance monitoring was identified as the best means of assessing the effect of biofouling on the vessel performance. A detailed review of the existing SPMSs (**Objective A**) was then given in Chapter 3. Such review justified the choice of the deterministic approach (**Objective B**) by highlighting the capability of a deterministic SPMS to be used immediately after installation, to maintain a good accuracy over time and to be employed in a wide range of applications.

All the data acquisition, management and analysis stages used in a deterministic SPMS were therefore investigated in detail (**Objective C**) in Chapter 4. Since the fundamental principle of the deterministic approach stands in the use of physical relationships to exclude the effects of disturbances from the ship performance, a deterministic SPMS must be designed according to the capabilities of the normalization method. Each of the disturbances earlier identified was analysed considering its effects on the vessel resistance and on the propeller performance (i.e. wake fraction) and the resources required to measure and correct the measurements for such effects (Section 4.2). It was concluded that the direct

wind resistance, the added wave resistance and the effects of currents and of changes of displacement should be corrected within the limits of applicability of their corrections. It was further remarked that, due to their limited influence and/or the extensive resources they require, added resistance caused by steering, drift and yaw and the effects of changes in water properties may be neglected. The Author finally suggests that when sailing in shallow waters or with a trim different from the reference trim, performance monitoring should simply be avoided unless dedicated experiments or numerical computations are available to describe the respective effects. Additionally, it was reckoned that the wake distortions caused by the disturbances are generally very difficult to be corrected. Therefore, suitable conditional filters must be devised to prevent excessive changes in wake fraction to affect the vessel performance.

Having investigated the normalization of each disturbance and consequently the required secondary measurements, the data acquisition system could be defined in Section 4.3. The means to measure accurately and automatically the primary variables (speed through water, propulsive power) and secondary variables were reviewed in line with the state-of-the-art technology. Most notably, Doppler Logs were identified, in accordance to recent research, as the most accurate sensors available at the time of writing to measure the speed through water.

An original empirical equation was also found to obtain the ship time constant, defined as the estimation of the mean phase lag between a low-energy excitation and the response of a vessel based on its principal characteristics. The time constant is used to tune several time-related variables — e.g. the sampling frequency.

As measured, the data is not suitable for immediate analysis and a preparation of some sort is needed. This is described in Section 4.4 of Chapter 4. A critical aspect of raw data preparation concerns identifying steady-state periods (suitable for performance monitoring) in a measurement dataset that may contain outliers. A detailed investigation was therefore carried out on steady-state identification, finding that the standardised standard deviation trimmed at the 5% delivers a better performance compared to other steady-state indicators. To use this indicator, the data was binned with bins having size $f\vartheta$, where $f$ is the sampling frequency of a primary parameter and $\vartheta$ is the vessel time constant.

Based on the normalization methods presented earlier, conditional filters were defined. These are boundary conditions beyond which ship performance monitoring must be avoided to limit the effects of the influencing factors. The sea trial boundary conditions recommended by the most recent ITTC were adopted in most cases. With respect to waves, however, a directional filtering criterion was devised in accordance with the strength of the effect of waves on ship resistance and propulsion. For instance, in case the added wave resistance transfer function is only available for head seas, the wave height

filter will allow a higher wave height for waves bearing 150 deg–210 deg. At the same time, a $\cos^2$ function was suggested to define the wave height at other angles, considering that lower thresholds must be forced to the following waves given their heavy impact on the propeller wake. Ocean currents should not be an issue in most cases — provided that the speed log is calibrated. Since depth-dependent or very strong tidal currents may affect the speed log measurements, it is suggested to avoid monitoring where the difference between the speed over ground and the speed through water is higher than 2kn. Based on manoeuvrability simulations, drift and yaw filters were suggested.

An extensive study was also devoted to the selection of an outlier-handling technique which would better the performance of the commonly used Chauvenet criterion. If outliers are to be *rejected*, it was found that the generalised Extreme Studentized Deviate (ESD) has a superior performance for normally distributed datasets contaminated by multiple outliers.

Speed through water, torque, thrust on one side and wind speed and direction measurements on the other are respectively known to be prone to sensor drift and shadowing from the vessel superstructures. A section was therefore dedicated to explore means to periodically verify the calibration of the formers and to assess the consistency of the latter after its installation.

Section 4.5 described the expanded revision of the Taniguchi–Tamura method that was chosen to apply the corrections. According to its principles, the propeller open water curves are not corrected for propeller fouling, allowing the discrepancy between thrust-identity and torque-identity wake fraction to be employed as an indication of the increase of propeller roughness.

Four Key Performance Indicators (KPIs) were derived to allow the effect of biofouling to be estimated (**Objective D**). Their derivation is described in detail in Section 4.6. The KPIs all show a fractional increase of a certain parameter with respect to a reference baseline. The reference performance may therefore be chosen at will, but it was stressed the importance of a careful selection of the baseline model to avoid introducing large biases in the KPIs. The first KPI is a customary power increase, which is both robust and intuitive. Since it cannot provide a deeper insight into the causes of the performance degradation, three novel KPIs were introduced, namely the wake fraction gain, the apparent wake fraction gain and the fouling coefficient. The wake fraction gain describes the increase of the torque-identity effective wake fraction caused by hull fouling. The apparent wake gain estimates the amount of torque-identity wake fraction which is fictitiously caused by the combination of propeller fouling and clean propeller open water curves. Finally, the fouling coefficient estimates the increase of the ship viscous drag due to hull biofouling. Additionally, a novel method is presented to make use of thrust measurements to derive the full-scale ITTC'78 frictional coefficient increase $\Delta C_f$. Most notably, it was found that

the cross-comparison of multiple KPIs is extremely beneficial to the assessment of the vessel performance.

In fulfilment of **Aim 2**, the ship performance monitoring method hitherto described was applied to the case study vessel *The Princess Royal*, Newcastle University's R/V (Chapter 5). In Section 5.3 the possible normalizations of the various influencing factors were investigated, which led to conducting a series of experimental and numerical campaigns to obtain the added wave resistance transfer functions, the direct wind resistance coefficients and other performance parameters (**Objective F**). A normalization procedure was chosen for the effects on the R/V resistance of waves, winds, displacement changes and water properties changes.

Based on this, the sensors already installed on *The Princess Royal* were reviewed, calibrated, upgraded and complemented were necessary and feasible (**Objective E**). Notably, a Doppler speed log was installed following the review. The sensors were all found to provide very acceptable measurements (Section 5.4).

The results of the performance assessment were reviewed in Section 5.7. The SPMS was finalised on *The Princess Royal* in January 2017. A few trials were conducted after this date (**Objective G**), which were limited to an small number mainly by a prolonged emergency dry-docking and by the weather state. The reference performance baselines were selected with care for each KPI and were decided to cover the displacing and semi-planing speed ranges separately to avoid erroneous model fitting in the transition region. Within a period of just over a year, the KPIs were able to capture the growth of biofouling from slime to medium-heavy calcareous hull fouling and the build-up of propeller algal fouling. The performance analysis method also allowed a propeller fault to be spotted. Comparison between all KPIs allowed the effect of biofouling to be also quantified, for instance, as a 20% to 25% power increase with medium-heavy hull calcareous fouling at 15kn, respectively with relatively clean and fouled propeller. This corresponded to an increase of frictional drag of up to 75%.

In fulfilment of **Aim 3**, an Uncertainty Analysis (UA) was conducted on *The Princess Royal* data (**Objective H**) and described in Chapter 6. Monte Carlo methods were combined with the distributions of measurements obtained in different dates and sailing conditions to provide a combined uncertainty originated from the systematic error of the SPMS and the analysis and the random error caused by weather and other circumstances. The uncertainty of the speed through water measurement was found to reach at most 3%. A total expanded uncertainty in power ranging 2–3%, at the higher (semi-planing) speeds and rising up to 7% at the lowest displacing speed. These results are found in very good agreement with the literature. An effort was also made to quantify the uncertainty related to the four KPIs. These were found to have uncertainties in the range 2%–40%, depending on speed and KPI. In general, the simpler KPIs (i.e. power increase and wake fraction

gain) met the expectations of being more accurate, whereas the only thrust based KPI (the apparent wake fraction gain) proved to be the more volatile. It was also noticed that the speed through water measurement has the largest impact on the KPIs' accuracy. It is however remarked that the limited data at disposal certainly biased the UA and that future work will attempt at updating the SPMS' uncertainty estimation.

Overall, considering all the difficulties of the application, the results supported the proposed deterministic method. The principal limitations of the application were identified in the vessel operational profile (often sailing in conditions not suitable for performance monitoring), the yearly maintenance schedule and the weather factor. All these elements contributed to heavily reduce the sample size at the Author's disposal, weakening the statistical strength of the analysis. Experience and literature alike show that the application on a larger vessel would undoubtedly improve the performance data quality and quantity.

Among the most critical aspects of the SPMS development, three were found to be fundamental:

- Quality of the measurement system and selection of a suitable sampling frequency in relation to the size of the vessel
- Thorough investigation of the capabilities and limitations of the normalization method, which accordingly is complemented by the definition of sensible steady-state and conditional filters
- Careful selection of the reference baseline performance, which may have a heavy impact on the KPIs if wrongly chosen

If these aspects are correctly taken into account, the proposed deterministic ship performance monitoring method was shown to be capable of identifying within reasonable uncertainty levels the little changes of hydrodynamic performance caused by hull and propeller fouling even on a small-sized research catamaran.

## 7.3 Contributions

Given the above review, the Author identifies the following contributions to the field of ship performance monitoring:

- This study presented the first published deterministic SPMS and analysis method purposely designed and implemented for the identification and estimation of the effect on vessel performance of hull and propeller biofouling and for the comparison of the performance of different fouling control strategies.

- A clearer perspective regarding the effects of the disturbances on ship performance was given together with a detailed review of the possible methods that can be used to correct them.

- New raw data preparation techniques were proposed, which are an improvement of the modern standards. Among these, the employment of the trimmed standard deviation as a steady-state identifier and the ESD as the outlier-handling algorithm.

- Three novel KPIs were proposed, which proved very useful in cross-comparison to identify and quantify the fouling effect. One of these KPIs (the apparent wake gain) is regarded as an efficient way to 'calibrate' the thrust measurements, excessively volatile to be used otherwise.

- Accordingly, an equation is proposed to derive the full-scale $\Delta C_f$ from the above KPIs and with respect to the reference fouling state.

- A complete UA was attempted on the working SPMS, proving to be the first uncertainty estimation of this kind. The UA confirmed the general understanding that the uncertainty of the speed log has the greatest impact on the performance analysis.

- The SPMS developed on *The Princess Royal* has been the first SPMS dedicated to biofouling that was successfully applied on a small sized vessel.

## 7.4 Future work

The performance of a SPMS is ultimately related to the uncertainty of its KPIs, which can be reduced by improving all the data treatment stages — measurement, preparation, normalization and performance analysis. Accordingly, the following are suggested as future improvements of the proposed methodology:

- The implementation of automatic on-board draught and wave spectra measurements, for example by means of an on-board X-band radar would refine the characteristic of the SPMS.

- A longer monitoring period is necessary to verify the long-term behaviour of the monitoring system and improve the calculation of the KPIs by using a wealthier dataset.

- Coherently, implementing the proposed SPMS on a larger vessel would confirm the goodness of the method and reduce the data scatter observed on *The Princess Royal*. A commercial application of the SPMS would in addition allow further improvements to the system by receiving feedback from the crew members of the vessel.

- The F-type statistic explored in this research for steady-state identification appeared to be promising, although further research is needed to verify its full suitability for an SPMS application.

- The performance analysis method should be improved by integrating a procedure to compare KPIs calculated at different speeds.

- Further data and/or a different analysis method should be used to improve the UA presented in this thesis, giving a stronger confidence in the presented results.

- One of the strengths of the proposed SPMS is the relatively high accuracy and low uncertainty levels. This feature makes it suitable to be potentially used to determine the performance of different coatings and novel drag reduction systems on a small vessel such as *The Princess Royal*. It is suggested that this capability be explored in future work.

- Also, the proposed SMPS should be in the future used to validate CFD simulations aimed at estimating the effect of biofouling on ship performance (e.g. Demirel *et al.*, 2017*a*; Atlar *et al.*, 2018; Demirel *et al.*, 2019). By using state-of-the-art instrumentation, the strength of full-scale trials may then be brought together to CFD and laboratory experiments by reverse analysis.

Finally, should the above be taken into account, a more detailed UA should be conducted to confirm the final uncertainty of the proposed deterministic ship performance monitoring and analysis method.

### *7.4.1 Commercial exploitation*

The SPMS presented in this thesis may be implemented on board a larger commercial vessel. Broadly speaking, the ship performance monitoring method is suitable to be applied to a commercial vessel 'as-is', classifying it as a *deterministic* SPMS in the commercial framework defined in Section 3.4. However, data acquisition and performance analysis stages deserve some additional comment.

***Data acquisition.***—The performance analysis method was *per se* conceived to be applicable to any vessel fitted with a suitable performance monitoring system. In case the vessel is not provided with most of the measuring equipment required by the method, the criteria proposed in Section 4.2 should be followed in aid to the selection of the most suitable data acquisition system. However, more often the ship performance practitioner has to make good use of the data acquisition instrumentation already existing on the vessel. In such cases, it is of great importance to verify the compliance of the data acquisition system with the minimum requirements of the presented method. Failure to do

so would significantly jeopardise the purposes of the SPMS. The requirements particularly concern:

- Sampling frequency, which needs to be sufficient to capture enough datapoints, particularly with respect to the primary variables. In Section 4.3, a sampling frequency above $100/\vartheta$ was stated to be good, whereas the suggested minimum for statistical relevance is $20/\vartheta$, with $\vartheta$ being the ship time constant.

- Sensor quality should be ensured by their correct installation (particularly location, e.g. speed log and anemometer) and maintenance.

- Signal communication must be secured against interference and data corruption in general. On larger ships, the data cabling will necessarily run across greater lengths. Because of the significant interference that metal ship structures have on data transfer, it is strongly recommended that all the analogue signals be converted to digital at the sensor side. This greatly simplifies the data quality assessment. Alternatively, suitable cable shielding must be provided.

***Performance analysis.***—The biofouling development on a regularly sailing ship is subjected to significantly slower rates than on *The Princess Royal*. As a consequence, consistently larger datasets are acquired. Thus, the baseline performance would mostly be obtained from a much greater wealth of datapoints, which allows for a better definition of the reference curves. Coherently, the trend of the KPIs over time will be observed more easily. On the other hand, the operational profile of most vessels will greatly reduce the data variability, concentrating most datapoints in a small speed range. This might results in a reduced confidence in the definition of the reference trends but also in a more accurate trend analysis of the KPIs.

Due to the larger size of the commercial vessels, the effects of disturbances on the performance will also be proportionally reduced and the scatter of the KPIs lowered.

# References


Aage, C. (1971) *Wind coefficients for nine ship models*. Tech. Rep. No. A-3, Hydro-og Aerodynamisk Laboratorium, Lyngby, DK.

Abkowitz, M. A. (1989) 'The Use of System Identification Techniques to Measure the Ship Resistance, Powering and Manoeuvering Coefficients of the Exxon Philadelphia and a Submarine from Simple Trials during a Routine Voyage'. *Proc. of 15th ATTC*, St. John, US.

Abkowitz, M. A. and Liu, G.-s. (1988) 'Measurement of Ship Resistance, Powering and Manoeuvering Coefficients from Simple Trials during a Regular Voyage'. *Trans. Society of Naval Architects and Marine Engineers (SNAME)*, **96**:97–128.

Aertssen, G. (1953) 'Sea trials on a Victory ship,AP3, in Normal Merchant Service'. *Trans. Institution of Naval Architects (INA)*, **95**:J21.

Aertssen, G. (1961) 'New Sea Trials of the Sandblasted Lubumbashi'. *Trans. Institution of Marine Engineers (IMarE)*, **73**.

Aldous, L. G. (2016) *Ship Operational Efficiency: Performance Models and Uncertainty Analysis*. PhD Thesis, University College London, London, UK.

Aldous, L., Smith, T. and Bucknall, R. (2013) 'Noon report Data Uncertainty'. *Proc. of the Low Carbon Shipping & Shipping in Changing Climates Conference (LCS 2013)*, London, UK.

Aldous, L., Smith, T., Bucknall, R. and Thompson, P. (2015) 'Uncertainty Analysis in ship performance monitoring'. *Ocean Engineering*, **110**:29–38.

Andersen, P., Borrod, A.-S. and Blanchot, H. (2005) 'Evaluation of the Service Performance of Ships'. *Marine technology and SNAME News*, **45**(4).

Anderson, C. D. (2013) *How antifouling coatings affect ship performance*. External Lecture MAR8024, Newcastle University, Newcastle upon Tyne, UK.

Anderson, C. D., Atlar, M., Callow, M., Candries, M., Milne, A. and Townsin, R. L. (2003) 'The development of foul-release coatings for seagoing vessels'. *Proc. of the Institute of*

*Marine Engineering, Science and Technology. Part B: Journal of Marine Design and Operations*, **B4**:11–23.

Anderson, C. D. and Hunter, J. E. (2000) 'Whither Antifouling paints after TBT?' *Proc. of the 13th International Conference on Ship and Shippping Research (NAV 2000)*, vol. 1, Venice, IT.

Antola, M., Solonen, A. and Pyörre, J. (2017*a*) 'Notorious speed through water'. *Proc. of the 2nd Hull Performance & Insight Conference (HullPIC '17)*, Ulrichshusen, DE.

Antola, M., Solonen, A. and Straboulis, S. (2017*b*) 'The Art of Scarcity: Combining High-Frequency Data with Noon Reports in Ship Modeling'. *Proc. of the 2nd Hull Performance & Insight Conference (HullPIC '17)*, Ulrichshusen, DE.

ASME (1998) *Test Uncertainty*. Tech. rep., American Society of Mechanical Engineers.

Atlar, M. (2013) *Ship Performance at sea*. Lecture notes MAR8024, Newcastle University, Newcastle upon Tyne, UK.

Atlar, M. (2014) *The Princess Royal Full-Scale Data & Operating Conditions*. Internal Report, Newcastle University, Newcastle upon Tyne, UK.

Atlar, M., Aktas, B., Sampson, R., Seo, K.-C., Viola, I. M., Fitzsimmons, P. and Fetherstonhaugh, C. (2013*a*) 'A multi-purpose marine science & technology research vessel for full-scale observations and measurements'. *Proc. of the 3rd International Conference on Advanced Model Measurement Technology for The Maritime Industry (AMT'13)*, Gdansk, PL.

Atlar, M., Bashir, M., Turkmen, S., Yeginbayeva, I. A., Carchen, A. and Politis, G. (2015) 'Design, manufacture and operation of a strut system deployed on a research catamaran to collect samples of dynamically grown biofilms in-service'. *Proc. of the 4th International Conference on Advanced Model Measurement Technology for The Maritime Industry (AMT'15)*, Istanbul, TR.

Atlar, M., Glover, E. J., Candries, M., Mutton, R. and Anderson, C. D. (2002) 'The effect of a Foul Release coating on propeller performance'. *Proc. of the 2nd International Conference on Marine Science and Technology for Environmental Sustainability (ENSUS2001)*, Newcastle upon Tyne, UK.

Atlar, M., Glover, E. J., Mutton, R. J. and Anderson, C. D. (2003) 'Calculation of the effects of new generation coatings on high speed propeller performance'. *Proc. of the 2nd International Warship Cathodic Protection Symposium and Equipment Exhibition*, Shrivenham, UK.

Atlar, M., Sampson, R., Wightman, S., Seo, K.-C., Glover, E. J., Danisman, D. B. and Mantouvalos, A. (2010) 'An innovative research vessel replacement for Newcastle University'. *Proc. of the 7th International Conference on High-Performance Marine Vehicles (HIPER 2010)*, Melbourne, US.

Atlar, M., Seo, K.-C., Sampson, R. and Danisman, D. B. (2013*b*) 'Anti-slamming bulbous bow and tunnel stern applications on a novel Deep-V catamaran for improved performance'. *Int. J. Naval Archit. Ocean Eng.*, **5**:302˜312.

Atlar, M., Yeginbayeva, I. A., Turkmen, S., Demirel, Y. K., Carchen, A., Marino, A. and Williams, D. (2018) 'A rational approach to predicting the effect of antifouling systems on "in-service" ship performance'. *Proc. of the 3rd International Symposium on Naval Architecture and Maritime*, Istanbul, TR.

Axiotis, D. (2016) *A CFD analysis for the calculation of wind loading on Newcastle University research vessel*. Master's thesis, Newcastle University, Newcastle upon Tyne, UK.

Barnett, V. and Lewis, T. (1994) *Outliers in Statistical Data*. Wiley Series in Probability and Mathematical Statistics, John Wiley & Sons Ltd., Norwich, UK.

Bengough, G. D. and Shepheard, V. G. (1943) 'The Corrosion and Fouling of Ships'. *Trans. Institution of Naval Architects (INA)*, **85**:1.

Bertram, V. (2016) 'Added Power in Waves – Time to Stop Lying (to Ourselves)'. *Proc. of the 1st Hull Performance & Insight Conference (HullPIC '16)*, Castello di Pavone, IT.

Betke, K. (2001) 'The NMEA 0183 Protocol'. URL `http://www.tronico.fi/OH6NT/docs/NMEA0183.pdf`.

Bhattacharyya, R. (1978) *Dynamics of marine vehicles*. Ocean engineering, a Wiley series, Wiley, New York.

Bialystocki, N. and Konovessis, D. (2016) 'On the estimation of ship's fuel consumption and speed curve: A statistical approach'. *Journal of Ocean Engineering and Science*, **1**:157–166.

Blendermann, W. (1996) *Wind Loading of Ships - Collected Data from Wind Tunnel Tests in Uniform Flow*. Tech. Rep. 574, Institut für Schiffbau der Universität Hamburg, Hamburg, DE.

Blok, J. J. (1993) *The Resistance Increase of a Ship in Waves*. PhD Thesis, Technische Universiteit Delft, Delft, NL.

Boese, P. (1970) *Eine einfache Methode zur Berechnung der Widerstandserhöhung eines Schiffes im Seegang*. Tech. Rep. 258, Institut für Schiffbau der Universität Hamburg, Hamburg, DE.

Bonebakker, J. W. (1951) 'The application of statistical methods to the analysis if service performance data'. *Trans. North East Coast Institution of Engineers & Shipbuilders (NECIES)*, **67**:277.

Bonebakker, J. W. (1953) 'Analysis of Model experiments trials and service performance data of a single-screw tanker'. *Trans. North East Coast Institution of Engineers & Shipbuilders (NECIES)*, **70**:475.

Bos, M. (2016) 'How MetOcean Data Can Improve Accuracy and Reliability of Vessel Performance Estimates'. *Proc. of the 1st Hull Performance & Insight Conference (HullPIC '16)*, Castello di Pavone, IT.

Bos, M. (2018) 'An Ensemble Prediction of Added Wave Resistance to Identify the Effect of Spread of Wave Conditions on Ship Performance'. *Proc. of the 3rd Hull Performance & Insight Conference (HullPIC '18)*, Redworth, UK.

Bouscasse, B., Broglia, R. and Stern, F. (2013) 'Experimental investigation of a fast catamaran in head waves'. *Ocean Engineering*, **72**:318–330, doi:10.1016/j.oceaneng.2013.07.012.

Broersma, G. and Tasseron, K. (1967) 'Propeller maintenance – propeller efficiency and blade roughness'. *International Shipbuilding Progress*, **14**(157):347–356, doi:10.3233/ISP-1967-1415701.

Bruzzone, D., Grasso, A. and Zotti, I. (2009) 'Experiments and computations of nonlinear effects on the motions of catamaran hulls'. *Proc. of the 10th International Conference on Fast Sea Transportation (FAST 2009)*, Athens, GR.

BSRA (1981) 'Ship Performance at Sea'. *Ship Design Manual - Hydrodynamics*, vol. 2.

Burton, T., Jenkins, N., Sharpe, D. and Bossanyi, E. (eds.) (2011) *Wind energy handbook*. Wiley, Chichester, West Sussex, 2nd edn.

Bustard, E. E. (1978) 'The Propeller as a Power Meter or Speed Log'. *Proc. of the CIMarE and SNAME Joint Meeting*, Toronto, CA.

Cao, S. and Rhinehart, R. R. (1995*a*) 'Critical Values for a Steady-State Identifier'. *Journal of Process Control*, **7**(2):149–152.

Cao, S. and Rhinehart, R. R. (1995*b*) 'An Efficient Method for On-Line Identification of Steady-State'. *Journal of Process Control*, **5**(6):363–374.

Carchen, A. (2015*a*) *Open Water test of the NPT propeller model ECT-TPR-002. Cavitation Tunnel performance and Full-Scale extrapolation.* Internal Report, Newcastle University, Newcastle upon Tyne, UK.

Carchen, A. (2015*b*) *Preliminary analysis of shaft measurements discrepancies onboard the R/V The Princess Royal.* Internal Report, Newcastle University, Newcastle upon Tyne, UK.

Carchen, A. (2017) 'Field Trials and in-situ coating Performance Monitoring'. *8th SeaFRONT Project Meeting*, Bologna, IT.

Carchen, A., Sasaki, N., Aktas, B., Turkmen, S. and Atlar, M. (2015) 'Design and review of the new 'NPT' propeller for The Princess Royal'. *Proc. of the 4th International Conference on Advanced Model Measurement Technology for The Maritime Industry (AMT'15)*, Istanbul, TR.

Carchen, A., Shi, W., Sasaki, N. and Atlar, M. (2016) 'A prediction program of manoeuvrability for a ship with a Gate Rudder system'. *Proc. of the 2nd International 'A. Yücel Odabaşı' Colloquium*, A. Yücel Odabaşı Colloquium series, Istanbul, TR.

Carchen, A., Turkmen, S., Pazouki, K., Murphy, A., Aktas, B. and Atlar, M. (2017) 'Uncertainty Analysis of full-scale ship performance monitoring onboard The Princess Royal'. *Proc. of the 5th International Conference on Advanced Model Measurement Technology for The Maritime Industry (AMT'17)*, Glasgow, UK.

Carlton, J. S. (2012) *Marine propellers and propulsion.* Butterworth-Heinemann, Amsterdam, NL, 3rd edn.

Castiglione, T., Stern, F., Bova, S. and Kandasamy, M. (2011) 'Numerical investigation of the seakeeping behavior of a catamaran advancing in regular head waves'. *Ocean Engineering*, **38**(16):1806–1822, doi:10.1016/j.oceaneng.2011.09.003.

CCO (2017) 'Regional coastal monitoring programmes'. URL `http://www.channelcoast.org/`.

CEFAS (2019) 'WaveNet interactive map'. URL `http://wavenet.cefas.co.uk/Map`.

Chauvenet, W. (1863) 'Method of Least Squares'. *Manual of Spherical and Practical Astronomy*, vol. 2, pp. 469–566, New York, US, 5th edn.

Clarksons Platou (2018) *Market Report - Shipping and Offshore.* Tech. rep., CPPF AS, Oslo, NO.

Clements, R. E. (1957) 'A method of analysing voyage data'. *Trans. North East Coast Institution of Engineers & Shipbuilders (NECIES)*, **73**:197–230.

Coleman, H. W. and Steele, W. G. (1989) *Experimentation and uncertainty analysis for engineers*. John Wiley & Sons.

Conn, J. F. C., Lackenby, H. and Walker, W. P. (1953) 'BSRA resistance experiments on the Lucy Ashton. Part II. The ship-model correlation for the naked hull conditions'. *Trans. Institution of Naval Architects (INA)*, **95**:350–436.

Coraddu, A., Oneto, L., Baldi, F. and Anguita, D. (2017) 'Vessel fuel consumption forecast and trim optimization: A data analytics perspective'. *Ocean Engineering*, **130**.

Crowe, E. L., Davis, F. A. and Maxfield, M. W. (1955) *Statistics Manual*. Dover Publications, New York, US.

Cusano, G., Garbarino, M., Qualich, S. and Stranieri, G. (2016) 'Monitoring, Reporting, Verifying and Optimizing Ship Propulsive Performance: A Support System to Ship Management Focused on Energy Efficiency'. *Proc. of the 1st Hull Performance & Insight Conference (HullPIC '16)*, Castello di Pavone, IT.

Dückert, T., Schmode, D. and Tullberg, M. (2016) 'Computing Hull & Propeller Performance: Ship Model Alternatives and Data Acquisition Methods'. *Proc. of the 1st Hull Performance & Insight Conference (HullPIC '16)*, Castello di Pavone, IT.

Demirel, Y. K., Song, S. and Turan, O. (2019) 'Added resistance diagrams to predict fouling impact on ship performance'. *Ocean Engineering*, **(under review)**.

Demirel, Y. K., Turan, O. and Incecik, A. (2017*a*) 'Predicting the effect of biofouling on ship resistance using CFD'. *Applied Ocean Research*, **62**:100–118, doi:10.1016/j.apor.2016.12.003.

Demirel, Y. K., Uzun, D., Zhang, Y., Fang, H.-C., Day, A. H. and Turan, O. (2017*b*) 'Effect of barnacle fouling on ship resistance and powering'. *Biofouling*, **33**(10):819–834, doi:10.1080/08927014.2017.1373279.

Dinham-Peren, T. A. and Dand, I. W. (2010) 'The need for full scale measurement'. *Proc. of the William Froude Conference: advances in Theoretical and Applied Hydrodynamics - Past and Future*, Royal Institution of Naval Architects, Portsmouth, UK.

EC (2015) 'On the monitoring, reporting and verification of carbon dioxide emissions from maritime transport, and amending Directive 2009/16/EC'.

EC (2016) 'On determination of cargo carried for categories of ships other than passenger, ro-ro and container ships pursuant to Regulation (EU) 2015/757 of the European Parliament and of the Council on the monitoring, reporting and verification of carbon dioxide emissions from maritime transport'.

Faltinsen, O. M. (2005) *Hydrodynamics of high-speed marine vehicles*. Cambridge University Press, Cambridge, UK, URL `http://www.loc.gov/catdir/toc/ecip059/2005006328.html`.

Faltinsen, O. M. and Helmers, J. B. (1991) 'Speed loss and operability of catamarans and SES in a seaway'. *Proc. of the 1st International Conference on Fast Sea Transportation (FAST'91)*, vol. 2, Tapir Publishers, Trondheim, NO.

Faltinsen, O. M., Minsaas, K., Liapis, N. and Skjørdal, S. O. (1980) 'Prediction of resistance and propulsion of a ship in a seaway'. *Proc. of the 13th Symposium on Naval Hydrodynamics*, The Shipbuilding Research Association of Japan, Tokyo, JP.

Faltinsen, O., Zhao, R. and Umeda, N. (1991) 'Numerical Predictions of Ship Motions at High Forward Speed'. *Philosophical Transactions of the Royal Society A: Mathematical, Physical and Engineering Sciences*, **334**(1634):241–252, doi:10.1098/rsta.1991.0011.

Fang, C. C., Chan, H. S. and Incecik, A. (1996) 'Investigation of motions of catamarans in regular waves - I'. *Ocean Engineering*, **23**(1):89–105.

Fathi, D. E. and Hoff, J. R. (2016) *ShipX Vessel Responses (VERES) - Theory Manual*. ShipX Manual, MARINTEK A/S.

Fisher, N. I. (1993) *Statistical Analysis of Circular Data*. Cambridge University Press, Cambridge, doi:10.1017/CBO9780511564345.

Fofonoff, N. P. and Millard Jr., R. C. (1983) 'Algorithms for computation of fundamental properties of seawater'. *UNESCO technical papers in marine science*, (44).

Foteinos, M. I., Tzanos, E. I. and Kyrtatos, N. P. (2017) 'Ship Hull Fouling Estimation Using Shipboard Measurements, Models for Resistance Components, and Shaft Torque Calculation Using Engine Model'. *Journal of Ship Research*, **61**(2):64–74, doi:10.5957/JOSR.61.2.160053.

Fujiwara, T. and Nimura, T. (2005) 'New Estimation Method of Wind Forces Acting On Ships On the Basis of Mathematical Model'. *Proc. of the Fifteenth International Offshore and Polar Engineering Conference*, International Society of Offshore and Polar Engineers (ISOPE), Seoul, KR.

Fumi, Y. (2016) 'Observational Study on Powers Estimated by Shaft Torque and Fuel Consumption'. *Proc. of the 1st Hull Performance & Insight Conference (HullPIC '16)*, Castello di Pavone, IT.

Furuno (2003) *DS-80 Doppler speed log*. Operator's manual, Furuno Electric Co. Ltd.

Gangeskar, R., Prytz, G. and Bertelsen, V. S. (2018) 'On-Board Real-Time Wave & Current Measurements for Decision Support'. *Proc. of the 3rd Hull Performance & Insight Conference (HullPIC '18)*, Redworth, UK.

Gerritsma, J. and Beukelman, W. (1972) 'Analysis of the resistance increase in waves of a fast cargo ship'. *International Shipbuilding Progress*, **19**.

Greeley, D. S. and Kerwin, J. E. (1982) 'Numerical methods for propeller design and analysis in steady flow'. *Trans. Society of Naval Architects and Marine Engineers (SNAME)*, **90**:415–453.

Grønlie, i. (2004) 'Wave radars - A comparison of concepts and techniques'. *Hydro International*, **8/5**.

Górski, W. (2016) 'Role of Reference Model in Ship Performance Management'. *Proc. of the 1st Hull Performance & Insight Conference (HullPIC '16)*, Castello di Pavone, IT.

Guldhammer, H. E. and Harvald, S. A. (1974) *Ship Resistance. Effect of form and principal dimensions*. Akademisk Forlag, Copenhagen, DK, revised edn.

Hagestuen, E., Lund, B. and Gonzalez, C. (2016) 'Continuous Performance Monitoring – A Practical Approach to the ISO 19030 Standard'. *Proc. of the 1st Hull Performance & Insight Conference (HullPIC '16)*, Castello di Pavone, IT.

Halfhide, R. (2018) 'Switching on to the Internet of Things'. *The Naval Architect*, (September):82–84.

Hamer, A. (2015) *RV Princess Royal port shaft instrumentation fit*. Client Rep. DU5723 R2 V0, Design Unit, Newcastle upon Tyne, UK.

Hamer, A. (2016) *RV Princess Royal stbd shaft upgrade (summary)*. Client Rep. DU5912 R3 V0, Design Unit, Newcastle upon Tyne, UK.

Hansen, S. V. (2011) *Performance Monitoring of Ships*. PhD Thesis, Technical University of Denmark.

Haranen, M., Pakkanen, P., Kariranta, R. and Salo, J. (2016) 'White, Grey and Black-Box Modelling in Ship Performance Evaluation'. *Proc. of the 1st Hull Performance & Insight Conference (HullPIC '16)*, Castello di Pavone, IT.

Harvald, S. A. (1983) *Resistance and propulsion of ships*. Ocean engineering, a Wiley series, Wiley, New York.

Haslbeck, E. G. and Bohlander, G. S. (1992) 'Microbial biofilm effects on drag – Lab and field'. *Proc. of the Ship Production Symposium*, SNAME, New Orleans, US.

Hasselaar, T. W. (2011) *An investigation into the development of an advanced ship performance monitoring and analysis system*. PhD Thesis, Newcastle University, Newcastle upon Tyne, UK.

Hasselaar, T. W. (2015) 'Speed measurement for ships in service'. *GST Seminar*, Copenhagen, DK.

Havelock, T. H. (1940) 'The Pressure of Water Waves upon a Fixed Obstacle'. *Proc. of the Royal Society of London*, **175**(963):409–421.

HBM (2019) 'The Wheatstone Bridge Circuit'. URL `https://www.hbm.com/en/7163/wheatstone-bridge-circuit/`.

He, S., Kellett, P., Yuan, Z., Incecik, A., Turan, O. and Boulougouris, E. (2016) 'Manoeuvring prediction based on CFD generated derivatives'. *Journal of Hydrodynamics*, **28**(2):284–292, doi:10.1016/S1001-6058(16)60630-3.

Hiam, S. (2003) *EM2000 Ship's Log System*. Operator's manual, Aeronautical & General Instruments Ltd„.

Hinostroza, M. A. and Guedes Soares, C. (2016) 'Parametric estimation of the Directional Wave Spectrum from ship motions'. *International Journal of Maritime Engineering*, **158**(A2), doi:10.3940/rina.2016.a2.356.

Hirano, M. (1980) 'A practical calculation method of ship maneuvering motion at initial design stage'. *Journal of the Society of Naval Architects of Japan*, **147**:68–80.

Hollenbach, K. U. (1998) 'Estimating Resistance and Propulsion for Single-Screw and Twin-Screw Ships'. *Ship Technology Research*, **45**.

Holtrop, J. and Chan, H. (1984) 'A statistical re-analysis of resistence and propulsion data'. *International Shipbuilding Progress*, **31**:p.272–276.

Holtrop, J. and Mennen, G. G. J. (1982) 'An approximate power prediction method'. *International Shipbuilding Progress*, **29**.

Huber, P. J. (1972) 'Robust Statistics: A Review (The 1972 Wald Lecture)'. *The Annals of Mathematical Statistics*, **43**(4):1041–1067.

Huber, P. J. (1981) *Robust Statistics*. Wiley Series in Probability and Mathematical Statistics, John Wiley & Sons, 1st edn.

Hughes, G. (1954) 'Friction and form resistance in turbulent flow and a proposed formulation for use in model and ship correlation'. *Trans. Institution of Naval Architects (INA)*, **96**:314–376.

Hunsucker, J. T. (2016) *Quantification of frictional drag due to biofouling on in-service ships*. PhD Thesis, Florida Institute of Technology, Melbourne, US.

Hydrex (2018) 'Underwater ship hull cleaning'. URL `https://hydrex.be/service/navy/underwater_maintenance`.

IEC (2005) *Wind turbines – Part 1: Design requirements*. Tech. Rep. International Standard 61400–1, International Electrotechnical Commission.

IMO (2002) *Guidelines on Voyage Data Recorder (VDR) ownership and recovery*. Guidelines MSC/Circ. 1024, International Maritime Organization, London, UK.

IMO (2009) *Guidelines for voluntary use of the Ship Energy Efficiency Operational Indicator (EEOI)*. Guidelines MEPC.1/Circ.684, International Maritime Organization, London, UK.

IMO (2011) *Inclusion of regulations on energy efficiency for ships in MARPOL Annex VI*. Resolution MEPC.203(62), International Maritime Organization, London, UK.

IMO (2016) *Guidelines for the development of a Ship Energy Efficiency Management Plan (SEEMP)*. Resolution MEPC.282(70), International Maritime Organization, London, UK.

IMO (2018) *Initial IMO strategy on reduction of GHG emissions from ships*. Resolution MEPC.304(72), International Maritime Organization, London, UK.

Inoue, S., Hirano, M., Hirakawa, Y. and Mukai, K. (1979*a*) 'The Hydrodynarnic Derivatives on Ship Maneuverability in Even Keel Condition'. *Trans. West-Japan Society of Naval Architects*, **57**.

Inoue, S., Hirano, M., Kijima, K. and Takashina, J. (1981) 'A practical calculation method of ship maneuvering motion'. *International Shipbuilding Progress*, **28**(325):207–222, doi: 10.3233/ISP-1981-2832502.

Inoue, S., Hirano, M. and Mukai, K. (1979*b*) 'The Non-linear Terms of Lateral Force and Moment Acting on Ship Hull in the Case of Maneuvering'. *Trans. West-Japan Society of Naval Architects*, **58**.

Insel, M. (2008) 'Uncertainty in the analysis of speed and powering trials'. *Ocean Engineering*, **35**(11-12):1183–1193, doi:10.1016/j.oceaneng.2008.04.009.

Isdale, J., Spence, C. and Tudhope, J. (1972) 'Physical properties of sea water solutions: viscosity'. *Desalination*, **10**(4):319–328, doi:10.1016/S0011-9164(00)80002-8.

Isherwood, R. M. (1973) 'Wind resistance of merchant ships'. *Trans. Royal Institution of Naval Architects (RINA)*, **115**:327.

ISO (2002) *Guidelines for the assessment of speed and power performance by analysis of speed trial data.* International Standard 15016:2002, International Standardization Organization.

ISO (2015*a*) *Guidelines for the assessment of speed and power performance by analysis of speed trial data.* International Standard 15016:2015, International Standardization Organization.

ISO (2015*b*) *Manufacturing tolerances of ship screw propellers. Part 2: Propellers of diameter between 0,80 and 2,50 m inclusive.* International Standard 484-2:2015, International Standardization Organization.

ISO (2016) *Measurement of changes in hull and propeller performance.* International Standard 19030, International Standardization Organization.

ITTC (1993) 'On-Board Monitoring Session'. *Proc. of 20th ITTC*, San Francisco, US.

ITTC (2002*a*) 'Report of the Specialist Committee on Speed and Powering Trials'. *Proc. of 23rd ITTC*, vol. II, Venice, IT.

ITTC (2002*b*) *Uncertainty analysis, Example for Open Water Test.* Recommended Procedures and Guidelines 7.5-02-03-02.2, International Towing Tank Conference.

ITTC (2002*c*) *Uncertainty analysis for Propulsion Test.* Recommended Procedures and Guidelines, International Towing Tank Conference.

ITTC (2008) 'Report of the Specialist Committee on Uncertainty Analysis'. *Proc. of 25th ITTC*, vol. II, Fukuoka, JP.

ITTC (2011*a*) *1978 ITTC Performance Prediction Method.* Recommended Procedures and Guidelines 7.5-02-03-01.4, International Towing Tank Conference.

ITTC (2011*b*) 'Report of the Specialist Committee on Uncertainty Analysis'. *Proc. of 26th ITTC*, vol. I, Rio de Janeiro, BR.

ITTC (2014*a*) *Analysis of Speed/Power Trial Data.* Recommended Procedures and Guidelines 7.5-04-01-01.2, International Towing Tank Conference.

ITTC (2014*b*) *Guide to the Expression of Uncertainty in Experimental Hydrodynamics.* Recommended Procedures and Guidelines 7.5-02-01-01, International Towing Tank Conference.

ITTC (2014*c*) *Preparation and Conduct of Speed/Power Trial Data.* Recommended Procedures and Guidelines 7.5-04-01-01.1, International Towing Tank Conference.

Izubuchi, T. (1934) 'Increase in Hull Resistance Through Shipbottom Fouling'. *Zosen Kiokai*, **55**.

Jain, R. B. (1981*a*) 'Detecting Outliers: Power and some other considerations'. *Communications in statistics - Theory and Methods*, **10**.

Jain, R. B. (1981*b*) 'Percentage Points of Many-Outlier detection procedures'. *Technometrics*, **23**(1):71–75.

Jazwinski, A. H. (1969) 'Adaptive Filtering'. *Automatica*, **5**.

JCGM (2008*a*) *Guide to the expression of uncertainty in measurement (GUM)*. Tech. rep.

JCGM (2008*b*) *Supplement 1: Propagation of distributions using a Monte Carlo method*. Tech. rep.

Jonsson, S. and Fridriksson, H. (2016) 'Continuous Estimate of Hull and Propeller Performance Using Auto-Logged Data'. *Proc. of the 1st Hull Performance & Insight Conference (HullPIC '16)*, Castello di Pavone, IT.

Journée, J. M. J., Rijke, R. J. and Verleg, G. J. H. (1987) *Marine performance surveillance with a personal computer*. Tech. Rep. No. 753-P, TUDelft, Faculty of Marine Technology, Ship Hydromechanics Laboratory, Helsinki, FI.

Kakuta, R., Ando, H. and Yonezawa, T. (2016) 'Utilization of Vessel Performance Management System in a Shipping Company'. *Proc. of the 1st Hull Performance & Insight Conference (HullPIC '16)*, Castello di Pavone, IT.

Kempf, G. (1937) 'On the effect of roughness on the resistance of ships'. *Trans. Institution of Naval Architects (INA)*, **79**:109–119.

Kent, J. L. (1959) *Ships in Rough Water*. Nelson's Nautical Series, Thomas Nelson and Sons Ltd., Edinburgh, UK.

Kijima, K. and Tanaka, S. (1993) 'On a Prediction Method of Ship Manoeuvring characteristics'. *Proc. of the International Conference on Marine Simulation and Ship Manoeuvrability (MARSIM'93)*, St. John's, CA.

Kongsberg (2019) 'Shaft power meter, Torque and power measurement system for rotating shafts'. URL `https://www.km.kongsberg.com/ks/web/nokbg0240.nsf/AllWeb/ECC998CE82FE3801C125758300448E97?OpenDocument`.

Korkut, E. and Takinaci, A. C. (2013) *18m Research Vessel Propulsion Tests and Powering Calculations*. Tech. Rep. 2013-UNEW-P03, Istanbul Technical University, Istanbul, TR.

Korvin-Kroukovsky, B. V. and Jacobs, W. R. (1957) *Pitching and heaving motions of a ship in regular waves*. Tech. Rep. 659, Stevens Institute of Technology, Hoboken, US.

Krapp, A. and Bertram, V. (2016) 'Hull Performance Analysis – Aspects of Speed-Power Reference Curves'. *Proc. of the 1st Hull Performance & Insight Conference (HullPIC '16)*, Castello di Pavone, IT.

Krapp, A. and Schmode, D. (2017) 'A Detailed Look at the Speed-Power Relation of Different Vessel Types at Different Loading Conditions'. *Proc. of the 2nd Hull Performance & Insight Conference (HullPIC '17)*, Ulrichshusen, DE.

Kreitner, J. (1939) 'Heave, Pitch and Resistance of Ships in a Seaway'. *Trans. Institution of Naval Architects (INA)*, **81**:203–241.

Lackenby, H. (1952) 'On the acceleration of ships'. *Trans. Institution of Engineers and Shipbuilders in Scotland (IESS)*.

Lackenby, H. (1963) 'The Effect of Shallow Water on Ship Speed'. *The Shipbuilder and the Marine Engine-Builder*, **70**(672).

Lainiotis, D. G. (ed.) (1976) *Special Issue on Adaptive Systems*, *Proceedings of the IEEE*, vol. 64, Issue 8. Institute of Electrical and Electronics Engineers, New York, US.

Larsson, L. and Raven, H. C. (2010) *Ship resistance and flow*. Principles of naval architecture, Society of Naval Architects and Marine Engineers, Jersey City, US.

Leifsson, L. ., Sævarsdóttir, H., Sigurðsson, S. . and Vésteinsson, A. (2008) 'Grey-box modeling of an ocean vessel for operational optimization'. *Simulation Modelling Practice and Theory*, **16**(8):923–932, doi:10.1016/j.simpat.2008.03.006.

Lemnius, L. (1571) *Occulta naturae miracula*.

Lewis, E. V. (ed.) (1988) *Principles of Naval Architecture*, vol. II: Resistance, Propulsion and Vibration. The Society of Naval Architects and Marine Engineers (SNAME), Jersey City, US, 2nd edn.

Lewthwaite, J. C., Molland, A. F. and Thomas, K. W. (1985) 'An investigation into the variation of ship skin frictional resistance with fouling.' *Trans. Royal Institution of Naval Architects (RINA)*, **127**:268–279.

Li, C. (2019) *Effect of Cuprous Oxide particles on the drag characteristics of marine coatings*. PhD Thesis, Newcastle University, Newcastle upon Tyne, UK.

Livingston Smith, S. (1955) 'BSRA resistance experiments on the Lucy Ashton. Part IV. Miscellaneous investigations and general appraisal'. *Trans. Institution of Naval Architects (INA)*, **97**:525–561.

Lloyd, A. R. J. M. (1989) *Seakeeping: ship behaviour in rough weather*. Ellis Horwood series in marine technology, E. Horwood ; Halsted Press, Southampton, UK.

Loeb, G. I., Laster, D., Gracik, T. and Taylor, D. W. (1984) 'The Influence of Microbial Fouling Films on Hydrodynamic Drag of Rotating Discs'. Costlow, J. D. and Tipper, R. C. (eds.), *Marine Biodeterioration: An Interdisciplinary Study.*, pp. 88–94, Springer US, Boston, US, doi:10.1007/978-1-4615-9720-9_13.

Logan, K. P. (2011) 'Using a Ship's Propeller for Hull Condition Monitoring'. *Proc. of the ASNE Intelligent Ships Symposium IX*, Philadelphia, US.

Lutkenhouse, C., Brady, B., Delbridge, J., Haslbeck, E. G., Holm, E., Dana, L., Michael, T., Ross, A., Stamper, D., Tseng, C. and Webb, A. (2016) 'Baseline Propeller Roughness Condition Assessment and its Impact on Fuel Efficiency'. *Proc. of the 1st Hull Performance & Insight Conference (HullPIC '16)*, Castello di Pavone, IT.

Maki, A., Akimoto, Y., Nagata, Y., Kobayashi, S., Kobayashi, E., Shiotani, S., Ohsawa, T. and Umeda, N. (2011) 'A new weather-routing system that accounts for ship stability based on a real-coded genetic algorithm'. *Journal of Marine Science and Technology*, **16**(3):311–322, doi:10.1007/s00773-011-0128-z.

Maruo, H. (1960) 'On the increase of the resistance of a ship in rough seas (2nd report)'. *Journal of the Society of Naval Architects of Japan*, **108**.

Millero, F. J. and Poisson, A. (1981) 'International one-atmosphere equation of state of seawater'. *Deep-Sea Research*, **28**:625–629.

Moat, B. I., Yelland, M. J., Pascal, R. W. and Molland, A. F. (2006*a*) 'Quantifying the Airflow Distortion over Merchant Ships. Part I: Validation of a CFD Model'. *Journal of Atmospheric and Ocean Technology*, **23**.

Moat, B. I., Yelland, M. J., Pascal, R. W. and Molland, A. F. (2006*b*) 'Quantifying the Airflow Distortion over Merchant Ships. Part II: Application of the Model Results'. *Journal of Atmospheric and Ocean Technology*, **23**.

Molland, A. F. and Turnock, S., R. (2002) 'Flow straightening effects on a ship rudder due to upstream propeller and hull'. *International Shipbuilding Progress*, **49**(3):195–214.

Molland, A. F., Wellicome, J. F. and Couser, P. R. (1994) *Resistance experiments on a systematic series of high speed displacement catamaran forms: variation of length-displacement ratio and breadth-draught ratio*. Ship Science Report 71, University of Southampton, Southampton, UK.

Mosaad, M. A. (1986) *Marine Propeller Roughness Penalties*. PhD Thesis, Newcastle University, Newcastle upon Tyne, UK.

Munk, T. (2006) 'Fuel Conservation through Managing Hull Resistance'. *Proc. of the Motorship Propulsion Conference*, Copenhagen, DK.

Munk, T. and Kane, D. (2011) 'Technical fuel conservation policy and Hull and Propeller Performance'. *Proc. of the International Conference on Design and Operation of Tankers*, Royal Institution of Naval Architects, Athens, GR.

Nakamura, S. and Naito, S. (1975) 'Propulsive performance of a container ship in waves'. *Journal of the Society of Naval Architects Kansai Japan*, **158**.

Nielsen, U. D. (2005) *Estimations of directional wave spectra from measured ship responses*. PhD Thesis, Tehnical University of Denmark.

Nielsen, U. D. (2006) 'Estimations of on-site directional wave spectra from measured ship responses'. *Marine Structures*, **19**.

NOAA (2009) 'National Data Buoy Center'. URL `https://www.ndbc.noaa.gov/`.

Ogawa, A., T., K. and Kijima, K. (1977) *MMG report-I, on the mathematical model of Ship manoeuvring.* Tech. rep.

Oliveira, D., Larsson, A. I. and Granhag, L. (2018) 'Effect of ship hull form on the resistance penalty from biofouling'. *Biofouling*, **34**(3):262–272, doi:10.1080/08927014.2018.1434157.

Orihara, H. and Tsujimoto, M. (2017) 'Performance prediction of full-scale ship and analysis by means of on-board monitoring. Part 2: Validation of full-scale performance predictions in actual seas'. *Journal of Marine Science and Technology.*

Park, D.-M., Kim, Y., Seo, M.-G. and Lee, J. (2016) 'Study on added resistance of a tanker in head waves at different drafts'. *Ocean Engineering*, **111**.

Pedersen, B. P. and Larsen, J. (2009*a*) 'Modeling of Ship Propulsion Performance'. *Proc. of the World Maritime Technology Conference (WMTC 2009)*, Institute of Marine Engineers, Mumbai, IN.

Pedersen, B. P. and Larsen, J. (2009*b*) 'Prediction of full-scale propulsion power using Artificial Newral Networks'. *Proc. of the 8th International Conference on Computer and Applications in the Maritime Industries (COMPIT 09)*, Budapest, HU.

Pedersen, B. P. and Larsen, J. (2013) 'Gaussian Process Regression for Vessel Performance Monitoring'. *Proc. of the 12th International Conference on Computer and Applications in the Maritime Industries (COMPIT 13)*, Cortona, IT.

Peirce, B. (1852) 'Criterion for the Rejection of Doubtful Observations'. *The Astronomical Journal*, **II**(21).

Petersen, J. P., Jacobsen, D. J. and Winther, O. (2012*a*) 'Statistical modelling for ship propulsion efficiency'. *Journal of Marine Science and Technology*, **17**(1):30–39, doi: 10.1007/s00773-011-0151-0.

Petersen, J. P., Winther, O. and Jacobsen, D. J. (2012*b*) 'A Machine-Learning Approach to Predict Main Energy Consumption under Realistic Operational Conditions'. *Ship Technology Research*, **59**(1):64–72, doi:10.1179/str.2012.59.1.007.

Ponsford, P. J. (1978) *Wind forces and moments measured on a waterline model of the container ship 'Tokyo Bay'*. Tech. Rep. R29, National Maritime Institute, Feltham, UK.

Prochaska, F. (1977) 'A Contribution to the Design of Service Adapted Propellers'. *Trans. Institution of Engineers and Shipbuilders in Scotland (IESS)*, **121**(2).

Raven, H. C. (2016) 'A new correction for Shallow-Water effects in ship Speed Trials'. *Proc. of the 13th International Symposium on PRActical Design of Ships and Other Floating Structures (PRADS 2016)*, Copenhagen, DK.

Reid, R. E. (1985) 'A Condition and Performance Monitoring System with Application to U.S. Navy Ship Operations'. *Naval Engineers Journal*, **97**(7):29–38, doi:10.1111/j. 1559-3584.1985.tb01876.x.

Rhinehart, R. R. (2013) 'Automated Steady and Transient State Identification in Noisy Processes'. *Proc. of the 2013 American Control Conference (ACC)*, Washington, US.

R.M. Young Company (2019) 'Mechanical wind sensors'. URL `http://www.youngusa.com/products/7/74.html`.

Rosner, B. (1975) 'On the Detection of Many Outliers'. *Technometrics*, **17**(2):221–227.

Sage, A. P. (1972) 'Estimation and Identification'. *Proc. of the IFAC World Congress*, Paris, FR.

Sannino, S. (2007) *Storia della navigazione*. la Tribuna, Poggiomarino, IT.

Sasaki, N. and Carchen, A. (2015) *Data quality assessment of The Princess Royal service trials data from 5th March 2015 sea trials*. Internal Report, Newcastle University, Newcastle upon Tyne, UK.

Schmiechen, M. (1991) 'Propulsive performance of METEOR and her model identified from quasisteady ropulsion tests'.

Schultz, M. P. (2004) 'Frictional Resistance of Antifouling Coating Systems'. *Journal of Fluids Engineering*, **126**(6):1039, doi:10.1115/1.1845552.

Schultz, M. P. (2007) 'Effects of coating roughness and biofouling on ship resistance and powering'. *Biofouling*, **23**(5):331–341, doi:10.1080/08927010701461974.

Schultz, M. P. and Swain, G. W. (2000) 'The influence of biofilms on skin friction drag'. *Biofouling*, **15**(1-3):129–139, doi:10.1080/08927010009386304.

Scott, J. R. (1971) 'Voyage performance of M.V. Protesilaus'. *Trans. Royal Institution of Naval Architects (RINA)*, **113**:287.

Söding, H. (2006) *Program PDSTRIP: Public Domain Strip Method*. Manual.

Seo, K.-C., Atlar, M. and Goo, B. (2016) 'A Study on the Hydrodynamic Effect of Biofouling on Marine Propeller'. *Journal of the Korean Society of Marine Environment and Safety*, **22**(1):123–128, doi:10.7837/kosomes.2016.22.1.123.

Sfakianos, N. (2016) *Prediction of Added Wave Resistance of Princess Royal Research Vessel using model tests*. Master's thesis, Newcastle University, Newcastle upon Tyne, UK.

Shigunov, V. (2017) 'Added Power in Seaway'. *Ship Technology Research*, **64**(2):65–75, doi:10.1080/09377255.2017.1331953.

Solonen, A. (2016) 'Experiences with ISO-19030 – and Beyond'. *Proc. of the 1st Hull Performance & Insight Conference (HullPIC '16)*, Castello di Pavone, IT.

Steen, S. and Faltinsen, O. M. (1998) 'Added Resistance of a Ship Moving in Small Sea States'. *Proc. of the 7th International Symposium on Practical Design of Ships and Mobile Units (PRADS '98)*, The Hague, NL.

Stewart, R. H. (2008) *Introduction to physical oceanography*. Texas A & M University, Texas, US.

Stopford, M. (2019) 'A workable agenda for the merchant shipping's technical development?' *The Naval Architect*, (Future Ship 2050).

Strasser, G., Takagi, K., Werner, S., Hollenbach, U., Tanaka, T., Yamamoto, K. and Hirota, K. (2015) 'A verification of the ITTC/ISO speed/power trials analysis'. *Journal of Marine Science and Technology*, **20**, doi:10.1007/s00773-015-0304-7.

Svensen, T. E. and Medhurst, J. S. (1984) 'A Simplified Method for the Assessment of Propeller Roughness Penalties'. *Marine Technology*, **21**(1).

Taniguchi, K. and Tamura, K. (1966) 'On a new method of correction for wind resistance relating to the analysis of speed trial results'. *Proc. of ITTC '66*, Performance Session, Tokyo, JP.

Taskar, B., Yum, K. K., Steen, S. and Pedersen, E. (2016) 'The effect of waves on engine-propeller dynamics and propulsion performance of ships'. *Ocean Engineering*, **122**:262–277, doi:10.1016/j.oceaneng.2016.06.034.

Telfer, E. V. (1926) 'The Practical Analysis of Merchant Ship Trials and Service Performance'. *Trans. North East Coast Institution of Engineers & Shipbuilders (NECIES)*, **43**:63–98.

Telfer, E. V. (1972) 'Some Loose Ends in Retrospect'. *Trans. North East Coast Institution of Engineers & Shipbuilders (NECIES)*.

Tezdogan, T., Demirel, Y. K., Kellett, P., Khorasanchi, M., Incecik, A. and Turan, O. (2015) 'Full-scale unsteady RANS CFD simulations of ship behaviour and performance in head seas due to slow steaming'. *Ocean Engineering*, **97**.

Townsin, R. L. (2003) 'The Ship Hull Fouling Penalty'. *Biofouling*, **19**(sup1):9–15, doi:10.1080/0892701031000088535.

Townsin, R. L., Moss, B., Wynne, J. B. and Whyte, I. M. (1975) 'Monitoring the Speed Performance of Ships'. *Trans. North East Coast Institution of Engineers & Shipbuilders (NECIES)*, **91**(5):pp. 159–175.

Townsin, R. L. and Svensen, T. E. (1980) 'Monitoring speed and power for fuel economy'. *Proc. of the Shipboard Energy Conservation '80 Symposium*, SNAME, New York, US.

Ueno, M., Tsukada, Y. and Tanizawa, K. (2013) 'Estimation and prediction of effective inflow velocity to propeller in waves'. *Journal of Marine Science and Technology*, **18**(3):339–348, doi:10.1007/s00773-013-0211-8.

van Ballegooijen, E., Munteau, T. and Timmer, M. (2017) 'Measuring the Full-Scale Performance of a Propeller and Bulbous Bow Retrofit via Propeller Thrust Measurements'. *Proc. of the 2nd Hull Performance & Insight Conference (HullPIC '17)*, Ulrichshusen, DE.

van den Boom, H. J. and Hasselaar, T. W. (2014) 'Ship Speed-Power Performance Assessment'. *Proc. of the SNAME Annual Meeting*, SNAME.

van den Boom, H., Huisman, H. and Mennen, F. (2015) 'New Guidelines for Speed/Power Trials'.

Van der Hoven, I. (1957) 'Power spectrum of horizontal wind speed in the frequency range from 0.0007 to 900 cycles per hour'. *Journal of Meteorology*, **14**(2):160–164, doi:10.1175/1520-0469(1957)014<0160:PSOHWS>2.0.CO;2.

van Lammeren, W. P. A., van Manen, J. and Oosterveld, M. W. C. (1969) 'The Wageningen B-Screw Series'. *Trans. Society of Naval Architects and Marine Engineers (SNAME)*, **77**.

Vargas, A. and Shan, H. (2017) 'Modeling of ship resistance as a function of biofouling type, coverage and spatial variation'. *Proc. of the 2nd Hull Performance & Insight Conference (HullPIC '17)*, Ulrichshusen, DE.

vom Baur, M. (2016) 'Acquisition and Integration of Meaningful Performance Data on Board - Challenges and Experiences'. *Proc. of the 1st Hull Performance & Insight Conference (HullPIC '16)*, Castello di Pavone, IT.

Vranakis, E. (2016) *An investigation into the wind loadings applied to a Deep-V catamaran using model testing*. Master's thesis, Newcastle University, Newcastle upon Tyne, UK.

Vranakis, E., Axiotis, D., Carchen, A., Trodden, D. and Atlar, M. (2017) 'Investigation into the wind loadings applied to a deep-v catamaran using experimental and numerical approaches'. *Proc. of the 5th International Conference on Advanced Model Measurement Technology for The Maritime Industry (AMT'17)*, Glasgow, UK.

Wahab, R., Pritchett, C. and Ruth, L. C. (1971) 'On the Behavior of the ASR catamaran in waves'. *Marine Technology*, **8**:334–360.

Wang, H. and Freise, C. (1997) 'Error analysis of the directional wave spectra obtained by the NDBC 3-m pitch-roll discus buoy'. *IEEE Journal of Oceanic Engineering*, **22**(4):639–648, doi:10.1109/48.650830.

Wellicome, J. F., Temarel, P., Molland, A. F., Cic, J. and Taunton, D. J. (1999) *Experimental measurements of the seakeeping characteristics of fast displacement catamarans in oblique waves*. Ship Science Report 111, University of Southampton, Southampton, UK.

Wellicome, J. F., Temarel, P., Molland, A. F. and Couser, P. R. (1995) *Experimental measurements of the seakeeping characteristics of fast displacement catamarans in oblique waves*. Ship Science Report 89, University of Southampton, Southampton, UK.

WHOI (1952) *Marine Fouling and Its Prevention*. Tech. Rep. 580, Woods Hole Oceanographic Institute, Massachusetts, US, george Banta Publishing Co., Menasha, WI.

Yamaguchi, Y., Furukawa, Y., Mutou, H. and Kijima, K. (2009) 'Study on Prediction Method of Hydrodynamic Derivatives for Full Ships'. *Journal of the Japan Society of Naval Architects and Ocean Engineers*, **10**:105–113, doi:10.2534/jjasnaoe.10.105.

Yasukawa, H. (1992) 'Hydrodynamic interactions among hull, rudder and propeller of a turning thin ship'. *Trans. West-Japan Society of Naval Architects*, (84):59–83.

Yasukawa, H. and Yoshimura, Y. (2015) 'Introduction of MMG standard method for ship maneuvering predictions'. *Journal of Marine Science and Technology*, **20**:37–52.

Yebra, D. M., Kiil, S. and Dam-Johansen, K. (2004) 'Antifouling technology—past, present and future steps towards efficient and environmentally friendly antifouling coatings'. *Progress in Organic Coatings*, **50**(2):75–104, doi:10.1016/j.porgcoat.2003.06.001.

Yeginbayeva, I. A. (2017) *An investigation into hydrodynamic performance of marine coatings "in-service" conditions*. PhD Thesis, Newcastle University, Newcastle upon Tyne, UK.

Young, K. (2012) 'USS Harry S. Truman sea trials'. URL `https://www.dvidshub.net/image/621007/uss-harry-s-truman-sea-trials`.

# Relevant publications

### Journal papers

Carchen, A., Atlar, M., Turkmen, S., Pazouki, K., Murphy, A. J. (2019), 'Ship performance monitoring dedicated to biofouling analysis: development on a small size research catamaran'. *Applied Ocean Research*, **89**.

### Conference papers

Carchen, A., Sasaki, N., Aktas, B., Turkmen, S., Atlar, M. (2015) 'Design and review of the new NPT propeller for The Princess Royal'. *Proc. of the 4th International Conference on Advanced Model Measurement Technology for The Maritime Industry (AMT'15)*, Istanbul, TR.

Lim, S., Carchen, A., Pazouki, K., Murphy, A. J., Younessi, S., Graham, N., (2016) 'Systematic rationale for assessing energy flow across the entire vessel operation', *Proc. of the Energy Efficient Ships Conference (EES)*, London, UK.

Carchen, A., Pazouki, K., Atlar, M. (2017) 'Development of an Online Ship Performance Monitoring System Dedicated for Biofouling Analysis', *Proc. of the 2nd Hull Performance & Insight Conference (HullPIC '17)*. Ulrichshusen, DE.

Carchen, A., Turkmen, S., Pazouki, K., Murphy, A. J., Aktas, B., Atlar, M. (2017) 'Uncertainty analysis of full-scale ship performance monitoring onboard The Princess Royal'. *Proc. of the 5th International Conference on Advanced Model Measurement Technology for The Maritime Industry (AMT'17)*. Glasgow, UK.

Vranakis, M., Axiotis, D., Carchen, A., Trodden, D., Atlar. (2017)' Investigation into the wind loadings applied to a deep-v catamaran using experimental and numerical approaches'. *Proc. of the 5th International Conference on Advanced Model Measurement Technology for The Maritime Industry (AMT'17)*. Glasgow, UK.

Atlar, M., Yeginbayeva, I., Turkmen, S., Demirel, Y. K., Carchen, A., Marino, A., Williams, D. (2018) 'A rational approach to predicting the effect of

antifouling systems on'in-service' ship performance'. *Proc. of the 3rd International Symposium on Naval Architecture and Maritime (INT-NAM 18)*, Istanbul, TR.

Lim, S., Turkmen, S., Rostami, A. B., Prini, F., Kurniawati, V. R., Carchen, A., Gibson, M., Benson, S., Birmingham, R., Dow, R. S., Murphy, A. J., Pazouki, K. (2018) 'Ship performance – using the real world as a laboratory'. *Full Scale Ship Performance Conference*. London, UK.